Tampere University

TAINA VIHERIÄLÄ

In Vitro Maturation and Functionality Assessment of Human Pluripotent Stem Cell-Derived Retinal Pigment Epithelium for Therapeutic Applications

Tampere University Dissertations 857

Tampere University Dissertations 857

TAINA VIHERIÄLÄ

In Vitro Maturation and Functionality Assessment of Human Pluripotent Stem Cell-Derived Retinal Pigment Epithelium for Therapeutic Applications

ACADEMIC DISSERTATION
To be presented, with the permission of
the Faculty of Medicine and Health Technology
of Tampere University,
for public discussion in the F114 auditorium
of the Arvo building, Arvo Ylpön katu 34, Tampere,
on 6 October 2023, at 12 o'clock.

ACADEMIC DISSERTATION
Tampere University, Faculty of Medicine and Health Technology
Finland

Responsible supervisor and Custos	Associate Professor (tenure track) Soile Nymark Tampere University Finland	
Supervisors	Professor Heli Skottman Tampere University Finland	Adjunct Professor Tanja Ilmarinen Tampere University Finland
Pre-examiners	Professor Paavo Honkakoski University of Eastern Finland Finland	PhD André Helder Karolinska Institutet Sweden
Opponent	Lecturer Amanda Carr University College London United Kingdom	

The originality of this thesis has been checked using the Turnitin OriginalityCheck service.

Cover design: Roihu Inc.

ISBN 978-952-03-3043-9 (print)
ISBN 978-952-03-3044-6 (pdf)
ISSN 2489-9860 (print)
ISSN 2490-0028 (pdf)
http://urn.fi/URN:ISBN:978-952-03-3044-6

Carbon dioxide emissions from printing Tampere University dissertations have been compensated.

PunaMusta Oy – Yliopistopaino
Joensuu 2023

"You gain strength, courage, and confidence by every experience in which you really stop to look fear in the face. You must do the thing which you think you cannot do."

Eleanor Roosevelt

ACKNOWLEDGEMENTS

This thesis was carried out in collaboration with the Biophysics of the Eye group and the Eye Regeneration group at Tampere University's Faculty of Medicine and Health Technology between 2017 and 2023. The Doctoral Programme of Medicine and Life Sciences, the Academy of Finland, and the Emil Aaltonen Foundation are thanked for funding this research and associated conference journeys. I would also like to thank the Finnish Cultural Foundation, the Instrumentarium Foundation, Evald and Hilda Nissi Foundation, and the Finnish Eye and Tissue Bank Foundation for supporting me with personal grants.

Most importantly, my deepest gratitude goes to my supervisors Associate Professor Soile Nymark, PhD, Professor Heli Skottman, PhD, and Adjunct Professor Tanja Ilmarinen, PhD. Thank you for trusting me with these projects and for guiding and supporting me through this journey. Soile, you are truly an inspiration, and I admire your enthusiasm and never-ending knowledge. You never ceased to amaze me with your skill in solving our scientific problems in a blink of an eye. Your effectiveness and optimism are beyond words. Thank you for always making me feel welcome in your office and lifting me up with your encouraging words. Heli, thank you for providing me with an inspirational work atmosphere. Thank you for the endless patience and sophisticated pushes you have given me whenever I was struggling. Your experience as a scientist is tremendous, and it has been an honour to work with you. Last but definitely not least, Tanja, you have a huge passion for science, and you have the amazing ability to spread that passion around you. You have the power of multitasking, and you somehow seem to have more than 24 hours in your days. I am extremely grateful to you for always being there for me and always finding the time even though it was not that easy in this hectic world.

I want to warmly thank the members of my thesis committee, Professor Jari Hyttinen, PhD, Professor Anu Kauppinen, PhD, and Adjunct Professor Giedrius Kalesnykas, PhD, for our annual meetings and the guidance and support provided. I also want to thank Professor Paavo Honkakoski, PhD, and Dr André Helder, PhD, for reviewing this thesis and giving invaluable comments that improved the quality

of this work. My co-authors are thanked for their contribution. Without their work, the publications would not have been possible.

I am truly grateful to the past and present members of both research groups. It is nearly impossible to succeed without a supportive team around you. Without your scientific and technical skills, this thesis would not exist. In particular Heidi Hongisto, Anni Mörö, Meri Vattulainen, and Maija Kauppila, I thank you for being there and providing your ears to my worries. You kept me going when times were tough, and I always knew I could count on you not only as co-workers but also as friends. I am sincerely grateful that we have such competent laboratory technicians as Hanna Pekkanen, Outi Melin, and Outi Heikkilä. Without you, this project would never have finished. Thank you for your constant help and support. Also, I feel lucky to have such skilful and helpful colleagues around me. Thank you Iina Korkka, Julia Fadjukov, Viivi Karema-Jokinen, and many others for your peer support. I would also like to thank the Tampere Imaging Facility, especially Teemu Ihalainen, for your help and technical expertise.

I have been blessed with a loving and caring family and friends. You have supported and helped me in many ways throughout these years. Mum and Dad, thank you for caring and believing in me and being there for me. I want to thank my brother, Jukka, who showed me the way to an academic career. I also want to thank my other family, Liisa, Vesa, Sanna, and Jenna, for your constant support and always making me feel at home.

Finally, my deepest gratitude goes to my little family! You have always believed in me, supported me, and loved me unconditionally. You have helped me to remember what this life is all about. Tommi, there are no words to describe my gratitude, appreciation, and love. My dearest Miko, Luka, and Mila, you are my everything!

Taina Viheriälä
Tampere, August 25, 2023

ABSTRACT

Vision can be regarded as a critical sense in everyday life, and vision loss is associated with a deterioration in quality of life. The visual function is partly ensured by the retinal pigment epithelium (RPE), a monolayer of pigmented cells supporting the welfare of the neural retina, which itself has many essential functions. Age-related macular degeneration (AMD) is a retinal degenerative disease where the degeneration of the RPE can lead to impaired or total loss of vision. To date, no curative treatment is available for AMD. However, replacement of the damaged and dysfunctional RPE cells with *in vitro* differentiated and cultured RPE cells is considered as a potential approach to cure AMD and other RPE degeneration-related diseases. Human embryonic stem cell-derived RPE (hESC-RPE) cells have been shown to be a promising cell source for the transplantation studies. Current clinical trials have shown no safety issues, but the efficacy of the transplantation remains to be studied in further clinical trials. One possible issue with clinical efficacy can be the immature state of the transplanted RPE cells. The work presented in this thesis focuses on the *in vitro* maturation of cryopreserved hESC-RPE cells with three approaches: I) to study the influence of the surface protein coating to the maturation of hESC-RPE cells on the functional level and in the expression of RPE-related proteins during maturation, II) to study the tolerance to cellular stress in different maturation levels of hESC-RPE cells, and III) to investigate the functional Ca^{2+} channels in hESC-RPE.

Based on the results obtained in this thesis, there are three main findings. First, adding more complexity to the culture substrate protein coatings is advantageous in improving the functionality of hESC-RPE cells and producing a more homogenous RPE cell layer. Secondly, a prolonged culture time was observed to have positive effects on the ability of hESC-RPE cells to tolerate cellular stress, which is important, for example, for the success of cell transplant therapy. Thirdly, the results showed that the intracellular localization of the Ca^{2+} channel, in particular the voltage-gated $Ca_V1.3$ subtype, changed as the culture time increased. In addition, the results indicate that the $Ca_V1.3$ channel is involved in the regulation of phagocytosis and vascular endothelial growth factor (VEGF) secretion.

To conclude, this thesis provides new insights into the phenotypic changes of cryopreserved hESC-RPE cells, which can be altered with culture conditions such as substrate protein coatings and culture time. Importantly, the results from this thesis can be utilized in RPE studies in general but also in the development of transplantation therapies.

TIIVISTELMÄ

Näkökyky on ihmisen hyvinvoinnin ja elämän laadun kannalta tärkein aistimme. Näkökykyä ylläpitää verkkokalvon pigmenttiepiteeli (engl. retinal pigment epithelium, RPE), joka sijaitsee silmän takaosassa verkkokalvon ja suonikalvon välissä huolehtien erityisesti verkkokalvon näköaistinsolujen toiminnasta ja täten koko näköaistista. RPE:n toimintahäiriöt voivat johtaa verkkokalvon rappeumasairauksiin kuten ikärappeumaan, joihin liittyy heikentynyt näkökyky tai jopa sokeus. Tällä hetkellä hoitokeinot ikärappeumaan ovat varsin rajalliset. Solusiirtohoitoa, jossa vaurioituneet RPE-solut korvataan terveillä RPE-soluilla, pidetään potentiaalisena tulevaisuuden hoitokeinona verkkokalvon rappeumasairauksiin. Ihmisen alkion kantasoluista erilaistetut RPE-solut (hESC-RPE) ovat osoittautuneet lupaavaksi solulähteeksi näihin soluterapiahoitoihin. Nykyiset kliiniset kokeet ovat osoittaneet hoitojen turvallisuuden, mutta hoitojen tehokkuuden saavuttamiseksi tarvitaan vielä lisää tutkimusta sekä lisätietoa siirrettävien solujen kypsyystasojen vaikutuksesta hoitotuloksiin. Tässä väitöskirjassa keskityttiin laboratoriossa kasvatettujen hESC-RPE-solujen ominaisuuksien analysointiin kolmella eri lähestymistavalla: I) tutkittiin kasvatusalustassa käytetyn proteiinipinnoitteen vaikutusta solujen ominaisuuksiin ja RPE:lle tyypillisten proteiinien ilmentymiseen, II) tutkittiin kasvatusajan vaikutusta solujen kykyyn sietää solustressiä ja III) tutkittiin Ca^{2+} -kanavien ilmentymistä ja roolia hESC-RPE:ssä.

Työn tulokset voidaan tiivistää kolmeen päätulokseen. Ensinnäkin, kasvatusalustana käytettävällä proteiinipinnoitteella huomattiin olevan merkittävä rooli hESC-RPE:n ominaisuuksiin. Solujen toiminnallisuus parani ja solukerroksesta tuli tasalaatuisempi. Toiseksi, pidemmällä viljelyajalla huomattiin olevan positiivisia vaikutuksia solujen kykyyn sietää paremmin solustressiä, jolla on tärkeä merkitys esimerkiksi solusiirtohoidon onnistumisen kannalta. Kolmanneksi, tutkimustulokset myös osoittivat, että Ca^{2+}-kanavan, erityisesti jänniteohjatun $Ca_V1.3$ alatyypin, sijainti hESC-RPE-soluissa muuttui viljelyajan pidentyessä. Lisäksi osoitimme $Ca_V1.3$-kanavan osallistuvan hESC-RPE-solujen fagosytoosiin sekä verisuonten endoteelin kasvutekijän (VEGF) erityksen säätelyyn.

Yhteenvetona tämä väitöskirja tuo merkittävästi uutta tietoa hESC-RPE-solujen ominaisuuksista, joihin pystytään vaikuttumaan viljelyolosuhteilla kuten

kasvatusalustan pinnoitteella sekä viljelyajalla. Työn tuloksia voidaan hyödyntää RPE-solututkimuksissa, mutta myös soluterapiahoidon kehityksessä.

CONTENT

ABBREVIATIONS

AMD	Age-related macular degeneration
ATP	Adenosine triphosphate
bFGF	basic fibroblast growth factor
BM	Bruch's membrane
BRB	Blood-retina barrier
Ca^{2+}	Calcium ion
$[Ca^{2+}]_i$	Intracellular Ca^{2+} concentration
Ca_V	Voltage-gated Ca^{2+} channel
Cl^-	Chloride ion
CL3	Claudin-3
CL-19	Claudin-19
Col-IV	Collagen IV
CRALBP	Cellular retinaldehyde-binding protein
Cx43	Connexin 43
DIC	Differential interference contrast
EB	Embryonic body
ECM	Extracellular matrix
EMT	Epithelial-mesenchymal transition
ER	Endoplasmic reticulum
FF	Feeder free
Fluo-4	Fluo-4-acetoxymethyl ester
GMP	Good manufacturing process
H_2O_2	Hydrogen peroxide
hESC	Human embryonic stem cell
hiPSC	Human induced pluripotent stem cell
hPSC	Human pluripotent stem cell
IL6	Interleukin 6
IL8	Interleukin 8
IP3	Inositol-1,4,5-trisphosphate
IVF	*In vitro* fertilization

K^+	Potassium ion
Keap 1	Kelch ECH-associated protein 1
KO-SR	Knockout serum replacement
LN521	Laminin 521
MerTK	Mer tyrosine kinase
Mg^{2+}	Magnesium ion
MITF	Microphthalmia-associated transcription factor
MMP	Mitochondrial membrane potential
Na^+	Sodium ion
Nid-1	Nidogen-1
OTX2	Orthodenticle homolog 2
PAX	Paired box protein-6
PCNT	Pericentrin
PEDF	Pigment epithelium growth factor
PET	Polyethylene terephthalate
PIP2	Phosphatidylinositol 4,5-bisphosphate
PLC	Phospholipase C
POS	Photoreceptor outer segment
ROI	Region of interest
ROS	Reactive oxygen species
RPE	Retinal pigment epithelium
RPE65	Retinal pigment epithelium-specific protein 65 kDa
TER	Transepithelial resistance
VEGF	Vascular endothelial growth factor
ZO-1	Zonula occludens 1

ORIGINAL PUBLICATIONS

This dissertation is based on the following original peer-reviewed publications, referred to as Studies I-III in the text. The original publications are reported at the end of this thesis with the permission of the copyright holders.

Publication I **Viheriälä T***, Sorvari J*, Ihalainen TO, Mörö A, Grönroos P, Schlie-Wolter S, Chichkov B, Skottman H, Nymark S*, Ilmarinen T*. Culture surface protein coatings affect the barrier properties and calcium signalling of hESC-RPE. Scientific Reports, 2021, 11:933

Publication II **Viheriälä T**, Hongisto H, Sorvari J, Skottman H*, Nymark S*, Ilmarinen T. Cell maturation influences the ability of hESC-RPE to tolerate cellular stress. Stem Cell Research & Therapy. 2022, 13:30

Publication III Korkka I, **Viheriälä T**, Juuti-Uusitalo K, Uusitalo-Järvinen H, Skottman H, Hyttinen J, Nymark S. Functional voltage-gated calcium channels are present in human embryonic stem cell-derived retinal pigment epithelium. Stem Cells Translational Medicine, 2019, 8:179-193. **

* These authors contributed equally

** Publication was included in the doctoral dissertation "Ionic Signaling in Retinal Pigment Epithelium" by Iina Korkka at the Faculty of Medicine and Health Technology, Tampere University, Finland, 2022

AUTHOR'S CONTRIBUTIONS

Publication I Experimental design and execution were performed mainly by Viheriälä and the last author Ilmarinen except for the cell adhesion and spreading data. Viheriälä analysed all the data except the Ca^{2+} imaging analysis tools were developed by the shared first author Sorvari. The manuscript was written by Viheriälä with major contribution from the last author Ilmarinen.

Publication II Viheriälä designed and performed the experiments and analysed all the data. The manuscript was written by Viheriälä as the first author.

Publication III The study was primarily designed by the first author Korkka and the last author Nymark with Viheriälä's independent role in the design of RPE maturation experiments. Viheriälä conducted and analysed all the maturation-related experiments of the study. Viheriälä participated in writing the manuscript as the second author.

1 INTRODUCTION

The retinal pigment epithelium (RPE) is a monolayer of pigmented cells located between the photoreceptors and choroid. The RPE has multiple functions and RPE ensures the proper functioning of the neural retina, thus ensuring vision. The RPE is responsible for forming the tight blood-retina barrier, epithelial trafficking, controlling subretinal ionic homeostasis, phagocytosing photoreceptor outer segments, secreting growth factors, and reisomerization of retinal in the visual cycle (Strauss, 2005). Malfunction in any of these functions can lead to retinal degenerative diseases such as age-related macular degeneration (AMD), which could impair vision and even lead to blindness (Dehghan et al., 2022). AMD is a major health issue affecting millions of people worldwide. Currently, despite several clinical trials, no curative treatment is available for the dry form of the AMD and wet AMD is treated with intravitreal injections of anti-VEGF agents (S. Yang et al., 2021).

Stem cell-based replacement therapy has been proposed as an approach for cell therapy to cure retinal diseases like AMD, especially the dry AMD. It utilizes technology where damaged and malfunctioning RPE cells are replaced with healthy, *in vitro* cultured RPE cells (Maeda et al., 2021). Promising sources for the therapies are human pluripotent stem cell-derived RPE cells (hPSC-RPE), including human embryonic stem cell-derived RPE (hESC-RPE) cells (Maeda et al., 2021; Plaza Reyes et al., 2016). First clinical trials have not shown any major safety issues, but the efficacy of the treatment has been incomplete (Kashani et al., 2021; Mehat et al., 2018; Schwartz et al., 2015, 2016; Song et al., 2015). The transplanted RPE cells must function rapidly after the transplantation to secure the well-being of the retina. Therefore, the incomplete restoration of vision could be due to the immaturity of the transplanted hPSC-RPE cells.

Among all the essential functions of the RPE, a key characteristic is Ca^{2+} signalling, which contributes to several RPE functions (Berridge et al., 2003; Mamaeva et al., 2021; Müller et al., 2014; Rosenthal et al., 2007). Light increases the subretinal adenosine triphosphate (ATP) concentration, which induces the activation of Ca^{2+} signalling in the RPE (Wimmers et al., 2007). To date, only a few studies focusing on the Ca^{2+} signalling of hPSC-RPE cells exist, even though Ca^{2+} signalling

is highly relevant for the overall physiology of the RPE (Abu Khamidakh et al., 2016; Miyagishima et al., 2016; Singh et al., 2013; Sorvari et al., 2019).

This thesis focuses on the maturation of hESC-RPE in culture and studies how the culture conditions and timing affect maturation *in vitro*. The overarching goal is to improve our understanding of the maturation process, especially related to gaining the functionality of the native RPE, which is a prerequisite for the success of future cell replacement therapies.

2 LITERATURE REVIEW

2.1 Retinal pigment epithelium

Sensing our visual environment begins with the eye. All information is carried in the form of visible light that passes through the cornea, lens, and vitreous humour, finally reaching the retina and retinal pigment epithelium (RPE) at the back of the eye (Figure 1). The retina is the light-detective neural tissue that converts light into electric signals, which, after additional signal processing, are sent to the brain where the actual sense of vision takes place. The retina contains several types of neuronal cells that are organized in layers (Figure 1) and have functional specializations. The cells responsible for detecting light and converting it into electric signals consists of two types of photoreceptors, rods and cones. These cells are supported by the RPE, a tight monolayer of highly pigmented epithelial cells residing under the neural retina. (Strauss, 2005; Wimmers et al., 2007) With different extracellular milieus on both sides of the monolayer, RPE cells are polarized by forming apical and basolateral structures with different distributions of membrane proteins and organelles (Bok, 1993). The apical cell membrane is facing the photoreceptors and neural retina, while the basolateral membrane faces Bruch's membrane (BM), which is the interface of the RPE and choriocapillaris. Long microvilli cover the apical side, whereas the basolateral side has deep infoldings. (Strauss, 2005) Between the RPE and photoreceptors is a narrow subretinal space where nutrient and waste exchange between the RPE and photoreceptors occurs (Gonzalez-Fernandez, 2003).

Positioned between the neural retina and the choroid, RPE cells form a tight blood-retina barrier (BRB) to control trafficking between the bloodstream and retinal neurons (Bok, 1993). Besides the barrier formation, the RPE has many supportive functions which all together ensure the welfare and functionality of the retina. The RPE is involved in epithelial transport, the visual cycle, phagocytosis, secretion, ion buffering, immune modulation, and absorption of scattered light (Strauss, 2005). These functions are discussed below.

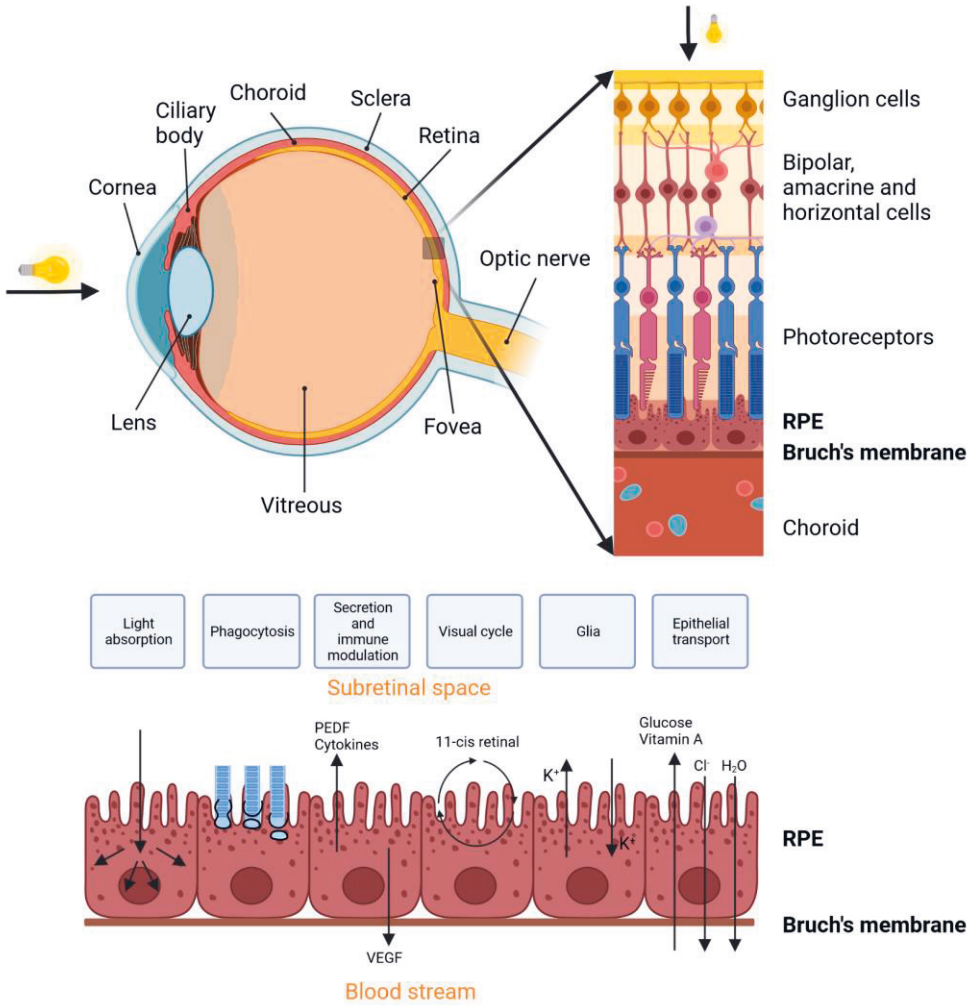

Figure 1. Structures of the human eye and the retina – the RPE complex together with an illustration of the functions of the RPE. The figure was created with BioRender.com by reconstruction with modifications from (Strauss, 2005).

2.1.1 Blood-retina barrier and controlled epithelial transport

The RPE forms a blood-retina barrier (BRB) together with BM and the vascular endothelial cells. The main function of the BRB is to form a tight and controlled barrier between the inner eye and blood circulation, thus preventing the free diffusion of molecules between the two spaces. Electrolytes, water, and metabolic end products are transported from the subretinal space to the bloodstream, while

glucose and nutrients are transported from the bloodstream to the inner eye via the RPE. (Rizzolo et al., 2011; Strauss, 2005) The barrier is composed of adherens and tight junctions, which form a distinguishable polarized cell structure (Rizzolo, 2014). As a polarized monolayer, the tight junctions encircle the cell, separating the distinct apical and basolateral membranes (Rajasekaran et al., 2003). Tight junctions are expressed in the apical junctional complex, where over 30 different proteins including transmembrane proteins and scaffolding proteins are involved in the formation and regulatory properties of the barrier (Anderson, 2001). The zonula occludens (ZO) covers the main protein group of scaffolding proteins that act as a linker between the tight junctional transmembrane proteins and cytoskeleton to form a junctional network (Naylor et al., 2020). The selectivity of the tight junctions is maintained by transmembrane claudin proteins, especially claudin-19 (CL-19) in the RPE (Peng et al., 2011). The expression of CL-19 can directly affect the ion selectivity and permeability of the tight junction. Therefore, CL-19 is referred to as the structural basis of the tight junctions. (F. Liu et al., 2020, 2021) Besides the junctional proteins, formation of the tight junctions and therefore formation of the tight barrier is affected by various factors, including the endothelial cell-secreted factors, which enhance the barrier function (Benedicto et al., 2017). Altogether, the expression and correct localization of tight junctional proteins ensure the proper function of tight junctions.

The formation and integrity of the epithelial barrier can be measured *in vitro* with transepithelial electrical resistance (TER), which can be conducted in real-time without damaging the cells. With TER measurements, the tightness of the tight junctions and therefore the tightness of the whole epithelium can be evaluated. (Anderson, 2001; Fronk & Vargis, 2016). In principle, a higher TER indicates a confluent, well-polarized, and properly formed epithelium (Fronk & Vargis, 2016). TER values of the *in vitro* RPE vary depending on the RPE cell line used and the culture age. Blenkinsop et al. (Blenkinsop et al., 2015) cultured human adult RPE cells for 2 months, after which the TER value was 178.7 ± 9.9 $\Omega \cdot cm^2$, while Peng et al. (Peng et al., 2011) reported a TER value of 900-1400 $\Omega \cdot cm^2$ from human fetal RPE cells cultured for 6-8 weeks. Typical TER values for human pluripotent stem cell-derived RPE (hPSC-RPE) cells range between 150 and 1000 $\Omega \cdot cm^2$ (Hongisto, Ilmarinen, et al., 2017; Ilmarinen et al., 2019; Li et al., 2021; May-Simera et al., 2018; Sharma et al., 2019; A. Sorkio et al., 2014).

In addition to the tight junctions, RPE cells possess gap junctions that are composed of transmembrane protein connexins, of which connexin 43 (Cx43) is the major subtype expressed in RPE cells (Fadjukov et al., 2022; Kojima et al., 2008).

Cell-to-cell communication occurs through gap junctions, but in addition, Cx43 takes part in differentiation, proliferation, and cell viability (Hutnik et al., 2008; Kojima et al., 2008; Pearson et al., 2005).

Na^+/K^+-ATPase pumps in the apical membrane of RPE cells are responsible for the regulation of the apical transport system (Hu et al., 1994; Korte & Wanderman, 1993; Rajasekaran et al., 2003). Intracellular Na^+ and K^+ homeostasis is regulated by Na^+/K^+-ATPase by transporting sodium ions to the subretinal space and potassium ions into the cell in 3:1 stoichiometry (Marmorstein, 2001; Rajasekaran et al., 2003). This transport needs and consumes energy due to the pumping of ions against their electrochemical gradient. Energy is provided by the hydrolysis of adenosine triphosphate (ATP) (Rajasekaran et al., 2003). Maintaining the Na^+ gradient across the cell membrane is essential for the transport of various ions, molecules, and metabolic end products into the RPE from the subretinal space (Wimmers et al., 2007).

Due to the tight epithelial structure, water has to be actively transported, and this is maintained by Cl^- and K^+ cotransporters and the functional presence of aquaporin-1 (Quinn & Miller, 1992). Photoreceptors secrete metabolic end products to the subretinal space, and RPE cells are responsible for their degradation (Strauss, 2005). The most common metabolic end product is lactic acid, whose pathway goes through the RPE's basolateral membrane to the choroid (Léveillard et al., 2019; Strauss, 2005).

Photoreceptors require energy to function and therefore glucose and nutrients are transported to the photoreceptors by the RPE (Strauss, 2005). However, the RPE must minimize its own glucose consumption to ensure enough glucose for the photoreceptors and other retinal cells. Photoreceptors can convert glucose into lactate, which suppresses glycolysis in the RPE. (Hurley, 2021) Glucose is actively transported by glucose transporters, which are located both in the apical and the basolateral membranes (Ban & Rizzolo, 2000). The malate-succinate shuttle has been revealed to be an important factor in the RPE metabolism. Succinate is produced in the retina, from where it is imported into the RPE to be oxidized. Succinate is an excellent fuel for the RPE since it increases the consumption of O_2 to H_2O threefold compared to glucose. RPE modifies succinate to malate, which is transported back to the retina where through the reverse succinate dehydrogenase reaction it is converted to fumarate to accept electrons. Thus, the malate-succinate shuttle transfers reducing power from the low O_2 retinal environment to the rich O_2 RPE environment. (Bisbach et al., 2020)

2.1.2 Phagocytosis

RPE cells are responsible for maintaining the welfare of photoreceptors with the circadian-regulated phagocytosis of photoreceptor outer segments (POS) (Strauss, 2005; Young & Bok, 1969). Photoreceptors renew 10% of their outer segments daily in interaction with RPE cells that digest and phagocytose the aged segments (Lakkaraju et al., 2020; Mazzoni et al., 2014). Typically in mammals, phagocytosis is initiated at light onset for rods and light offset for cones (Laurent et al., 2017; Young, 1978). POS interact closely with surrounding microvilli in the apical membrane of RPE cells (Wimmers et al., 2007). Phagocytosis is tightly regulated between the RPE and photoreceptors, and malfunction in this process can lead to the uncontrolled lengthening or shortening of POS (Strauss, 2005). One RPE cell is responsible, on average, for phagocytosing POS from 23 photoreceptors, and the entire outer segments are renewed every 11 days (Wimmers et al., 2007). POS are exposed to high levels of light, radicals, photo-damaged proteins, and lipids, which initiate accumulation in the POS, and the highest concentration of these radicals can be observed in the outermost POS tips. The tips are detached and new POSs are formed at the base of the outer segments so that the length of the POS stays constant. (Strauss, 2005)

Phagocytosis contains three phases: binding, internalization, and degradation. Specific RPE receptors in the apical membrane recognize POS, after which POS are bound to the apical membrane. The internalization phase transfers the bound POS to the intracellular space of the RPE. Phagocytosis is regulated and controlled with specific proteins by the RPE. CD36, Mer tyrosine kinase (MerTK), and αvβ5 integrin are responsible for the regulation of the phagocytosis. While αvβ5 integrin is required for the binding of POS, MerTK initiates the internalization of POS and CD36 regulates the rate of POS internalization. (Finnemann & Nandrot, 2006; Lakkaraju et al., 2020; Mazzoni et al., 2014) After internalization, POS migrates to the basolateral regions of the RPE, where it unites with lysosome, forming a phagolysosome (Lakkaraju et al., 2020; Mazzoni et al., 2014). Lack of MerTK expression does not affect the binding of POS but the RPE is unable to digest the bound POS (Chaitin & Hall, 1983; Schreiter et al., 2020). MerTK and αvβ5 integrin interact with each other since αvβ5 integrin plays a role not only in the binding of POS but also in the activation of MerTK (Finnemann, 2003).

Phagocytic capacity can be studied *in vitro* with isolated POS particles typically of porcine or bovine origin (Mazzoni et al., 2014). However, the measurement methodology used is known to affect the results of phagocytosis making the

comparison between different studies difficult (Vargas & Finnemann, 2022). In addition, phagocytosis occurs in the mammalian eye with a diurnal rhythm; therefore the *in vitro* studies differ from natural phagocytosis since the POS are added *in vitro* typically in single pulses with high concentration (Mazzoni et al., 2014).

2.1.3 Secretion and immune modulation

RPE produces and secretes various growth factors, such as vascular endothelial growth factor (VEGF) and pigment epithelium-derived factor (PEDF), to support the photoreceptors and choriocapillaris (Strauss, 2005). VEGF and PEDF are secreted in a polarized manner with the pronounced apical secretion of PEDF, whereas the VEGF is primarily secreted basolaterally (Becerra et al., 2004; Maminishkis et al., 2006). The role of PEDF is to inhibit endothelial proliferation and to stabilize the structure of the retina and choriocapillaris (Strauss, 2005), while VEGF prevents endothelial cell apoptosis and acts as a stabilizer of the endothelium fenestrations (Dawson et al., 1999). In addition, the secretion of VEGF is essential for the formation and maintenance of the intact endothelium of the choriocapillaris (Strauss, 2005).

RPE is known to participate in ocular immunity to secure the immune privilege of the eye (Strauss, 2005; Streilein et al., 2002). It is involved in both innate and adaptive immunity by secreting immune components such as cytokines and chemokines (Detrick & Hooks, 2020). To protect the eye in inflammatory conditions, the RPE is the main source of complement activators and inhibitors at the retina-choroid interface and subretinal space, thus indicating RPE involvement in immunological defence. (Sugita et al., 2018) For immune suppression, RPE cells express a variety of receptors to secrete immunoregulatory factors, for example, to suppress the activation of T-cells (Sugita et al., 2009, 2018).

2.1.4 Visual cycle

The visual cycle is one of the most crucial integrative functions of the RPE and the retina that ensures photoreceptor light sensitivity. The process requires close interaction between the photoreceptors and RPE cells. During light exposure, light is absorbed in the photoreceptors by rhodopsin molecules, which are composed of opsin protein and retinaldehyde chromophore. Light causes a *cis-trans* conformation to the retinaldehyde chromophore, and for retained light sensitivity the all-*trans*-

retinal needs to be converted back to 11-*cis*-retinal. However, photoreceptors lack the *cis-trans* isomerase function that is needed for this conversion. The reisomerization of all-*trans*-retinal into light-sensitive 11-*cis*-retinal (stored form, 11-*cis*-retinol, also known as vitamin A) is provided by the RPE. The 11-*cis*-retinal is then transferred back to the photoreceptors and combined with opsin. (Goldstein, 1970; Strauss, 2005; Xue et al., 2015).

The two key proteins in the RPE cells that participate in the visual cycle are retinal pigment epithelium-specific protein 65 kDa (RPE65) and cellular retinaldehyde-binding protein (CRALBP). RPE65 regenerates all-*trans*-retinal into its photoactive form, 11-*cis*-retinal. (Redmond. et al., 1998; Simó et al., 2010; Strauss, 2005) CRALBP, on the other hand, participates in the retinoid metabolism with a high affinity to bind 11-*cis*-retinol and 11-*cis*-retinal. The precise function of the CRALBP is still unknown, although it has been shown that reisomerization of retinaldehyde was impaired in the absence of CRALBP. (Saari et al., 2001; Xue et al., 2015)

2.1.5 Other functions of the RPE

RPE cells are highly pigmented, and therefore they have the capability to absorb scattered light and protect the retina against photo-oxidation. Melanin is the main factor responsible for light absorption. (Strauss, 2005) Pigment granules are formed from melanosomes, which contain high amounts of melanin. Pigmentation can be observed as the dark colour of the RPE cells. Melanin concentration decreases with age due to high levels of light exposure and oxidative stress. Melanin cannot be reproduced, therefore the loss of melanin indicates ocular senescence. (Shu et al., 2017) Melanin is formed during embryogenesis, whereas during life, RPE cells tend to accumulate another pigment called lipofuscin, which consists mostly of indigestible waste products (Juel et al., 2013). At first, lipofuscin is beneficial for light absorption but as the accumulation continues, the high amount of lipofuscin starts to become toxic to RPE cells (Strauss, 2005).

RPE cells contain a variety of different ion channels. Similar to cells in general, RPE cells keep intracellular calcium (Ca^{2+}), sodium (Na^{+}), and chloride (Cl^{-}) concentrations lower compared to the extracellular space. For K^{+}, the concentration gradient is the opposite. RPE cells express Cl^{-} channels whose one function is to enable the transport of water from the subretinal space to the bloodstream. The subretinal space contains water from the metabolic processes and also from the vitreous humour due to an intraocular pressure. This osmotic transport occurs

together with the transportation of Cl^- and K^+. (Wimmers et al., 2007) K^+ channels are known to participate in several RPE functions, including phagocytosis (Müller et al., 2014) and VEGF and PEDF secretions (Mamaeva et al., 2021) but also in the protection of the RPE against oxidative stress (Huang et al., 2018). The relevance of Na^+ homeostasis in normal RPE function is known, although the identification of Na^+ channels is still partly unclear (Johansson et al., 2019; Wimmers et al., 2007). RPE cells express epithelial Na^+ channels and voltage-gated Na^+ channels (Johansson et al., 2019; Wimmers et al., 2007) from which the voltage-gated Na^+ channels are shown to be a part of the regulatory machine of POS phagocytosis (Johansson et al., 2019). The Ca^{2+} channels expressed in the RPE are described in Chapter 2.2.

2.1.6 Oxidative stress in the RPE

RPE cells are exposed to chronic oxidative stress due to their metabolically active role and the daily absorption of scattered light. Oxygen consumption increases during light exposure, which leads to the formation of reactive oxygen species (ROS) in the RPE at a high rate (Upadhyay et al., 2020). ROS are produced in the mitochondria even under normal conditions in high amounts, thereby forcing RPE cells to adapt to the oxidative conditions (Bellezza, 2018; Datta et al., 2017). The production of ROS is essential for normal cellular functions, such as redox signalling. However, over-production of ROS is harmful and even fatal for the RPE cells. During ageing, mitochondria-derived ROS increases. (Datta et al., 2017) Thus, RPE cells must tolerate oxidative stress and protect themselves and the whole retina from the over-production of ROS. The RPE has a method to overcome the intracellular overload of ROS and pathogens through autophagy. As oxidative stress increases in the RPE cells, the level of autophagy increases as well, although the efficiency of autophagy decreases during ageing. (Hyttinen et al., 2011; Kaarniranta et al., 2010)

Since mitochondria are highly active in RPE cells, the number of malfunctioning mitochondria increases during the lifetime. Cells have a unique way to dismantle damaged mitochondria in a process called mitophagy. If this function is impaired, redundant and non-functional cellular elements increase which is sufficient to initiate the degeneration of the RPE. (Bellezza, 2018; Hyttinen et al., 2018)

Like most cell types, RPE cells have developed mechanisms to protect themselves from oxidative damage. The antioxidant defence is composed of multiple enzymes such as catalase and SODs and non-enzymatic molecules such as vitamin E and β-

carotene. (Bellezza, 2018; Miranda & Romero, 2019) Transcription factor Nrf2 plays a key role in the regulation of enzymatic antioxidant defence in RPE (Bellezza, 2018; Bellezza et al., 2018). Normally, Nrf2 is bound to its inhibitor Kelch ECH-associated protein 1 (Keap1) which maintains the level of Nrf2 relatively low. Over-produced ROS disrupts the interaction between Keap1 and Nrf2. Antioxidant responses initiate as Nrf2 is translocated to nucleus where it binds to antioxidant response element sequences leading to the activation of its target genes such as glutamate cysteine ligase modifier subunit, NAD(P)H:quinone oxidoreductase, glutathione S-transferase and thioredoxin. (Bellezza, 2018; Bellezza et al., 2018; Sachdeva et al., 2014)

2.1.7 Development and early maturation of RPE cells

The RPE and the neural retina derive from the neuroepithelium tissue. A patch of cells forms the eye field, from which, with specific and tightly regulated signals and interactions, the differentiation of the RPE and retinal cells is initiated. Initially, an optic vesicle and eventually an optic cup with inner and outer layers are formed. The inner layer of the optic cup is responsible for the formation of the neural retina, while the outer layer of the optic cup forms the RPE. (Bowes Rickman et al., 2016) The first visible signs of RPE development are the formation of distinguishable pigmentation and the cuboidal morphology of the cells. Further development of the RPE requires interactions with extraocular mesenchyme, which controls the process with specific signalling molecules such as transforming growth factor-beta. (George et al., 2021) Wnt signalling is mediated by β-catenin and its direct targets are transcription factors related to the differentiation of RPE cells such as microphthalmia-associated transcription factor (Mitf), paired box protein-6 (Pax6) and orthodenticle homolog 2 (Otx2). On the other hand, activation of Wnt signalling in mature RPE leads to a deformation of epithelial morphogenesis and induces an epithelial-mesenchymal transition (EMT). Mitf, Pax6 and Otx2 are considered as three key transcription factors in the RPE development. Pax6 is referred to as a master regulator since it is essential for the whole ocular development (Gehring, 1996). Otx2, on the other hand, is essential in the embryogenesis where it is required for the specification of the RPE after the formation of the optic vesicle (Beby & Lamonerie, 2013). Mitf transactivates genes such as tyrosinase for terminal pigment differentiation and malfunctions in Mitf would lead to defects in the RPE development (Bharti et al., 2012), pigmentation and also hyperproliferative RPE (Ma

et al., 2019; Nguyen & Arnheiter, 2000; Ramón Martínez-Morales et al., 2004). Besides Mitf, also Pax6 and Otx2 are known to participate in pigmentation and melanogenesis of RPE by binding and transactivating their target genes such as tyrosinase (Cavodeassi & Bovolenta, 2014; Ramón Martínez-Morales et al., 2004).

Tissue development in the human body is tightly controlled by multiple different factors, including primary cilia, which are sensory organelles found in nearly all human cell types. Primary cilia are referred to as the antenna of the cell as they are located on the apical membrane to face the extracellular space to sense and transduce extracellular signals. (May-Simera et al., 2018; Sun et al., 2021) The primary cilium is a nonmotile and interestingly only one primary cilium exists per cell with a 9+0 microtubule structure. The base of the primary cilium (known as the basal body) is docked in the cytoplasmic site under the apical membrane. (Wheway et al., 2018) Pericentrin (PCNT), which is an integral component of the basal body, serves as the anchoring for multiple proteins (Delaval & Doxsey, 2010). The primary cilium membrane is a continuum of the cell membrane, although a transition zone separates the membranes from each other so that the membranes have, for example, their own protein compositions (Wheway et al., 2018). The primary cilium has been shown to be an important factor during RPE development and maturation, but, RPE cells also require a functional primary cilium to polarize properly (May-Simera et al., 2018). The primary cilium is disassembled upon maturation in some cell types, like corneal epithelial cells, but in the case of the RPE, the disassembly is yet to be studied (Blitzer et al., 2011). Defects in generation of primary cilium (ciliogenesis) lead to incomplete RPE maturation with incomplete functionality where RPE-specific gene expressions are reduced and the morphology of the apical microvilli is deformed (May-Simera et al., 2018).

Retinoic acid, a derivative of vitamin A, is synthesized in multiple sites in the developing eye; it contributes to the retinal development and the maintenance of the developed RPE cells (Compochioro et al., 1991; George et al., 2021). Once the RPE cells are developed as an individual monolayer of cells, the maturation of the cells is initiated. The interphotoreceptor layer is formed between the RPE and retina and it is involved in the maturation of RPE cells. The RPE starts to gain a polarized cell structure simultaneously with the development of BM. Apical microvilli start to emerge with elongation due to apical microvilli protein ezrin and junctional tightness is initiated to finalize the apical-basal polarization. At first, the tight junctions are relatively leaky, but during the maturation of RPE, the expression of tight junctional proteins such as ZO-1 and CL-19 develops to ensure the tightness of the junctions. (George et al., 2021)

2.1.8 Bruch's membrane

BM resides strategically between the RPE monolayer and the choroid. Its main functions are to provide structural support for the RPE and to control the exchange of biomolecules between the retina and blood circulation. BM is prone to modifications. Especially ageing and some retinal diseases can alter and modify the structure of BM, which could lead to the loss of its supportive function. (Gullapalli et al., 2005; Saari et al., 2001) BM is a multilayered membrane that is highly concentrated with specific extracellular matrix (ECM) proteins. It is composed of five different protein layers, and the layer underneath the RPE cells is called the basement membrane of the RPE. This layer is rich in proteins like collagen IV (Col-IV), laminin (LN) and nidogen-1 (Nid-1). All the proteins have their unique role in the architecture of the membrane. (Curcio & Johnson, 2013) LNs are responsible for the attachment of the RPE cells to BM through interactions with integrins; Col-IV gives the elasticity to BM; and Nid-1 acts as a crosslinker between the LN and Col-IV, thus forming a protein network (Curcio & Johnson, 2013; May, 2012). LNs are cell-adhesive glycoproteins made from three distinct polypeptide chains with a binding site for integrins (Hohenester, 2019). LNs play a vital role together with Col-IV to provide the structural stability of BM. Nid-1 links LN and Col-IV together, which enhances the stability even further. (Jayadev & Sherwood, 2017; Yurchenco, 2011) Nid-1 consists of three subdomains from which the G2 domain fuses with Col-IV while the G3 domain binds to LN (Yurchenco, 2011).

2.2 Ca^{2+} signalling in RPE

Ca^{2+} signalling is one of the most prominent ways for the cell to affect the functionality of cellular proteins (Berridge et al., 2003; Wimmers et al., 2007). It contributes to nearly all cell functions, starting from fertilization all the way to apoptosis. Dysfunctions in Ca^{2+} signalling are linked to various diseases such as tumorigenesis (Berridge et al., 2000), and some retinal degenerative diseases such as Best Disease (Singh et al., 2013). Ca^{2+} signalling must therefore be tightly controlled and regulated. (Berridge et al., 2003) In RPE cells, Ca^{2+} signalling is known to be involved in cell functions including phagocytosis (Mamaeva et al., 2021; Müller et al., 2014; Wimmers et al., 2007), secretion of VEGF (Mamaeva et al., 2021; Rosenthal et al., 2007; Strauss, 2005; Wimmers et al., 2007, 2008), transepithelial transport of

ions and water (Wimmers et al., 2007), and apoptosis (D. Yang et al., 2011) (Table 1).

Ca^{2+} ions have a high affinity to binding the cellular proteins by acting as a second messenger. Protein conformation and function are changed due to the binding of Ca^{2+}. Basically, Ca^{2+} can initiate an intracellular response either by binding to a protein or by detaching from the protein. (Berridge et al., 2003; Wimmers et al., 2007) Ca^{2+}-mediated signalling is regulated by Ca^{2+}-sensing proteins such as calmodulin which is activated after the binding of Ca^{2+}. Once bound, calmodulin goes through conformational changes which enables it to modify the interactions with its target proteins and activate Ca^{2+}-sensitive cellular processes. (Berridge et al., 2003; Chin & Means, 2000). Interestingly, the speed of Ca^{2+} signalling from the stimulus to the cellular response varies from microseconds even to hours, depending on the cell function. The most crucial factor in Ca^{2+} signalling is controlling the free intracellular Ca^{2+} concentration ($[Ca^{2+}]_i$), which is usually around 100 nM. (Berridge et al., 2003) This low concentration is maintained by actively pumping Ca^{2+} into the extracellular space and cytoplasmic Ca^{2+} stores using Ca^{2+} pumps and Ca^{2+} exchangers (Berridge et al., 2003; Wimmers et al., 2007). Thus, Ca^{2+} signalling can be divided into two phases: 1) maintaining low $[Ca^{2+}]_i$ and 2) increasing cytoplasmic $[Ca^{2+}]_i$ by releasing Ca^{2+} from the intracellular stores and/or the extracellular space. However, Ca^{2+}-binding proteins exist in the cytoplasm, thus all the released Ca^{2+} will not end up as free intracellular Ca^{2+}. These proteins with a high affinity to Ca^{2+} are involved in the fine-tuning of the spatial and temporal properties of Ca^{2+} signalling. (Berridge et al., 2003) In the RPE, the intracellular Ca^{2+} stores are in the endoplasmic reticulum (ER), mitochondria, and especially in the melanosomes. (Berridge et al., 2000; Boulton, 1991; Salceda & Sánchez-Chávez, 2000; Strauß, 2013) The storage of Ca^{2+} consumes energy, which is produced during ATP hydrolysis (Clapham, 2007).

Ca^{2+} signals occur on multiple time scales, yet even short spikes can initiate a cellular response. Occasionally, multiple repeated spikes with proper frequencies are necessary to trigger a response. Ca^{2+} signalling occurs in response to different stimuli but also spontaneous $[Ca^{2+}]_i$ increases are common. (Berridge et al., 2000) Both of these signalling types are present in the RPE (Abu Khamidakh et al., 2016). Ca^{2+} signalling in the RPE can be studied *in vitro* by observing the changes in the $[Ca^{2+}]_i$ using fluorescent dyes (Abu Khamidakh et al., 2016; Sorvari et al., 2019; Stalmans & Himpens, 1997).

Table 1. Summary of Ca^{2+} channels participating in RPE functions. Factors that influence the functioning of the channels are named, if known.

RPE function	Ca^{2+} channels	Influencing factor	Ref
VEGF secretion	$Ca_V1.1$	n/a	(Mamaeva et al., 2021; Rosenthal et al., 2007)
	$Ca_V1.3$	Best-1, bFGF, TKs	
	$Ca_V3.1$, $Ca_V3.3$	n/a	(Mamaeva et al., 2021)
	TRPV	n/a	(Cordeiro et al., 2010)
PEDF secretion	$Ca_V1.1$	n/a	(Mamaeva et al., 2021)
	$Ca_V1.3$	Best-1, bFGF, TKs	
Phagocytosis	$Ca_V1.1$	n/a	(Mamaeva et al., 2021; Müller et al., 2014)
	$Ca_V1.3$	Best-1, bFGF, TKs	
	$Ca_V3.1$, $Ca_V3.3$	n/a	(Mamaeva et al., 2021)
	TRPV	n/a	(Kennedy et al., 2010; Müller et al., 2014)
Transepithelial transport	P_2Y	Extracellular ATP	(Peterson et al., 1997)
Apoptosis	P_2X	Extracellular ATP	(D. Yang et al., 2011)

2.2.1 ATP-mediated Ca^{2+} signalling in RPE cells

Small molecules like ATP can initiate a Ca^{2+} signalling cascade that leads to changes in the intracellular Ca^{2+} concentration. ATP-mediated Ca^{2+} signalling is largely involved in the RPE physiology, and it can be divided into paracrine signalling and autocrine signalling. (Wimmers et al., 2007) ATP in the subretinal space can be light-induced (paracrine signalling) or ATP can be released from the RPE cells (autocrine signalling) (Mitchell, 2001; Peterson et al., 1997). ATP initiates Ca^{2+} signalling by binding to purinergic receptors (P_2Y and P_2X) in the apical membrane of the RPE cells (Figure 2) (Wimmers et al., 2007). P_2Y is a G protein-coupled receptor, whereas P_2X is a ligand-activated channel (North, 2002), and both exist in the RPE (Peterson et al., 1997; Sullivan et al., 1997; D. Yang et al., 2011). P_2Y and P_2X are connected to various RPE functions, and the malfunction of these receptors can contribute to the formation of age-related macular degeneration (AMD) (Peterson et al., 1997; D. Yang et al., 2011).

Activation of G-protein coupled P_2Y_2 by ATP leads to the activation of phospholipase C (PLC). At the cell membrane, PLC hydrolyses phosphatidylinositol 4,5-bisphosphate (PIP2) to inositol-1,4,5-trisphosphate (IP3) and diacylglycerol. (Berridge et al., 2003; Lemon et al., 2003) Ca^{2+} is then released from the intracellular stores to the cytoplasm after the IP3 interacts with its receptor, IP3R in the ER membrane. However, IP3R is a Ca^{2+} sensitive receptor and the increased $[Ca^{2+}]_i$ inhibits IP3R and prevents the release of Ca^{2+} from the ER. (Berridge et al., 2003)

Altogether, this cascade requires the interactions of ATP, P_2Y_2, PLC, PIP2, IP3 and IP3R will lead to the increase of $[Ca^{2+}]_i$.

As RPE cells are connected to adjacent cells via gap junctions, cell-cell communication can occur through these junctions. Therefore, Ca^{2+} signals are able to spread between the adjacent cells to influence even the whole monolayer (Abu Khamidakh et al., 2013; Himpens et al., 1999; Stalmans & Himpens, 1997; Wimmers et al., 2007). Ca^{2+} signalling has not been studied in hPSC-RPE extensively, and much is still unknown about its function and pathways (Abu Khamidakh et al., 2016; Miyagishima et al., 2016; Singh et al., 2013; Sorvari et al., 2019).

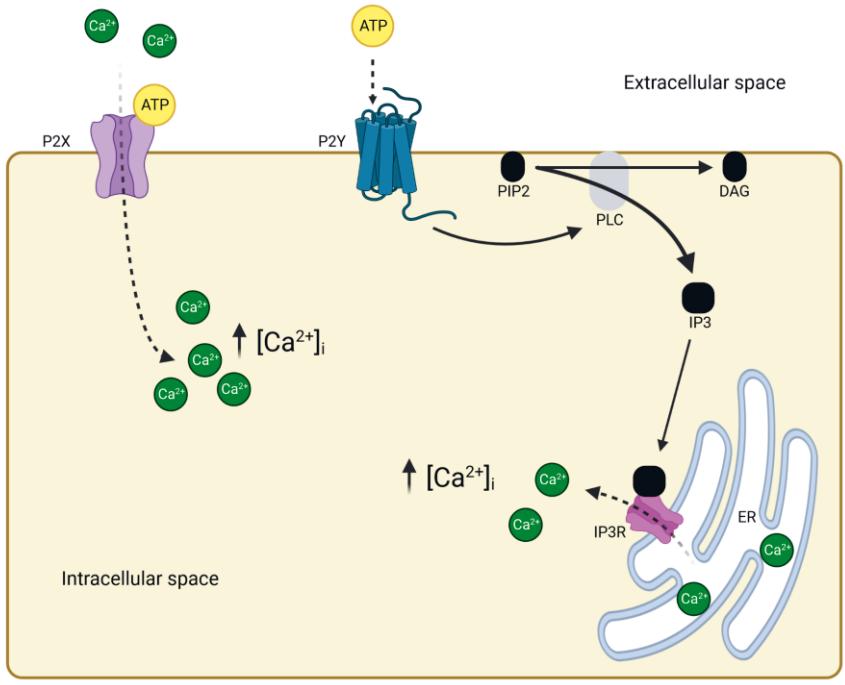

Figure 2. Schematic illustration of the ATP-mediated Ca^{2+} signalling. ATP: adenosine triphosphate, DAG: diacylglycerol, PLC: phospholipase C, PIP2: phosphatidylinositol 4,5-bisphosphate, IP3: inositol-1,4,5-trisphosphate, IP3R: inositol-1,4,5-trisphosphate receptor, ER: endoplasmic reticulum, $[Ca^{2+}]_i$: free intracellular Ca^{2+}. Figure created with BioRender.com.

2.2.2 Ca^{2+} channels in the RPE

The correct physiology of RPE cells is largely dependent on the proper function and activity of ion channels in the apical and basal cell membranes of the RPE. A set of different voltage- and ligand-dependent Ca^{2+}, K^+, Na^+, and Cl^- channels are expressed in RPE cells. One of the highly important ion channel types in RPE cells are the Ca^{2+} channels, which contribute to most of the functions of the RPE. Ca^{2+} channels participate in Ca^{2+} signalling by providing a route for Ca^{2+} ions into the cytoplasm from the extracellular space. (Wimmers et al., 2007)

As described previously, Ca^{2+} acts as a second messenger intracellularly, and to act properly, its concentration must be altered very quickly. Within a stimulus from the intracellular or extracellular space, Ca^{2+} is actively transported to the cytoplasm. (Strauß, 2013; Wimmers et al., 2007) The most rapid way for the cell to change the $[Ca^{2+}]_i$ is via the Ca^{2+} channels, especially voltage-gated Ca^{2+} channels that can change the Ca^{2+} levels within milliseconds (Clapham, 2007). Voltage-gated L-type Ca^{2+} (Ca_V) channel subtypes $Ca_V1.1$- $Ca_V1.3$ and T-type channels $Ca_V3.1$ and $Ca_V3.3$ have been shown to be expressed in cultured ARPE-19 cells (spontaneously immortalized human ARPE-19 line) (Wimmers et al., 2008) of which $Ca_V1.3$ is the main subtype in RPE cells (Müller et al., 2014; Rosenthal et al., 2007; Wimmers et al., 2008; Wollmann et al., 2006). Opening upon cell membrane depolarization, these Ca_V channels enable the transfer of Ca^{2+} from the extracellular space to the cytoplasm down the electrochemical gradient (Wimmers et al., 2007). L-type Ca^{2+} channels have been shown to participate in several RPE functions, including the secretion of VEGF (Rosenthal et al., 2007) and phagocytosis (Karl et al., 2008; Mamaeva et al., 2021; Müller et al., 2014). For example, the rate of the VEGF secretion is dependent on the activation of L-type Ca^{2+} channels which is regulated by cytosolic tyrosine kinases (Rosenthal et al., 2007). Therefore, it is not surprising that defects in Ca^{2+} signalling have been shown to be related in the pathogenesis of certain retinal diseases (Mergler et al., 1998). For example, the increased activity of L-type Ca^{2+} channels can lead to the over-secretion of VEGF, which can lead to choroidal neovascularization and eventually to the formation of retinal degenerative diseases such as AMD (Strauss, 2005).

The functions of Ca^{2+} and certain K^+ channels are coupled since an increase in intracellular Ca^{2+} concentration can activate Ca^{2+}-activated K^+ channels and lead to membrane hyperpolarization. On the other hand, voltage-gated K^+ channels limit the activation of L-type Ca^{2+} channels through their hyperpolarizing effect, thus preventing the overload of Ca^{2+} in the intracellular space. This supports the rapid

change in intracellular Ca^{2+} homeostasis. (Strauss, 2005; Wimmers et al., 2007) In addition, transport molecules such as Na^{+}/Ca^{2+} exchanger control the intracellular Ca^{2+} concentration by eliminating Ca^{2+} from the cytoplasm (Wimmers et al., 2007).

The functionality of Ca^{2+} channels can be studied *in vitro* with the patch-clamp technique. In a whole cell configuration, it measures the Ca^{2+} currents across the RPE cell membrane simultaneously from all active channels. In patch clamp recordings, the different channel types can be analysed by varying measurement protocols and using channel-specific pharmacological modulators. (Reichhart & Strauß, 2014)

2.3 Pathophysiology of RPE

The dysfunction of RPE cells have been linked to the retinal degenerative diseases, such as retinitis pigmentosa, AMD, and Stargardt disease. The causes of the retinal diseases vary depending on the disease type. Some forms are inherited, whereas some are multifactorial. (S. Yang et al., 2021) Of all these retinal diseases, AMD is the most common, affecting millions of people worldwide. Currently, no curative therapy is available for AMD, although wet AMD can be managed using monthly anti-VEGF injections (Fabre et al., 2022; S. Yang et al., 2021).

2.3.1 Age-related macular degeneration

As the RPE is responsible for multiple physiological tasks and its proper functionality is crucial for the welfare of the whole retina, any malfunctions of the RPE can be fatal for vision. AMD is the leading cause of vision impairment or loss in developed countries (Resnikoff et al., 2004). AMD affects the macular area which is responsible for the sharp vision and colour sensation in daylight conditions (Dehghan et al., 2022). AMD does not in its early stage cause total blindness since the RPE damage occurs in the macula and thus peripheral vision is retained. A consequence of the loss of the RPE is the loss of photoreceptors, which eventually can spread to the peripheral area and lead to total blindness. (Dehghan et al., 2022) AMD can be categorized as dry AMD and wet AMD (Higuchi et al., 2017). The dry form is the most common one (approximately 90% of all the cases), and it progresses slowly in the area of central vision (Jager et al., 2008). In the wet form of AMD, the

most severe symptom is a growth of new blood vessels in the subretinal space (Dehghan et al., 2022).

AMD is a multifactorial disease, although the most common unifying factor among patients is age. In addition, other risk factors such as smoking, genetics, and even family history can affect the formation of AMD. (Ambati et al., 2003; Datta et al., 2017; Dehghan et al., 2022). It is well known that the RPE and its degeneration plays a crucial role in the development of AMD, but also BM and the choroid are involved in AMD pathogenesis (Farazdaghi & Ebrahimi, 2019). One of the main symptoms and also a requirement for the diagnosis of AMD is the formation of drusen (lipid and protein aggregates) between the RPE and BM and also inside BM in dry AMD. Choroidal neovascularization is a symptom in the wet form of the AMD and also the most severe symptom since it can lead to intraocular bleeding and eventually to the loss of vision. (Strauss, 2005) However, intravitreal anti-VEGF injections are used to treat the wet AMD which prevents the uncontrolled bleeding and leaking from the blood vessels (Fabre et al., 2022; Kaiser et al., 2021; Modi et al., 2015; Schmidt-Erfurth et al., 2014).

Immunological aspects like inflammation have been noted in AMD studies as one of the leading causes of AMD (Ambati et al., 2013; de Jong et al., 2023; Hollyfield et al., 2008; Kauppinen et al., 2016). Damaged cells use inflammation as a sign of foreign or damaged material, but as the inflammation continues to be chronic, various diseases are initiated, such as retinal degenerative diseases (Kauppinen et al., 2016). Overactivation of immune responses is suggested to be related to AMD pathogenesis (Ambati et al., 2013). Certain pro-inflammatory cytokines like interleukin-6 (IL6), interleukin-8 (IL8), and tumour necrosis factor-α are observed in AMD patients and are therefore considered as markers for AMD (Knickelbein et al., 2015). The role of cytokines is to activate and attract leukocytes to the inflamed site (Kauppinen et al., 2016).

As drusen contain multiple inflammatory proteins like cytokines, local inflammation could increase and cause retinal stress reactions (Hageman et al., 2001; Kauppinen et al., 2016). As mentioned previously, RPE and the whole retina are under constant exposure to oxidative stress from multiple sources, such as scattered light, lipofuscin, and a high metabolism, and all these lead to the generation of ROS. Oxidative stress can be studied *in vitro* with the use of oxidative chemicals such as hydrogen peroxide (H_2O_2). Treatment with H_2O_2 can result in the decreased expression of specific RPE proteins, such as the visual cycle proteins RPE65 and CRALBP (Alizadeh et al., 2001). The most severe effect of H_2O_2 treatment is the cellular death of the RPE (Juel et al., 2013), which together with the decreased

protein expressions indicate the possible role of oxidative stress in AMD. Even though the RPE cells have mechanisms to protect themself and the retina from oxidative stress, antioxidant defence is not capable of protecting the cells endlessly as ROS is produced in excessive amounts. (Bellezza, 2018; Datta et al., 2017)

One of the causes that leads to AMD is the loss of the RPE's capability to absorb light (Ambati et al., 2003). Even in normal conditions, the RPE must tolerate enormous amounts of oxygen radicals due to the phagocytosis and light exposure, and the malfunction in the degradation of the radicals enhances the increase in radicals even further. Oxygen radicals are accumulated in the POS and end up in the RPE during phagocytosis, and the RPE itself is exposed to high amounts of oxygen radicals due to high light energy exposure. In addition, the consequence of RPE loss is a higher number of photoreceptors per single RPE cell, which again causes a greater amount of accumulated oxygen radicals in the remaining RPE cells. Thus, phagocytosis might take part in the formation of AMD. (Strauss, 2005)

2.3.2 Treatments for AMD

Retinal degenerative diseases such as AMD form a group of diseases that affect millions of people worldwide. AMD affects mostly elderly people, and globally it is a major health issue. As the world population ages, the total global burden will increase, which could test healthcare systems to their limits. (Pascolini & Mariotti, 2012) Therefore, there is an urgent need for treatment for AMD, but no curative treatment is currently available, especially for the dry form of AMD (Higuchi et al., 2017). Several clinical trials are ongoing for dry AMD (Table 2), but for wet AMD, the stabilization of the disease progression can be achieved with current therapies (such as monthly anti-VEGF injections), although a curative treatment to restore vision is still missing (Dehghan et al., 2022; Higuchi et al., 2017). A potential treatment approach to dry AMD is based on hPSC-RPE cells, where healthy RPE cells are transplanted to replace the degenerated RPE cells as an intact sheet or as a suspension (Figure 3) (Maeda et al., 2021). To be effective, the transplantation should occur in the early stage of AMD, before the total loss of the RPE and the degeneration of the photoreceptors (Bennis et al., 2017). Sheet transplantation requires a surgical procedure, as the intact RPE monolayer is delivered and transplanted in the subretinal space (Dehghan et al., 2022). In addition, the sheet transplantation usually requires the use of biodegradable biomaterials as a carrier for the cells, whereas the suspension method uses a suspension of single RPE cells

(Sharma et al., 2020). The main requirements for the carrier are permeability and a surface that allows the RPE cells to adhere and proliferate on the substrate (Higuchi et al., 2017). The sheet transplantation method may be more suitable for the therapies since the suspension approach requires detaching the RPE cells from the culture substrate, and this leads to the loss of polarization of the RPE cells. In addition, detached RPE cells must adhere to the retina and possible dedifferentiation of the already differentiated RPE cells could occur. (Higuchi et al., 2017) However, sheet transplantation is more invasive, therefore the risk of surgical complications is higher compared to the suspension method, where the cells are injected with a thin needle (Maeda et al., 2021). The survival rate of the transplanted RPE cells is nevertheless higher after sheet transplantation when compared to suspension (Hsiung et al., 2015).

Table 2. Summary of ongoing clinical trials for dry AMD. Table modified from Guimaraes et al. (Guimaraes et al., 2022)

Treatment	Drug	Route of delivery	ClilinalTrials.gov identifier
Antioxidative	AREDS/2	Oral	NCT00000145, NCT00345176
	OT-551	Topical	NCT00306488
Reduction of toxic byproducts	GSK933776	IV	NCT01342926
	RN6G	IV	NCT01577381
Visual cycle modulators	ACU-4429	Oral	NCT01802866
	Fenretinide	Oral	NCT00429936
	C20-D3-vitamin-A	Oral	NCT03845582
Anti-inflammatory and complement inhibition	Eculizumab	IV	NCT00935883
	Lampalizumab	Intravitreal	NCT02247531 NCT02247479
	Sirolimus	Subconjuctival	NCT00766649
	Zimura	Intravitreal	NCT02686658
	Pegcetacoplan	Intravitreal	NCT02503332 NCT03525600 NCT03525613
	Tedisolimab	Intravitreal	NCT01527500
	Risuteganib	Intravitreal	NCT03626636
Neuroprotection	Ciliary nerve trophic factor	Intravitreal	NCT00063765 NCT00447954
	Brimonidine tartrate	Intravitreal	NCT00658619 NCT02087085
Gene therapy	AAVCAGsCD59	Intravitreal	NCT03144999
	GT005	Subretinal	NCT03846193
Mitochondrial enhancers	Elamipretide	Subcutaneous	NCT02848313 NCT03891875
Nanosecond laser therapy	2RT nanosecond laser	Retinal active laser therapy	NCT01790802

The most promising cell source for the stem cell therapies are hPSCs, and remarkably, clinical trials have already been initiated with hPSC-derived RPE cells

(Table 3) (Da Cruz et al., 2018; Kashani et al., 2018, 2021; Mandai et al., 2017; Schwartz et al., 2015, 2016; Song et al., 2015). The first clinical trials I/II have proved the safety of the hPSC-derived RPE cells in transplantation (Kashani et al., 2021; Mehat et al., 2018; Schwartz et al., 2015, 2016; Song et al., 2015) but also the efficacy of the treatment (Da Cruz et al., 2018; Kashani et al., 2021; Mehat et al., 2018; Schwartz et al., 2015, 2016; Song et al., 2015). However, behaviour and the proper functionality of the transplanted cells after the transplantation is still unknown.

In addition, adult or fetal donor RPE cells and human adipose-derived stem cells are under consideration for the therapies (Higuchi et al., 2017). The hPSCs are differentiated to RPE cells before transplantation, whereas adult or fetal stem cells are transplanted directly into the subretinal space without differentiation to RPE cells (Higuchi et al., 2017). The differentiation of the hPSC cells into RPE cells is relatively efficient, albeit time-consuming (Chapter 2.4) (Dehghan et al., 2022).

Table 3. Summary of ongoing clinical trials utilizing hPSC-RPEs for AMD.

Cell source	Dry/wet AMD	Cell delivery method	Phase of trial	ClinicalTrials.gov identifier	Ref
hESC-RPE	Advanced dry AMD	n/a	Phase I/II	NCT01674829	(Song et al., 2015)
hESC-RPE	Advanced dry AMD	Suspension	Phase I/II	NCT01344993	(Schwartz et al., 2012, 2015, 2016)
hESC-RPE	Advanced dry AMD	Suspension	Phase I/II	NCT02463344	(Schwartz et al., 2012, 2015, 2016)
hESC-RPE	Advanced dry AMD	Cells on parylene-C film	Phase I/II	NCT02590692	(Kashani et al., 2018, 2021)
hESC-RPE	Acute wet AMD	Cells on polyester membrane	Phase I	NCT01691261	(Da Cruz et al., 2018)
iPSC-RPE	Wet AMD	Sheet	n/a	n/a	(Mandai et al., 2017)

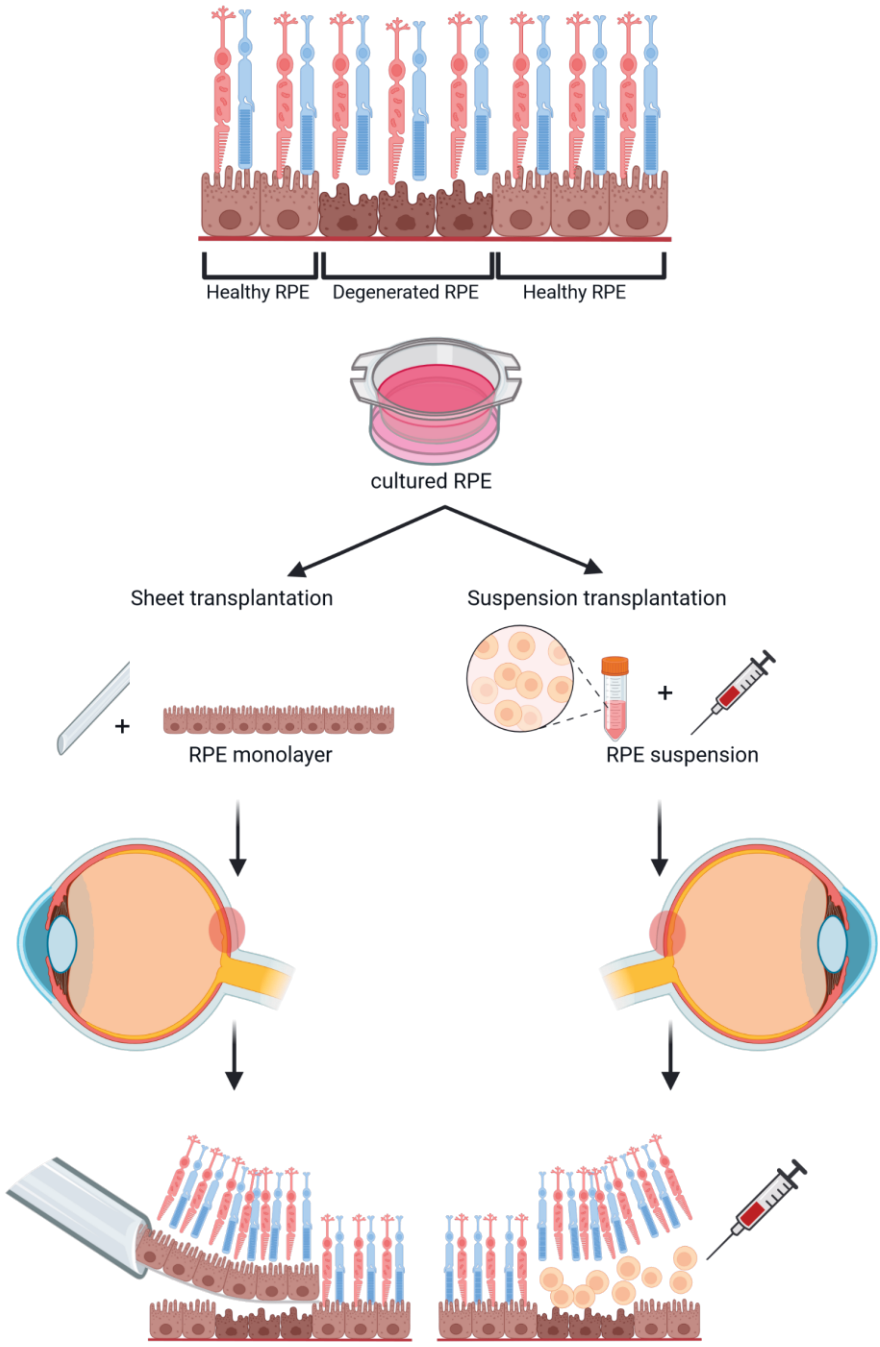

Figure 3. Schematic illustration of the two transplantation approaches. Figure created with BioRender.com.

2.4 Human pluripotent stem cell-derived RPE cells

2.4.1 *In vitro* differentiation and maturation of hPSC-RPE cells

RPE cells can be differentiated from ESCs and iPSCs (Figure 4). Stem cells have a unique ability to self-renew and differentiate into multiple different types of cells (Takahashi & Yamanaka, 2006). Thus, stem cells provide an unlimited source of RPE cells (Dehghan et al., 2022). The differentiation of stem cells into RPE cells can be conducted with two differentiation methods: spontaneous or directed differentiation (Choudhary et al., 2017; Geng et al., 2017; Pennington et al., 2015; Plaza Reyes et al., 2016; Reichman et al., 2017). In the spontaneous method, stem cells can freely differentiate into many cell types. However, this method is relatively inefficient (efficiency of ~1%) and requires multiple purification steps to obtain the pure RPE cells. (Leach et al., 2016; Sharma et al., 2020) An alternative and more efficient (efficiency up to ~80%) method to produce RPE cells is to add growth factors such as Noggin and Activin A and small molecules such as nicotinamide in the culture media that guides the stem cells to differentiate into the desired cell type. This method is called directed differentiation. (Buchholz et al., 2013; Dehghan et al., 2022; Leach et al., 2016; Sharma et al., 2020; Zahabi et al., 2012)

Human embryonic stem cell (hESC) lines are generated from surplus embryos from fertility treatments. The hESCs are then differentiated to hESC-RPE cells. The iPSC-RPE cells, on the other hand, can be obtained through the generation of iPSC cell lines from tissues such as skin or blood, after which the iPSC cell lines are differentiated to iPSC-RPE cells. (Dehghan et al., 2022) Our group and others have previously shown the successful differentiation of hESC-RPE cells (Dehghan et al., 2022; Hongisto, Ilmarinen, et al., 2017; Hongisto, Jylhä, et al., 2017; Vaajasaari et al., 2011). Recently, research aiming towards safer cell therapies, xenogeneic- and feeder free (FF) culture and differentiation of hPSCs are used to produce RPE cells (Choudhary et al., 2017; Geng et al., 2017; Hongisto, Ilmarinen, et al., 2017; McGill et al., 2017; Pennington et al., 2015; Plaza Reyes et al., 2016). Hongisto et al. showed that the FF-hESCs are not karyotypically as stable as the hESC cells produced with presence of the feeder cells, thus the safe window of FF-hESCs for usage is short (approximately 7.5 weeks compared to up to 100 weeks) (Hongisto, Ilmarinen, et al.,

2017). However, high efficiency was achieved compared to feeder-based method (efficiency approximately threefold higher). (Hongisto, Ilmarinen, et al., 2017)

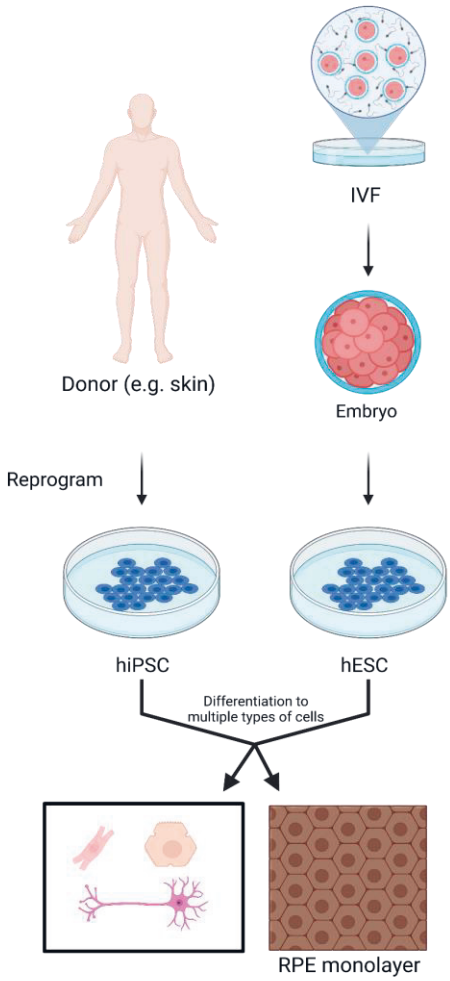

Figure 4. Basic concept of the cell differentiation from human pluripotent stem cells. IVF: *in vitro* fertilization. Figure created with BioRender.com.

Since RPE differentiation from hESCs is time-consuming, cryopreservation is urgently needed after the differentiation. This will decrease the waiting time of the transplanted cells in cell therapy (Hongisto, Ilmarinen, et al., 2017). In addition, RPE cells can be cultured only for a limited time before the cells start to lose their phenotype (Buchholz et al., 2009). After differentiation, the cells require time to mature and gain functions and characteristics specific to the RPE (Figure 5). The

outcome of the successful differentiation of stem cell-derived RPE cells is cells resembling their native counterparts regarding characteristics such as their proteome (Hongisto, Jylhä, et al., 2017), phagocytosis capacity (Hongisto, Ilmarinen, et al., 2017), barrier formation (A. Sorkio et al., 2014), secretion of VEGF (Skottman et al., 2017), and functional visual cycle (Maeda et al., 2013).

Pigmentation has been widely used as an indicator for mature RPE cells *in vitro*. However, Bennis et al. (Bennis et al., 2017) revealed that the pigmentation level does not reflect the expression level of specific RPE marker genes. In addition, they stated that appearance of pigmentation is rather an early maturation marker for RPE cells, and a higher pigmentation does not indicate a more mature monolayer. (Bennis et al., 2017)

As RPE cells mature in time *in vitro*, the polarized structure and expression of functionally important proteins are gained, and therefore functionality increases as well. It is still unclear whether the transplanted cells should be as mature as possible or if an early maturation level is more suitable in order for the transplantation to be successful.

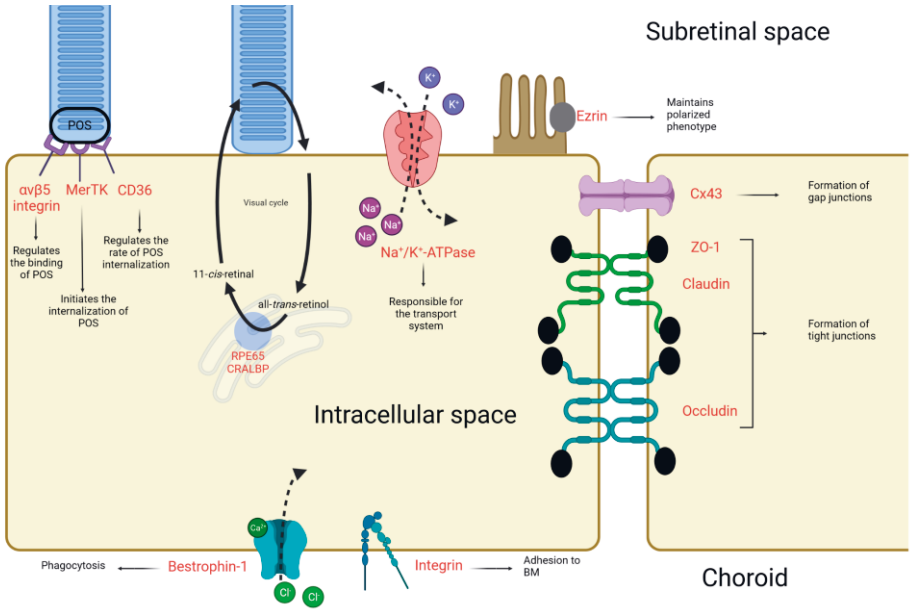

Figure 5. Illustration of RPE-related proteins and their localizations and functions. BM: Bruch's membrane, CRALBP: Cellular retinaldehyde-binding protein, Cx43: Connexin 43, MerTK: Mer tyrosine kinase, POS: photoreceptor outer segment, RPE65: Retinal pigment epithelium-specific protein 65 kDa, ZO-1: zonula occludens. Figure created with BioRender.com.

2.4.2 RPE culture substrates

The goal of the RPE cultures is to produce RPE cells that mimic native RPE cells. The growth conditions, such as the culture surface and culture media, are known to affect the maturity of the cultured RPE cells. RPE cells are cultured with a spectrum of different culture protocols that all support the maturation and functionality of RPE cells to varying degrees. (Fronk & Vargis, 2016)

Since RPE cells are polarized cells with two distinct cell membranes, the *in vitro* culture of RPE cells should support the polarized structure. When RPE cells are cultured on a porous surface, the polarized secretion of the RPE is enabled as the basolateral secretion occurs through the pores of the culture surface. A commonly used culture surface for the RPE cells is the porous polyethylene terephthalate (PET) insert, which is coated with different protein compositions to mimic BM (Da Cruz et al., 2018; Hongisto, Ilmarinen, et al., 2017). It has been shown that the protein coating used affects, for example, the structure and barrier properties of RPE cells (A. Sorkio et al., 2014). Commercially available protein mixes such as Matrigel and Synthemax II-SC (Pennington et al., 2015) are used to coat the culture substrate, although the use of Matrigel has limitations in clinical applications due to the animal-derived xenomaterial (Bharti et al., 2014; Rowland et al., 2013). Use of the commercially available protein mixes in the substrate coating is based on the resembling protein compositions compared to the ECM proteins (Guo et al., 2016; Weber et al., 2010). Purified or recombinant ECM proteins like Col-IV and LN can be used in the substrate coating individually or in combination. By mixing the purified ECM proteins, an environment more or less mimicking BM can be achieved. (Hongisto, Ilmarinen, et al., 2017; Rowland et al., 2013) However, the protein composition has a key role in the efficiency of RPE differentiation, maturation, cell structure, and functions (Rowland et al., 2013; A. Sorkio et al., 2014). For example, laminin supports the differentiation and maintenance of hESC to RPE since undifferentiated hESC cells express a variety of integrins which are known to have high affinity to laminin (Rowland et al., 2013).

2.4.3 Requirements for successful transplantation

For transplantation, the *in vitro* RPE cells must be well-characterized and the quality of the cells should be consistent. As mentioned earlier, cryopreservation of transplanted cells is essential. A requirement for the cryopreservation is that the cells must survive the cryopreservation and thawing, and they must start to mature rather

quickly after thawing. It is important to note that the cryopreservation should occur at the right time during the differentiation. (Zhang et al., 2022) The differentiation and maturation should be conducted in such an environment that is suitable for transplantation. A good manufacturing process (GMP) is required for the therapies, but the conditions should preferably be xeno-free (Higuchi et al., 2017; Pennington et al., 2015).

Since RPE cells have many crucial functions in the welfare of the retina, the transplanted RPE cells should also have the functionality of the same level compared to the native RPE cells. At the very least, they should gain the functions rapidly after the transplantation. Our group have previously shown that the cryopreserved hESC-RPE cells gain RPE characteristics during the culture (Hongisto, Ilmarinen, et al., 2017; Ilmarinen et al., 2019; A. Sorkio et al., 2014). The immunostainings of key RPE proteins and functional studies revealed the RPE cells to be functional after the cryopreservation (Hongisto, Ilmarinen, et al., 2017). However, the functional improvement during the culture is still unclear.

Since the suspension approach for the transplantation has been mostly unsuccessful so far, sheet transplantation may aid the survival or functionality of the transplanted cells, but it requires a carrier that can be transplanted together with the cells. The material requirements for the carrier are to be permeable to support the polarized structure of the transplanted cells and to be biocompatible causing no side effects such as rejection or toxicity reactions. (Da Cruz et al., 2018) In addition, the surgical procedure should be carried out by such a method that the retina or other parts of the eye are not damaged (G. S. W. Tan et al., 2021).

The cultured RPE cells may not fully mature compared to the native RPE cells and the influence of the maturation status of the transplanted hESC-RPE to the success of the transplantation could be one potential aspect to be studied.

3 AIMS OF THE STUDY

The study aimed to investigate the maturation of hESC-RPE cells *in vitro* with a focus on RPE functionality. The general hypothesis was that the culture conditions and duration influence the functionality of the hESC-RPE cells.

The specific aims of this study are outlined below:

1) To study the influence of basement membrane proteins on the molecular characteristics and functionality of hESC-RPE cells with specific focus on ATP-mediated Ca^{2+} signalling (**Study I**).

2) To investigate how the *in vitro* culture time of hESC-RPE cells affects their ability to tolerate cellular stress, i.e. maintain critical RPE functions, after treatment with chemicals leading to oxidative stress and proteasome impairment (**Study II**).

3) To analyse the presence of functional voltage-gated Ca^{2+} channels, especially $Ca_V1.3$, of hESC-RPE cells *in vitro* and to determine how the culture time of the RPE cells affects the expression and localization of this channel (**Study III**).

4 MATERIALS AND METHODS

4.1 Culture and differentiation of hESC cells into RPE cells

4.1.1 Culture of undifferentiated hESC cells

Four different hESC lines were used in the studies. All the lines - namely Regea 08/017 (46, XX) (**Studies I, II, III**), Regea 11/013 (46, XY) (**Studies I and III**), Regea 13/012 (46, XY) (**Study I**), and Regea 08/023 (**Study III**) - were derived and characterized as described previously (Skottman, 2010). The culturing of the hESC lines was carried out in the presence of feeder cells in **Studies I and III**, whereas a feeder-free hESC culture was used in **Study II**. The feeder-cultured cells were maintained in serum-free culture conditions with culture medium containing KnockOut™ Dulbecco's Modified Eagle Medium supplemented with 20% xeno-free KnockOut™ Serum Replacement (KO-SR), 2 mM Glutamax, 0.1 mM 2-mercaptoethanol, 1% non-essential amino acids, 50 U/ml penicillin-streptomycin (all from Thermo Fisher Scientific), and 8 mg/ml human basic fibroblast growth factor (bFGF, PreproTech Inc.) on inactivated human foreskin fibroblast feeder cells (CRL-2429TM American Type Culture Collection) (**Studies I and III**). The feeder-cultured undifferentiated stem cell colonies were enzymatically passaged with TrypLE Select (Thermo Fisher Scientific) onto a fresh feeder cell layer every 10 days. In the feeder-free culture, the hESC lines were cultured in Essential 8 Flex medium (Thermo Fisher Scientific) supplemented with 50 U/ml penicillin-streptomycin (**Study II**) on human recombinant laminin-521 (LN521, Biolamina) and passaged to culture plates coated with LN521 diluted in Ca^{2+}- and Mg^{2+}-containing 1x phosphate-buffered saline (Thermo Fisher Scientific) twice a week.

4.1.2 Differentiation of hESC cultures

The hESCs were spontaneously differentiated into RPE cells in one of two ways: in suspension from feeder-cultured hESCs (**Studies I and III**) or adherent from feeder

free -cultured hESCs (**Study II**) (Figure 6). In both methods, the colonies were dissociated with TrypLe Select and transferred to Corning™ Costar™ Low Attachment well plates (Sigma Aldrich) for differentiation. 5 μM blebbistatin (Sigma Aldrich) was used to induce embryoid body formation. The next day, blebbistatin was removed and replaced with culture media. In adherent differentiation method, after 4-6 days of suspension culturing, the embryoid bodies were plated on culture wells coated with LN521 and Col-IV (Sigma Aldrich) for further differentiation. The adherent differentiation in **Study II** was conducted in xeno-free conditions. In both methods, differentiation was performed in a feeder-hESC culture medium with a reduced (15%) KO-SR concentration and no bFGF. Pigmented areas began to form in both methods, and the areas were manually separated with a scalpel and dissociated with 1x Trypsin-EDTA/TrypLe Select. The cells were then seeded on Col-IV +/- LN521 for the enrichment of the RPE cells. After the differentiation, the RPE cells were cryopreserved, thawed, and seeded as described in each study.

4.1.3 Culture of differentiated hESC-RPE cells

After differentiation and cryopreservation, the hESC-RPE cells were thawed and seeded to mature. Depending on the assay, 1 μm PET culture inserts (Millipore or Sarstedt) or 48 well plates were used. The culture surfaces were dip-coated with RPE basement membrane proteins. In **Study I**, five different protein compositions were used: Col-IV alone, LN521 alone, and a combination of Col-IV and LN521 with or without the addition of Nid-1 (R&D Systems, 2570-ND) with the Nid-1 used at two different concentrations. In **Studies II and III**, a combination of Col-IV and LN521 was used. The specific details of the protocols are described in each study. Differentiated hESC-RPE cells were cultured and analysed at desired time points, depending on each study (summarized in Figure 7, Chapter 4.2).

In **Study II**, the differentiated hESC-RPE cells were exposed for 24 hours to cellular stress with two different chemical stressors, separately with 1 μM MG132 protease inhibitor (from now on referred to only as MG132, Calbiochem) and 600 μM H_2O_2 (Sigma Aldrich). The control cells received a fresh medium without the stressors.

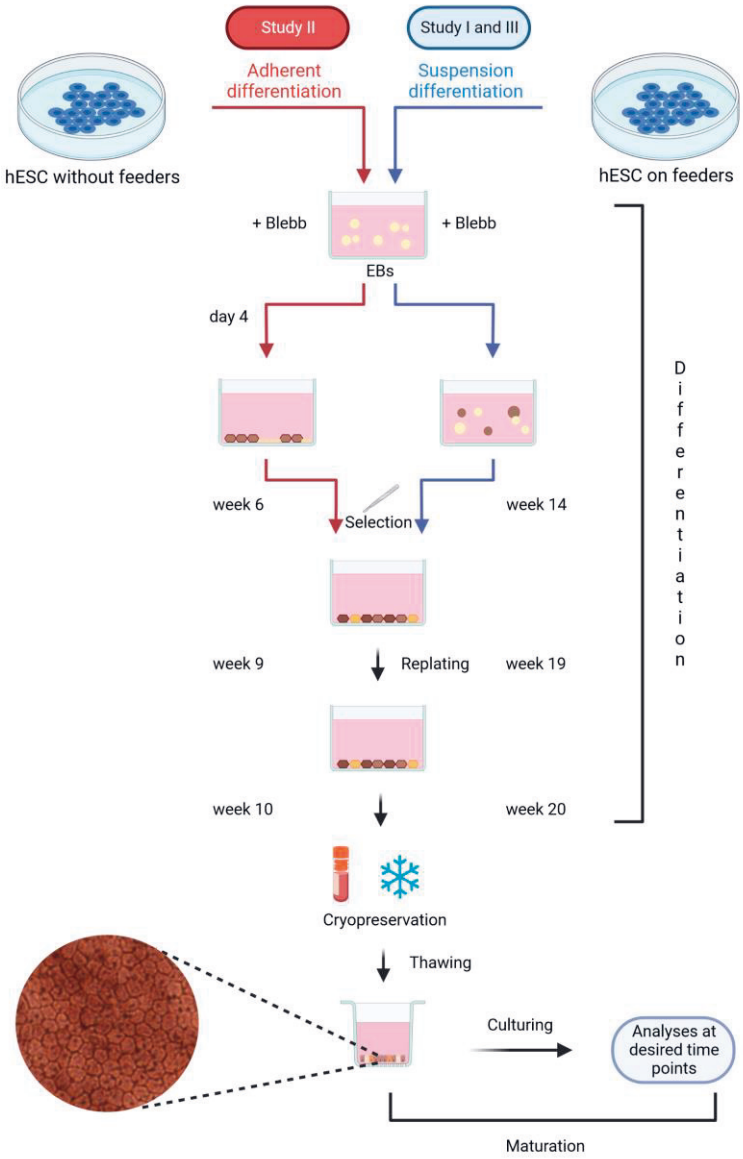

Figure 6. Illustration of both RPE differentiation methods used in this thesis. Blebbistatin was used to induce the EB formation. The protocols are explained in more detail in Chapter 4.1.2. Timelines are visible next to each step of the differentiation methods. After thawing, differentiated hESC-RPE cells are cultured for a desired time, depending on each study. hESC-RPE cultures can be divided into two distinct parts: differentiation of hESC-RPE and maturation of differentiated hESC-RPE. hESC-RPE: human embryonic stem cell-derived retinal pigment epithelium, EB: embryonic body. Figure created with BioRender.com.

4.2 Methods to study the differentiated hESC-RPE cells

All cell cultures used in this thesis were characterized and monitored throughout the culturing. The typical cobblestone morphology and the development of RPE cells' pigmentation were monitored with a Nikon Eclipse TE2000-S phase contrast microscope (Nikon Instruments Europe B.V., Amstelveen, Netherlands) and imaged with a Nikon DS-Fi1 camera. TER was measured to ensure the proper development of the barrier properties and the intactness of the RPE monolayer. At the endpoints of culturing (depending on the study), characterizations with different methods were conducted (Figure 7).

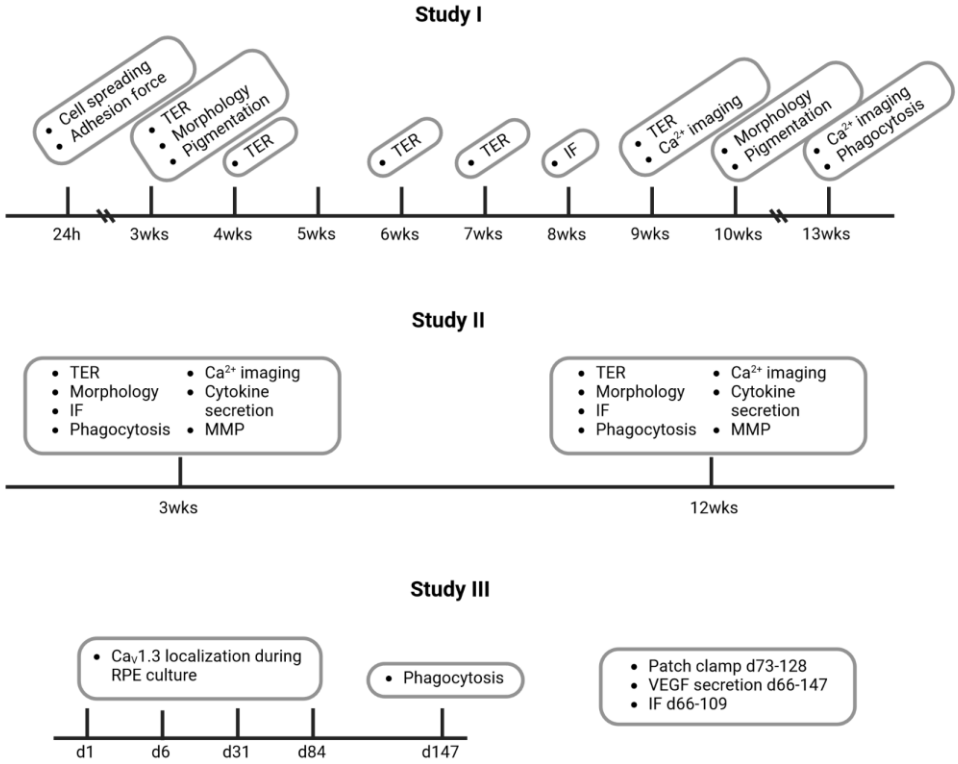

Figure 7. Time points and analyses conducted in each study. TER: transepithelial resistance, IF: immunofluorescence stainings, MMP: mitochondrial membrane potential, VEGF: vascular endothelial growth factor. Figure created with BioRender.com

4.2.1 Transepithelial resistance

TER was comprehensively measured in **Studies I and II,** and routinely checked during the culturing in **Study III**. The cells were cultured on PET culture inserts (Millipore) and measurements were carried out with a Millicell electrical resistance volt-ohm meter (Merck Millipore). Inserts without cells were measured to obtain background values, which were subtracted from the original values. The surface area ($0.3cm^2$) of the PET insert was acknowledged in the final values.

4.2.2 Analysis of pigmentation

For pigmentation analysis conducted in **Study I**, differential interference contrast (DIC) images were obtained with confocal microscopy (LSM 800, Carl Zeiss) with a 20x air immersion objective. Images were taken from five randomly selected areas per sample. Average intensities were calculated with ImageJ (Schneider et al., 2012) from each image.

4.2.3 Immunofluorescence stainings

Immunofluorescence staining was used to detect protein expression and localization from RPE monolayers (all studies). The primary antibodies are listed with details in Table 4. In addition, phalloidin-tetramethylrhodamine B isothiocyanate (Sigma Aldrich) was used to detect the filamentous F-actin cytoskeleton. Imaging of samples was conducted with confocal microscopes (LSM 700, Carl Zeiss (**Study II and III**), LSM 780, Carl Zeiss (**Study II and III**), or LSM 800, Carl Zeiss (**Studies I and II**); see imaging details in each publication) with a 63x/1.4 oil immersion objective. Detailed protocols of the stainings are described in the original publications (**Study II and III**) and in (A. E. Sorkio et al., 2015). The images were processed with ImageJ (linear brightness and contrast adjustment). Final figures were created with GraphPad Prism (version 8, GraphPad Software, La Jolla, CA, USA) and CorelDRAW Graphics Suite 2019 (Corel Corporation, Ottawa, Canada).

Table 4. Antibodies used in this study.

Antibody	Manufacturer	Cat.no	Dilution	Study
Acetylated α-tubulin	Sigma Aldrich	T6793	1:1000	III
$Ca_V1.3$	Alomone Labs	ACC-005	1:100	III
CL3	Thermo Fisher Scientific	34-1700	1:80-1:100	I, III
CL-19	R&D Systems	MAB6970	1:100-1:200	I, II
Cx43	Abcam	ab11730	1:200	II
CRALBP	Abcam	ab15051	1:500	I, III
Ezrin	Abcam	ab4069	1:100	III
Na^+/K^+-ATPase	Abcam	ab7671	1:200	I, II
Opsin	Sigma Aldrich	O4886	1:200	All studies
ZO-1	Thermo Fisher Scientific	61-7300	1:50-1:200	All studies
$P2Y_2$	Invitrogen	PAI-46150	1:200	II
PCNT	Abcam	ab28144	1:200	III
Vinculin	Sigma Aldrich	V4139	1:400	I
Phalloidin-Atto 500	Sigma Aldrich	19083	1:100	I
Phalloidin-Atto 633	Sigma Aldrich	68825	1:100	III
Phalloidin tetramethyl-rhodamine B	Sigma Aldrich	P1951	1:800	II
Anti-mouse Alexa Fluor A488	Thermo Fisher Scientific	A21202 A21042	1:200-1:400	I, II
Anti-mouse Alexa Fluor A568	Thermo Fisher Scientific	A10037 A21043	1:200	III
Anti-rabbit Alexa Fluor A488	Thermo Fisher Scientific	A21206	1:200	III
Anti-rabbit Alexa Fluor A568	Thermo Fisher Scientific	A10042, A11011	1:200-1:400	I, II

4.2.4 Phagocytosis analysis

The capability of the cells to phagocytose (**all Studies**) was analysed as follows. POS particles were isolated and purified from porcine eyes as described previously (Hongisto, Ilmarinen, et al., 2017). The POS challenge was applied to the apical side of the hESC-RPE cells, and cells with POS-containing media were incubated for 2h. After the challenge, the cells were fixed and immunostained with anti-opsin, anti-ZO-1, or phalloidin, depending on the study. Confocal microscopy (LSM 800 or LSM780, Carl Zeiss) with a 63x/1.4 oil immersion objective was used to obtain Z-stack images of randomly selected areas from each sample. The images were further processed with ImageJ to evaluate the overall capability of the cells to bind and internalize POS particles (**all Studies**) and to count internalized POS particles (**Studies I and II**) (Figure 8). The protocol is explained in more detail in each Study.

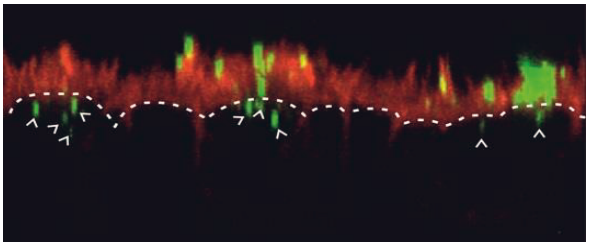

Figure 8. Orthogonal view of the hESC-RPE monolayer during the phagocytosis assay. POS particles are shown in green and F-actin in red. The white line illustrates the localization of the apical cell membrane and cytoplasm, and white arrows point to the internalized POS particles. Figure modified from **Study I**.

4.2.5 Ca^{2+} imaging

For Ca^{2+} imaging (**Studies I and II**), cells were washed with Elliot buffer (pH 7.4, 330 mOsm) containing 137 mM NaCl, 5 mM KCl, 0.44 mM KH_2PO_4, 20 mM HEPES, 4.2 mM $NaHCO_3$, 5 mM glucose, 1.2 mM $MgCl_2$, and 2 mM $CaCl_2$. Ca^{2+} -sensitive dye fluo-4-acetoxymethyl ester (fluo-4 AM; Molecular Probes, Thermo Fischer Scientific) was diluted in Elliot buffer with a final concentration of 1 mM. Cells were incubated for 45 min in 1 mM fluo-4 followed by washing with Elliot buffer for 15 min. Imaging was conducted with a Nikon Eclipse FN1 upright fluorescence microscope with a 25x/1.1 water immersion objective. A gravity-fed solution exchange system (AutoMate Scientific) was used during the imaging to keep the cells in a constant flow of Elliot buffer with or without 100 μM ATP (Sigma Aldrich). The total imaging time per sample was 10 min (with 500 ms intervals) containing 2 min of baseline imaging, 2 min of imaging after bath-applied ATP, and 6 min of imaging after ATP washout. All the steps during the assay were performed at room temperature protected from light.

Data analysis of Ca^{2+} imaging

Timelapse imaging of the fluorescent Ca^{2+} indicator in the hESC-RPE cells was used to follow the cellular Ca^{2+} -response to the ATP stimulation. The data analysis was carried out so that the timelapse videos were processed with ImageJ (version 1.52e) where three randomly chosen region of interests (ROIs) (200x200 pixels, 104x104 μm) were cropped from each video. All the reasonably recognizable cells were

outlined as circles, resulting in approximately 70-120 cells per ROI. The data were then converted to MATLAB (version R2017b, The MathWorks Inc.) form and analysed with specific MATLAB scripts (Sorvari et al., 2019).

In **Study I**, the outlined cells were analysed with a set of parameters (shown in Figure 9). The rise of the response indicates the release of Ca^{2+} from the intracellular stores as well as the Ca^{2+} influx from the extracellular solution (Tovell & Sanderson, 2008). Decay of the response reflects the activation of Ca^{2+} extrusion mechanisms and the return of intracellular Ca^{2+} concentration back to the resting level. In principle, fast response rise and decay kinetics are desirable for the RPE (Tovell & Sanderson, 2008). In **Study II**, the cells were first subcategorized as cells that respond to ATP stimulus and cells that do not respond to the ATP stimulus. Responding cells were further analysed to determine the relative maximum amplitude of the Ca^{2+} response.

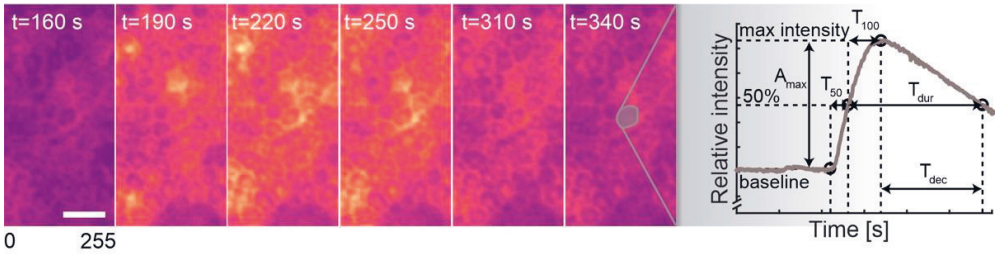

Figure 9. Pseudo-coloured image time series of ATP-induced Ca^{2+} response in hESC-RPE with Fluo-4 Ca^{2+} indicator and schematic curve representing the parameters determined from each single cell Ca^{2+} response. The pseudocoloured intensities are linearly scaled from 0 to 255. Scale bar 10 μm. Figure modified from **Study I** (Viheriälä et al., 2021).

4.2.6 Mitochondrial membrane potential

For the mitochondrial membrane potential (MMP) assay (**Study II**), the RPE cells were seeded and cultured on a 48-well plate. A TMRE-Mitochondrial Membrane Potential Assay Kit (Abcam, ab113852) with a microplate reader was used to detect changes in the mitochondrial membrane potentials. Results were obtained as intensity values. The protocol is presented in more detail in **Study I** (Viheriälä et al., 2022).

4.2.7 Cytokine secretion

Secretion of several cytokines were analysed in **Study II** with a Cytokine Array Kit (ARY005B, R&D Systems) from apical media collected from the RPE cell cultures. Results were obtained as intensity values, which were then compared between the samples. Specific details about the protocol are presented in **Study II** (Viheriälä et al., 2022).

4.3 Statistical analysis

Normality was tested with the Shapiro-Wilk test. Statistical differences were performed with the Mann-Whitney U test. A p-value of < 0.05 was considered statistically significant.

4.4 Ethical issues

Tampere University, Faculty of Medicine and Health Technology, has the approval of the National Supervisory Authority Fimea (Dnro FIMEA/2020/003758) to conduct research with human embryos. The Ethics Committee of the Pirkanmaa Hospital District has given the research group a supportive statement to derive, culture, and differentiate hESC lines (R05116) and to use the lines for research purposes. New cell lines were not derived for any of the studies in this thesis.

5 SUMMARY OF RESULTS

5.1 Cell surface protein coatings affect the formation of the intact and pigmented hESC-RPE monolayer

The aim of **Study I** was to investigate the effect of the culture surface protein coatings on the maturation of cultured hESC-RPE cells after cryopreservation. To address this, different basement membrane proteins were used: Col-IV alone, LN521 alone, and a combination of Col-IV and LN521 with or without the addition of Nid-1 (at two different concentrations). Adhesion and initial spreading 24h after thawing were first examined. Cell spreading indicates the formation of actin stress fibres, which provides the force for the maturation of cell adhesion and focal adhesion. Except for the cells on Col-IV, the hESC-RPE cells showed a well-spread morphology and the formation of organized actin stress fibres and initial focal adhesions and adherens junctions, as indicated by vinculin immunostaining. However, using centrifugation force, differences in the adhesion force were not observed between different coatings (**Study I**, Figure 1c).

In addition to poor spreading, cells cultured for a longer time with Col-IV alone were not able to form an intact epithelium based on morphology, and they were also lacking the RPE-like cobblestone morphology (Figure 10). Therefore, this coating was omitted from the upcoming analysis. All other protein coatings supported the formation of the intact epithelium monolayer, and the cobblestone morphology was detected during maturation. The results in more detail are described in the following chapters.

The effect of protein coatings on the pigmentation of hESC-RPE cells was measured. Modest changes were observed between the different coatings except with cells cultured on LN521, which yielded the highest pigmentation level.

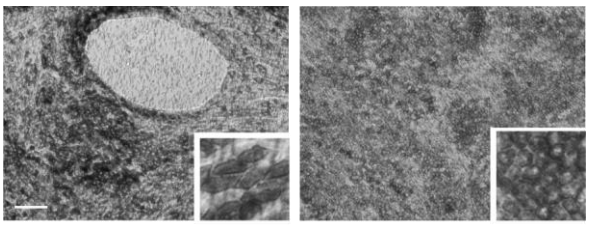

Figure 10. Comparative phase contrast images demonstrating the formation of the intact epithelium of hESC-RPE. The hESC-RPE cells on PET insert coated with Col-IV (left image) and Col-IV + LN521 + Nid-1 (right image) are shown. The hESC-RPE cells were not able to form an intact epithelium when cultured on Col-IV alone. Scale bar 20μm. Figure modified from **Study I** (Viheriälä et al., 2021).

5.2 Protein expression and localization were changed during hESC-RPE maturation

RPE-characteristic protein expression and their correct localization are a prerequisite for proper functionality. The localization of proteins differs depending on their tasks. RPE cells are polarized cells, which can be exhibited as the polarized localizations of proteins, as well. The apical membrane facing the neural retina has its own protein composition compared to the choroid facing the basolateral membrane.

Studies I, II, and III demonstrated the expression and localization of key RPE proteins in cultured hESC-RPE cells. In **Study I**, protein expressions and localizations were studied on RPE cells cultured for 8 weeks using different coating proteins. Functionally relevant proteins, CRALBP, Na^+/K^+-ATPase, claudin-3 (CL3), CL-19, and ZO-1, were selected, immunostained and imaged with confocal microscopy. In this study, the protein coatings used did not majorly affect the expression of these proteins, except for the cells cultured on LN521 alone, which yielded a less frequent expression of junctional protein CL-19. On the contrary, cells cultured in a combination of Col-IV, LN521, and Nid-1 (both concentrations) gained an improved localization of CL-19 (**Study I**, Figure 2).

Study II investigated and compared more closely the maturation of hESC-RPE since two different time points were chosen to represent RPE cells at an early (3 weeks) and late (12 weeks) maturation status (Figure 11). Immunostainings revealed

that tight junction protein ZO-1 was expressed and localized correctly in the cell-cell junctions already in the early phase of the maturation, and further culturing for 12 weeks did not affect the localization. CL-19, on the other hand, shifted its localization during maturation. At the 3-week time point, CL-19 was expressed apically, from where the localization shifted to be junctional at the 12 weeks.

RPE cells communicate with neighbouring cells via gap junctions, which are located near the tight junctions in cell borders. Gap junctions are composed of connexin protein hexamers, and Cx43 is the major connexin in the RPE (Fadjukov et al., 2022; Kojima et al., 2008). In **Study II**, the Cx43 localization in the hESC-RPE cells with a late maturation status (12 weeks) is primarily on the cell borders (**Study II**, Figure 3), resembling its native localization (Lobato-Álvarez et al., 2016). This can be observed also in the cells with early maturation status (3-week time point), although not as clearly as the cells with late maturation status.

Na^+/K^+-ATPases generate and maintain the gradients of Na^+ and K^+ in the RPE. In native and polarized RPE cells, Na^+/K^+-ATPase is expressed highly apically (Lobato-Álvarez et al., 2016). In **Study II**, cells at both maturation time points expressed Na^+/K^+-ATPase apically with a slight intracellular localization.

Furthermore, the expression and localization of Ca^{2+} signalling-related protein $P2Y_2$ was studied in **Study II**. $P2Y_2$ is an apical receptor initiating the cascade that transforms the apically applied ATP stimulus to intracellular Ca^{2+} transients. The hESC-RPE cells at early and late maturation time points expressed the $P2Y_2$ receptor both apically and laterally.

In **Study III**, CRALBP, ZO-1, and CL3 were immunostained from RPE monolayers, and the polarization of RPE cells was verified by immunostaining paraffin-embedded hESC-RPE sections with Na^+/K^+-ATPase and Best-1. CRALBP and Na^+/K^+-ATPase were localized in the apical membrane, Best-1 on the basolateral side and ZO-1 and CL3 in the cell-cell junctions. All these localizations resemble those in native RPE, as demonstrated by Luo et al. (Luo et al., 2006). Notably, the immunostainings in **Study III** were conducted with cells cultured for 9-15 weeks as compared to the culture times of 3 and 12 weeks in **Study II**.

All these results obtained from immunostainings indicate that hESC-RPE cells mature *in vitro* since proper proteins are expressed and their localizations are shifted during the maturation to resemble the native tissue.

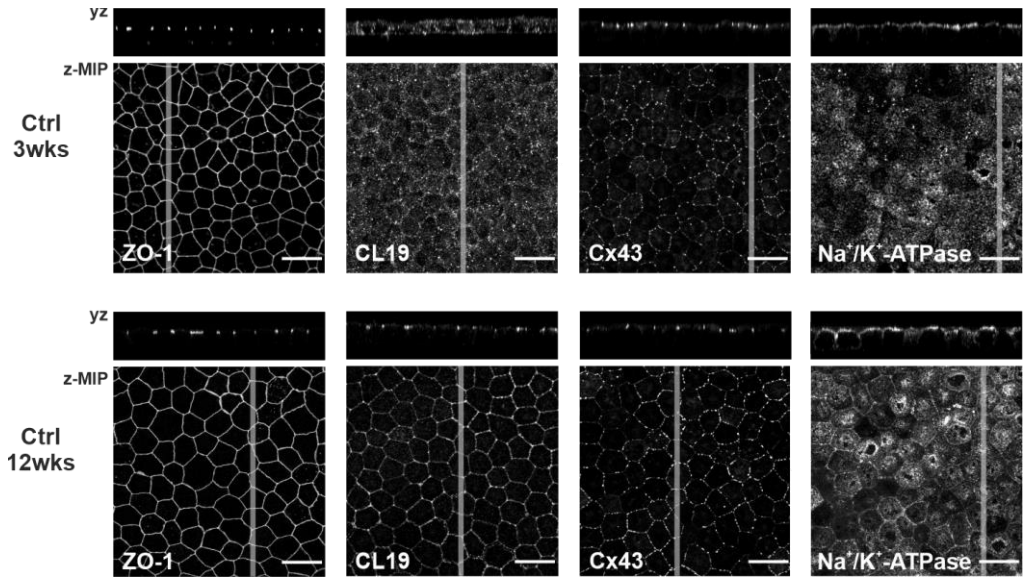

Figure 11. Immunostaining images of the hESC-RPE with two maturity statuses to compare the marker expression and localization during maturation. Scale bar 20μm. Figure modified from **Study II** (Viheriälä et al., 2022).

5.2.1 Functional $Ca_V1.3$ channel in hESC-RPE cells

Voltage-gated $Ca_V1.3$ channels take part in several RPE functions and are therefore a crucial factor for the proper development of the physiology of the RPE cells. The aim of **Study III** was to analyse the presence and localization of L-type $Ca_V1.3$ channels in the hESC-RPE cultures and to determine their functionality. At first, the channels were immunostained from hESC-RPE monolayers cultured for 13 weeks. This staining showed the apical localization of the channels, but to analyse the possible basolateral localization, immunostaining of paraffin-embedded hESC-RPE sections was conducted. Paraffin sections revealed also a basolateral localization of $Ca_V1.3$. Mouse eyecups were used as controls to verify the localization of $Ca_V1.3$ in native tissue. The localization of $Ca_V1.3$ was similarly in the apical membrane in the whole mount preparations, but the paraffin-embedded mouse eyecups revealed also a distinct basolateral localization.

$Ca_V1.3$ channels during RPE maturation

Another aim of **Study III** was to follow the expression and localization of $Ca_V1.3$ during hESC-RPE maturation. As stated above, immunostaining of mouse RPE revealed the localization of the channel in mature RPE cells to be both apical and basolateral. In our hESC-RPE cultures, the localization of $Ca_V1.3$ was in concordance with this in cells cultured for 13 weeks (**Study III**, Figure 3H). Cultured hESC-RPE cells reached confluency around day 5, after which the immunostainings were conducted at four time points to follow the localization of $Ca_V1.3$ during RPE maturation. $Ca_V1.3$ was immunostained on day 1, day 6, day 31, and day 84 post-confluency. $Ca_V1.3$ was present already at the beginning of the maturation process, but the localization shifted during maturation. Quite soon after confluency (day 6), $Ca_V1.3$ was localized at the apical and basolateral membranes. Apical localization enhanced during maturation (although the detection of basolateral localization was hindered by the increase in pigmentation).

The hESC-RPE immunostainings revealed not only the presence and the shifting localization of the $Ca_V1.3$ channels during maturation, but also a colocalization of the channel with PCNT. This was observed as a clear and small apical cluster (1 per cell), and immunostaining with PCNT antibody verified the colocalization. This finding was further verified by immunostaining with a primary cilium marker, acetylated α-tubulin. $Ca_V1.3$ localization was near the base of the primary cilium. The co-localization of $Ca_V1.3$ and PCNT remained during maturation. Mouse RPE were immunostained as control cells where $Ca_V1.3$ was clearly visible in the apical membrane but lacking the co-localization with PCNT, which may be due to the strong apical $Ca_V1.3$ expression that hinders the PCNT localization. The results of this thesis work revealed the localization of $Ca_V1.3$ (and PCNT) near the centre at the time point of 84 days post-confluence.

5.3 Changes in functionality during hESC-RPE maturation

The functionality of hESC-RPE cultures was assessed in all studies of the thesis. TER, Ca^{2+} signalling, and phagocytosis experiments were conducted from maturing RPE cells. These analyses can be utilized to address several aspects of RPE functionality and to gain a better understanding of the maturation status of the RPE cell monolayer.

5.3.1 TER increased during hESC-RPE maturation

Measuring TER and its changes during RPE maturation is highly important since the barrier formation and its maintenance are among the key functions of the RPE. TER measurements were conducted from cells cultured on hanging inserts. In principle, higher TER values indicate a stronger polarization and better-developed tight junctions between the cells (Fronk & Vargis, 2016). In **Study I**, TER measurements were initiated after 3 weeks post-seeding and continued up to 9 weeks. The results clearly revealed the increase in TER values from ~200 Ω·cm^2 to 630-730 Ω.cm^2, although the RPE cells cultured on LN521 alone showed a decrease in TER values at 9 weeks (TER value decreased back to ~200 Ω·cm^2). The combination of Col-IV, LN521 and Nid-1 yielded the highest TER values (730±80 Ω·cm^2), with a significant difference compared to the combination of Col-IV and LN521 (630±200 Ω·cm^2, p=0.014) (**Study I**, Figure 2a).

The TER results of **Study II** supported the results obtained from **Study I**. TER values increased during RPE maturation *in vitro*. Cells with a culture time of 3 weeks gained TER values of >160 Ω·cm^2, while the values after 12 weeks of culturing was >840 Ω·cm^2.

5.3.2 Phagocytosis

Phagocytosis was investigated in all studies. In **Study I**, a new analysis method was developed to count only the internalized POS particles. The same method was utilized in **Study II**. Phagocytosis is crucial for the welfare of the whole retina since RPE cells phagocytose POS daily to enable their continuous renewal. In **Study I**, phagocytosis was studied from cells cultured for 13 weeks. After the counting of the internalized particles from the obtained z-stack images, all the protein coatings used produced RPE cells with phagocytic capacity with minor differences. The addition of Nid-1 to the culture substrate yielded the highest mean number of internalized POS but also the lowest variation between the samples. The number of internalized POS in cells cultured on LN521 was 4.8±1.6/cell (506±180 POS/imaged field), Col-IV + LN521 3.4±1.2/cell (367±130 POS/imaged field), Col-IV + LN521 + 1xNid-1 6.2±0.5/cell (650±49 POS/imaged field), and Col-IV + LN521 + 10xNid-1 6.2±0.8/cell (629±72 POS/imaged field) (**Study I,** Figure 3).

In **Study II**, phagocytosis efficiency was measured in hESC-RPE cells with the culture time points of 3 and 12 weeks. Internalized POS particles were calculated as described above. No major differences were observed when comparing cells with 3

weeks and 12 weeks of culturing. The number of internalized POS were 521±140 POS/imaged field and the number of POS/cell was 3.9±1 at 3 weeks and 567±228 POS/imaged field and 4.8±2 POS/cell at 12 weeks (**Study II**, Figure 4). The results obtained from **Study I and II** were consistent indicating the phagocytosis machinery to be functional already in cells with an early maturation status.

5.3.3 ATP-mediated Ca^{2+} signalling

In **Study I and II**, two different time points were used to measure and calculate the ATP-mediated Ca^{2+} signalling in the RPE monolayer. The hESC-RPE cells were exposed to ATP and the response to the ATP stimulus was imaged along with imaging before and after the stimulus. All the calculated parameters are shown in Figure 10. The monitored Ca^{2+} signal includes the release of Ca^{2+} from the intracellular stores but also the influx of Ca^{2+} from the extracellular space. This can be observed as a biphasic response (Figure 12a and **Study I**, Figure 4).

In **Study I**, RPE cells showed quite large heterogeneity in their Ca^{2+} responses, regardless of the protein coating used. However, biphasic responses were observed as well as the increase of the mean amplitudes between 9- and 13-week culture times in all coatings. Cells cultured on LN521 alone showed altered Ca^{2+} signalling compared to the other coatings, especially after 13 weeks of culturing. These cells showed the largest cell-to-cell variation in response properties, the initiation of the responses was delayed, the decay time was longer, and only a few cells produced fast responses. Combining LN521 and Col-IV produced cells with improved Ca^{2+} signalling kinetics compared to LN521 alone: the initial rise of the responses was faster and the decay time was shorter. Nevertheless, even more improved Ca^{2+} signalling kinetics were achieved with the combination of Col-IV, LN521, and Nid-1 at both concentrations. Not only the number of cells with the fast initial rise were increased but also cell-to-cell variation was decreased. In addition, Nid-1 at the higher concentration produced cells with fast response and fast decay kinetics. Altogether, hESC-RPE cells cultured on a coating consisting of Col-IV, LN521, and Nid-1 produced Ca^{2+} response kinetics that best resembled the characteristics of native RPE tissue (Tovell & Sanderson, 2008).

Ca^{2+} imaging was conducted also in **Study II,** where the hESC-RPE cells were categorized as responsive or non-responsive (Figure 12b). Responsive cells were counted from the RPE monolayer and their maximum amplitude intensities were measured. The majority of the cells were responsive at both time points: 97 ± 3 %

at the 3-week time point and 98 ± 3 % at the 12-week time point (**Study II**, Figure 5a). However, at 3 weeks, considerable heterogeneity between the cells was observed and the maximum amplitude intensities were widely distributed.

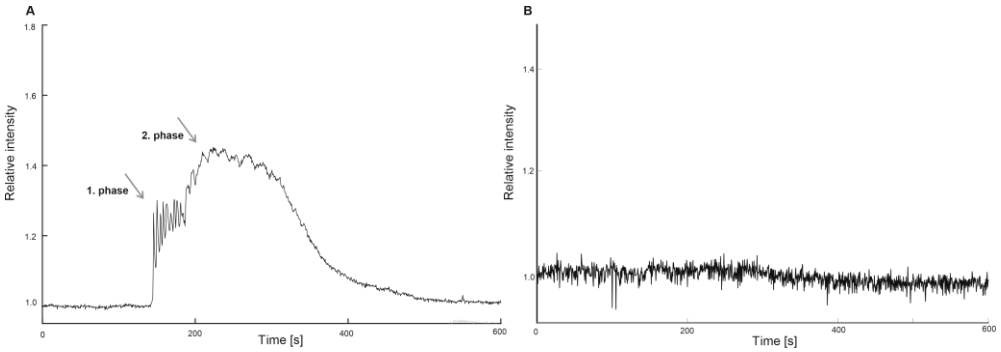

Figure 12. The representative images of the Ca^{2+} signalling responses. a) Illustrates the biphasic response with two arrows pointing the first and the second phases. Modified from Figure 4 in **Study I**. b) Example of a non-responsive cell from **Study II**. Cells were manually categorized into two subcategories: responsive and non-responsive cells. Response curves with no increase in intensity were considered as non-responsive cells.

5.3.4 Functional assays of Ca^{2+} channels

Whole-cell patch-clamp recordings, phagocytosis capacity and VEGF secretion were measured to analyse the functionality of Ca_V channels in hESC-RPE cultures in **Study III**. Notably, these experiments are not included in this thesis but are introduced here since the results are highly relevant to the overall view of **Study III**. For the patch-clamp measurements, single cells were dissociated from the monolayer. Two types of currents were detected: the slowly inactivating current and fast inactivating current from which the slowly inactivating was the main current type. Further analysis indicated the slowly inactivating current to be through L-type Ca^{2+} channels, and the presence of functional $Ca_V1.3$ channels in the hESC-RPE was concluded based on the similarity of the results to previous studies (Rosenthal et al., 2007; Wimmers et al., 2008) as well as the recordings from mouse RPE in **Study III**.

VEGF secretion was observed to be polarized in the hESC-RPE, as is characteristic of RPE physiology. When pharmacologically modulating the Ca^{2+}

channels, the overall secretion (apical and basal secretion) of VEGF was altered. Activation of Ca^{2+} channels increased the VEGF secretion, whereas the inhibition decreased the secretion, thus indicating the interplay between Ca^{2+} channels and VEGF secretion.

Phagocytosis was analysed by modulating Ca_V channels during the phagocytosis assay. Activation of L-type Ca^{2+} channels reduced the number of bound and internalized POS particles by 30% compared to the control cells. The inhibition of L-type Ca^{2+} channels reduced the number of POS particles by 62%. Thus, the results from the immunostainings, patch-clamp recordings, VEGF secretion, and phagocytosis assays indicate the presence and functionality of the voltage-gated L-type Ca^{2+} channels in hESC-RPE.

5.4 Tolerance of cellular stress in hESC-RPE

Transplantation requires the transplanted RPE cells to tolerate cellular stress caused by multiple different sources such as live-cell shipment to the clinic and oxidative stress in the diseased microenvironment of the eye. The main aim of **Study II** was to investigate the effect of the maturation status of hESC-RPE in terms of tolerance of cellular stress. In addition, the goal was to resolve if the maturation status of the cultured cells affects the capability of the cells to maintain their functions immediately after exposure to cellular stress. Two time points were chosen: 3 weeks and 12 weeks post-seeding. In addition, two different chemical stressors were used: MG132 and H_2O_2, both with sublethal concentrations to avoid cell death. The viability of the cells was monitored during the study and no cell death was observed since the hESC-RPE cells maintained the RPE-like cobblestone morphology during the treatments. In addition, no changes in the pigmentation were observed (**Study II,** Figure 2b).

A mitochondrial membrane potential (MMP) assay was used to monitor the viability of the cells and to verify the sublethal concentrations of the stressors since MMP is known to decrease in apoptosis (Gottlieb et al., 2003; C. Wang & Youle, 2019) and disperse in necrosis (Webster, 2012). Both time points and treatments revealed an increase in MMP compared to the control cells (**Study III**, Figure 1). These results indicate the concentrations of the treatments to be sublethal.

5.4.1 Barrier properties were altered especially in hESC-RPE with early maturation status

Since the transplanted RPE cells need to maintain the proper barrier function after transplantation, the barriers were studied with immunostainings of junctional markers CL-19 and ZO-1 and with measurements of TER. The results revealed the decreased TER values of MG132- and H_2O_2-treated cells in comparison to the untreated control cells (**Study II**, Figure 2a). This was especially observed in cells with an early maturation status (3-week time point). Although the TER was decreased, the expression and localization of tight junction protein ZO-1 were not affected by the treatments. Localization of ZO-1 remained in the cell-cell junctions at both time points and after both treatments. Localization of CL-19, on the other hand, was affected by the treatments. This was observed most clearly in cells with an early maturation status after both treatments as the apical localization was shifted to the cytoplasm (**Study II**, Figure 3).

In addition to ZO-1 and CL-19 immunostainings, gap junction protein Cx43 and Na^+/K^+-ATPase were immunostained (**Study II**, Figure 3). Cx43 participates in the intercellular communication of adjacent RPE cells, while Na^+/K^+-ATPase forms the Na^+ and K^+ gradients. MG132 treatment shifted the localization of Cx43 from the junctional to the apical in cells with early maturation status. After H_2O_2 treatment, the localization of Cx43 was shifted to the apical membrane or the cytoplasm. After both treatments, Cx43 was not detectable in some cells, pointing to a loss of expression. Na^+/K^+-ATPase localization shifted more visibly to the apical membrane after MG132 treatment, which resembles the native localization of Na^+/K^+-ATPase. After H_2O_2 treatment, Na^+/K^+-ATPase expression and localization were not altered.

5.4.2 Phagocytosis and Ca^{2+} signalling were altered particularly in cells with early maturation status

Phagocytosis was conducted with isolated POS particles as described previously in this thesis. POS were added to the cells immediately after the MG132 and H_2O_2 treatments and incubated for 2h. Internalized POS particles were counted from z-stack images obtained from a confocal microscope. Interestingly, the H_2O_2 treatment did not affect the phagocytosis efficiency at either of the time points. However, the treatment with MG132 reduced the number of internalized POS particles in cells

cultured for 3 weeks (3.9±1 POS/cell to 2.5±1 POS/cell). No changes at the 12-week time point were observed (**Study II,** Figure 4c).

Ca^{2+} imaging is a sensitive method for analysing the functionality of the RPE monolayer since the measurement is conducted from the whole monolayer, but the analysis can be targeted to individual cells. When almost all the control cells (97 ± 3%) were responsive to the ATP stimulus at 3 weeks, only 3 ± 3% of the MG132-treated cells and 43 ± 33% of the H_2O_2-treated cells responded. As the cells reached the culture age of 12 weeks, the relative number of responsive cells was 31 ± 43% after MG132 treatment and 99 ± 0% after H_2O_2 treatment, while 98 ± 3% of the control cells were responsive. In addition, at 12 weeks only cells treated with MG132 showed reduced maximum amplitude values compared to the control cells. (**Study II,** Figure 5a-e)

Localization of the $P2Y_2$ protein was altered after both treatments. Apical and lateral localizations observed in control cells were shifted to cytoplasmic and lateral localizations at both time points with enhancement at 12 weeks (**Study II**, 5f).

5.4.3 Cytokine expression after induction of cellular stress

Transplantation itself is a procedure that may initiate the expression and secretion of cytokines and chemokines to reject the RPE graft. In **Study II,** the secretion of different cytokines in the control cells but also in the cells after the MG132 and H_2O_2 treatments was analysed. Most of the cytokines expressed in control cells at 3 weeks were downregulated or not expressed at 12 weeks. IL6 and IL8 were expressed only after the treatments. IL6 was expressed after the treatment with H_2O_2 at 12 weeks. IL8 was expressed after the treatment with MG132 at 3 weeks. (**Study II,** Figure 6)

6 DISCUSSION

RPE cells derived from hPSCs present a potential cell source for the treatment of retinal degenerative diseases caused by RPE degeneration. RPE cells form a tight monolayer at the back of the eye and together with the underlying BM, trafficking between the retina and blood circulation is closely controlled. Due to this BRB, RPE cells are responsible for the formation of the immune privilege of the eye. Route for delivery of drugs for dry AMD are mostly oral administrations and intravitreal injections as summarized in Table 2. However, BRB sets its own limitations on treating retinal diseases; for example, some therapeutic drugs are not able to pass the barrier. The use of eye drops could be a potential approach to treat retinal diseases, but the challenge with the eye drops is that they must pass multiple cell layers before reaching the retina located at the back of the eye. (Choi et al., 2020) Transplantation of healthy RPE cells to replace the degenerated RPE has been proposed as a treatment option for the future to cure retinal diseases such as dry AMD. (Choi et al., 2020; Fronk & Vargis, 2016) The ideal outcome of the cell replacement therapy would be to restore the vision and reverse the damage caused in the retina, or at least to stop the progression of the disease. Since patients with dry AMD do not suffer from the loss of photoreceptors (except at the late stage of the disease), they might benefit from the RPE cell replacement therapy. Therefore, the transplantation should occur at the early stages of AMD to pre-empt the irreversible damage. (Markert et al., 2022)

RPE cells can be successfully cultured *in vitro*. With proper culture conditions, RPE cells form a monolayer, which represents in many aspects the native RPE of the eye. Since RPE cells have been associated with several retinal diseases, transplantation research has advanced significantly. Clinical trials have been initiated that have proven the safety of the treatment, but at the same time, the treatment has not been completely successful, mostly due to the patients' advanced stage of AMD (Sharma et al., 2020). Thus, the efficacy of the treatments remains to be verified with further clinical studies involving patients with less advanced AMD. One possible aspect affecting the clinical outcome and efficacy is the maturation level of the transplanted RPE cells. (Markert et al., 2022) The overarching goal of this thesis was

to study the *in vitro* maturation and functionality of hESC-RPE cells with a focus on cell culture parameters, which are important for cell replacement therapies as well.

6.1 Maturation of hESC-RPE cells

The time points for the studies in this thesis were based on our experience of RPE cultures. Since the culturing of hESC-RPE is time-consuming, cryopreservation of differentiated hESC-RPE cells is required, although it could slow down the maturation of the cells after cryopreservation. All the studies in this thesis were conducted with cryopreserved cells. Our group and others have previously shown that the cryopreserved RPE cells gain RPE characteristics and functions after thawing (Hongisto, Ilmarinen, et al., 2017; Li et al., 2021; Reichman et al., 2017). To study this further, the aim here was to investigate more specifically how the culture conditions and duration affect the characteristics of the hESC-RPE after cryopreservation.

6.1.1 The effects of culture substrate coating to hESC-RPE

Culture conditions were studied in **Study I** regarding the culture surface protein coatings. Various protocols exist for the differentiation and maturation of the hPSC-RPE cells, but comparative studies of the effect of the substrate protein coatings on the functionality of the cells after cryopreservation were lacking. RPE cells are commonly cultured on a permeable membrane to support transepithelial transport and basolateral secretions. PET inserts are already being used as a membrane for RPE cells in transplantation studies (Da Cruz et al., 2018; Z. Liu et al., 2021), and therefore it was chosen as the culture substrate. Proteins for coatings were chosen from the proteins that exist in the native BM, which gives structural support to the RPE cells by forming a protein network to which the RPE cells attach with interactions of specific proteins, like integrins, which are the main protein group responsible for the attachment of the cells (Aisenbrey et al., 2006; Gullapalli et al., 2005). We have previously shown that hESC-RPE cultured on fibronectin did not produce well-pigmented monolayer compared to the RPE cells on Col-IV and LN521 protein coatings (A. Sorkio et al., 2014). In addition, since the role of the Nid-1 is to act as a linker between Col IV and LNs (May, 2012), it was included in the **Study I**. Laminin isoform LN521 is the main laminin isoform in BM. In addition,

it has been previously shown that LN521 supports the differentiation and maturation of hESC-RPE cells (Aisenbrey et al., 2006). In **Study I**, the hESC-RPE cells cultured on Col-IV alone were not able to produce an intact epithelium based on phase contrast microscopy imaging, and therefore the tight barrier was lacking, yielding low TER values. It has been previously shown that ARPE-19 cells preferentially adhere to laminins over Col-IV (Aisenbrey et al., 2006) which could also explain the unfavourable conditions in our study when using Col-IV alone for the coating. Even though ARPE-19 is a widely used cell model to study RPE cells, the comparison between ARPE-19 and iPSC-RPE may be difficult, for example, because ARPE-19 cells do not form a pigmented and hexagonal cell monolayer (Abu Khamidakh et al., 2013; Markert et al., 2022). In addition, ARPE-19 cells have other RPE gene expressions at lower levels compared to the iPSC-RPE cells (Markert et al., 2022). As a comparison to Col-IV in **Study I**, the hESC-RPE cultured on LN521 showed improved attachment and barrier formation compared to cells on Col-IV, although a significant decrease in the TER values at 9 weeks of culturing was observed with cells cultured on LN521. It has been previously reported that freshly differentiated iPSC-RPE cells on mouse LN coating did not show any decrease in TER values during 10 weeks of culturing (Hazim et al., 2017). However, LN is known to have a high affinity with ECM proteins and growth factors (Ishihara et al., 2018), which are present in the serum-containing culture media they used. Thus, the maintained TER values in Hazim et al. could be explained by the presence of serum as compared to the more defined serum replacement used here in **Study I**.

In this thesis work, a decrease in TER was not observed after the addition of more complexity to the protein coatings with the combination of Col-IV and LN521 and finally with the addition of Nid-1. TER values increased during 9 weeks of maturation, especially with the combination of Col-IV + LN521 + Nid-1. Functional analyses (more details in the following chapters) were conducted that all showed improved results with the more complex protein coating. Nid-1 is a glycoprotein that cross-links Col-IV and LN521 together to enhance the stability of BM (Yurchenco, 2011). To study the effects of the presence of Nid-1 in the coating, the morphological properties were first analysed. No morphological differences of the hESC-RPE cells between the different protein coatings were observed except in the cells cultured on Col-IV alone, where the RPE cells were not able to form the cobblestone cell shape. All the results obtained from **Study I** indicate the unfavourable coatings of Col-IV and LN521 used alone on the maturation and functionality of the hESC-RPE cells. In addition, the presence of Nid-1 in the protein coating produced cells with the least heterogeneity.

6.1.2 Culture conditions affecting pigmentation

In addition to the coating, other culture condition parameters may significantly influence the hESC-RPE cells. In **Study I**, the hESC cells were cultured in the presence of feeder cells, whereas in **Study II**, the feeder-free cultures for hESCs were used before RPE differentiation. In comparison, the pigmentation level appeared to be higher in the hPSCs cultured with the feeder cells, but also multiple other aspects could affect the pigmentation, such as the cell line used, the different chemical components used during the differentiation, and even hESC line-to-line variability. Leach et al. reported variability between different cell lines as they compared three iPSC-RPE cell lines differentiated with both spontaneous and directed methods. All their cell lines produced pigmented monolayer and the RPE-related proteins were localized similarly between the cell lines when spontaneous differentiation method was used. However, one cell line differentiated with directed differentiated method showed a reduced pigmentation and different localization of MITF, OTX2 and ZO-1 compared to the other cell lines. (Leach et al., 2016) In **Study II**, only one hESC-RPE cell line was used. However, to minimize the batch-to-batch variability, three different batches were used in all the experiments.

In **Study II**, the pigmentation was measured after 3 and 12 weeks of culturing, compared to **Study I**, which featured 8 weeks of culturing. The pigmentation level in **Study II** was clearly lower even at the later time point. Notably, it was not possible to measure the pigmentation (the brightness of the image) of the cells in **Study II** since the pigmentation was too light and therefore the pores from the culture insert were visible, especially at 3 weeks of culturing. Pigmentation is one of the hallmarks of RPE cells. In the eye, RPE cells appear as a black/dark brown layer of cells. Pigmentation has also been taken as one of the maturity marks of cultured RPE cells (Al-Ani et al., 2020; Bennis et al., 2017; Da Cruz et al., 2018). However, Sorkio et al. revealed that higher pigmentation does not indicate a more mature monolayer, since they observed that TER values were low simultaneously with high pigmentation (A. Sorkio et al., 2014). In addition, RPE cells with higher pigmentation have shown reduced expression of the visual cycle and oxidative stress-related pathways (Bennis et al., 2017). However, it is known that the pigmentation during lifetime decreases and can eventually be a part of the degeneration of RPE cells and the retina (Shu et al., 2017). To conclude, based on the pigmentation results from **Studies I and II**, pigmentation alone should not be considered as a maturity mark for cultured hESC-RPE cells, especially when comparing the pigmentation levels of different cell lines.

6.1.3 Protein expression and shifting localization during hESC-RPE cell maturation

A common method to study the maturation of cultured RPE cells is to immunolabel proteins related to RPE functions, such as Na^+/K^+-ATPase, CRALBP, ZO-1, and CL-19. It is known that the expression and localization of proteins changes during RPE maturation (Burke, 2008). **Studies I and II** both showed the tight junctional protein ZO-1 localizing in the cell borders indicating the formation of tight junctions and thereby the formation of a tight barrier. Combining the immunostaining of ZO-1 and CL-19 and the measurement of TER, barrier formation and functionality can be studied and evaluated. The junctional association of ZO-1 was observed already at the 3-week time point (**Study II**), but the TER was still relatively low (>160 $\Omega \cdot cm^2$). Therefore, ZO-1 can be considered as an early marker of the maturation of tight junctions and does not alone indicate a functional barrier. Neither the localization nor the expression of ZO-1 changed during the maturation.

CL-19 is closely associated with tight junctions, as it is a transmembrane protein of four transmembrane regions with a high affinity to bind ZO-1 in the cytoplasmic site. Both cytoplasmic domains of CL-19 are bound to ZO-1 in neighbouring cells, thus connecting the cells to each other via tight junctions (O'Leary & Campbell, 2021). In **Study I**, the expression of CL-19 was visible at 8 weeks of culturing with all the protein coatings used, but the highest expression level when examining immunofluorescence stainings was in cells cultured in the presence of Nid-1. In **Study II,** the expression of proteins was observed to be initiated with an earlier culture time point compared to **Study I** (an 8-week time point in **Study I** compared to the 3-week time point in **Study II**). In **Study II**, junctional expression of CL-19 was mostly lacking after 3 weeks of culturing, whereas the expression was correctly junctional after 12 weeks of culturing. This was in agreement with our previous experience, where we have observed the expression of CL-19 to initiate rather late during maturation (data not shown). As ZO-1 can be considered as an early marker of the formation of the barrier, CL-19 on the other hand can be considered as a marker of a functional or at least nearly functional barrier, since the TER values were high simultaneously with the proper localization of CL-19. In ARPE-19, junctional proteins ZO-1 and occludin are expressed, but detectable claudin expression is mostly missing (Peng et al., 2016). The TER of ARPE-19 is low, ~50-100 $\Omega \cdot cm^2$, reflecting leaky junctions (Dunn et al., 1996). Based on these earlier studies, our results of late CL-19 expression together with the concurrently achieved high TER values indicate the importance of CL-19 in barrier formation.

Besides the tight junctions, RPE cells are coupled to neighbouring cells via gap junctions that are composed of connexins, with Cx43 being the dominant in the RPE (Fadjukov et al., 2022; Kojima et al., 2008). Cx43 is expressed in the apical and intercellular membranes in mouse RPE and ARPE-19 cells (Akanuma et al., 2018) and also in the hESC-RPE (Fadjukov et al., 2022). Here in **Study II**, the expression and proper localization of Cx43 were observed already at 3 weeks of culturing, but they were slightly enhanced when 12 weeks of culturing was reached.

Na^+/K^+-ATPase (**Studies I and II**) was observed distinctly apically already after 3 weeks of culturing (**Study II**), and it did not significantly change during the maturation. Based on the obtained data, proteins with no significant alterations in the expression or localization during RPE maturation should not be considered as ideal maturity markers. Instead, they can be used as an initial step in the evaluation of the quality and functionality of the cells.

The expression of ATP-mediated Ca^{2+} signalling receptor P_2Y_2 was enhanced during RPE maturation (**Study II**). Under normal conditions, the localization of the P_2Y_2 is highly apical, since the function of the receptor is to bind extracellular ATP and therefore to act as a first step in Ca^{2+} signalling events (Mitchell & Reigada, 2008). During maturation, the localization was shifted from the cytoplasmic to the apical (**Study II**) which resembles the native localization of the receptor. Thus, to evaluate RPE maturity, P_2Y_2 can be considered as one maturity marker.

RPE cells gain pigmentation during maturation, as described earlier. Pigmentation can hinder the visualization of fluorescent staining with microscopy. Since RPE cells are cultured on a substrate, the substrate together with pigmentation cause challenges when observing the immunolabelled proteins even with a transparent substrate. Basolateral and cytoplasmic proteins in particular could be difficult to observe with microscopy since the pigment granules are located in the apical regions of the RPE cell and the microscopy light has to pass the granules to reach the proteins underneath them (Bermond et al., 2020). Paraffin-embedded sections or cryosections could have been used to avoid this challenge.

6.1.4 Improvement of the functionality of hESC-RPE cells during maturation

As previously described, immunolabelling most of the individual proteins alone cannot be used to evaluate functionality. Thus, in **Studies I and II**, TER,

phagocytosis, and Ca^{2+} signalling were evaluated to study the functionality of the hESC-RPE cells along with the maturation process.

TER

Even though the pigmentation was low in the hESC-RPE cells in **Study II**, the TER values were at the same level regardless of the differentiation method used. **Studies I and II** both revealed cells with barrier maturation since the TER values increased from ~200 Ω·cm2 at 3 weeks to ~800 Ω·cm2 at the later time point (8 weeks in **Study I** and 12 weeks in **Study II**). Based on these characteristics, hESC-RPE cells cultured for a longer period (8 weeks and 12 weeks in this thesis) can be considered as more mature compared to the shorter cultured cells (3 weeks). Also, in the native environment, the barrier matures as the BRB and tight junctions are formed during the development of the retina (Rahner et al., 2004). The increasing TER values are consistent with other studies conducted with hESC-RPE cells, such as that conducted by Plaza Reyes et al., which showed the barrier formation of hESC-RPE cells although the final time point for the measurement was only 31 days compared to 8 and 12 weeks in this thesis (Plaza Reyes et al., 2016).

Phagocytosis

Since phagocytosis is an essential function of the RPE for the welfare of the retina, the transplanted RPE cells must be able to phagocytose as well. Phagocytosis efficiency was measured in **Studies I and II** by calculating the internalized POS particles. All protein coatings produced RPE cells with functional phagocytotic machinery, although by adding Nid-1 to the coating, the number of internalized POS particles was increased when compared to other coatings. In addition, RPE cells cultured on Col-IV + LN521 + Nid-1 showed the lowest variation of internalized POS particles, indicating improved homogeneity compared to cells on other coatings. **Study II** revealed phagocytosis relatively early since the efficacy of the phagocytosis was not altered at least significantly by the maturation. The number of internalized POS particles was on average 4-5 per cell at 3 and 12 weeks of culturing.

The set-up for the phagocytosis experiment is relatively short; 2h incubation with POS. Since the phagocytosis can be divided into three phases - binding, internalization, and degradation - the analysis in **Studies I and II** measures only the internalized particles after the binding; but the degradation of the POS is beyond

this measurement. However, the binding and internalization of POS is already an indication of phagocytosis. In native tissue, RPE cells phagocytose POS daily. In culture conditions without constantly added POS, the proteins involved in the phagocytosis are expressed even though they are not actively needed. Thus, POS challenges indicate the expression and correct localization of the phagocytosis-related proteins in general. Based on the results obtained from **Study II**, hESC-RPE cells at 3 weeks are mature enough for active phagocytosis.

Ca^{2+} signalling

Intact Ca^{2+} signalling is highly important for cells since Ca^{2+} ions are known to participate and regulate a multitude of cellular functions due to their high affinity to proteins (Peterson et al., 1997; Strauß, 2013). Therefore, analysing ATP-induced Ca^{2+} signalling has been considered important when evaluating the quality of hPSC-RPE cells for transplantation purposes (Miyagishima et al., 2016). ATP is a well-known signalling molecule in the subretinal space, and it induces signalling pathways including ATP-mediated Ca^{2+} signalling in RPE cells. In native tissue, ATP can act as an autocrine or paracrine messenger to activate Ca^{2+} signalling cascades in the RPE (Mitchell & Reigada, 2008; Peterson et al., 1997). Fast response kinetics is mandatory for the cells, and delayed response could lead to impaired cell function and eventually, for example, to compromised fluid regulation of the subretinal space (Mitchell & Reigada, 2008; Peterson et al., 1997). ATP-mediated Ca^{2+} signalling can be measured *in vitro* by bathing RPE cells in an ATP-containing solution after the cells have loaded with Ca^{2+}-sensitive fluorescent dye. The stimulation of RPE with ATP results in releases of Ca^{2+} from the intracellular stores, and these $[Ca^{2+}]_i$ transients can be monitored with microscopy and observed as intensity changes. (Sorvari et al., 2019; Stalmans & Himpens, 1997) In **Studies I and II**, information about the population-level Ca^{2+} signalling was obtained without missing events from single cells as described in (Sorvari et al., 2019). Ca^{2+} imaging is a sensitive method to evaluate the quality and functionality of hESC-RPE cells. During maturation of the hESC-RPE cells, the Ca^{2+} response amplitudes increased, as observed in **Study I**. Cells cultured on LN521 showed altered Ca^{2+} response kinetics, especially at 13 weeks of culturing compared to cells cultured on other coatings. In **Study II**, the RPE cells were able to respond to the ATP stimulus relatively early (at 3 weeks). Surprisingly, at the later time point (12 weeks), the maximum intensity values were lower. This is in contradiction with the results obtained from **Study I**, where the maximum amplitudes increased during maturation from 9 weeks to 13 weeks.

Pigmentation of the hESC-RPE cells increased during maturation in **Study II**, which at least partly explains the decrease of the maximum amplitudes between the time points. Higher pigmentation influences the imaging, as the fluorescence peaks are more difficult to observe since the majority of the pigment granules are located in the apical region of the RPE cells and presumably at least most of the free Ca^{2+} in the cytoplasm is under them (Bermond et al., 2020). No increase in the pigmentation was observed from 9 weeks to 13 weeks in **Study I**, which makes the results more comparable regarding the maximum intensity values than in **Study II**. In addition, the expression of $P2Y_2$, which is involved in the Ca^{2+} signalling, was enhanced and localization was more visible in the apical membrane after 12 weeks of culturing (**Study II**). This indicates that the lower maximum amplitude values were not due to a decreased expression of the $P2Y_2$ in **Study II**. Ca^{2+} signalling during hESC-RPE maturation was studied also by Abu Khamidakh et al., and they demonstrated that spontaneous Ca^{2+} release from the intracellular stores increased during RPE maturation (Abu Khamidakh et al., 2016). However, the culture ages of hESC-RPE cells in the study by Abu Khamidakh et al. (Abu Khamidakh et al., 2016) were 9 days and 28 days, which are relatively early time points compared to the time points used in this thesis. Nevertheless, these data support our results, which demonstrated that hESC-RPE cells are capable of releasing Ca^{2+} from the intracellular stores already at 3 weeks.

Variation of the maximum relative amplitude values were observed at all the time points in both **Studies I and II**. The large distribution may be due to uneven maturation between the cells, but RPE cells are also naturally heterogeneous, as demonstrated by Korkka et al. (Korkka et al., 2022) regarding K^+ channel heterogeneity and Ortolan et al. (Ortolan et al., 2022) regarding heterogeneity related to cell morphology and disease sensitivity.

To conclude, using protein mixes that resemble more the native BM protein composition supports the functionality of hESC-RPE cells including TER and Ca^{2+} signalling. In addition, simultaneously with the increased culture time of hESC-RPE, the TER values increased and the localization of proteins including CL-19, Cx43, and $P2Y_2$ shifted to resemble their native localization. Interestingly, the functional studies revealed that phagocytosis was not improved during maturation. However, with Ca^{2+} signalling experiments, a more homogenous cell monolayer was observed even though the cells were able to produce responses after ATP stimulus already at 3 weeks.

6.2 Tolerance of cellular stress

RPE cells face a set of different stressors during transplantation, starting from the transportation of the cells to the clinic in the case of live-cell shipment. The already diseased microenvironment with inflammatory factors in the retina enhances the difficulties of the cells in surviving and functioning properly. Inflammation may have begun in the retina and therefore inflammatory factors may be present. (W. Tan et al., 2020) Thus, the transplanted RPE cells must be able to tolerate cellular stress caused by multiple sources, and the transplanted cells are required to function rapidly after the transplantation to replace the functions of the damaged RPE cells in the retina.

In **Study II**, two culture time points were chosen to represent cells with two different maturation statuses, early and late. Cells were exposed to oxidative stress with H_2O_2 and the function of proteases were inhibited with MG132. The chemicals were used separately and with sublethal concentrations. Functional assessments were conducted after the treatments both of the treated cells and the untreated control cells. H_2O_2 is a common chemical causing oxidative stress (Ransy et al., 2020), and it has been shown to induce cell death in the nonpolarized RPE monolayer (Hsiung et al., 2015). However, the nonpolarized cells were seeded only a day before the experiments compared to the 3-4 weeks of culturing used to obtain polarized cells (Hsiung et al., 2015). The role of the proteases in cells is to break down damaged or redundant proteins. If the function of proteases is inhibited, the accumulation of proteins is initiated in the cytoplasm. In addition, oxidative stress is known to inactivate proteases. (Blasiak et al., 2019)

Since the aim of **Study II** was not to measure or observe cell death, sublethal concentrations of H_2O_2 and MG132 were ensured by measuring MMP, which should decrease in the case of cell death (C. Wang & Youle, 2019). The decrease of the MMP enhances the leakage of ROS into the cytoplasm, which promotes cell death even further. The treatments were conducted for 24h, which is a relatively short period of time compared to the progression of AMD, which could take years with the accumulation of different factors. Mitochondria are known to react rapidly to stimuli (C. Wang & Youle, 2019), and therefore the 24h exposure to the stressors should be adequate to produce changes in the mitochondrial membrane potential. In our study, no decrease in MMP was observed at least at the population level. Surprisingly, the membrane potential increased after the treatments. As a possible explanation, defence mechanisms may have been activated in the mitochondria due

to oxygen damage (Ransy et al., 2020). This requires energy and could explain the increase in the membrane potential.

6.2.1 Barriers and junctions were altered by the treatments more pronouncedly at 3 weeks

Chemical treatments clearly affected the barriers of RPE cells, as TER values were decreased especially in the cells with an early maturation status (3 weeks). The localization of key barrier proteins CL-19 and ZO-1 was examined. The localization of CL-19 was altered at both time points after both chemical treatments, whereas ZO-1 localization was not altered and remained junctional. Although CL-19 was not localized at the cell borders at 3 weeks in the control cells either, the treatments shifted the localization more clearly to the cytoplasm. Since ZO-1 was still junctional after the treatments but CL-19 was mislocalized, this indicates that the decrease in TER was due to the shift of CL-19 localization. CL-19 is known to participate in the determination of junctional properties such as permeability (F. Liu et al., 2021). Therefore, it was not surprising that since the localization of CL-19 was altered, the TER values were decreased. The same observation was made by F. Liu et al. (F. Liu et al., 2021), where they showed that the knockdown of CL-19 reduced TER while the ZO-1 remained unaltered. However, in **Study II** the barriers could be at least partly functional due to the junctional localization of ZO-1. Altogether, the findings of reduced TER, CL-19 mislocalization and unaltered localization of ZO-1 are in agreement with previous studies. Based on our results in **Study II**, a longer culture time (12 weeks) supports the maintenance of the barrier and junctions after the chemical treatments. Thus, regarding RPE transplantation in general, disruption of the barriers would enable the uncontrollable leakage of molecules and nutrients, which would be non-beneficial. In addition, the deletion of ZO-1 is shown to be lethal in mouse embryogenesis (Phua et al., 2014), which could explain why the cells try to maintain the expression of tight junction proteins as long as possible to avoid cell death. Therefore, this could explain why in **Study II** ZO-1 is still expressed even though other tight junctional proteins are mislocalized or the expression is already disrupted. Based on earlier studies, a dramatic decrease in the TER values indicate dramatic consequences for the cell, as Hsiung et al. (Hsiung et al., 2015) have demonstrated. They observed a decrease in the TER when cell death occurred. However, in **Study II** cell death was not observed even though the TER decreased, at least within the 24h time window.

Connexins, especially Cx43 in RPE cells, form gap junctions in intercellular membranes and hemichannels in apical membranes (Fadjukov et al., 2022). Both treatments in **Study II** altered the localization of Cx43 at both time points, but more visibly at 3 weeks. The localization was shifted more to the cytoplasm, which could be due to the inhibited function of proteasomes. The same observation has been seen in other studies as well (Kimura & Nishida, 2010; Laing et al., 1997; Laing & Beyer, 1995). In addition, Cx43 has been revealed to shift more to the cytoplasm as oxidative stress occurs (Giardina et al., 2007; Hutnik et al., 2008) which could explain the shifting localization in **Study II**, especially after H_2O_2 treatment. However, to study in more detail the expression level of proteins, quantitative methods such as western blot should be used.

Autophagy is a way for the cells to degrade proteins, and it is upregulated if the proteasomes are inhibited (Zhan et al., 2016). The autophagic machinery could try to compensate for the functions of proteasomes and take a more dominant role in the degradation of proteins. However, it is not known how autophagy matures in RPE cells and when it becomes functional for degradation.

Altogether, hESC-RPE cells at 3 weeks are more susceptible to losing their barrier function and the junctional localization of CL-19 and Cx43 after the chemical treatments compared to cells cultured for 12 weeks.

6.2.2 Pigmentation has antioxidative role in RPE

RPE cells are highly pigmented cells and melanin, which is one of the components of pigment granules, is participating in the antioxidant defence of RPE cells by demolishing free radicals (Z. Wang et al., 2006). In **Study II**, the pigmentation of control cells or chemically treated cells was not particularly high at 3 weeks of culturing. However, the pigment was clearly visible although it was not measurable, at least with the analysis method used in the **Study I** (as discussed in Chapter 6.1.2). Wang et al showed that melanin is capable to inhibit the formation of A2E (a major chromophore in lipofuscin) photo-oxidation products (Z. Wang et al., 2006). However, during RPE differentiation, the amount of melanin is known to increase which could have a significant impact on its protecting properties (Buchholz et al., 2009; Vaajasaari et al., 2011). In **Study II**, the pigmentation increased between the time points (3 weeks and 12 weeks) (**Study II**, Figure 2b) which could explain at least partly why the cells cultured for 12 weeks were not as susceptible to cellular stress as the cells cultured for 3 weeks, especially after the H_2O_2 treatment.

6.2.3 Phagocytosis and Ca^{2+} signalling after the treatments

Phagocytosis is needed rapidly after the transplantation, and it has been proposed that malfunctions in the phagocytic machinery could contribute to AMD pathophysiology due to the accumulation of undegraded POS material and lipofuscin, resulting in increased ROS in the RPE (Boulton et al., 2004; Juuti-Uusitalo et al., 2015; F. Liu et al., 2021). In our studies, phagocytosis efficacy was reduced only at the early time point (3 weeks) and only after the MG132 treatment. Since the analysis measures only the internalized particles and the number of internalized POS was lower in treated cells compared to the control cells, this could be due to the unsuccessful binding of POS and/or unsuccessful internalization and/or enhanced degradation. Interestingly, the knockdown of CL-19 has been shown to reduce the degradation of phagocytosis in human induced pluripotent stem cell-derived RPE (hiPSC-RPE) (F. Liu et al., 2021). In addition, CL-19 knockdown activates AMPK (F. Liu et al., 2021), which is known to take part in the reassembly of the tight junctions. AMPK has also been shown to inhibit phagocytosis in ARPE-19 cells (Qin, 2016). This could at least partly explain the reduced number of POS particles in the cells as CL-19 expression was altered at 3 weeks and therefore the reassembly of the tight junctions could have been initiated by AMPK. MG132 is known to activate AMPK (Jiang et al., 2015). However, the activation of AMPK using MG132 does not alone explain the reduced phagocytosis, since the efficacy of phagocytosis was reduced only at the 3-week time point.

Ca^{2+} signalling was highly altered by the treatments, especially at the earlier time point where the ability to respond was either weaker or completely lost compared to the control cells. The expression of ATP-mediated Ca^{2+} signalling receptor $P2Y_2$ was altered after the treatments at 3 weeks, which could explain the compromised results of Ca^{2+} responses as the ATP-binding receptor was missing at least in the majority of the cells after the MG132 treatment. Ca^{2+} signals are spread via gap junctions to neighbouring cells. Since the gap junction protein Cx43 localization was shifted, the spreading of the Ca^{2+} signals may also be reduced. Treated cells at 12 weeks were able to produce ATP-induced Ca^{2+} responses (31% of MG132 treated cells and 99% of H_2O_2 treated cells), which could reflect the involvement of $P2Y_2$ since it was better-preserved after the treatments compared to the earlier time point.

To conclude, hESC-RPE cells cultured for 3 weeks reduced their phagocytosis efficiency after the MG132 treatment. In addition, after both treatments, Ca^{2+} signalling was altered especially at 3 weeks, making the hESC-RPE at 3 weeks more

prone to cellular stress and thereby reduced in functionality when compared to cells cultured for 12 weeks.

6.2.4 Cytokine secretion, especially IL-6 and IL-8, were upregulated by the treatments

Since the eye has its own immunoregulatory system, RPE cells are known to secrete immunomodulatory cytokines (Holtkamp et al., 2001). The cytokine secretion by RPE is highly upregulated via pathogens and in diseases such as AMD (Shi et al., 2008). After the treatments in **Study II**, the secretion of interleukins (IL6 and IL8) was upregulated compared to the control cells where the secretion of interleukin was absent. This result is consistent with previous studies where the H_2O_2 and MG132 upregulated the secretion of IL6 and IL8 (Detrick & Hooks, 2020; Wu et al., 2010). Although cytokine secretion is advantageous in the retina, harmful side effects could occur regarding transplantation. Secretion of certain cytokines like IL8 could enhance the rejection of the transplanted graft (Z. Liu et al., 2016). Since RPE cells possess a vital role in inflammatory responses in normal and pathological conditions, ATP-mediated signalling could be involved in the modulation of inflammation. The ATP in the subretinal space could arise from the RPE cells themselves, especially from the damaged RPE cells indicating a communication pathway between nearby cells to alert the other cells of the damage. (Peterson et al., 1997) RPE cells must then respond quickly to the ATP stimulus to initiate inflammatory responses. Since RPE cells are metabolically active, they possess a high number of mitochondria to generate enough ATP to ensure the normal functions of the cells (Bellezza, 2018), and since mitochondria are known to react rapidly (C. Wang & Youle, 2019), the production and release of the ATP could occur rapidly in the case of cell damage.

6.3 Functional $Ca_V1.3$ channels in hESC-RPE cells

The expression, localization, and functionality of the Ca^{2+} channel $Ca_V1.3$, which is highly relevant for the RPE physiology, was followed during RPE maturation in **Study III**. Previously, the presence of $Ca_V1.3$ had not been shown in cultured hESC-RPE cells. In **Study III**, the localization of $Ca_V1.3$ in the cells with early maturation status (day 1 post-confluence) was significantly different compared to the cells with late maturation status (day 84 post-confluence). $Ca_V1.3$ was localized homogenously

in the apical and basolateral membranes in cells with late maturation status, while in cells with early maturation status, the localization was cytoplasmic. Thus, the maturation status of the RPE cells influenced the localization of $Ca_V1.3$. Apically localized $Ca_V1.3$ was a new observation in our study, as only basolateral localization had been reported before in murine and porcine RPE (Reichhart et al., 2010, 2015). Intriguingly, $Ca_V1.3$ channels on the apical membrane could provide a route for Ca^{2+} between the subretinal space and RPE. Since phagocytosis takes place on the apical side of the RPE (Lakkaraju et al., 2020; Mazzoni et al., 2014) and VEGF is secreted both apically and basolaterally (Becerra et al., 2004; Blaauwgeers et al., 1999; Klettner et al., 2015), the regulatory role of $Ca_V1.3$ in these processes could be supported with the apical and basolateral localizations as observed in **Study III**. Interestingly, apical $Ca_V1.3$ also colocalized with the base of the primary cilia, PCNT, which is a centrosome component. PCNT takes part in cell functions like the assembly of the primary cilia by recruiting proteins. May-Simera et al. (May-Simera et al., 2018) showed PCNT localization at the centre of mature RPE cells. In addition, PCNT is involved in Ca^{2+} signalling, which could explain the colocalization of the $Ca_V1.3$ channel and PCNT (Jurczyk et al., 2004). Several different Ca^{2+} channels including subtype $Ca_V1.2$ have been shown to localize and function in the primary cilium (Muntean et al., 2014; Pablo et al., 2017). The expression level of $Ca_V1.2$ is regulated by Wnt signalling, which is known to be involved in the RPE development (Westenskow et al., 2009) and maturation (May-Simera et al., 2018). Since primary cilia are signalling organelles, their function is often dependent on the presence of Ca^{2+}. Therefore, the $Ca_V1.3$ channels could be involved in the regulation of Ca^{2+} trafficking between the cytoplasm and primary cilia and eventually take part in the regulation of primary cilia functions (Saternos et al., 2020). Mouse RPE has a strong apical membrane localization of $Ca_V1.3$, but single punctum localization was not observed. This could be due to the strong apical staining that could hinder or cover the single puncta of $Ca_V1.3$. Alternatively, since the mouse RPE used in **Study III** was mature RPE and primary cilium is disassembled in some cell types upon maturation (Blitzer et al., 2011), the localization of $Ca_V1.3$ in the PCNT could have already been disassembled. To study this in more detail, multiple paraffin-embedded sections of mouse RPE should be used. However, detecting a single punctum from the sections could be difficult or even impossible.

To study channel functionality and to assess the influence of $Ca_V1.3$ channels in hESC-RPE physiology, phagocytosis, VEGF secretion, and whole-cell patch-clamp recordings were conducted. Slowly inactivating Ca^{2+} currents from patch-clamp recordings were considered as L-type Ca^{2+} currents based on comparisons to earlier

studies in native RPE as well as the use of channel modulators (-)BayK8644 (Rosenthal et al., 2007; Wimmers et al., 2008) and nifedipine (Rosenthal et al., 2007). VEGF secretion and phagocytosis were both altered after the modification of $Ca_V1.3$ with either an inhibitor or activator. After the activation of L-type Ca^{2+} channels, VEGF secretion increased and the inhibition of L-type Ca^{2+} channels, VEGF secretion decreased, respectively. L-type Ca^{2+} channels have been shown to be involved in the VEGF secretion (Mamaeva et al., 2021; Rosenthal et al., 2007) in hiPSC-RPE (Mamaeva et al., 2021), which supports the results obtained in **Study III** indicating the regulatory role of $Ca_V1.3$ in VEGF secretion in hESC-RPE as well. In addition, the regulatory role of L-type Ca^{2+} channels in phagocytosis has been established also by other studies (Karl et al., 2008; Mamaeva et al., 2021; Müller et al., 2014). In **Study III**, the phagocytosis capacity was reduced after the inhibition of L-type Ca^{2+} channels. Ion channels are known to cooperate with each other and abnormal lysosome morphology or defective vesicle trafficking occurs if the channel cooperation is in imbalance (Xiong & Zhu, 2016). For example, Bestrophin-1 (a Ca^{2+} activated Cl^- channel) is suggested to control the phagocytosis by altering the activity of L-type Ca^{2+} channels (Müller et al., 2014). This could explain the reduced phagocytosis capacity when the Ca^{2+} channels were inhibited and thus, the normal cooperation between the ion channels was blocked. These functional studies indeed indicate the presence of functional L-type Ca^{2+} channels in hESC-RPE cells, and since $Ca_V1.3$ is the major L-type Ca^{2+} channel subtype in the RPE, the immunostaining results together with functional studies verified the presence of $Ca_V1.3$ channels in hESC-RPE cells.

The correct localization of specific proteins can indicate proper maturation, but the functionality of the cells cannot be fully evaluated based on the immunofluorescence staining. When evaluating the maturity and functionality of the hESC-RPE cells, pigmentation, gene expression, functionality, and barrier properties should all be taken into consideration.

6.4 Limitations and future perspectives

hPSC-RPE research aiming for cell therapy applications to cure retinal degenerative diseases such as dry AMD must meet various criteria, as discussed in this thesis, for the therapy to be successful. RPE has a vital role in the well-being of photoreceptors and the whole neural retina. Therefore, the transplanted hPSC-RPE must resemble their native counterparts in many ways. (Sharma et al., 2020) In many studies, the

functional aspects of the hESC-RPE are poorly characterized. In clinical trials utilizing hPSC-RPE transplants, different culture times and quality criteria of hPSC-RPE are used. Although the current clinical trials mainly aim to secure the safety of the treatments, the overall maturity of the cells aimed for transplantation should be evaluated and well-defined criteria for functionality/maturation status set. This thesis provides a new insight of the *in vitro* maturation of the hESC-RPE cells and particularly, how the maturation status of the hESC-RPE cells affects the functions and characteristics of the hESC-RPE cells.

Native human RPE provides the best tissue to compare the quality and functions of the hESC-RPE cells in the research aiming for cell therapy. However, the access of native human tissue is limited which sets challenges when comparing RPE characteristics between native human RPE and hESC-derived RPE cells. Mouse tissue is commonly used cell model in RPE research due to its easy access, and freshly isolated mouse RPE was used in this thesis. However, it is worth noting that human and mouse RPE tissues do not fully match each other (Bennis et al., 2015).

In vitro maturation status of differentiated hPSC-RPE cells could play a crucial role in the stem cell therapies and currently, most studies evaluate the maturity of the hPSC-RPE cells based on their protein expression and phenotype such as pigmentation. In this thesis, the evaluation of protein expression by immunocytochemistry was also used as a routine assay. Culturing hESC-RPE cells is time-consuming and cell line-to-line and even batch-to-batch variation is common (Leach et al., 2016), making assessment of e.g. optimal culture times to gain various characteristics challenging. RPE-related protein expressions emerge in cultures gradually. For example, tight junction-associated protein ZO-1 is expressed relatively early whereas the other junctional proteins such as CL-19 is usually expressed later during the culture, coinciding with maturation/selective properties of RPE tight junctions. To gain a better overall view of the protein expressions, methods such as western blot or proteomics should be used to measure the quantity of the proteins. Another method to evaluate barrier property of RPE is TER measurement which is a quite simple, fast, and economical method. However, judging barrier properties by TER values alone is difficult due to the lack of reliable control cultures for comparison. E.g. human fetal RPE which is considered as the gold standard for cultured RPE, has TER values reported ranging from 500 to 2000 $\Omega \cdot cm^2$ (Peng et al., 2011) depending on the culture conditions used and it is not known which cell model resembles the native RPE the most.

Functional ion channels in hESC-RPE cells are important since the compromised functioning of the channels has been linked to various RPE malfunctions. Ca^{2+}

signalling is a versatile cell characteristic due to the high affinity of Ca^{2+} to bind cellular proteins and thus, modify the proteins. In this thesis, we showed that the prolonged culture time of the hESC-RPE affects the Ca^{2+} signalling properties advantageously. Ca^{2+} signalling is typically analysed from a few single cells. Here, analysis was performed from hundreds of cells on a single cell level revealing significant cell-cell heterogeneity within RPE populations. Another potential approach to measure the heterogeneity of the RPE population could be the use of single-cell transcriptomics (Parikh et al., 2023). The prospective implications of this heterogeneity to RPE functionality on population level or to cell therapy remain to be further studied.

As data presented in this thesis suggests, the level of *in vitro* maturation of the RPE cells at the time of transplantation may affect treatment efficacy via the ability of the cells to function post-transplantation. Nevertheless, more studies including *in vivo* transplantation experiments are needed to provide more in-depth knowledge on this aspect. To this date, hESC-RPE-related research has progressed significantly all the way to clinical trials even though the research still meets its challenges. The current status of the research holds great promise of the suitability of stem cells to be the cell source for future cell therapies.

7 CONCLUSIONS

The aim of this thesis was to understand the maturation of hESC-RPE cells *in vitro* by focusing on the achievement of functional characteristics similar to the native RPE and evaluating how maturation affects the ability of cells to tolerate cellular stress. Cultured hESC-RPE cells tend to be lacking fully mature status *in vitro*, which could cause unsuccessful outcomes in cell replacement therapies when attempting to cure retinal degenerative diseases such as AMD. Based on **Studies I-III**, the following main conclusions can be drawn:

1. Culture surface protein coatings affect the maturation and especially the homogeneity of the cryopreserved RPE cells (**Study I**).

    - A culture surface coated with Col-IV alone did not produce RPE cells with a proper morphology, and an intact epithelium was not formed.

    - By adding complexity to the protein coating used with the addition of linker protein Nidogen-1 to the combination of Col-IV and laminin 521, the hESC-RPE cells gained improved functionality regarding ATP-induced Ca^{2+} signalling.

    - The hESC-RPE cells matured with improved homogeneity when cultured with the combination of Col-IV + LN521 + Nid-1.

2. The maturation status of hESC-RPE cells affects their tolerance of cellular stress (**Study II**).

    - The hESC-RPE cells cultured for 3 weeks are more susceptible to cellular stress than longer cultured cells (12 weeks) since the hESC-RPE cells cultured for 3 weeks were not able to fully maintain their

functions, including ATP-mediated Ca^{2+} signalling and phagocytosis after the chemical treatments.

- Barrier properties, such as TER and the localization of CL-19, were altered especially at 3 weeks after the chemical treatments.

3. The maturation of hESC-RPE cells influences the L-type Ca^{2+} channels $Ca_V1.3$ that are essential for RPE physiology (**Study III**).

    - Localization of $Ca_V1.3$ shifted during RPE maturation from the cytoplasmic to the apical and basal membranes, resembling its localization *in vivo*.

    - Co-localization of $Ca_V1.3$ with the base of the primary cilium, pericentrin, was observed during RPE maturation.

8 REFERENCES

Abu Khamidakh, A. E., dos Santos, F. C., Skottman, H., Juuti-Uusitalo, K., & Hyttinen, J. (2016). Semi-automatic Method for Ca2+ Imaging Data Analysis of Maturing Human Embryonic Stem Cells-Derived Retinal Pigment Epithelium. *Annals of Biomedical Engineering*, *44*(11), 3408–3420. https://doi.org/10.1007/s10439-016-1656-9

Abu Khamidakh, A. E., Juuti-Uusitalo, K., Larsson, K., Skottman, H., & Hyttinen, J. (2013). Intercellular Ca2+ wave propagation in human retinal pigment epithelium cells induced by mechanical stimulation. *Experimental Eye Research*. https://doi.org/10.1016/j.exer.2013.01.009

Aisenbrey, S., Zhang, M., Bacher, D., Yee, J., Brunken, W. J., & Hunter, D. D. (2006). Retinal Pigment Epithelial Cells Synthesize Laminins, Including Laminin 5, and Adhere to Them through α3- and α6-Containing Integrins. *Investigative Opthalmology & Visual Science*, *47*(12), 5537. https://doi.org/10.1167/iovs.05-1590

Akanuma, S., Higashi, H., Maruyama, S., Murakami, K., Tachikawa, M., Kubo, Y., & Hosoya, K. (2018). Expression and function of connexin 43 protein in mouse and human retinal pigment epithelial cells as hemichannels and gap junction proteins. *Experimental Eye Research*, *168*(January 2017), 128–137. https://doi.org/10.1016/j.exer.2018.01.016

Al-Ani, A., Sunba, S., Hafeez, B., Toms, D., & Ungrin, M. (2020). In Vitro Maturation of Retinal Pigment Epithelium Is Essential for Maintaining High Expression of Key Functional Genes. *International Journal of Molecular Sciences*, *21*(17), 6066. https://doi.org/10.3390/ijms21176066

Alizadeh, M., Wada, M., Gelfman, C. M., Handa, J. T., & Hjelmeland, L. M. (2001). Downregulation of Differentiation Specific Gene Expression by Oxidative Stress in ARPE-19 Cells. *Retinal Cell Biology*, *42*(11), 2706–2713.

Ambati, J., Ambati, B. K., Yoo, S. H., Ianchulev, S., & Adamis, A. P. (2003). Age-Related Macular Degeneration: Etiology , Pathogenesis , and Therapeutic Strategies. *Survey of Ophthalmology*, *48*(3), 257–293. https://doi.org/10.1016/S0039-6257(03)00030-4

Ambati, J., Atkinson, J. P., & Gelfand, B. D. (2013). Immunology of age-related macular degeneration. *Nature Reviews. Immunology*, *13*(6), 438–451. https://doi.org/10.1038/nri3459

Anderson, J. M. (2001). Molecular Structure of Tight Junctions and Their Role in Epithelial Transport. *Physiology*, *16*(3), 126–130. https://doi.org/10.1152/physiologyonline.2001.16.3.126

Ban, Y., & Rizzolo, L. J. (2000). Regulation of glucose transporters during development of the retinal pigment epithelium. *Developmental Brain Research*, *121*, 89–95.

Beby, F., & Lamonerie, T. (2013). The homeobox gene Otx2 in development and disease. *Experimental Eye Research*, *111*, 9–16. https://doi.org/10.1016/j.exer.2013.03.007

Becerra, S. P., Fariss, R. N., Wu, Y. Q., Montuenga, L. M., Wong, P., & Pfeffer, B. A. (2004). Pigment epithelium-derived factor in the monkey retinal pigment epithelium and

interphotoreceptor matrix: Apical secretion and distribution. *Experimental Eye Research*, *78*, 223–234. https://doi.org/10.1016/j.exer.2003.10.013

Bellezza, I. (2018). Oxidative Stress in Age-Related Macular Degeneration: Nrf2 as Therapeutic Target. *Frontiers in Pharmacology*, *9*, 1280. https://doi.org/10.3389/fphar.2018.01280

Bellezza, I., Giambanco, I., Minelli, A., & Donato, R. (2018). Nrf2-Keap1 signaling in oxidative and reductive stress. *Biochimica et Biophysica Acta (BBA) - Molecular Cell Research*, *1865*(5), 721–733. https://doi.org/10.1016/j.bbamcr.2018.02.010

Benedicto, I., Lehmann, G. L., Ginsberg, M., Nolan, D. J., Bareja, R., Elemento, O., Salfati, Z., Alam, N. M., Prusky, G. T., Llanos, P., Rabbany, S. Y., Maminishkis, A., Miller, S. S., Rafii, S., & Rodriguez-Boulan, E. (2017). Concerted regulation of retinal pigment epithelium basement membrane and barrier function by angiocrine factors. *Nature Communications*, *8*(1), 15374. https://doi.org/10.1038/ncomms15374

Bennis, A., Gorgels, T. G. M. F., ten Brink, J. B., van der Spek, P. J., Bossers, K., Heine, V. M., & Bergen, A. A. (2015). Comparison of Mouse and Human Retinal Pigment Epithelium Gene Expression Profiles: Potential Implications for Age-Related Macular Degeneration. *PLoS ONE*, *10*(10), e0141597. https://doi.org/10.1371/journal.pone.0141597

Bennis, A., Jacobs, J. G., Catsburg, L. A. E., ten Brink, J. B., Koster, C., Schlingemann, R. O., van Meurs, J., Gorgels, T. G. M. F., Moerland, P. D., Heine, V. M., & Bergen, A. A. (2017). Stem Cell Derived Retinal Pigment Epithelium: The Role of Pigmentation as Maturation Marker and Gene Expression Profile Comparison with Human Endogenous Retinal Pigment Epithelium. *Stem Cell Reviews and Reports*, 659–669. https://doi.org/10.1007/s12015-017-9754-0

Bermond, K., Wobbe, C., Tarau, I.-S., Heintzmann, R., Hillenkamp, J., Curcio, C. A., Sloan, K. R., & Ach, T. (2020). Autofluorescent Granules of the Human Retinal Pigment Epithelium: Phenotypes, Intracellular Distribution, and Age-Related Topography. *Investigative Opthalmology & Visual Science*, *61*(5), 35. https://doi.org/10.1167/iovs.61.5.35

Berridge, M. J., Bootman, M. D., & Roderick, H. L. (2003). Calcium signalling: Dynamics, homeostasis and remodelling. *Nature Reviews Molecular Cell Biology*, *4*(7), Article 7. https://doi.org/10.1038/nrm1155

Berridge, M. J., Lipp, P., & Bootman, M. D. (2000). The versatility and universality of calcium signalling. *Nature Reviews Molecular Cell Biology*, *1*, 11–21.

Bharti, K., Gasper, M., Ou, J., Brucato, M., Clore-Gronenborn, K., Pickel, J., & Arnheiter, H. (2012). A Regulatory Loop Involving PAX6, MITF, and WNT Signaling Controls Retinal Pigment Epithelium Development. *PLOS Genetics*, *8*(7), e1002757. https://doi.org/10.1371/journal.pgen.1002757

Bharti, K., Rao, M., Hull, S. C., Stroncek, D., Brooks, B. P., Feigal, E., van Meurs, J. C., Huang, C. A., & Miller, S. S. (2014). Developing Cellular Therapies for Retinal Degenerative Diseases. *Investigative Ophthalmology & Visual Science*, *55*(2), 1191–1202. https://doi.org/10.1167/iovs.13-13481

Bisbach, C. M., Hass, D. T., Robbings, B. M., Rountree, A. M., Sadilek, M., Sweet, I. R., & Hurley, J. B. (2020). Succinate Can Shuttle Reducing Power from the Hypoxic Retina to the O2-Rich Pigment Epithelium. *Cell Reports*, *31*(5), 107606. https://doi.org/10.1016/j.celrep.2020.107606

Blaauwgeers, H. G. T., Holtkamp, G. M., Rutten, H., Witmer, A. N., Koolwijk, P., Partanen, T. A., Alitalo, K., Kroon, M. E., Kijlstra, A., van Hinsbergh, V. W. M., &

Schlingemann, R. O. (1999). Polarized Vascular Endothelial Growth Factor Secretion by Human Retinal Pigment Epithelium and Localization of Vascular Endothelial Growth Factor Receptors on the Inner Choriocapillaris. *The American Journal of Pathology*, *155*(2), 421–428.

Blasiak, J., Pawlowska, E., Szczepanska, J., & Kaarniranta, K. (2019). Interplay between Autophagy and the Ubiquitin-Proteasome System and Its Role in the Pathogenesis of Age-Related Macular Degeneration. *International Journal of Molecular Sciences*, *20*(1). https://doi.org/10.3390/ijms20010210

Blenkinsop, T. A., Saini, J. S., Maminishkis, A., Bharti, K., Wan, Q., Banzon, T., Lotfi, M., Davis, J., Singh, D., Rizzolo, L. J., Miller, S., Temple, S., & Stern, J. H. (2015). Human Adult Retinal Pigment Epithelial Stem Cell–Derived RPE Monolayers Exhibit Key Physiological Characteristics of Native Tissue. *Investigative Ophthalmology & Visual Science*, *56*(12), 7085–7099. https://doi.org/10.1167/iovs.14-16246

Blitzer, A. L., Panagis, L., Gusella, G. L., Danias, J., Mlodzik, M., & Iomini, C. (2011). Primary cilia dynamics instruct tissue patterning and repair of corneal endothelium. *Proceedings of the National Academy of Sciences of the United States of America*, *108*(7), 2819–2824. https://doi.org/10.1073/pnas.1016702108

Bok, D. (1993). The retinal pigment epithelium: A versatile partner in vision. *Epithelial and Neuronal Cell Polarity and Differentiation*, 189–195.

Boulton, M. (1991). Ageing of the retinal pigment epithelium. *Progress in Retinal Research*, *11*, 125–151.

Boulton, M., Rózanowska, M., Rózanowski, B., & Wess, T. (2004). The photoreactivity of ocular lipofuscin. *Photochemical and Photobiological Sciences*, *3*(8), 759–764. https://doi.org/10.1039/b400108g

Bowes Rickman, C., LaVail, M. M., Anderson, R. E., Grimm, C., Hollyfield, J., & Ash, J. (Eds.). (2016). *Retinal Degenerative Diseases: Mechanisms and Experimental Therapy* (Vol. 854). Springer International Publishing. https://doi.org/10.1007/978-3-319-17121-0

Buchholz, D. E., Hikita, S. T., Rowland, T. J., Friedrich, A. M., Hinman, C. R., Johnson, L. V., & Clegg, D. O. (2009). Derivation of Functional Retinal Pigmented Epithelium from Induced Pluripotent Stem Cells. *Stem Cells*, *27*(10), 2427–2434. https://doi.org/10.1002/stem.189

Buchholz, D. E., Pennington, B. O., Croze, R. H., Hinman, C. R., Coffey, P. J., & Clegg, D. O. (2013). Rapid and Efficient Directed Differentiation of Human Pluripotent Stem Cells Into Retinal Pigmented Epithelium. *Stem Cells Translational Medicine*, *2*(5), 384–393. https://doi.org/10.5966/sctm.2012-0163

Burke, J. (2008). Epithelial phenotype and the RPE: Is the answer blowing in the Wnt? *Progress in Retinal and Eye Research*, *27*(6), 579–595. https://doi.org/10.1016/j.preteyeres.2008.08.002

Cavodeassi, F., & Bovolenta, P. (2014). New functions for old genes: Pax6 and Mitf in eye pigment biogenesis. *Pigment Cell & Melanoma Research*, *27*(6), 1005–1007. https://doi.org/10.1111/pcmr.12308

Chaitin, M. H., & Hall, M. O. (1983). Defective Ingesfion of Rod Outer Segments by Cultured Dystrophic Rot Pigment Epithelial Cells. *Investigative Ophthalmology & Visual Science*, *24*(7), 812–820.

Chin, D., & Means, A. R. (2000). Calmodulin: A prototypical calcium sensor. *Trends in Cell Biology*, *10*(8), 322–328. https://doi.org/10.1016/S0962-8924(00)01800-6

Choi, E.-J., Choi, G.-W., Kim, J. H., Jang, H.-W., Lee, J.-H., Bae, H. J., Kim, Y. G., Lee, Y.-B., & Cho, H.-Y. (2020). A Novel Eye Drop Candidate for Age-Related Macular

Degeneration Treatment: Studies on its Pharmacokinetics and Distribution in Rats and Rabbits. *Molecules*, *25*(3), 663. https://doi.org/10.3390/molecules25030663

Choudhary, P., Booth, H., Gutteridge, A., Surmacz, B., Louca, I., Steer, J., Kerby, J., & Whiting, P. J. (2017). Directing Differentiation of Pluripotent Stem Cells Toward Retinal Pigment Epithelium Lineage. *Stem Cells Translational Medicine*, *6*(2), 490–501. https://doi.org/10.5966/sctm.2016-0088

Clapham, D. E. (2007). Calcium Signaling. *Cell*, *131*(6), 1047–1058. https://doi.org/10.1016/j.cell.2007.11.028

Compochioro, P. A., Hackeit, S. F., & Conway, B. P. (1991). Retinoic Acid Promotes Density-Dependent Growth Arrest in Humon Retinal Pigment Epithelial Cells. *INVESTIGATIVE OPHTHALMOLOGY*, *1*.

Cordeiro, S., Seyler, S., Stindl, J., Milenkovic, V. M., & Strauss, O. (2010). Heat-sensitive TRPV channels in retinal pigment epithelial cells: Regulation of VEGF-A secretion. *Investigative Ophthalmology & Visual Science*, *51*(11), 6001–6008. https://doi.org/10.1167/iovs.09-4720

Curcio, C. A., & Johnson, M. (2013). Structure, Function, and Pathology of Bruch's Membrane. In *Anatomy and Physiology* (pp. 465–481).

Da Cruz, L., Fynes, K., Georgiadis, O., Kerby, J., Luo, Y. H., Ahmado, A., Vernon, A., Daniels, J. T., Nommiste, B., Hasan, S. M., Gooljar, S. B., Carr, A. J. F., Vugler, A., Ramsden, C. M., Bictash, M., Fenster, M., Steer, J., Harbinson, T., Wilbrey, A., … Coffey, P. J. (2018). Phase 1 clinical study of an embryonic stem cell-derived retinal pigment epithelium patch in age-related macular degeneration. *Nature Biotechnology*, *36*(4), 328–337. https://doi.org/10.1038/nbt.4114

Datta, S., Cano, M., Ebrahimi, K., Wang, L., & Handa, J. T. (2017). The impact of oxidative stress and inflammation on RPE degeneration in non-neovascular AMD. *Progress in Retinal and Eye Research*, *60*, 201–218. https://doi.org/10.1016/j.preteyeres.2017.03.002

Dawson, D. W., Volpert, O. V., Gillis, P., Crawford, S. E., Xu, H., Benedict, W., & Bouck, N. P. (1999). Pigment Epithelium – Derived Factor: A Potent Inhibitor of Angiogenesis. *Science*, *285*(July), 245–249.

de Jong, S., Tang, J., & Clark, S. J. (2023). Age-related macular degeneration: A disease of extracellular complement amplification. *Immunological Reviews*, *313*(1), 279–297. https://doi.org/10.1111/imr.13145

Dehghan, S., Mirshahi, R., Shoae-Hassani, A., & Naseripour, M. (2022). Human-induced pluripotent stem cells-derived retinal pigmented epithelium, a new horizon for cells-based therapies for age-related macular degeneration. *Stem Cell Research & Therapy*, *13*(1), 217. https://doi.org/10.1186/s13287-022-02894-0

Delaval, B., & Doxsey, S. J. (2010). Pericentrin in cellular function and disease. *The Journal of Cell Biology*, *188*(2), 181–190. https://doi.org/10.1083/jcb.200908114

Detrick, B., & Hooks, J. J. (2020). The RPE Cell and the Immune System. In A. K. Klettner & S. Dithmar (Eds.), *Retinal Pigment Epithelium in Health and Disease* (pp. 101–114). Springer International Publishing. https://doi.org/10.1007/978-3-030-28384-1_6

Dunn, K. C., Aotaki-keen, A. E., Putkey, F. R., & Hjelmeland, L. M. (1996). ARPE-19, A Human Retinal Pigment Epithelial Cell Line with Differentiated Properties. *Experimental Eye Research*, *62*(2), 155–170. https://doi.org/10.1006/exer.1996.0020

Fabre, M., Mateo, L., Lamaa, D., Baillif, S., Pagès, G., Demange, L., Ronco, C., & Benhida, R. (2022). Recent Advances in Age-Related Macular Degeneration Therapies. *Molecules*, *27*(16), 5089. https://doi.org/10.3390/molecules27165089

Fadjukov, J., Wienbar, S., Hakanen, S., Aho, V., Vihinen-Ranta, M., Ihalainen, T. O., Schwartz, G. W., & Nymark, S. (2022). Gap junctions and connexin hemichannels both contribute to the electrical properties of retinal pigment epithelium. *Journal of General Physiology*, *154*(4), e202112916. https://doi.org/10.1085/jgp.202112916

Farazdaghi, M., & Ebrahimi, K. (2019). Role of the choroid in age-related macular degeneration: A current review. *Journal of Ophthalmic and Vision Research*, *14*(1), 78. https://doi.org/10.4103/jovr.jovr_125_18

Finnemann, S. C. (2003). Focal adhesion kinase signaling promotes phagocytosis of integrin-bound photoreceptors. *EMBO Journal*, *22*(16), 4143–4154.

Finnemann, S. C., & Nandrot, E. F. (2006). MERTK ACTIVATION DURING RPE PHAGOCYTOSIS IN VIVO REQUIRES αVβ5 INTEGRIN. *Advances in Experimental Medicine and Biology*, *572*, 499–503. https://doi.org/10.1007/0-387-32442-9_69

Fronk, A. H., & Vargis, E. (2016). Methods for culturing retinal pigment epithelial cells: A review of current protocols and future recommendations. *Journal of Tissue Engineering*, *7*, 204173141665083. https://doi.org/10.1177/2041731416650838

Gehring, W. J. (1996). The master control gene for morphogenesis and evolution of the eye. *Genes to Cells*, *1*(1), 11–15. https://doi.org/10.1046/j.1365-2443.1996.11011.x

Geng, Z., Walsh, P. J., Truong, V., Hill, C., Ebeling, M., Kapphahn, R. J., Montezuma, S. R., Yuan, C., Roehrich, H., Ferrington, D. A., & Dutton, J. R. (2017). Generation of retinal pigmented epithelium from iPSCs derived from the conjunctiva of donors with and without age related macular degeneration. *PLoS ONE*, *12*(3), e0173575. https://doi.org/10.1371/journal.pone.0173575

George, S. M., Lu, F., Rao, M., Leach, L. L., & Gross, J. M. (2021). The retinal pigment epithelium: Development, injury responses, and regenerative potential in mammalian and non-mammalian systems. *Progress in Retinal and Eye Research*, *85*, 100969. https://doi.org/10.1016/j.preteyeres.2021.100969

Giardina, S. F., Mikami, M., Goubaeva, F., & Yang, J. (2007). Connexin 43 Confers Resistance to Hydrogen Peroxide-Mediated Apoptosis. *Biochemical and Biophysical Research Communications*, *362*(3), 747–752.

Goldstein, E. B. (1970). Cone pigment regeneration in the isolated frog retina. *Vision Research*, *10*(10), 1065–1068. https://doi.org/10.1016/0042-6989(70)90082-9

Gonzalez-Fernandez, F. (2003). Interphotoreceptor retinoid-binding protein — an old gene for new eyes. *Vision Research*, *43*(28), 3021–3036. https://doi.org/10.1016/j.visres.2003.09.019

Gottlieb, E., Armour, S. M., Harris, M. H., & Thompson, C. B. (2003). Mitochondrial membrane potential regulates matrix configuration and cytochrome c release during apoptosis. *Cell Death & Differentiation*, *10*(6), Article 6. https://doi.org/10.1038/sj.cdd.4401231

Guimaraes, T. A. C. de, Varela, M. D., Georgiou, M., & Michaelides, M. (2022). Treatments for dry age-related macular degeneration: Therapeutic avenues, clinical trials and future directions. *British Journal of Ophthalmology*, *106*(3), 297–304. https://doi.org/10.1136/bjophthalmol-2020-318452

Gullapalli, V. K., Sugino, I. K., Van Patten, Y., Shah, S., & Zarbin, M. A. (2005). Impaired RPE survival on aged submacular human Bruch's membrane. *Experimental Eye Research*, *80*(2), 235–248. https://doi.org/10.1016/j.exer.2004.09.006

Guo, X., Zhu, D., Lian, R., Han, Y., Guo, Y., Li, Z., Tang, S., & Chen, J. (2016). Matrigel and Activin A promote cell-cell contact and anti-apoptotic activity in cultured human

retinal pigment epithelium cells. *Experimental Eye Research*, *147*, 37–49. https://doi.org/10.1016/j.exer.2016.04.021

Hageman, G. S., Luthert, P. J., Chong, N. H. V., Johnson, L. V., Anderson, D. H., & Mullins, R. F. (2001). An Integrated Hypothesis That Considers Drusen as Biomarkers of Immune-Mediated Processes at the RPE-Bruch ' s Membrane Interface in Aging and. *Progress in Retinal and Eye Research*, *20*(6), 705–732.

Hazim, R. A., Karumbayaram, S., Jiang, M., Dimashkie, A., Lopes, V. S., Li, D., Burgess, B. L., Vijayaraj, P., Alva-Ornelas, J. A., Zack, J. A., Kohn, D. B., Gomperts, B. N., Pyle, A. D., Lowry, W. E., & Williams, D. S. (2017). Differentiation of RPE cells from integration-free iPS cells and their cell biological characterization. *Stem Cell Research & Therapy*, *8*(1), 217. https://doi.org/10.1186/s13287-017-0652-9

Higuchi, A., Kumar, S. S., Benelli, G., Alarfaj, A. A., Munusamy, M. A., Umezawa, A., & Murugan, K. (2017). Stem Cell Therapies for Reversing Vision Loss. *Trends in Biotechnology*, *35*(11), 1102–1117. https://doi.org/10.1016/j.tibtech.2017.06.016

Himpens, B., Stalmans, P., Gomez, P., Malfait, M., & Vereecke, J. (1999). Intra- and intercellular Ca2+ signaling in retinal pigment epithelial cells during mechanical stimulation. *The FASEB Journal*, *13*(9001), S63–S68. https://doi.org/10.1096/fasebj.13.9001.s63

Hohenester, E. (2019). Structural biology of laminins. *Essays in Biochemistry*, *63*(3), 285–295. https://doi.org/10.1042/EBC20180075

Hollyfield, J. G., Bonilha, V. L., Rayborn, M. E., Yang, X., Shadrach, K. G., Lu, L., Ufret, R. L., Salomon, R. G., & Perez, V. L. (2008). Oxidative damage–induced inflammation initiates age-related macular degeneration. *Nature Medicine*, *14*(2), Article 2. https://doi.org/10.1038/nm1709

Holtkamp, G. M., Kijlstra, A., Peek, R., & De Vos, A. F. (2001). Retinal pigment epithelium-immune system interactions: Cytokine production and cytokine-induced changes. *Progress in Retinal and Eye Research*, *20*(1), 29–48. https://doi.org/10.1016/S1350-9462(00)00017-3

Hongisto, H., Ilmarinen, T., Vattulainen, M., Mikhailova, A., & Skottman, H. (2017). Xeno- and feeder-free differentiation of human pluripotent stem cells to two distinct ocular epithelial cell types using simple modifications of one method. *Stem Cell Research and Therapy*, *8*(1), 1–15. https://doi.org/10.1186/s13287-017-0738-4

Hongisto, H., Jylhä, A., Nättinen, J., Rieck, J., & Ilmarinen, T. (2017). Comparative proteomic analysis of human embryonic stem cell-derived and primary human retinal pigment epithelium. *Scientific Reports*, *7*(June). https://doi.org/10.1038/s41598-017-06233-9

Hsiung, J., Zhu, D., & Hinton, D. R. (2015). Polarized Human Embryonic Stem Cell-Derived Retinal Pigment Epithelial Cell Monolayers Have Higher Resistance to Oxidative Stress-Induced Cell Death Than Nonpolarized Cultures. *STEM CELLS Translational Medicine*, *4*(1), 10–20. https://doi.org/10.5966/sctm.2014-0205

Hu, J. G., Gallemore, R. P., Bok, D., Lee, A. Y., & Frambach, D. A. (1994). Localization of NaK ATPase on cultured human retinal pigment epithelium. *Investigative Ophthalmology & Visual Science*, *35*(10), 3582–3588.

Huang, H., Li, H., Shi, K., Wang, L., Zhang, X., & Zhu, X. (2018). TREK-TRAAK two-pore domain potassium channels protect human retinal pigment epithelium cells from oxidative stress. *International Journal of Molecular Medicine*, *42*(5), 2584–2594. https://doi.org/10.3892/ijmm.2018.3813

Hurley, J. B. (2021). Retina Metabolism and Metabolism in the Pigmented Epithelium: A Busy Intersection. *Annual Review of Vision Science*, *7*, 665–692. https://doi.org/10.1146/annurev-vision-100419-115156

Hutnik, C. M. L., Pocrnich, C. E., Liu, H., Laird, D. W., & Shao, Q. (2008). The Protective Effect of Functional Connexin43 Channels on a Human Epithelial Cell Line Exposed to Oxidative Stress. *Investigative Ophthalmology & Visual Science*, *49*(2), 800–806. https://doi.org/10.1167/iovs.07-0717

Hyttinen, J. M. T., Petrovski, G., Salminen, A., & Kaarniranta, K. (2011). 5 ' -Adenosine Monophosphate-Activated Protein Kinase – Mammalian Target of Rapamycin Axis As Therapeutic Target for Age-Related Macular Degeneration. *Rejuvenation Research*, *14*(6).

Hyttinen, J. M. T., Viiri, J., Kaarniranta, K., & Błasiak, J. (2018). Mitochondrial quality control in AMD: Does mitophagy play a pivotal role? *Cellular and Molecular Life Sciences: CMLS*, *75*(16), 2991–3008. https://doi.org/10.1007/s00018-018-2843-7

Ilmarinen, T., Thieltges, F., Hongisto, H., Juuti-uusitalo, K., Koistinen, A., Kaarniranta, K., Brinken, R., Braun, N., Holz, F. G., Skottman, H., & Stanzel, B. V. (2019). Survival and functionality of xeno-free human embryonic stem cell – derived retinal pigment epithelial cells on polyester substrate after transplantation in rabbits. *Acta Ophthalmologica*, 688–699. https://doi.org/10.1111/aos.14004

Ishihara, J., Ishihara, A., Fukunaga, K., Sasaki, K., White, M. J. V., Briquez, P. S., & Hubbell, J. A. (2018). Laminin heparin-binding peptides bind to several growth factors and enhance diabetic wound healing. *Nature Communications*, *9*(1), Article 1. https://doi.org/10.1038/s41467-018-04525-w

Jager, R. D., Mieler, W. F., & Miller, J. W. (2008). Age-related macular degeneration. *The New England Journal of Medicine*, *358*(24), 2606–2617. https://doi.org/10.1056/NEJMra0801537

Jayadev, R., & Sherwood, D. R. (2017). Basement membranes. *Current Biology*, *27*(6), R207–R211. https://doi.org/10.1016/j.cub.2017.02.006

Jiang, S., Park, D. W., Gao, Y., Ravi, S., Darley-Usmar, V., Abraham, E., & Zmijewski, J. W. (2015). Participation of proteasome-ubiquitin protein degradation in autophagy and the activation of AMP-activated protein kinase. *Cell Signal*, *27*(6), 1186–1197.

Johansson, J. K., Karema-jokinen, V. I., Hakanen, S., Jylhä, A., Uusitalo, H., Vihinen-ranta, M., Skottman, H., Ihalainen, T. O., & Nymark, S. (2019). Sodium channels enable fast electrical signaling and regulate phagocytosis in the retinal pigment epithelium. *BMC Biology*, *17*(63).

Juel, H. B., Faber, C., Svendsen, S. G., Vallejo, A. N., & Nissen, M. H. (2013). Inflammatory Cytokines Protect Retinal Pigment Epithelial Cells from Oxidative Stress-Induced Death. *PLoS ONE*, *8*(5). https://doi.org/10.1371/journal.pone.0064619

Jurczyk, A., Gromley, A., Redick, S., Agustin, J. S., Witman, G., Pazour, G. J., Peters, D. J. M., & Doxsey, S. (2004). Pericentrin forms a complex with intraflagellar transport proteins and polycystin-2 and is required for primary cilia assembly. *Journal of Cell Biology*, *166*(5), 637–643. https://doi.org/10.1083/jcb.200405023

Juuti-Uusitalo, K., Nieminen, M., Treumer, F., Ampuja, M., Kallioniemi, A., Klettner, A., & Skottman, H. (2015). Effects of cytokine activation and oxidative stress on the function of the human embryonic stem cell–derived retinal pigment epithelial cells. *Investigative Ophthalmology and Visual Science*, *56*(11), 6265–6274. https://doi.org/10.1167/iovs.15-17333

Kaarniranta, K., Hyttinen, J., Ryhänen, T., Viiri, J., Paimela, T., Toropainen, E., Sorri, I., & Salminen, A. (2010). Mechanisms of protein aggregation in the retinal pigment epithelial cells. *Frontiers in Bioscience-Elite*, *1*(2), 1374–1384.

Kaiser, S. M., Arepalli, S., & Ehlers, J. P. (2021). Current and Future Anti-VEGF Agents for Neovascular Age-Related Macular Degeneration. *Journal of Experimental Pharmacology*, *13*, 905–912. https://doi.org/10.2147/JEP.S259298

Karl, M. O., Kroeger, W., Wimmers, S., Milenkovic, V. M., Valtink, M., Engelmann, K., & Strauss, O. (2008). Endogenous Gas6 and Ca2+-channel activation modulate phagocytosis by retinal pigment epithelium. *Cellular Signalling*, *20*(6), 1159–1168. https://doi.org/10.1016/j.cellsig.2008.02.005

Kashani, A. H., Lebkowski, J. S., Rahhal, F. M., Avery, R. L., Salehi-Had, H., Chen, S., Chan, C., Palejwala, N., Ingram, A., Dang, W., Lin, C.-M., Mitra, D., Pennington, B. O., Hinman, C., Faynus, M. A., Bailey, J. K., Mohan, S., Rao, N., Johnson, L. V., … Humayun, M. S. (2021). One-Year Follow-Up in a Phase 1/2a Clinical Trial of an Allogeneic RPE Cell Bioengineered Implant for Advanced Dry Age-Related Macular Degeneration. *Translational Vision Science & Technology*, *10*(10), 13. https://doi.org/10.1167/tvst.10.10.13

Kashani, A. H., Lebkowski, J. S., Rahhal, F. M., Avery, R. L., Salehi-Had, H., Dang, W., Lin, C. M., Mitra, D., Zhu, D., Thomas, B. B., Hikita, S. T., Pennington, B. O., Johnson, L. V., Clegg, D. O., Hinton, D. R., & Humayun, M. S. (2018). A bioengineered retinal pigment epithelial monolayer for advanced, dry age-related macular degeneration. *Science Translational Medicine*, *10*(435), 1–11. https://doi.org/10.1126/scitranslmed.aao4097

Kauppinen, A., Paterno, J. J., Blasiak, J., Salminen, A., & Kaarniranta, K. (2016). Inflammation and its role in age-related macular degeneration. *Cellular and Molecular Life Sciences*, *73*(9), 1765–1786. https://doi.org/10.1007/s00018-016-2147-8

Kennedy, B. G., Torabi, A. J., Kurzawa, R., Echtenkamp, S. F., & Mangini, N. J. (2010). Expression of transient receptor potential vanilloid channels TRPV5 and TRPV6 in retinal pigment epithelium. *Molecular Vision*, *16*, 665–675.

Kimura, K., & Nishida, T. (2010). Role of the Ubiquitin-Proteasome Pathway in Downregulation of the Gap-Junction Protein Connexin43 by TNF-α in Human Corneal Fibroblasts. *Investigative Ophthalmology & Visual Science*, *51*(4), 1943–1947. https://doi.org/10.1167/iovs.09-3573

Klettner, A., Kaya, L., Flach, J., Lassen, J., Treumer, F., & Roider, J. (2015). Basal and apical regulation of VEGF-A and placenta growth factor in the RPE/choroid and primary RPE. *Molecular Vision*, *21*, 736–748.

Knickelbein, J. E., Chan, C.-C., Sen, H. N., Ferris, F. L., & Nussenblatt, R. B. (2015). Inflammatory mechanisms of age-related macular degeneration. *International Ophthalmology Clinics*, *55*(3), 63–78. https://doi.org/10.1097/IIO.0000000000000073

Kojima, A., Nakahama, K. ichi, Ohno-Matsui, K., Shimada, N., Mori, K., Iseki, S., Sato, T., Mochizuki, M., & Morita, I. (2008). Connexin 43 contributes to differentiation of retinal pigment epithelial cells via cyclic AMP signaling. *Biochemical and Biophysical Research Communications*, *366*(2), 532–538. https://doi.org/10.1016/j.bbrc.2007.11.159

Korkka, I., Skottman, H., & Nymark, S. (2022). Heterogeneity of Potassium Channels in Human Embryonic Stem Cell-Derived Retinal Pigment Epithelium. *Stem Cells Translational Medicine*, *11*(7), 753–766. https://doi.org/10.1093/stcltm/szac029

Korte, G. E., & Wanderman, M. C. (1993). Distribution of Na+ K+-ATPase in Regenerating Retinal Pigment Epithelium in the Rabbit. A Study by Electron Microscopic Cytochemistry. *Experimental Eye Research*, *56*(2), 219–229. https://doi.org/10.1006/exer.1993.1029

Laing, J. G., & Beyer, E. C. (1995). The Gap Junction Protein Connexin43 Is Degraded via the Ubiquitin Proteasome Pathway (*). *Journal of Biological Chemistry*, *270*(44), 26399–26403. https://doi.org/10.1074/jbc.270.44.26399

Laing, J. G., Tadros, P. N., Westphale, E. M., & Beyer, E. C. (1997). Degradation of Connexin43 Gap Junctions Involves both the Proteasome and the Lysosome. *Experimental Cell Research*, *236*(2), 482–492. https://doi.org/10.1006/excr.1997.3747

Lakkaraju, A., Umapathy, A., Tan, L. X., Daniele, L., Philp, N. J., Boesze-Battaglia, K., & Williams, D. S. (2020). The cell biology of the retinal pigment epithelium. *Progress in Retinal and Eye Research*, 100846. https://doi.org/10.1016/j.preteyeres.2020.100846

Laurent, V., Sengupta, A., Sánchez-Bretaño, A., Hicks, D., & Tosini, G. (2017). Melatonin signaling affects the timing in the daily rhythm of phagocytic activity by the retinal pigment epithelium. *Experimental Eye Research*, *165*, 90–95. https://doi.org/10.1016/j.exer.2017.09.007

Leach, L. L., Croze, R. H., Hu, Q., Nadar, V. P., Clevenger, T. N., Pennington, B. O., Gamm, D. M., & Clegg, D. O. (2016). Induced Pluripotent Stem Cell-Derived Retinal Pigmented Epithelium: A Comparative Study Between Cell Lines and Differentiation Methods. *Journal of Ocular Pharmacology and Therapeutics*, *32*(5), 317–330. https://doi.org/10.1089/jop.2016.0022

Lemon, G., Gibson, W. G., & Bennett, M. R. (2003). Metabotropic receptor activation, desensitization and sequestration—I: Modelling calcium and inositol 1,4,5-trisphosphate dynamics following receptor activation. *Journal of Theoretical Biology*, *223*(1), 93–111. https://doi.org/10.1016/S0022-5193(03)00079-1

Léveillard, T., Philp, N. J., & Sennlaub, F. (2019). Is Retinal Metabolic Dysfunction at the Center of the Pathogenesis of Age-related Macular Degeneration? *International Journal of Molecular Sciences*, *20*(3), 762. https://doi.org/10.3390/ijms20030762

Li, Q.-Y., Zou, T., Gong, Y., Chen, S.-Y., Zeng, Y.-X., Gao, L.-X., Weng, C.-H., Xu, H.-W., & Yin, Z.-Q. (2021). Functional assessment of cryopreserved clinical grade hESC-RPE cells as a qualified cell source for stem cell therapy of retinal degenerative diseases. *Experimental Eye Research*, *202*, 108305. https://doi.org/10.1016/j.exer.2020.108305

Liu, F., Peng, S., Adelman, R. A., & Rizzolo, L. J. (2021). Knockdown of claudin-19 in the retinal pigment epithelium is accompanied by slowed phagocytosis and increased expression of SQSTM1. *Investigative Ophthalmology and Visual Science*, *62*(2), 1–3. https://doi.org/10.1167/IOVS.62.2.14

Liu, F., Xu, T., Peng, S., Adelman, R. A., & Rizzolo, L. J. (2020). Claudins regulate gene and protein expression of the retinal pigment epithelium independent of their association with tight junctions. *Experimental Eye Research*, *198*(198), 108157. https://doi.org/10.1016/j.exer.2020.108157

Liu, Z., Ilmarinen, T., Tan, G. S. W., Hongisto, H., Wong, E. Y. M., Tsai, A. S. H., Al-nawaiseh, S., Holder, G. E., Su, X., & Barathi, V. A. (2021). Submacular integration of hESC-RPE monolayer xenografts in a surgical non-human primate model. *Stem Cell Research and Therapy*, *12*, 1–16.

Liu, Z., Qin, T., Zhou, J., Taylor, A., Sparrow, J. R., & Shang, F. (2016). *Impairment of the ubiquitin-proteasome pathway in rpe alters the expression of inflammation related genes*. *854*, 237–250. https://doi.org/10.1007/978-3-319-17121-0

Lobato-Álvarez, J. A., Roldán, M. L., López-Murillo, T. del C., González-Ramírez, R., Bonilla-Delgado, J., & Shoshani, L. (2016). The Apical Localization of Na+, K+-ATPase in Cultured Human Retinal Pigment Epithelial Cells Depends on Expression of the β2 Subunit. *Frontiers in Physiology*, *7*, 450. https://doi.org/10.3389/fphys.2016.00450

Luo, Y., Zhuo, Y., Fukuhara, M., & Rizzolo, L. J. (2006). Effects of Culture Conditions on Heterogeneity and the Apical Junctional Complex of the ARPE-19 Cell Line. *Investigative Opthalmology & Visual Science*, *47*(8), 3644. https://doi.org/10.1167/iovs.06-0166

Ma, X., Li, H., Chen, Y., Yang, J., Chen, H., Arnheiter, H., & Hou, L. (2019). The transcription factor MITF in RPE function and dysfunction. *Progress in Retinal and Eye Research*, *73*, 100766. https://doi.org/10.1016/j.preteyeres.2019.06.002

Maeda, T., Lee, M. J., Palczewska, G., Marsili, S., Tesar, P. J., Palczewski, K., Takahashi, M., & Maeda, A. (2013). Retinal Pigmented Epithelial Cells Obtained from Human Induced Pluripotent Stem Cells Possess Functional Visual Cycle Enzymes in Vitro and in Vivo. *Journal of Biological Chemistry*, *288*(48), 34484–34493. https://doi.org/10.1074/jbc.M113.518571

Maeda, T., Sugita, S., Kurimoto, Y., & Takahashi, M. (2021). Trends of Stem Cell Therapies in Age-Related Macular Degeneration. *Journal of Clinical Medicine*, *10*(8), Article 8. https://doi.org/10.3390/jcm10081785

Mamaeva, D., Jazouli, Z., DiFrancesco, M. L., Erkilic, N., Dubois, G., Hilaire, C., Meunier, I., Boukhaddaoui, H., & Kalatzis, V. (2021). Novel roles for voltage-gated T-type Ca2+ and ClC-2 channels in phagocytosis and angiogenic factor balance identified in human iPSC-derived RPE. *The FASEB Journal*, *35*(4), e21406. https://doi.org/10.1096/fj.202002754R

Maminishkis, A., Chen, S., Jalickee, S., Banzon, T., Shi, G., Wang, F. E., Ehalt, T., Hammer, J. A., & Miller, S. S. (2006). Confluent Monolayers of Cultured Human Fetal Retinal Pigment Epithelium Exhibit Morphology and Physiology of Native Tissue. *Investigative Ophthalmology & Visual Science*, *47*(8), 3612–3624. https://doi.org/10.1167/iovs.05-1622

Mandai, M., Watanabe, A., Kurimoto, Y., Hirami, Y., Morinaga, C., Daimon, T., Fujihara, M., Akimaru, H., Sakai, N., Shibata, Y., Terada, M., Nomiya, Y., Tanishima, S., Nakamura, M., Kamao, H., Sugita, S., Onishi, A., Ito, T., Fujita, K., … Takahashi, M. (2017). Autologous Induced Stem-Cell–Derived Retinal Cells for Macular Degeneration. *New England Journal of Medicine*, *376*(11), 1038–1046. https://doi.org/10.1056/nejmoa1608368

Markert, E. K., Klein, H., Viollet, C., Rust, W., Strobel, B., Kauschke, S. G., Makovoz, B., Neubauer, H., Bakker, R. A., & Blenkinsop, T. A. (2022). Transcriptional comparison of adult human primary Retinal Pigment Epithelium, human pluripotent stem cell-derived Retinal Pigment Epithelium, and ARPE19 cells. *Frontiers in Cell and Developmental Biology*, *10*, 910040. https://doi.org/10.3389/fcell.2022.910040

Marmorstein, A. D. (2001). The Polarity of the Retinal Pigment Epithelium. *Traffic*, 867–872.

May, C. A. (2012). Distribution of Nidogen in the Murine Eye and Ocular Phenotype of the Nidogen-1 Knockout Mouse. *ISRN Ophthalmology*, *2012*, 1–6. https://doi.org/10.5402/2012/378641

May-Simera, H. L., Wan, Q., Jha, B. S., Hartford, J., Khristov, V., Dejene, R., Chang, J., Patnaik, S., Lu, Q., Banerjee, P., Silver, J., Insinna-Kettenhofen, C., Patel, D., Lotfi, M., Malicdan, M., Hotaling, N., Maminishkis, A., Sridharan, R., Brooks, B., … Bharti, K. (2018). Primary Cilium-Mediated Retinal Pigment Epithelium Maturation Is Disrupted in Ciliopathy Patient Cells. *Cell Reports*, *22*(1), 189–205. https://doi.org/10.1016/j.celrep.2017.12.038

Mazzoni, F., Safa, H., & Finnemann, S. C. (2014). Understanding photoreceptor outer segment phagocytosis: Use and utility of RPE cells in culture. *Exp Eye Res*, *Sep*(0), 51–60. https://doi.org/10.1016/j.exer.2014.01.010

McGill, T. J., Bohana-Kashtan, O., Stoddard, J. W., Andrews, M. D., Pandit, N., Rosenberg-Belmaker, L. R., Wiser, O., Matzrafi, L., Banin, E., Reubinoff, B., Netzer, N., & Irving, C. (2017). Long-Term Efficacy of GMP Grade Xeno-Free hESC-Derived RPE Cells Following Transplantation. *Translational Vision Science & Technology*, *6*(3), 17. https://doi.org/10.1167/tvst.6.3.17

Mehat, M. S., Sundaram, V., Ripamonti, C., Robson, A. G., Smith, A. J., Borooah, S., Robinson, M., Rosenthal, A. N., Innes, W., Weleber, R. G., Lee, R. W. J., Crossland, M., Rubin, G. S., Dhillon, B., Steel, D. H. W., Anglade, E., Lanza, R. P., Ali, R. R., Michaelides, M., & Bainbridge, J. W. B. (2018). Transplantation of Human Embryonic Stem Cell-Derived Retinal Pigment Epithelial Cells in Macular Degeneration. *Ophthalmology*, *125*(11), 1765–1775. https://doi.org/10.1016/j.ophtha.2018.04.037

Mergler, S., Steinhausen, K., Wiederholt, M., & Strauß, O. (1998). Altered regulation of L-type channels by protein kinase C and protein tyrosine kinases as a pathophysiologic effect in retinal degeneration. *FASEB Journal*, *12*(12), 1125–1134.

Miranda, M., & Romero, F. J. (2019). Antioxidants and Retinal Diseases. *Antioxidants*, *8*(12), 604. https://doi.org/10.3390/antiox8120604

Mitchell, C. H. (2001). Release of ATP by a human retinal pigment epithelial cell line: Potential for autocrine stimulation through subretinal space. *Journal of Physiology*, *534*(1), 193–202.

Mitchell, C. H., & Reigada, D. (2008). Purinergic signalling in the subretinal space: A role in the communication between the retina and the RPE. *Purinergic Signalling*, *4*(2), 101–107. https://doi.org/10.1007/s11302-007-9054-2

Miyagishima, K., Wan, Q., Corneo, B., Sharma, R., Lotfi, M., Boles, N. C., Hua, F., Maminishkis, A., Zhang, C., Blenkinsop, T., Khristov, V., Jha, B. S., Memon, O. S., D'Souza, S., Temple, S., Miller, S., & Bharti, K. (2016). In pursuit of authenticity: Induced pluripotent stem cell-derived retinal pigment epithelium for clinical applications. *Stem Cells Translational Medicine*, *5*, 1–13.

Modi, Y. S., Tanchon, C., & Ehlers, J. P. (2015). Comparative Safety and Tolerability of Anti-VEGF therapy in Age-Related Macular Degeneration. *Drug Safety*, *38*(3), 279–293. https://doi.org/10.1007/s40264-015-0273-0

Müller, C., Más, N., Ruth, P., & Strauß, O. (2014). CaV 1.3 L-type channels , maxiK Ca 2 + -dependent K + channels and bestrophin-1 regulate rhythmic photoreceptor outer segment phagocytosis by retinal pigment epithelial cells. *Cellular Signalling*, *26*(5), 968–978. https://doi.org/10.1016/j.cellsig.2013.12.021

Muntean, B. S., Jin, X., Williams, F. E., & Nauli, S. M. (2014). Primary Cilium Regulates CaV1.2 Expression Through Wnt Signaling: CILIUM AND POLYCYSTIC KIDNEY DISEASE. *Journal of Cellular Physiology*, *229*(12), 1926–1934. https://doi.org/10.1002/jcp.24642

Naylor, A., Hopkins, A., Hudson, N., & Campbell, M. (2020). Tight junctions of the outer blood retina barrier. *International Journal of Molecular Sciences*, *21*(1). https://doi.org/10.3390/ijms21010211

Nguyen, M.-T. T., & Arnheiter, H. (2000). Signaling and transcriptional regulation in early mammalian eye development: A link between FGF and MITF. *Development*, *127*(16), 3581–3591. https://doi.org/10.1242/dev.127.16.3581

North, R. A. (2002). Molecular Physiology of P2X Receptors. *Physiological Reviews*, *82*(4), 1013–1067.

O'Leary, F., & Campbell, M. (2021). The blood–retina barrier in health and disease. *The FEBS Journal*, febs.16330. https://doi.org/10.1111/febs.16330

Ortolan, D., Sharma, R., Volkov, A., Maminishkis, A., Hotaling, N. A., Huryn, L. A., Cukras, C., Di Marco, S., Bisti, S., & Bharti, K. (2022). Single-cell–resolution map of human retinal pigment epithelium helps discover subpopulations with differential disease sensitivity. *Proceedings of the National Academy of Sciences of the United States of America*, *119*(19), e2117553119. https://doi.org/10.1073/pnas.2117553119

Pablo, J. L., DeCaen, P. G., & Clapham, D. E. (2017). Progress in ciliary ion channel physiology. *Journal of General Physiology*, *149*(1), 37–47. https://doi.org/10.1085/jgp.201611696

Parikh, B. H., Blakeley, P., Regha, K., Liu, Z., Yang, B., Bhargava, M., Wong, D. S. L., Tan, Q. S. W., Wong, C. S. W., Wang, H. F., Al-Mubaarak, A., Chou, C., Cheung, C. M. G., Lim, K. L., Barathi, V. A., Hunziker, W., Lingam, G., Hu, T. X., & Su, X. (2023). Single-cell transcriptomics reveals maturation of transplanted stem cell–derived retinal pigment epithelial cells toward native state. *Proceedings of the National Academy of Sciences*, *120*(26), e2214842120. https://doi.org/10.1073/pnas.2214842120

Pascolini, D., & Mariotti, S. P. (2012). Global estimates of visual impairment: 2010. *British Journal of Ophthalmology*, *96*(5), 614–618. https://doi.org/10.1136/bjophthalmol-2011-300539

Pearson, R. A., Dale, N., Llaudet, E., & Mobbs, P. (2005). ATP Released via Gap Junction Hemichannels from the Pigment Epithelium Regulates Neural Retinal Progenitor Proliferation. *Neuron*, *46*(5), 731–744. https://doi.org/10.1016/j.neuron.2005.04.024

Peng, S., Rao, V. S., Adelman, R. A., & Rizzolo, L. J. (2011). Claudin-19 and the Barrier Properties of the Human Retinal Pigment Epithelium. *Investigative Opthalmology & Visual Science*, *52*(3), 1392. https://doi.org/10.1167/iovs.10-5984

Peng, S., Wang, S. B., Singh, D., Zhao, P. Y. C., Davis, K., Chen, B., Adelman, R. A., & Rizzolo, L. J. (2016). Claudin-3 and claudin-19 partially restore native phenotype to ARPE-19 cells via effects on tight junctions and gene expression. *Experimental Eye Research*, *151*, 179–189. https://doi.org/10.1016/j.exer.2016.08.021

Pennington, B. O., Clegg, D. O., Melkoumian, Z. K., & Hikita, S. T. (2015). Defined Culture of Human Embryonic Stem Cells and Xeno-Free Derivation of Retinal Pigmented Epithelial Cells on a Novel, Synthetic Substrate. *Stem Cells Translational Medicine*, *4*(2), 165–177. https://doi.org/10.5966/sctm.2014-0179

Peterson, W. M., Meggyesy, C., Yu, K., & Miller, S. S. (1997). Extracellular ATP Activates Calcium Signaling , Ion , and Fluid Transport in Retinal Pigment Epithelium. *The Journal of Neuroscience*, *17*(7), 2324–2337.

Phua, D. C. Y., Xu, J., Ali, S. M., Boey, A., Gounko, N. V., & Hunziker, W. (2014). ZO-1 and ZO-2 Are Required for Extra-Embryonic Endoderm Integrity, Primitive Ectoderm Survival and Normal Cavitation in Embryoid Bodies Derived from Mouse

Embryonic Stem Cells. *PLOS ONE*, *9*(6), e99532. https://doi.org/10.1371/journal.pone.0099532

Plaza Reyes, A., Petrus-Reurer, S., Antonsson, L., Stenfelt, S., Bartuma, H., Panula, S., Mader, T., Douagi, I., André, H., Hovatta, O., Lanner, F., & Kvanta, A. (2016). Xeno-Free and Defined Human Embryonic Stem Cell-Derived Retinal Pigment Epithelial Cells Functionally Integrate in a Large-Eyed Preclinical Model. *Stem Cell Reports*, *6*(1), 9–17. https://doi.org/10.1016/j.stemcr.2015.11.008

Qin, S. (2016). Blockade of MerTK Activation by AMPK Inhibits RPE Cell Phagocytosis. In C. Bowes Rickman, M. M. LaVail, R. E. Anderson, C. Grimm, J. Hollyfield, & J. Ash (Eds.), *Retinal Degenerative Diseases* (pp. 773–778). Springer International Publishing. https://doi.org/10.1007/978-3-319-17121-0_103

Quinn, R. H., & Miller, S. S. (1992). Ion Transport Mechanisms in Native Human Retinal Pigment Epithelium. *Investigative Ophthalmology & Visual Science*, *33*(13), 3513–3527.

Rahner, C., Fukuhara, M., Peng, S., Kojima, S., & Rizzolo, L. J. (2004). The apical and basal environments of the retinal pigment epithelium regulate the maturation of tight junctions during development. *Journal of Cell Science*, *117*(15), 3307–3318. https://doi.org/10.1242/jcs.01181

Rajasekaran, S. A., Hu, J., Gopal, J., Gallemore, R., Ryazantsev, S., Bok, D., & Rajasekaran, A. K. (2003). Na,K-ATPase inhibition alters tight junction structure and permeability in human retinal pigment epithelial cells. *American Journal of Physiology - Cell Physiology*, *284*(6 53-6), 1497–1507. https://doi.org/10.1152/ajpcell.00355.2002

Ramón Martínez-Morales, J., Rodrigo, I., & Bovolenta, P. (2004). Eye development: A view from the retina pigmented epithelium. *BioEssays*, *26*(7), 766–777. https://doi.org/10.1002/bies.20064

Ransy, C., Vaz, C., Lombès, A., & Bouillaud, F. (2020). Use of H2O2 to cause oxidative stress, the catalase issue. *International Journal of Molecular Sciences*, *21*(23), 1–14. https://doi.org/10.3390/ijms21239149

Redmond., T. M., Yu, S., Lee, E., Bok, D., Hamasaki, D., Chen, N., Goletz, P., Ma, J.-X., Crouch, R. K., & Pfeifer, K. (1998). Rpe65 is necessary for production of 11-cis-vitamin A in the retinal visual cycle. *Nature Genetics*, *20*(4), Article 4. https://doi.org/10.1038/3813

Reichhart, N., Markowski, M., Ishiyama, S., Wagner, A., Crespo-Garcia, S., Schorb, T., Ramalho, J. S., Milenkovic, V. M., Föckler, R., Seabra, M. C., & Strauß, O. (2015). Rab27a GTPase modulates L-type Ca2+ channel function via interaction with the II-III linker of CaV1.3 subunit. *Cellular Signalling*, *27*(11), 2231–2240. https://doi.org/10.1016/j.cellsig.2015.07.023

Reichhart, N., Milenkovic, V. M., Halsband, C.-A., Cordeiro, S., & Strauß, O. (2010). Effect of bestrophin-1 on L-type Ca2+ channel activity depends on the Ca2+ channel beta-subunit. *Experimental Eye Research*, *91*(5), 630–639. https://doi.org/10.1016/j.exer.2010.08.001

Reichhart, N., & Strauß, O. (2014). Ion channels and transporters of the retinal pigment epithelium. *Experimental Eye Research*, *126*, 27–37. https://doi.org/10.1016/j.exer.2014.05.005

Reichman, S., Slembrouck, A., Gagliardi, G., Chaffiol, A., Terray, A., Nanteau, C., Potey, A., Belle, M., Rabesandratana, O., Duebel, J., Orieux, G., Nandrot, E. F., Sahel, J.-A., & Goureau, O. (2017). Generation of Storable Retinal Organoids and Retinal Pigmented Epithelium from Adherent Human iPS Cells in Xeno-Free and Feeder-Free Conditions. *Stem Cells*, *35*(5), 1176–1188. https://doi.org/10.1002/stem.2586

Resnikoff, S., Pascolini, D., Etya, D., Kocur, I., Pararajasegaram, R., Pokharel, G. P., & Mariotti, S. P. (2004). Global data on visual impairment in the year 2002. *Bull World Health Organ*, *82*(11), 844–851.

Rizzolo, L. J. (2014). Barrier properties of cultured retinal pigment epithelium. *Experimental Eye Research*, *126*, 16–26. https://doi.org/10.1016/j.exer.2013.12.018

Rizzolo, L. J., Peng, S., Luo, Y., & Xiao, W. (2011). Integration of tight junctions and claudins with the barrier functions of the retinal pigment epithelium. *Progress in Retinal and Eye Research*, *30*(5), 296–323. https://doi.org/10.1016/j.preteyeres.2011.06.002

Rosenthal, R., Heimann, H., Agostini, H., Martin, G., Hansen, L. L., & Strauss, O. (2007). Ca2+ channels in retinal pigment epithelial cells regulate vascular endothelial growth factor secretion rates in health and disease. *Molecular Vision*, *13*, 443–456.

Rowland, T. J., Blaschke, A. J., Buchholz, D. E., Hikita, S. T., Johnson, L. V., & Clegg, D. O. (2013). Differentiation of human pluripotent stem cells to retinal pigmented epithelium in de fi ned conditions using purified extracellular matrix proteins. *Journal of Tissue Engineering and Regenerative Medicine*, *7*, 642–653. https://doi.org/10.1002/term.1458

Saari, J. C., Nawrot, M., Kennedy, B. N., Garwin, G. G., Hurley, J. B., Huang, J., Possin, D. E., & Crabb, J. W. (2001). Visual Cycle Impairment in Cellular Retinaldehyde Binding Protein (CRALBP) Knockout Mice Results in Delayed Dark Adaptation. *Neuron*, *29*(3), 739–748. https://doi.org/10.1016/S0896-6273(01)00248-3

Sachdeva, M. M., Cano, M., & Handa, J. T. (2014). Nrf2 signaling is impaired in the aging RPE given an oxidative insult. *Experimental Eye Research*, *119*, 111–114. https://doi.org/10.1016/j.exer.2013.10.024

Salceda, R., & Sánchez-Chávez, G. (2000). Calcium uptake, release and ryanodine binding in melanosomes from retinal pigment epithelium. *Cell Calcium*, *27*(4), 223–229. https://doi.org/10.1054/ceca.2000.0111

Saternos, H., Ley, S., & AbouAlaiwi, W. (2020). Primary Cilia and Calcium Signaling Interactions. *International Journal of Molecular Sciences*, *21*(19), 7109. https://doi.org/10.3390/ijms21197109

Schmidt-Erfurth, U., Kaiser, P. K., Korobelnik, J.-F., Brown, D. M., Chong, V., Nguyen, Q. D., Ho, A. C., Ogura, Y., Simader, C., Jaffe, G. J., Slakter, J. S., Yancopoulos, G. D., Stahl, N., Vitti, R., Berliner, A. J., Soo, Y., Anderesi, M., Sowade, O., Zeitz, O., … Heier, J. S. (2014). Intravitreal Aflibercept Injection for Neovascular Age-related Macular Degeneration: Ninety-Six–Week Results of the VIEW Studies. *Ophthalmology*, *121*(1), 193–201. https://doi.org/10.1016/j.ophtha.2013.08.011

Schneider, C. A., Rasband, W. S., & Eliceiri, K. W. (2012). NIH Image to ImageJ: 25 years of image analysis. *Nat Methods*, *9*, 671–675.

Schreiter, S., Vafia, K., Barsacchi, R., Tsang, S. H., Bickle, M., Ader, M., Karl, M. O., Tanaka, E. M., & Almedawar, S. (2020). A Human Retinal Pigment Epithelium-Based Screening Platform Reveals Inducers of Photoreceptor Outer Segments Phagocytosis. *Stem Cell Reports*, *15*(6), 1347–1361. https://doi.org/10.1016/j.stemcr.2020.10.013

Schwartz, S. D., Hubschman, J., Heilwell, G., Franco-cardenas, V., Pan, C. K., Ostrick, R. M., Mickunas, E., Gay, R., Klimanskaya, I., & Lanza, R. (2012). Embryonic stem cell trials for macular degeneration: A preliminary report. *The Lancet*, *379*, 713–720. https://doi.org/10.1016/S0140-6736(12)60028-2

Schwartz, S. D., Regillo, C. D., Lam, B. L., Eliott, D., Rosenfeld, P. J., Gregori, N. Z., Hubschman, J. P., Davis, J. L., Heilwell, G., Spirn, M., Maguire, J., Gay, R., Bateman,

J., Ostrick, R. M., Morris, D., Vincent, M., Anglade, E., Del Priore, L. V., & Lanza, R. (2015). Human embryonic stem cell-derived retinal pigment epithelium in patients with age-related macular degeneration and Stargardt's macular dystrophy: Follow-up of two open-label phase 1/2 studies. *The Lancet*, *385*(9967), 509–516. https://doi.org/10.1016/S0140-6736(14)61376-3

Schwartz, S. D., Tan, G., Hosseini, H., & Nagiel, A. (2016). Subretinal Transplantation of Embryonic Stem Cell – Derived Retinal Pigment Epithelium for the Treatment of Macular Degeneration: An Assessment at 4 Years. *Investigative Ophthalmology & Visual Science*, *57*(5). https://doi.org/10.1167/iovs.15-18681

Sharma, R., Bose, D., Maminishkis, A., & Bharti, K. (2020). Retinal Pigment Epithelium Replacement Therapy for Age-Related Macular Degeneration: Are We There Yet? *Annual Review of Pharmacology and Toxicology*, *60*(1), 553–572. https://doi.org/10.1146/annurev-pharmtox-010919-023245

Sharma, R., Khristov, V., Rising, A., Jha, B. S., Dejene, R., Hotaling, N., Li, Y., Stoddard, J., Stankewicz, C., Wan, Q., Zhang, C., Campos, M. M., Miyagishima, K. J., McGaughey, D., Villasmil, R., Mattapallil, M., Stanzel, B., Qian, H., Wong, W., … Bharti, K. (2019). Clinical-Grade Stem Cell-Derived Retinal Pigment Epithelium Patch Rescues Retinal Degeneration in Rodents and Pigs. *Science Translational Medicine*, *11*(475), eaat5580. https://doi.org/10.1126/scitranslmed.aat5580

Shi, G., Maminishkis, A., Banzon, T., Jalickee, S., Li, R., Hammer, J., & Miller, S. S. (2008). Control of Chemokine Gradients by the Retinal Pigment Epithelium. *Investigative Ophthalmology and Visual Science*, *49*(10), 4620–4630. https://doi.org/10.1167/iovs.08-1816

Shu, X., Li, H., Dong, B., Sun, C., & Zhang, H. F. (2017). Quantifying melanin concentration in retinal pigment epithelium using broadband photoacoustic microscopy. *Biomedical Optics Express*, *8*(6), 2851. https://doi.org/10.1364/BOE.8.002851

Simó, R., Villarroel, M., Corraliza, L., Hernández, C., & Garcia-Ramírez, M. (2010). The Retinal Pigment Epithelium: Something More than a Constituent of the Blood-Retinal Barrier—Implications for the Pathogenesis of Diabetic Retinopathy. *Journal of Biomedicine and Biotechnology*, *2010*, 1–15. https://doi.org/10.1155/2010/190724

Singh, R., Shen, W., Kuai, D., Martin, J. M., Guo, X., Smith, M. A., Perez, E. T., Phillips, M. J., Simonett, J. M., Wallace, K. A., Verhoeven, A. D., Capowski, E. E., Zhang, X., Yin, Y., Halbach, P. J., Fishman, G. A., Wright, L. S., Pattnaik, B. R., & Gamm, D. M. (2013). iPS cell modeling of Best disease: Insights into the pathophysiology of an inherited macular degeneration. *Human Molecular Genetics*, *22*(3), 593–607. https://doi.org/10.1093/hmg/dds469

Skottman, H. (2010). Derivation and characterization of three new human embryonic stem cell lines in Finland. *Report*, *46*, 206–209. https://doi.org/10.1007/s11626-010-9286-2

Skottman, H., Muranen, J., Lähdekorpi, H., Pajula, E., Mäkelä, K., Koivusalo, L., Koistinen, A., Uusitalo, H., Kaarniranta, K., & Juuti-Uusitalo, K. (2017). Contacting co-culture of human retinal microvascular endothelial cells alters barrier function of human embryonic stem cell derived retinal pigment epithelial cells. *Experimental Cell Research*, *359*(1), 101–111. https://doi.org/10.1016/j.yexcr.2017.08.004

Song, W. K., Park, K., Kim, H., Lee, J. H., Choi, J., Chong, S. Y., Shim, S. H., Priore, L. V. D., & Lanza, R. (2015). Treatment of Macular Degeneration Using Embryonic Stem Cell-Derived Retinal Pigment Epithelium: Preliminary Results in Asian Patients. *Stem Cell Reports*, *4*(5), 860–872. https://doi.org/10.1016/j.stemcr.2015.04.005

Sorkio, A. E., Vuorimaa-laukkanen, E. P., Hakola, H. M., Liang, H., Osterberg, M., Yliperttula, M. L., Ujula, T. A., & Jos, J. (2015). Biomimetic collagen I and IV double layer Langmuir-Schaefer films as microenvironment for human pluripotent stem cell derived retinal pigment epithelial cells. *Biomaterials*, *51*, 257–269. https://doi.org/10.1016/j.biomaterials.2015.02.005

Sorkio, A., Hongisto, H., Kaarniranta, K., Uusitalo, H., Juuti-Uusitalo, K., & Skottman, H. (2014). Structure and Barrier Properties of Human Embryonic Stem Cell–Derived Retinal Pigment Epithelial Cells Are Affected by Extracellular Matrix Protein Coating. *Tissue Engineering*, *20*(3, 4). https://doi.org/10.1089/ten.tea.2013.0049

Sorvari, J., Viheriälä, T., Ilmarinen, T., Ihalainen, T. O., & Nymark, S. (2019). Analysis of ATP-Induced Ca2+ Responses at Single Cell Level in Retinal Pigment Epithelium Monolayers. *Retinal Degenerative Diseases*, *1185*, 525–530.

Stalmans, P., & Himpens, B. (1997). Confocal Imaging of Ca2+ Signaling in Cultured Rat Retinal Pigment Epithelial Cells During Mechanical and Pharmacologic Stimulation. *Investigative Ophthalmology*, *38*(1).

Strauss, O. (2005). The retinal pigment epithelium in visual function. *Physiological Reviews*, *85*(3), 845–881. https://doi.org/10.1152/physrev.00021.2004

Strauß, O. (2013). Ca2+-Imaging Techniques to Analyze Ca2+ Signaling in Cells and to Monitor Neuronal Activity in the Retina.pdf. *Methods in Molecular Biology*. https://doi.org/10.1007/978-1-62703-080-9_21

Streilein, J. W., Ma, N., Wenkel, H., Ng, T. F., & Zamiri, P. (2002). Immunobiology and privilege of neuronal retina and pigment epithelium transplants. *Vision Research*, *42*, 487–495.

Sugita, S., Makabe, K., Fujii, S., & Takahashi, M. (2018). Detection of Complement Activators in Immune Attack Eyes After iPS-Derived Retinal Pigment Epithelial Cell Transplantation. *Investigative Ophthalmology & Visual Science*, *59*(10), 4198–4209. https://doi.org/10.1167/iovs.18-24769

Sugita, S., Usui, Y., Horie, S., Futagami, Y., Aburatani, H., Okazaki, T., Honjo, T., Takeuchi, M., & Mochizuki, M. (2009). T-Cell Suppression by Programmed Cell Death 1 Ligand 1 on Retinal Pigment Epithelium during Inflammatory Conditions. *Investigative Opthalmology & Visual Science*, *50*(6), 2862. https://doi.org/10.1167/iovs.08-2846

Sullivan, D. M., Erb, L., Anglade, E., Weisman, G. A., Turner, J. T., & Csaky, K. G. (1997). Identification and characterization of P2Y2 nucleotide receptors in human retinal pigment epithelial cells. *Journal of Neuroscience Research*, *49*(1), 43–52. https://doi.org/10.1002/(SICI)1097-4547(19970701)49:1<43::AID-JNR5>3.0.CO;2-D

Sun, C., Zhou, J., & Meng, X. (2021). Primary cilia in retinal pigment epithelium development and diseases. *Journal of Cellular and Molecular Medicine*, *25*(19), 9084–9088. https://doi.org/10.1111/jcmm.16882

Takahashi, K., & Yamanaka, S. (2006). Induction of Pluripotent Stem Cells from Mouse Embryonic and Adult Fibroblast Cultures by Defined Factors. *Cell*, *126*(4), 663–676. https://doi.org/10.1016/j.cell.2006.07.024

Tan, G. S. W., Liu, Z., Ilmarinen, T., Barathi, V. A., Chee, C. K., Lingam, G., Su, X., & Stanzel, B. V. (2021). Hints for Gentle Submacular Injection in Non-Human Primates Based on Intraoperative OCT Guidance. *Translational Vision Science & Technology*, *10*(1), 10. https://doi.org/10.1167/tvst.10.1.10

Tan, W., Zou, J., Yoshida, S., Jiang, B., & Zhou, Y. (2020). The Role of Inflammation in Age-Related Macular Degeneration. *International Journal of Biological Sciences*, *16*(15), 2989–3001. https://doi.org/10.7150/ijbs.49890

Tovell, V. E., & Sanderson, J. (2008). Distinct P2Y Receptor Subtypes Regulate Calcium Signaling in Human Retinal Pigment Epithelial Cells. *Investigative Opthalmology & Visual Science*, *49*(1), 350. https://doi.org/10.1167/iovs.07-1040

Upadhyay, M., Milliner, C., Bell, B. A., & Bonilha, V. L. (2020). Oxidative stress in the retina and retinal pigment epithelium (RPE): Role of aging, and DJ-1. *Redox Biology*, *37*, 101623. https://doi.org/10.1016/j.redox.2020.101623

Vaajasaari, H., Ilmarinen, T., Juuti-Uusitalo, K., Rajala, K., Onnela, N., Narkilahti, S., Suuronen, R., Hyttinen, J., Uusitalo, H., & Skottman, H. (2011). Toward the defined and xeno-free differentiation of functional human pluripotent stem cell–derived retinal pigment epithelial cells. *Molecular Vision*, *17*, 575.

Vargas, J. A., & Finnemann, S. C. (2022). Probing Photoreceptor Outer Segment Phagocytosis by the RPE In Vivo: Models and Methodologies. *International Journal of Molecular Sciences*, *23*(7), 3661. https://doi.org/10.3390/ijms23073661

Viheriälä, T., Hongisto, H., Sorvari, J., Skottman, H., Nymark, S., & Ilmarinen, T. (2022). Cell maturation influences the ability of hESC-RPE to tolerate cellular stress. *Stem Cell Research & Therapy*, *13*(1), 30. https://doi.org/10.1186/s13287-022-02712-7

Viheriälä, T., Sorvari, J., Ihalainen, T. O., Mörö, A., Grönroos, P., Schlie-Wolter, S., Chichkov, B., Skottman, H., Nymark, S., & Ilmarinen, T. (2021). Culture surface protein coatings affect the barrier properties and calcium signalling of hESC-RPE. *Scientific Reports*, *11*(1), 1–14. https://doi.org/10.1038/s41598-020-79638-8

Wang, C., & Youle, R. J. (2019). The Role of Mitochondria in Apoptosis. *Annu Rev Genet*, *43*, 95–118.

Wang, Z., Dillon, J., & Gaillard, E. R. (2006). Antioxidant Properties of Melanin in Retinal Pigment Epithelial Cells. *Photochemistry and Photobiology*, *82*(2), 474. https://doi.org/10.1562/2005-10-21-ra-725

Weber, J. L., Dolley-Sonneville, P., Weber, D. M., Fadeev, A. G., Zhou, Y., Yang, J., Priest, C. A., Brandenberger, R., & Melkoumian, Z. (2010). Corning® Synthemax™ Surface: A tool for feeder-free, xeno-free culture of human embryonic stem cells. *Nature Methods*, *7*(12), Article 12. https://doi.org/10.1038/nmeth.f.316

Webster, K. A. (2012). Mitochondrial membrane permeabilization and cell death during myocardial infarction: Roles of calcium and reactive oxygen species. *Future Cardiology*, *8*(6), 863–884. https://doi.org/10.2217/fca.12.58

Westenskow, P., Piccolo, S., & Fuhrmann, S. (2009). β-catenin controls differentiation of the retinal pigment epithelium in the mouse optic cup by regulating Mitf and Otx2 expression. *Development*, *136*(15), 2505–2510. https://doi.org/10.1242/dev.032136

Wheway, G., Nazlamova, L., & Hancock, J. T. (2018). Signaling through the Primary Cilium. *Frontiers in Cell and Developmental Biology*, *6*, 8. https://doi.org/10.3389/fcell.2018.00008

Wimmers, S., Coeppicus, L., Rosenthal, R., & Strauß, O. (2008). Expression profile of voltage-dependent Ca2+ channel subunits in the human retinal pigment epithelium. *Graefe's Archive for Clinical and Experimental Ophthalmology*, *246*(5), 685–692. https://doi.org/10.1007/s00417-008-0778-7

Wimmers, S., Karl, M. O., & Strauss, O. (2007). Ion channels in the RPE. *Progress in Retinal and Eye Research*, *26*(3), 263–301. https://doi.org/10.1016/j.preteyeres.2006.12.002

Wollmann, G., Lenzner, S., Berger, W., Rosenthal, R., Karl, M. O., & Strauss, O. (2006). Voltage-dependent ion channels in the mouse RPE: Comparison with Norrie disease mice. *Vision Research*, *46*(5), 688–698. https://doi.org/10.1016/j.visres.2005.08.030

Wu, W.-C., Hu, D.-N., Gao, H.-X., Chen, M., Wang, D., Rosen, R., & McCormick, S. A. (2010). Subtoxic levels hydrogen peroxide-induced production of interleukin-6 by retinal pigment epithelial cells. *Molecular Vision*.

Xiong, J., & Zhu, M. X. (2016). Regulation of lysosomal ion homeostasis by channels and transporters. *Science China Life Sciences*, *59*(8), 777–791. https://doi.org/10.1007/s11427-016-5090-x

Xue, Y., Shen, S. Q., Jui, J., Rupp, A. C., Byrne, L. C., Hattar, S., Flannery, J. G., Corbo, J. C., & Kefalov, V. J. (2015). CRALBP supports the mammalian retinal visual cycle and cone vision. *The Journal of Clinical Investigation*, *125*(2), 727–738. https://doi.org/10.1172/JCI79651

Yang, D., Elner, S. G., Clark, A. J., Hughes, B. A., Petty, H. R., & Elner, V. M. (2011). Activation of P2X Receptors Induces Apoptosis in Human Retinal Pigment Epithelium. *Investigative Ophthalmology & Visual Science*, *52*(3), 1522–1530. https://doi.org/10.1167/iovs.10-6172

Yang, S., Zhou, J., & Li, D. (2021). Functions and Diseases of the Retinal Pigment Epithelium. *Frontiers in Pharmacology*, *12*, 727870. https://doi.org/10.3389/fphar.2021.727870

Young, R. W. (1978). The daily rhythm of shedding and degradation of rod and cone outer segment membranes in the chick retina. *Investigative Ophthalmology & Visual Science*, *17*, 105–116.

Young, R. W., & Bok, D. (1969). PARTICIPATION OF THE RETINAL PIGMENT EPITHELIUM IN THE ROD OUTER SEGMENT RENEWAL PROCESS. *The Journal of Cell Biology*, *42*(2), 392–403.

Yurchenco, P. D. (2011). Basement Membranes: Cell Scaffoldings and Signaling Platforms. *Cold Spring Harbor Perspectives in Biology*, *3*(2), a004911. https://doi.org/10.1101/cshperspect.a004911

Zahabi, A., Shahbazi, E., Ahmadieh, H., Hassani, S.-N., Totonchi, M., Taei, A., Masoudi, N., Ebrahimi, M., Aghdami, N., Seifinejad, A., Mehrnejad, F., Daftarian, N., Salekdeh, G. H., & Baharvand, H. (2012). A New Efficient Protocol for Directed Differentiation of Retinal Pigmented Epithelial Cells from Normal and Retinal Disease Induced Pluripotent Stem Cells. *Stem Cells and Development*, *21*(12), 2262–2272. https://doi.org/10.1089/scd.2011.0599

Zhan, J., He, J., Zhou, Y., Wu, M., Liu, Y., Shang, F., & Zhang, X. (2016). Crosstalk Between the Autophagy-Lysosome Pathway and the Ubiquitin-Proteasome Pathway in Retinal Pigment Epithelial Cells. *Curr Mol Med*, *16*(5), 487–495.

Zhang, T., Huang, X., Liu, S., Bai, X., Zhu, X., Clegg, D. O., Jiang, M., & Sun, X. (2022). Determining the optimal stage for cryopreservation of human embryonic stem cell-derived retinal pigment epithelial cells. *Stem Cell Research & Therapy*, *13*(1), 454. https://doi.org/10.1186/s13287-022-03141-2

PUBLICATIONS

PUBLICATION I

Culture surface protein coatings affect the barrier properties and calcium signalling of hESC-RPE

Viheriälä T*, Sorvari J*, Ihalainen TO, Mörö A, Grönroos P, Schlie-Wolter S, Chichkov B, Skottman H, Nymark S*, Ilmarinen T*.

Scientific Reports (2021), 11:933
https://doi.org/10.1038/s41598-020-79638-8

scientific reports

Check for updates

OPEN

Culture surface protein coatings affect the barrier properties and calcium signalling of hESC-RPE

Taina Viheriälä[1,4], Juhana Sorvari[1,4], Teemu O. Ihalainen[1], Anni Mörö[1], Pyry Grönroos[1], Sabrina Schlie-Wolter[2], Boris Chichkov[3], Heli Skottman[1], Soile Nymark[1,4] & Tanja Ilmarinen[1,4]✉

Human pluripotent stem cell-derived retinal pigment epithelium (RPE) transplantation is currently under evaluation as treatment for macular degeneration. For therapeutic applications, cryostorage during cell production is typically needed with potential consequences to cell functionality. We have previously shown that the culture substrate affects human embryonic stem cell-derived RPE (hESC-RPE) properties in fresh cultures. Here, we aimed to further identify the role of RPE basement membrane proteins type IV collagen (Col-IV), laminin (LN), and nidogen-1 in the maturation and functionality of hESC-RPE after cryopreservation. In addition to cell attachment and morphology, transepithelial electrical resistance, expression of key RPE proteins, phagocytosis capacity and Ca^{2+} signalling were analysed. After cryostorage, attachment of hESC-RPE on culture surfaces coated with Col-IV alone was poor. Combining Col-IV and LN with or without nidogen-1 significantly improved cell attachment and barrier properties of the epithelium. Furthermore, functional homogeneity of the hESC-RPE monolayer was enhanced in the presence of nidogen-1. Our results suggest that the choice of coating proteins for the cell culture may have implications to the functional properties of these cells after cryostorage cell banking.

Retinal pigment epithelium (RPE) cells form a highly polarised pigmented monolayer between the neural retina and the choriocapillaris at the back of the eye. RPE plays a central role in the maintenance of a healthy retina. Photoreceptor function and survival is supported by RPE via multiple processes responsible for the transport of nutrients, waste products, ions and fluid between the choroidal blood supply and the subretinal space as well as photoreceptor outer segment (POS) phagocytosis and visual pigment regeneration[1]. Dysfunction of RPE cells leads to the death of photoreceptors, resulting in progressive retinal degenerative diseases, such as age-related macular degeneration (AMD), a major cause of blindness among the elderly in the developed countries[2]. Treatment options for these diseases are currently limited and mostly only delay disease progression. However, replacement of the damaged RPE with human pluripotent stem cell (hPSC)-derived healthy RPE (hPSC-RPE) has been considered as a promising treatment strategy[3].

For clinical applications, the hPSC-RPE cells need to be well-characterized, functionally competent and consistent in quality[4,5]. Cryopreservation of cells is an important part of clinical production process, enabling increased shelf-life and storage of large, quality-controlled, batches of cells[4,5]. However, cryopreservation may affect cellular properties such as adhesion to extracellular matrix (ECM) and following downstream signalling, which is vitally important for appropriate cell physiology and functionality. For example, it has been shown that cryopreservation decreases the expression of certain adhesion molecules on CD34 + hematopoietic progenitor cells[6]. Human umbilical vein endothelial cells have also been shown to be vulnerable to cryopreservation which can lead to lowered angiogenic functionality[7]. In the eye, RPE sits on an ECM called Bruch's membrane which provides structural support and cues affecting e.g. cell differentiation, morphology, and function. The upper part of the Bruch's membrane forms the RPE basement membrane, which is rich in collagen type IV (Col-IV), laminin (LN, types LN111, LN332, LN511, and LN521), nidogen-1 (Nid-1), fibronectin, hyaluronic acid, heparan sulfate, and chondroitin/dermatan sulfate[8–10]. RPE cells express various integrin subunits (i.e. α1-6, and β1), and proteoglycans (i.e. perlacan), forming receptors for ECM proteins such as laminins, collagens, and Nid-1[10–14].

[1]Faculty of Medicine and Health Technology, BioMediTech, Tampere University, Tampere, Finland. [2]Institute for Multiphase Processes, Leibniz University of Hannover, Hannover, Germany. [3]Institute of Quantum Optics, Leibniz University of Hannover, Hannover, Germany. [4]These authors contributed equally: Taina Viheriälä, Juhana Sorvari, Soile Nymark and Tanja Ilmarinen. ✉email: tanja.ilmarinen@tuni.fi

RPE cells can be differentiated and grown in vitro to form confluent monolayers on a variety of ECM mimicking culture surface coatings, such as mixed ECM substrates including Matrigel, purified/recombinant ECM proteins like Col-IV and LN, or synthetic substrates such as Synthemax II-SC[15–19]. Nevertheless, we and others have previously shown that the choice of protein composition for coating cell culture surfaces has major effects on RPE differentiation efficiency, as well as RPE structure, basal lamina production and barrier properties of hPSC-RPE in fresh cultures[16,20]. However, comparative studies on the functional consequences of different protein coatings after cryopreservation are lacking.

RPE is part of the outer blood-retinal barrier which regulates the composition of the subretinal space enabling proper photoreceptor function. Tight junctions are an important component of tissue barriers and their permeability and selectivity is regulated by claudins, especially claudin-19 in human RPE[21]. The barrier properties of RPE have been extensively studied, and it has been shown that endothelial cell secreted factors regulate RPE basement membrane assembly, launching integrin-mediated Rho GTPase signalling that modulate RPE tight junctions and enhance RPE barrier function[22,23]. However, the effects of the cell culture surface protein composition on the maturation of hPSC-RPE tight junctions during differentiation have not been reported before. Another essential aspect for RPE physiology is calcium (Ca^{2+}) signalling, as several critical RPE functions rely on Ca^{2+}-dependent regulatory mechanisms[24]. Light-induced increase of adenosine triphosphate (ATP) in the subretinal space is an important activator of Ca^{2+} signalling in RPE, affecting e.g. RPE transport processes that are involved in the regulation of subretinal space hydration and chemical composition, and influence retinal adhesion[25,26]. Consequently, faults in Ca^{2+} signalling in the transplanted hPSC-RPE cells could contribute to unsuccessful cell therapy. Yet, only a few studies on Ca^{2+} signalling of hPSC-RPE exist[5,27–29]. We have previously shown, that functional voltage-gated Ca^{2+} channels are present in human embryonic stem cell (hESC) –derived RPE[30]. However, the effects of different ECM protein coatings on hPSC-RPE Ca^{2+} signalling have not been previously studied.

To address the potential importance of ECM coatings in the orchestration of cellular functions and responses of hESC-RPE, we investigated the role of the key RPE basement membrane proteins Col-IV, LN, and Nid-1, to the in vitro maturation and functionality of the hESC-RPE after cryopreservation, focusing on barrier properties, phagocytosis and Ca^{2+} signalling. Here, we show that the composition of protein coating affects cell attachment after cryostorage and can lead to profound functional changes during hESC-RPE maturation. Our results also highlight the importance of examining the Ca^{2+} signalling properties, as previously suggested by others[5], when evaluating the quality of hPSC-RPE.

Results

Col-IV alone does not support the formation of an intact hESC-RPE monolayer on culture inserts after cryopreservation. For successful cell culture, an environment allowing appropriate cellular responses is critical. In addition to chemical signals, interactions at the cell-material interface affect cellular signalling through cell-ECM adhesions[31]. Thus, we examined the adhesion and morphology of cryopreserved hESC-RPE (Table 1) 24 h after thawing and seeding on coverslips dip-coated with Col-IV, LN, Col-IV + LN, or Col-IV + LN + Nid-1. Cell flattening/spreading, formation of actin stress fibres providing force for cell adhesion and focal adhesion maturation on different coatings was studied by labelling the hESC-RPE for filamentous actin and important focal adhesion linker protein vinculin. On all other coatings except on Col-IV, hESC-RPE were well-spread, formed organised actin stress fibres, and showed recruitment of vinculin to focal adhesions and adherens junctions (Fig. 1a,b). On Col-IV, punctate vinculin staining was observed, but the cells exhibited rare cell–cell contacts, poor stress fibre formation and weak cell spreading (Fig. 1a,b). The strength of cell adhesion was examined using centrifugation force. Despite the low cell density and poor spreading on Col-IV, no differences in adhesion force between coatings were observed (Fig. 1c). Over the following 10-week culture time, an intact hESC-RPE monolayer on Col-IV alone was never reached and the cells had a fusiform morphology, unlike on all other coatings where hESC-RPE formed an intact pigmented epithelium with cobblestone cell morphology (Fig. 1d). The results indicate that in our culture conditions, LN either alone or in combination with Col-IV + /-Nid-1 is superior to Col-IV alone in supporting hESC-RPE cell attachment and formation of an intact epithelium. LN coating condition also produced the highest level of pigmentation in hESC-RPE, although the differences between LN alone or in combination with Col-IV + /-Nid-1 were modest (Fig. 1e).

Culture substrate coating affects the barrier formation of hESC-RPE in culture. We have previously shown that hESC-RPE express important RPE marker proteins post-cryopreservation when seeded on Col-IV + LN[32]. Before performing more detailed analyses on different coatings after cryopreservation, we compared the RPE characteristics of the cells on Col-IV + LN by the expression of cellular retinaldehyde-binding protein (CRALBP, involved in visual cycle) and Na^+/K^+-ATPase (important for transepithelial ion transport) and transepithelial electrical resistance (TER) before and after cryopreservation and found no major differences (Supplementary Fig. S1). In order to examine the development of barrier properties and integrity of the hESC-RPE monolayer on different coatings, TER was measured during the culture (Fig. 2a, Table 1). In concordance with the morphology of the epithelium, culturing cells on Col-IV alone resulted in low TER reaching a maximum (mean ± SEM) of 56 ± 7 Ωcm^2 at 9 weeks. Surprisingly, compared to hESC-RPE seeded on Col-IV + LN and Col-IV + LN + Nid-1, TER remained lower on LN alone, reaching a maximum of 488 ± 27 Ωcm^2 at 7 weeks after which TER values began to decline. Combining Col-IV and LN yielded epithelia with TER reaching 617 ± 18 Ωcm^2 by week 7 after which TER plateaued. The highest TER values (731 ± 19 Ωcm^2 at 9 weeks) were observed with hESC-RPE seeded on Col-IV + LN + Nid-1 coating.

Because Col-IV coating alone constantly failed to support formation of an intact hESC-RPE monolayer with proper morphology, this coating condition was excluded from the subsequent analyses. The level of hESC-RPE

				Replicates/coating (n)						
				Technical replicates (total)						
	Cell lines	Coating	Biological n	24 h	Wk 3	Wk 4	Wk 6	Wk 7–8	Wk 9–10	Wk 13
Cell adhesion force	hESC-08/017	Col	3	6–9 [m]						
		LN	3	6–9 [m]						
		Col + LN	3	6–9 [m]						
		Col + LN + 1xNid	3	6–9 [m]						
Cell area	hESC-08/017	Col	1	80 [c]						
		LN	1	168 [c]						
		Col + LN	1	241 [c]						
		Col + LN + 1xNid	1	266 [c]						
Morphology	hESC-08/017, hESC-11/013, hESC-13/012	All coatings	n/a		n/a				n/a	
TER	hESC-08/017, hESC-11/013, hESC-13/012	Col	6		12 [m]	32 [m]	34 [m]	46 [m]	56 [m]	
		LN	3		12 [m]	18 [m]	20 [m]	12 [m]	28 [m]	
		Col + LN	6		24 [m]	44 [m]	44 [m]	46 [m]	52 [m]	
		Col + LN + 1xNid	4		24 [m]	38 [m]	36 [m]	48 [m]	36 [m]	
IF	hESC-08/017, hESC-11/013	LN	2					2 [s]		
		Col + LN	2					2 [s]		
		Col + LN + 1xNid	2					2 [s]		
Phagocytosis assay	hESC-08/017	LN	1							5 [i] 519 [c]
		Col + LN	1							5 [i] 540 [c]
		Col + LN + 1xNid	1							5 [i] 528 [c]
		Col + LN + 10xNid	1							5 [i] 510 [c]
Ca-imaging	hESC-08/017 hESC-11/013	LN	2						465 [c]	555 [c]
		Col + LN	2						473 [c]	545 [c]
		Col + LN + 1xNid	2						591 [c]	643 [c]
		Col + LN + 10xNid	2						551 [c]	531 [c]
Pigmentation assay	hESC-08/017	LN	1					5 [i]		
		Col + LN	1					5 [i]		
		Col + LN + 1xNid	1					5 [i]		
		Col + LN + 10xNid	1					5 [i]		

Table 1. Number of replicates for all experiments. [m] measurements, [c] cells, [s] stainings, [i] images, Col—collagen IV, LN—laminin, Nid—nidogen-1.

maturation on different coatings (Table 1) was further evaluated by expression and subcellular localisation of marker proteins important for RPE functionality. Due to the positive effect of the ECM linker protein Nid-1[33] for barrier formation observed with TER measurements, the subsequent experiments were performed with an additional 10-times higher concentration of Nid-1 (Col-IV + LN + 10xNid-1) to examine if Nid-1 concentration affected RPE maturation and functionality. After 8 weeks in culture, CRALBP, Na^+/K^+-ATPase and tight junction proteins claudin-3, claudin-19 (Fig. 2b), as well as tight junction associated protein zonula occludens-1 (ZO-1, Supplementary Fig. S2), were expressed on all coatings. Interestingly, the junctional localisation of claudin-19 was consistently less frequent on LN alone compared to other coatings and improved by the addition of Nid-1 (both 1x and 10x), being in line with the TER measurements. Overall, based on TER measurements and immunostainings, adding complexity to the protein coating enhanced or at least accelerated the maturation of hESC-RPE barrier properties.

Functionality of the hESC-RPE is affected by the culture substrate coating. Daily renewal of POS and the subsequent removal of the shed POS by RPE via phagocytosis is essential for vision, phagocytosis thus being one of the key indicators for functional RPE. The phagocytic capacity of the hESC-RPE (Table 1) on different coatings was studied with isolated porcine POS that were incubated with the cells for 2 h. This was followed by labelling the POS with anti-opsin (Fig. 3a) and counting the number of internalised particles (Fig. 3b-d). POS phagocytosis was observed in hESC-RPE on all culture substrate coatings with slight differences between the coatings. The mean number of internalised particles was lowest on Col-IV + LN and highest on Col-IV + LN + Nid-1 (both 1x and 10x) while the variation was highest on LN and lowest on Col-IV + LN + Nid-1 (both 1x and 10x).

Ca^{2+} acts as an important second messenger in diverse signalling pathways and the control of intracellular free Ca^{2+} concentration ($[Ca^{2+}]_i$) is involved in regulation of the majority of cellular reactions, including many

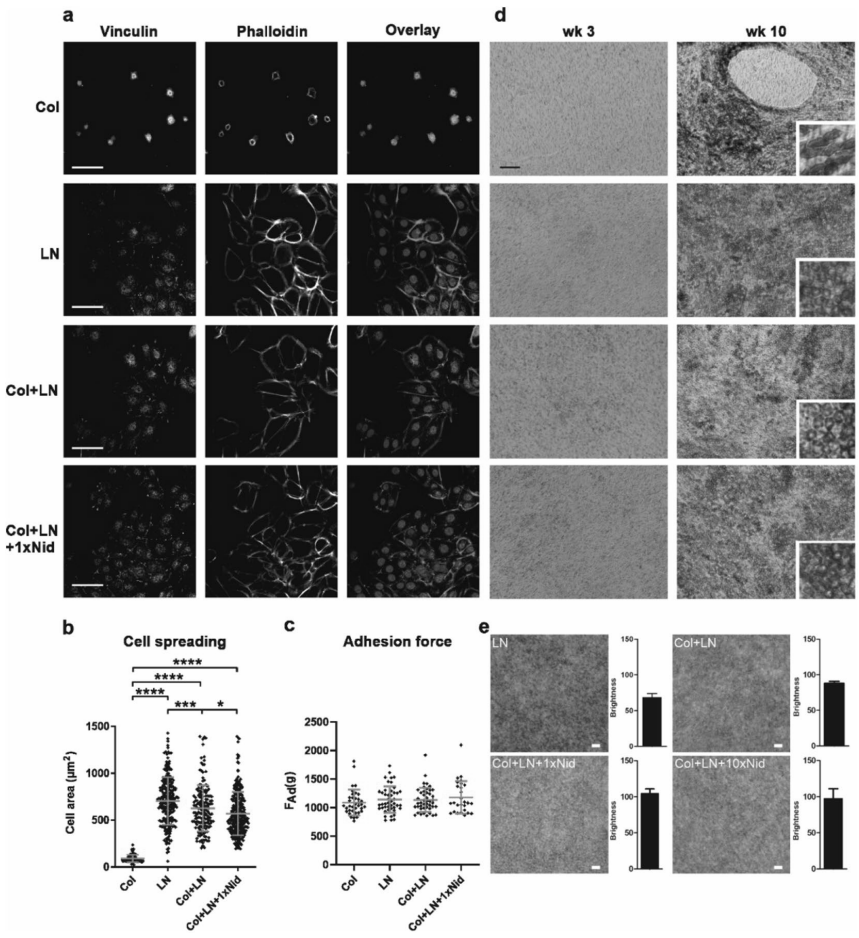

Figure 1. Adhesion of hESC-RPE on different protein coatings (all data shown for hESC-08/017). (**a**) Confocal single plane images showing the subcellular distribution of vinculin and filamentous actin 24 h after seeding. In the overlay, vinculin is shown in green, actin filaments are stained by phalloidin (red) and nucleus by DAPI (blue). Scale bar 50 µm. (**b**) Quantification of the cell area 24 h after seeding was done by outlining the periphery of cells based on F-Actin staining using ImageJ software. The analysed cell numbers were 80 (Col), 241 (LN), 168 (Col + LN) and 265 (Col + LN + Nid) and the results are given as mean ± SD. (**c**) Adhesion force (F_{ad}) correlates with the force (g) needed to detach half of the adherent cells after centrifugation, values are given as mean ± SD. Measurements were done 24 h after seeding from 3 biological and 2–3 technical replicates for each coating. (**d**) Phase contrast micrographs of RPE cell morphology on different coatings 3 and 10 weeks after seeding. *$p < 0.05$, ***$p < 0.001$, ****$p < 0.0001$. (**e**) Pigmentation analysis of hESC-RPE after 8 weeks of seeding. Each image and bar represent the average intensity of five differential interference contrast (DIC) images (LSM800, Carl Zeiss, air immersion objective 20x). Brightness from each image was calculated using ImageJ and represents as mean ± SD. Difference in brightness was statistically significant between LN and all other coatings; LN + Col ($p = 0.0079$), LN + Col + 1xNid ($p = 0.0079$) and LN + Col + 10xNid ($p = 0.0079$). In addition, difference in brightness of LN + Col was statistically significant compared to LN + Col + 1xNid ($p = 0.0079$). Scale bar 20 µm. All statistics were performed with Mann–Whitney U. Col—collagen IV, LN—laminin, Nid—nidogen-1.

RPE functions vital for the maintenance of healthy retina[34,35]. In our study, the RPE cells were loaded with the cell permeable Fluo-4 AM Ca^{2+} indicator dye, and with fluorescence time-lapse microscopy, we were able to monitor relative changes in $[Ca^{2+}]_i$ to analyse hESC-RPE Ca^{2+} dynamics on different protein coatings (Fig. 4a). We have previously developed tools to analyse Ca^{2+} imaging data from large populations of individual cells in intact RPE

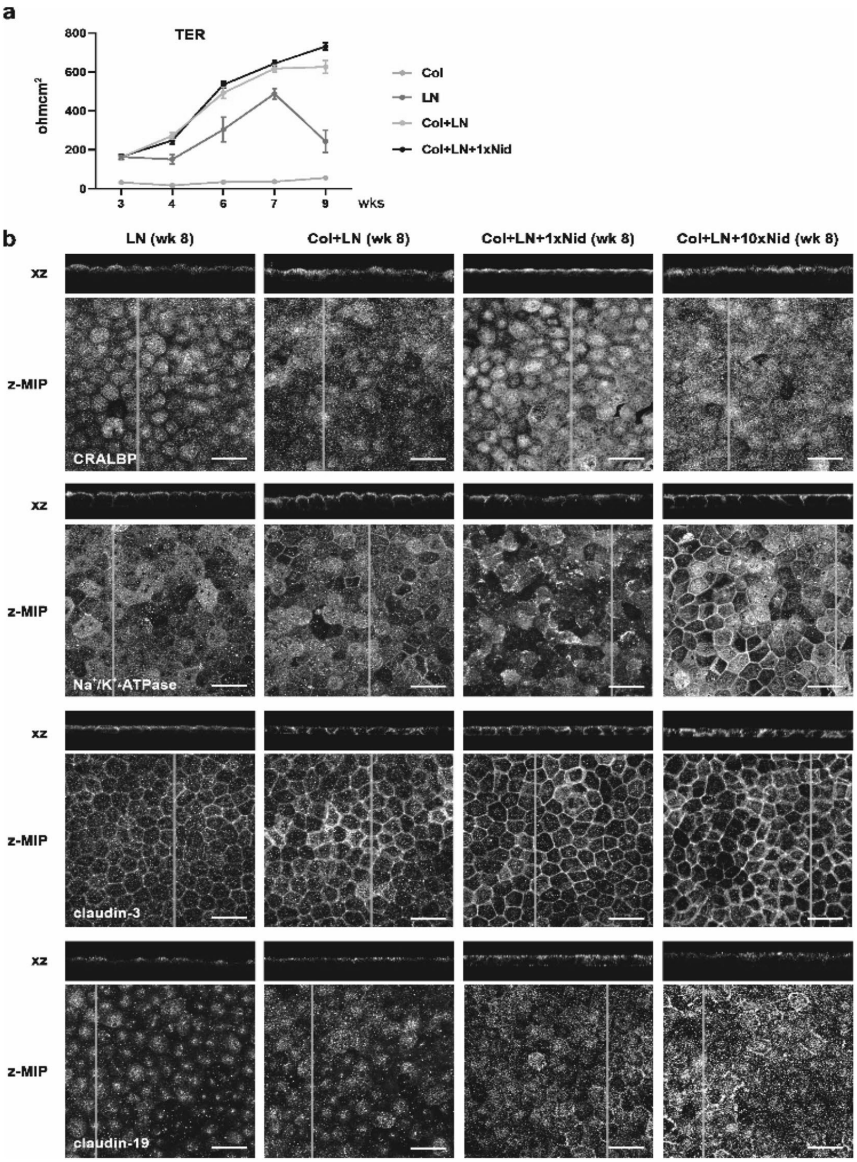

Figure 2. Barrier properties of hESC-RPE on different coatings. (**a**) TER of hESC-RPE on different coatings was measured over time. Data represents means ± SEM at 5 time points of 3 hESC-RPE lines from 3–6 biological and 6–28 technical replicates (Table 1). The differences in TER on LN compared to Col + LN are statistically significant at all time points (4 weeks $p = 0.001$, 6 weeks $p = 0.035$, 7 weeks $p = 0.001$, 9 weeks $p < 0.0001$). At 9-week time point the difference in TER between hESC-RPE on Col + LN + Nid and on Col + LN was statistically significant ($p = 0.014$). Statistical analysis was performed with Mann–Whitney U. (**b**) Representative (shown for hESC-08/017, Table 1) laser scanning confocal microscopy z-maximum intensity projections (z-MIP) and yz cross-sections (MIP from 10 sections) showing expression and subcellular localisation of functionally relevant proteins in hESC-RPE on different coatings after 8 weeks of culture. Scale bar 20 µm. Col—collagen IV, LN—laminin, Nid—nidogen-1.

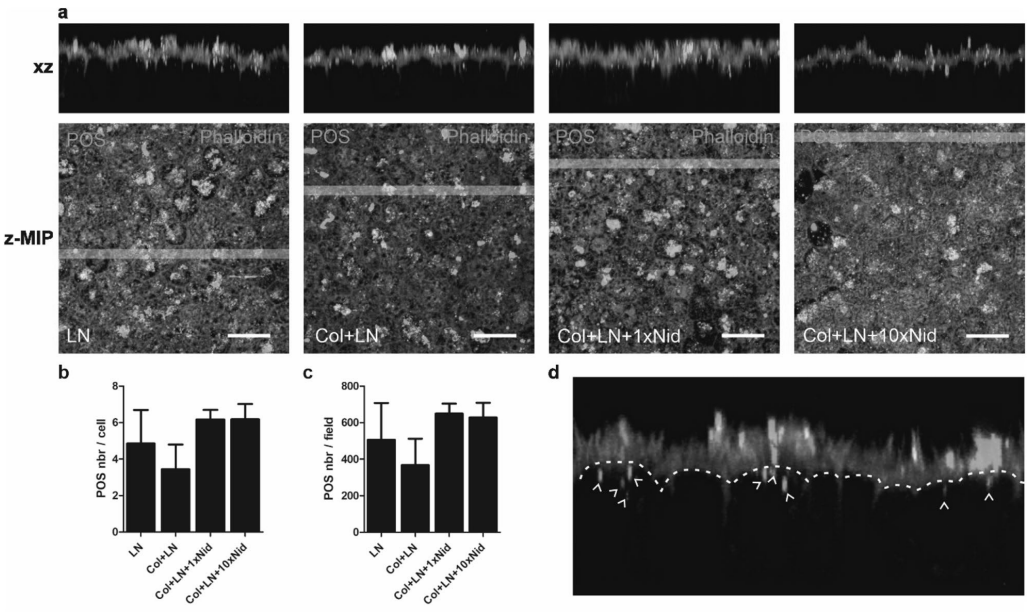

Figure 3. POS phagocytosis assay performed on hESC-RPE 13 weeks post-seeding with purified porcine POS (hESC-08/017, Table 1). (**a**) Representative laser scanning confocal microscopy z-maximum intensity y projections (z-MIP) and xz cross-sections (MIP from 20 sections) after 2-h phagocytic challenge showing the overall number, distribution and internalisation of the POS particles. The POS particles were labelled with anti-opsin (green) and filamentous actin with phalloidin (red). Scale bar 20 µm. Quantification of internalised POS particles (**b**) per cell and (**c**) per field. Each field contains cs. 100 cells. Internalised POS particles were manually calculated from each xz-MIP image (from five z-MIP images/coating). Both data represent means ± SD. The number of POS particles per cell between LN + Col and LN + Col + 1xNid ($p = 0.0079$) and LN + Col + 10xNid ($p = 0.0079$) was statistically significant. Similarly, POS number per field on Col + LN was statistically significant compared to LN + Col + 1xNid ($p = 0.0079$) and LN + Col + 10xNid ($p = 0.0159$). Statistical analysis was performed with Mann–Whitney U test. **(d)** A schematic image to demonstrate which POS particles (green) were calculated as internalised POS particles (white arrows). Col—collagen IV, LN—laminin, Nid—nidogen-1.

monolayers (Fig. 4b)[29]. These tools were applied here to identify population level events and potential differences between the culture conditions. We focused on ATP-induced purinergic signalling pathway that reflects both Ca^{2+} release from intracellular stores and its influx from the extracellular solution[36]. The hESC-RPE cells (Table 1) were exposed to 100 µM ATP for 2 min and several aspects of the recorded Ca^{2+} response were analysed including the amplitude as well as the rise and decay kinetics. Overall, on all surface coatings, an exposure to extracellular ATP induced Ca^{2+} responses that showed a wide cell-to-cell variation (Fig. 4c). Typical to RPE cells, most of the responses were biphasic with fast initial rise resulting from the release of Ca^{2+} from the intracellular stores followed by a slower secondary phase where extracellular Ca^{2+} influx plays a role. As the hESC-RPE cells matured in culture, the mean amplitude of the responses was observed to increase on all surfaces (Fig. 5a). However, on LN, the duration of the response was delayed compared to other surfaces, especially after long-term (13 weeks) culture (Figs. 4c, 5b). Further analysis of the response kinetics showed that purinergic Ca^{2+} signalling is altered on LN: although the majority of the hESC-RPE cells on this coating produced a fast initial $[Ca^{2+}]_i$ rise during early phases of maturation, after long-term culture, only few fast responding hESC-RPE cells with intact response characteristics were detected (Fig. 5c). In addition, a longer culture time was accompanied by the lengthening of the decay phase in the majority of cells cultured on LN (Fig. 5d) as well as by the more heterogenous response properties visible in the scatter graphs as more spread-out distribution (Fig. 5c, 5d). Addition of Col-IV to the coating together with LN supported the preservation of the fast initial response component better than LN alone during maturation. Although the number of cells with fast initial $[Ca^{2+}]_i$ rise on Col-IV + LN during early maturation (week 9) was reduced compared to LN alone, in the majority of cells at 13 weeks of culture, the fast response component was observed, unlike on LN alone (Fig. 5c). The response decay time on the Col-IV + LN surface coating was also shorter than on LN alone in both time points (Fig. 5b,d). Adding yet more complexity to the protein coating with Nid-1 (1x and 10x) increased the number of cells with the fast initial $[Ca^{2+}]_i$ rise and cell population homogeneity compared to Col-IV + LN (Fig. 5c). The higher Nid-1 concentration was beneficial for production of fast Ca^{2+} responses especially during the earlier phases (week 9) of RPE maturation (Figs. 4c, 5c), and this culture coating was superior in supporting cells with fast decay after long-term culture (week 13).

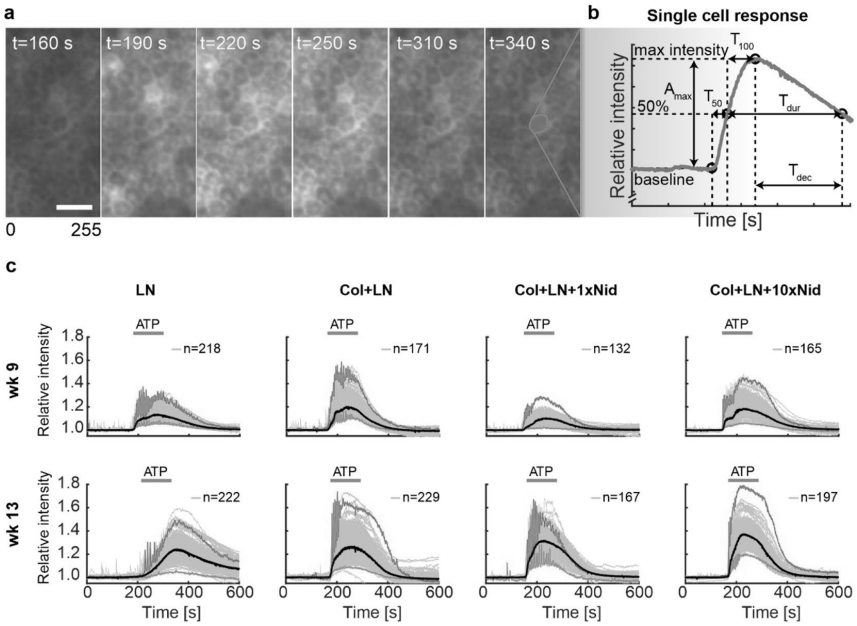

Figure 4. Ca^{2+}-imaging response characterization and grouping. (**a**) Pseudocolored image time series of ATP-induced Ca^{2+} response in hESC-RPE with Fluo-4 Ca^{2+}-indicator from the LN + Col + 10xNid surface. The pseudocolored intensities are linearly scaled from 0 to 255. Scale bar 10 μm. (**b**) Schematic curve representing the parameters calculated from a single cell Ca^{2+}-response: maximum relative intensity (A_{max}), first (T_{50}) and second (T_{100}) half of intensity rise time, intensity decay time from maximum to 50% (T_{dec}) and response duration at 50% intensity (T_{dur}). (**c**) The largest response groups with relative intensity as a function of time for each surface at 9 and 13 weeks. The parameters from (b) were used as inputs in the grouping algorithm. From each group, the strongest (magenta) and weakest (blue) responses are highlighted, in addition to the calculated median curve of the population (black). Col—collagen IV, LN—laminin, Nid—nidogen-1.

Taken together, in addition to the barrier properties and phagocytosis, adding complexity to the protein coating also increased functional maintenance and cell–cell homogeneity of hESC-RPE in terms of Ca^{2+} signalling.

Discussion

Although several clinical trials exploring the safety and surgical methods of hPSC-RPE transplantation have not revealed any major complications, the efficacy of RPE cell therapy remains to be evaluated[37]. For successful outcome, the transplanted cells need to be able to perform key RPE functions. Currently, several protocols for differentiation and culture of hPSC-RPE exist, utilising a variety of culture substrates and surface protein coatings, but lacking any comparative studies on how these culture conditions affect the functionality of hPSC-RPE. In this study, we examined the functional consequences of different cell culture surface protein coatings in the course of hESC-RPE culture and maturation, concentrating on the development of barrier properties, phagocytosis and ATP-induced Ca^{2+} response characteristics. In the Ca^{2+} signalling analysis, emphasis was put on analysing Ca^{2+} imaging data obtained from a large number of individual cells to obtain population level data. As cell banking with cryopreservation is an essential step in the production of cells for therapeutic applications, the study was conducted with cryopreserved cells. Previously, cryopreserved hESC- and human induced pluripotent stem cell (hiPSC)-derived RPE cells cultured on coatings like Matrigel and CellStart or more defined coatings like vitronectin or Col-IV + LN have been reported to maintain key RPE characteristics such as expression of functionally important proteins, phagocytosis and to some extent growth factor secretion[32,38–40]. However, to the best of our knowledge, there are no comparative studies on the functional consequences of different protein coatings after cryopreservation.

Since cell adhesion initiates a myriad of signalling cascades determining cell functions such as survival, growth or differentiation, we first compared the attachment of hESC-RPE on different basement membrane components. Cell attachment is mediated by multifunctional, heterodimeric transmembrane receptors, integrins. Previous studies of integrin expression in human RPE have identified several subunits which are highly expressed and bind to ECM proteins in Bruch's membrane[10,11,16,41]. For this current study, we included Col-IV, LN and Nid-1. LN type LN521 was chosen because it is one of the main isoforms in Bruch's membrane and has been previously shown to support differentiation and maturation of hESC-RPE[10,42]. When Col-IV coating alone was

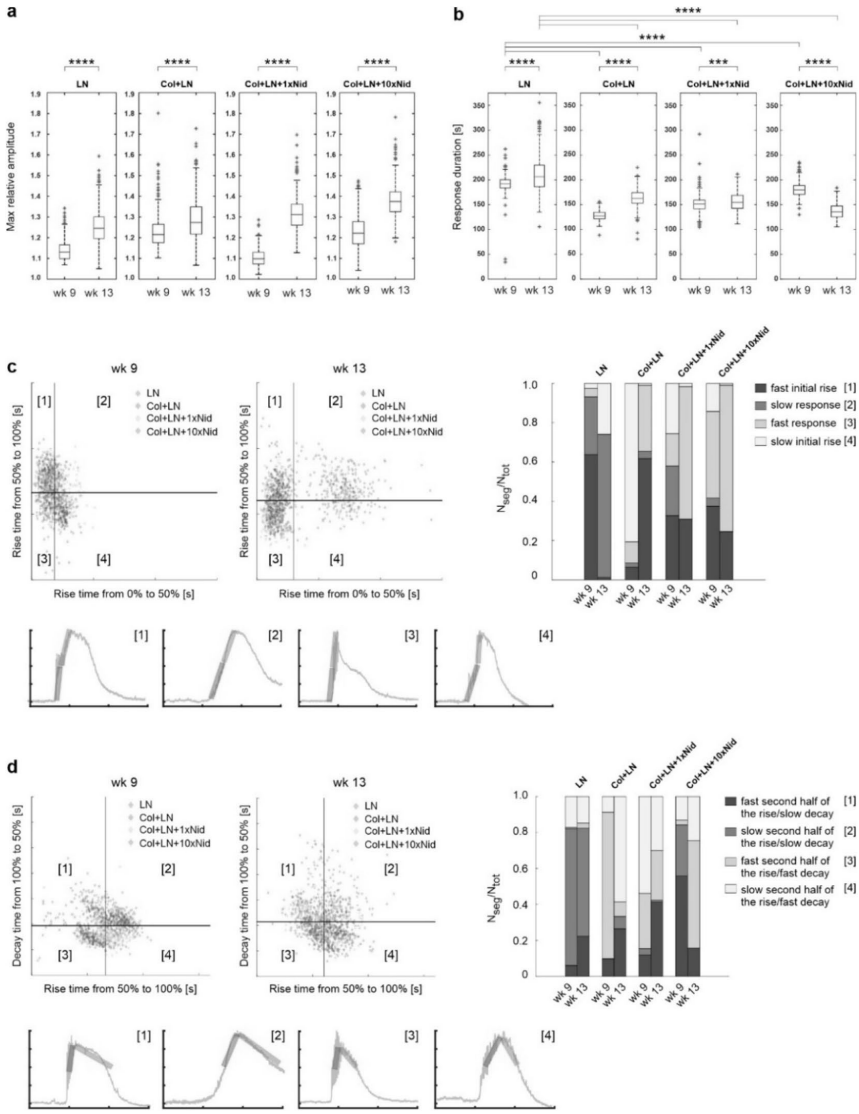

Figure 5. Visualization of the Ca^{2+} response parameters. Boxplots of maximum relative amplitude (**a**) and response duration at 50% intensity (**b**) at weeks 9 and 13. The red line represents the median value and the box extends to 25th and 75th percentiles. The red crosses mark values considered as outliers, outside approximately 99% of the population. (**c**) Upper left: Scatter graph between the first half (horizontal axis) and the second half (vertical axis) of the response rise time at weeks 9 (left) and 13 (right). The scatter fields are divided into four segments by taking the average value of each axis (black lines). Upper right: The number of responses in each segment per total number of responses is represented as a stacked bar graph for each culture surface coating at weeks 9 and 13 (right). Lower left: Examples of responses characterizing each segment. The response segment for the horizontal axis parameter is highlighted with a magenta bar and for the vertical axis parameter with a cyan bar. (**d**) Similar scatter and stacked bar graphs with example responses as in (c) for the second half of the response rise time (horizontal axis) and the intensity decay time from maximum to 50% intensity (vertical axis). ***$p < 0.001$, ****$p < 0.0001$ (Mann–Whitney U). Col—collagen IV, LN—laminin, Nid—nidogen-1.

used, cell density post-thawing was low and spreading poor, unlike on other coatings. Despite similar adhesion strength among coatings, formation of an intact epithelium was hindered on Col-IV alone. This was somewhat surprising, since previously, the culture of freshly differentiated hESC-RPE on Col-IV has been successful[20] and cultured RPE cells typically express several integrins binding both to collagens (α2β1) and laminins (α3β1, α6β1)[10,11]. LN on the other hand supported cell attachment and formation of an intact epithelium. Preference for binding LN instead of Col-IV has also been reported for a RPE cell line ARPE-19 by Aisenbrey et al[10]. The dominant role of LN in epithelial cell adhesion and formation of a functional basement membrane[43,44], may partly explain why LN as the coating matrix improves cell attachment dramatically. The hESC-RPE cells on LN were also more pigmented than on other coatings. The melanin pigment is an important factor in the RPE cells, minimizing light scatter and protecting the cells from cytotoxicity caused by light and inflammation[45]. In general, pigmentation has been considered as a differentiation marker for hPSC-RPE. However, the level of pigmentation in the in vitro hPSC-RPE cultures varies and the functional consequences of this remain elusive. It has been shown that increase in hESC-RPE pigmentation over time does not lead to significant changes in gene expression, suggesting that pigmentation does not reflect the maturation state of the cells[46], at least not at transcriptome level. Interestingly, among the few genes that were significantly differentially expressed between lightly and highly pigmented cells were genes involved in Ca^{2+} signaling and adherens junction remodeling[46].

Development of mature tight junctions is a crucial property of the RPE cells and required for maintenance of the outer blood-retinal barrier. Thus, the formation of barrier properties during maturation of hESC-RPE seeded on different culture surface coatings was followed. During development, the composition and functional properties of RPE tight junctions mature as the neural retina and choroid differentiate[47]. A gradual maturation of the tight junctions indicated by increase in TER over time can also be seen in the hESC-RPE cells in our culture system. Morphologically, on all other coatings except Col-IV alone, hESC-RPE formed an intact pigmented monolayer of cuboidal cells. However, TER of hESC-RPE seeded on LN alone was consistently lower compared to cells cultured on a combination of Col-IV and LN. In our previous study comparing the effects of ECM coatings using freshly differentiated cells cultured for 6 weeks, the lowest TER values were also obtained from cells seeded on human LN compared to other coatings, including Col-IV[20]. In the present study, the TER values on LN alone were not only lower than on other coatings but also started to decline after 7 weeks in culture. This phenomenon was not observed in the study by Hazim et al.[48] with freshly differentiated hiPSC-RPE and mouse LN during 10-week culture. However, in their study, the hiPSC-RPE were cultured in the presence of serum. As serum contains ECM proteins and growth factors which LN is known to bind with high affinity[49], this could explain why the TER values were maintained in serum culture but not in the more defined serum replacement based culture system used in our study. The TER values on LN521 used in our study during the first 4 weeks of culture were in line with a previous study by Plaza Reyes et al., also using serum-free culture conditions and LN521 for culture of hESC-RPE. However, in their work, the TER values were not reported after 4 weeks time point[42]. In contrast to Col-IV or LN alone, bringing more complexity and/or potentially increasing the amount of adsorpted protein in the coating by combining Col-IV and LN, led to higher TER that was maintained throughout the follow-up time of 9 weeks. In addition to TER, the barrier properties were evaluated by comparing the expression of the major human RPE claudins, claudin-3 and -19[21], by hESC-RPE seeded on different coatings. Claudins are a family of transmembrane proteins that bring specificity to tight junctions in a highly sophisticated manner. Claudins are tissue- and developmental stage-specific with only a subset of the so far identified 27 mammalian claudins being expressed by RPE. Based on their microenvironment or differing extracellular regions, claudins can form several types of paracellular barriers and channels, making the junctions for example cation- or anion-selective[50,51]. In our culture system, the expression of claudins typically appears after 7–8-weeks maturation time, initially in patches of claudin-immunopositive cells and as the cells mature, spreading across the whole epithelium and localising to the tight junctions. In this present study, after 8-week maturation time, claudins were expressed by cells on all coatings but especially claudin-19 was localised at this time point to tight junctions more in cells seeded in the presence of Nid-1.

Further functional analysis by phagocytosis assay suggested improved functionality in cells cultured on more complex protein coatings containing 1x or 10x Nid-1 in terms of the number of internalised POS particles and increased cell population homogeneity. In addition to phagocytosis, functionality of especially the ATP-mediated purinergic pathway has been considered an important criterion when assessing the quality of hiPSC-RPE for clinical applications due to the important role of ATP in the regulation of RPE physiology [5,26,52]. More generally, Ca^{2+} signalling is an important regulator of numerous cell functions, controlled by the temporal and spatial distribution of $[Ca^{2+}]_i$[53]. Yet, no comparisons have been reported of how different culture conditions such as culture surface coating affect hPSC-RPE Ca^{2+} signalling. We have previously reported marked cell–cell heterogeneity in ATP-induced Ca^{2+} responses regarding magnitude and response kinetics[29]. With the analysis tools developed[29], we could parametrise the response heterogeneity which allowed us to further group the cells according to their response characteristics and to assess population data on a single cell level from the RPE monolayer. When following the hESC-RPE cultures in time, maturation of the cultures was accompanied by increased Ca^{2+} response amplitudes on all coatings. Interestingly, although the functional analyses by phagocytosis assay did not indicate major defects in phagocytosis by cells on LN, further Ca^{2+} signalling analysis revealed differences in the $[Ca^{2+}]_i$ increase and decay characteristics. Initially, despite poor barrier properties at the 8–9 week time point, majority of cells on LN alone produced fast initial $[Ca^{2+}]_i$ rise reflecting intact ATP-induced release of Ca^{2+} from the intracellular stores. However, further maturation on LN was followed by deceleration of the responses. This was evident both in the rise and decay phase of the responses, yet the decay was affected already in the early maturation stage (week 9) cultures. The ATP-induced Ca^{2+} response in RPE is a result of complex molecular cascade where ATP first binds to $P2Y_2$ receptors resulting in IP_3 increase, release of Ca^{2+} from the ER and subsequent activation of several transporters and ion channels. Delayed or altered kinetics of the response indicate impaired downstream signalling following the ATP binding, and in the eye, it would result e.g. in compromised fluid regulation of the

subretinal space[25,26]. Ca^{2+} imaging also suggested increased cell population homogeneity with more complex protein coatings compared to LN alone in the cultures matured for 13 weeks. The TER and immunostaining studies on barrier properties suggested that adding Nid-1 to the coating both accelerated hESC-RPE maturation and supported the maintenance of the epithelium the best. These observations were further supported by the improved phagocytosis on Nid-1 and Ca^{2+} imaging data showing that compared to other coatings, on Nid-1, especially with the higher tested concentration, a larger number of cells produced fast responses during the earlier phases (week 9) of RPE maturation and also had a fast decay after long-term culture (week 13). Furthermore, our results indicate that analysing the population measurements on a single cell level is advisable as population-averaged measurements can mask cell–cell heterogeneity.

Acquisition of mature tight junctions and appropriate ATP-activated Ca^{2+} signalling in RPE are key for the correct formation of gradients that drive directional fluid transport between the neural retina and the choroid, which together with phagocytosis are essential for the maintenance of photoreceptors. Considering the central role of ECM and basement membrane interactions in cellular differentiation and signal transduction, it is not surprising that a more complex and thus native-like culture surface (Col-IV + LN + Nid-1) was beneficial for the development and maintenance of these characteristics by hESC-RPE in vitro.

Methods

For all experiments, the used cell lines and number of replicates have been indicated in Table 1.

Human ESC-RPE differentiation and culture. Derivation and characterization[54] as well as culture, subsequent differentiation[55,56] into hESC-RPE and cryopreservation[32] of cell lines Regea08/017 (46,XX), Regea11/013 (46,XY), and Regea13/012 (46,XY), was carried out as previously described. For experiments, hESC-RPE were conventionally thawed and seeded as described under each analysis. Culture of hESC-RPE was performed in serum-free medium (KO-DMEM) consisting of KnockOut Dulbecco's modified Eagle's medium (DMEM) supplemented with 15% KnockOut serum replacement, 2 mM GlutaMAX, 0.1 mM 2-mercaptoethanol, 1% MEM non-essential amino acids, and 50 U/ml penicillin–streptomycin (all from Gibco, Thermo Fisher Scientific).

Cell adhesion—adhesion force studies. For cell adhesion force tests, hESC-RPE (hESC-08/017, Table 1) were seeded at 150 000 cells/cm^2 on Thermanox plastic coverslips (Thermo Fisher Scientific) dip-coated at + 4 °C overnight with Col-IV (Sigma Aldrich C5533, 10 μg/cm^2) or LN521 (Biolamina, 0.75 μg/cm^2) alone or in combination, with and without nidogen-1 (R&D Systems, 2570-ND, 2.5 μg/cm^2). Cells were cultured in the KO-DMEM medium described above and analysis was performed 24 h after seeding. Justification of the method and formulas for calculating the cell adhesion force are described in[57]. Adhesion force was measured using a centrifugation system (Hettich Universal 320) as described before[57] with centrifugation force 750 g for 5 min. Cell number of adhered cells before and after centrifugation was evaluated with LDH assay according to the online protocol of OPS diagnostics. The absorbance was detected at 492 nm wavelength using a microplate reader (Tecan Infinite M200Pro and Tecan i-control software). LDH activity was measured at three different time points: after 5 min, 10 min and 15 min of incubation. The measured LDH activity was correlated with the cell number from a cell standard curve prepared under the same conditions.

Cell adhesion—immunolabeling. For immunolabeling vinculin and F-actin, hESC-RPE (hESC-08/017, Table 1) were seeded at 30 000 cells/cm^2 on dip coated Thermanox plastic coverslips and cultured in the KO-DMEM medium as described above. Immunolabeling of cells was performed 24 h after seeding as previously described[58] with the exception of not mounting the samples. Instead, the imaging was performed in PBS immediately after labelling. Antibody information and dilutions can be found in Table 2. Samples were incubated with primary antibodies at + 4 °C overnight, and with secondary antibodies for 1 h at RT. Nuclear label (Hoechst 33,342, 1:1000) and Phalloidin were stained simultaneously with the secondary antibody incubation. Images were captured with a confocal microscope (NikonEclipse TE2000-E, Nikon; 60 × oil immersion objective).

RPE functionality studies—hESC-RPE seeding and culture. For studying hESC-RPE functional properties, cells (Table 1) were seeded 200 000 cells/cm^2 on 1 μm Millicell polyethylene terephthalate (PET) culture inserts (Millipore) dip-coated at + 4 °C overnight with Col-IV (5 μg/cm^2) or LN521 (1.8 μg/cm^2) alone or in combination, with and without Nid-1 (2.5 μg/cm^2). For phagocytosis and Ca^{2+} imaging studies an additional coating with Col-IV (5 μg/cm^2) + LN521 (1.8 μg/cm^2) + Nid-1 (25 μg/cm^2) was used. The cells were matured in KO-DMEM culture medium described above for 8–13 weeks before end-point analyses. Medium was changed 3 times a week.

RPE functionality studies—TER. The barrier function of hESC-RPE (hESC-08/017, hESC-11/013, hESC-13/012, Table 1) on PET was assessed by TER measurements with a Millicell electrical resistance volt-ohm meter (Merck Millipore). Each hESC-RPE sheet was measured at least twice and the average TER values (Ωcm^2) were calculated by subtracting the background TER (PET without cells) and multiplying the result by the surface area of the substrate. Data was measured at five time points (Table 1).

RPE functionality studies—immunolabeling. Immunolabeling of hESC-RPE (hESC-08/017, hESC-11/013, Table 1) was performed as previously described[58]. Antibody information and dilutions can be found in Table 2. Samples were incubated with primary antibodies at + 4 °C overnight, and with secondary antibodies for

Antibody/dye name	Manufacturer	Host/clonality	Cat#	Primary/secondary	Dilution/ab amount
Vinculin	Sigma Aldrich	Rabbit polyclonal	V4139	Primary	1:400
CRALBP	Abcam	Mouse monoclonal	ab15051	Primary	1:500
Na + /K + -ATPase	Abcam	Mouse monoclonal	ab7671	Primary	1:200
Claudin-3	Invitrogen, Thermo Fisher Scientific	Rabbit polyclonal	34-1700	Primary	1:100
Claudin-19	R&D Systems	Mouse monoclonal	MAB6970	Primary	1:100
ZO-1	Invitrogen, Thermo Fisher Scientific	Rabbit polyclonal	61-7300	Primary	1:200
Opsin	Sigma Aldrich	Mouse monoclonal	O4886	Primary	1:200
Phalloidin-Atto 550	Sigma Aldrich	–	19083	Primary	1:100
Anti-mouse IgG Alexa Fluor 488-conjugated	Molecular Probes, Thermo Fisher Scientific	Donkey polyclonal	A-21202	Secondary	1:400
Anti-rabbit IgG Alexa Fluor 488-conjugated	Molecular Probes, Thermo Fisher Scientific	Goat polyclonal	A-11034	Secondary	1:400
Anti-rabbit IgG Alexa Fluor 568-conjugated	Molecular Probes, Thermo Fisher Scientific	Goat polyclonal	A-11011	Secondary	1:400

Table 2. Antibodies used in the study.

1 h at RT. Z-stack images were captured with a confocal microscope (LSM 800, Carl Zeiss; 63 × oil immersion objective).

RPE functionality studies—phagocytosis assay. The porcine POS particles were isolated and purified as previously described[32]. The POS particles were fed to the hESC-RPE cells (hESC-08/017, Table 1) in the KO-DMEM medium supplemented with 10% foetal bovine serum and incubated for 2 h at + 37 °C in 5% CO_2. Labelling with anti-opsin antibody (no POS primary antibody control in Supplementary Fig. S3) and Phalloidin (Table 2) was performed as preciously described[32]. Z-stack images were acquired with confocal microscope (LSM 800, Carl Zeiss, 63 × oil immersion objective) to visualise POS. For quantification of the internalised POS particles, z-stack images (5/coating) were resliced to 512 xz-slices. Maximum intensity projections (MIP) were sequentially generated in 20 xz-slice intervals using ImageJ. Internalised POS particles (illustrated in Fig. 3d) were manually calculated from each resliced xz-MIP. In addition, the cells were calculated from each z-stack image in order to obtain the average number of POS particles per cell.

RPE functionality studies—Ca^{2+} imaging and data analyses. Human ESC-RPE cell (hESC-08/017, hESC-11/013, Table 1) Ca^{2+} dynamics was assessed with the Ca^{2+}-sensitive dye fluo-4-acetoxymethyl ester (fluo-4 AM; Molecular Probes, Thermo Fischer Scientific) as previously described[29]. Briefly, the samples were washed with Elliot solution (pH 7.4, 330 mOsm) followed by incubation in 1 mM fluo-4 AM in Elliott buffer for 45 min at RT protected from light. During imaging, hESC-RPE cells were perfused with Elliot solution alone or Elliot containing 100 µM ATP (Sigma-Aldrich) using a gravity-fed solution exchange system (AutoMate Scientific). Imaging was performed at RT with Nikon Eclipse FN1 upright fluorescence microscope using a 25 × water immersion objective (NA = 1,10). The images were acquired every 500 ms with binning of 2 × 2 with Nikon Nis Elements Imaging Software (version 5,02). Excitation and emission wavelength of 494/506 nm for Fluo-4 was used with exposure time of 80 ms. 2 min of baseline imaging was performed before the cells were exposed to ATP for 2 min followed by imaging for additional 6 min in Elliot.

For data analysis, three 200 × 200 pixel (104 × 104 µm) regions of interest (ROIs) were cropped from each Ca^{2+} image stack in ImageJ and 70–120 individual cells were outlined from each ROI. The average intensity values of each cell as a function of time were extracted, and the intensity data was analysed using a self-developed MATLAB script package[29] (MATLAB R2017b, The MathWorks Inc.). For each cell response, a set of quantities to describe the intensity amplitude and dynamics was calculated: maximum relative amplitude, first (0% to 50% intensity) and second half (50% to 100%) of the intensity rise time, time to maximum amplitude (0% to 100%), decay time (100% to 50%) and response duration at 50% intensity (Fig. 4b). After the single-cell analysis, the intensity responses were sorted with a clustering algorithm, using the calculated intensity parameters of all cells from the three ROIs as input. As a result, the algorithm provided two to four groups of intensity responses having a unique set of response characteristics. The largest group of each measurement was chosen to represent the behaviour of each cell population (Fig. 4c).

Image processing. Images were processed with ImageJ[59,60] using only linear brightness and contrast adjustments for the pixel intensities. Final figures were generated using GraphPad Prism version 8 for Windows (GraphPad Software, La Jolla, CA, USA) and CorelDRAW Graphics Suite 2019 (Corel corporation, Ottawa, Canada).

Statistical analysis. Normality was tested with Shapiro–Wilk test and following statistical analysis between two groups was performed with the unpaired Mann–Whitney U test using GraphPad Prism. A p value of < 0.05 was considered statistically significant.

Ethical issues. Tampere University has the approval of the National Supervisory Authority for Welfare and Health Valvira (Dnro 1426/32/300/05) to conduct research on human embryos. The institute also has supportive statements of the Ethical Committee of the Pirkanmaa Hospital District to derive, culture, and differentiate hESC lines (Skottman/R05116). No new cell lines were derived for this study.

Data availability

The datasets generated during and/or analysed during the current study are available from the corresponding author on request.

Received: 16 May 2020; Accepted: 4 December 2020
Published online: 13 January 2021

References

1. Strauss, O. The retinal pigment epithelium in visual function. *Physiol. Rev.* **85**, 845–881 (2005).
2. Wong, W. L. *et al.* Global prevalence of age-related macular degeneration and disease burden projection for 2020 and 2040: a systematic review and meta-analysis. *Lancet Glob. Health* **2**, e106–e116 (2014).
3. Zarbin, M., Sugino, I. & Townes-Anderson, E. Concise review: update on retinal pigment epithelium transplantation for age-related macular degeneration. *Stem Cells Transl. Med.* **8**, 466–477 (2019).
4. French, A. *et al.* Enabling consistency in pluripotent stem cell-derived products for research and development and clinical applications through material standards. *Stem Cells Transl. Med.* **4**, 217–223 (2015).
5. Miyagishima, K. J. *et al.* In pursuit of authenticity: induced pluripotent stem cell-derived retinal pigment epithelium for clinical applications. *Stem Cells Transl. Med.* **5**, 1562–1574 (2016).
6. Koenigsmann, M. P. M. *et al.* Adhesion molecules on peripheral blood-derived CD34+ cells: effects of cryopreservation and short-term ex vivo incubation with serum and cytokines. *Bone Marrow Transplant.* **22**, 1077–1085 (1998).
7. Cai, G. *et al.* Effects of cryopreservation on excretory function, cellular adhesion molecules and vessel lumen formation in human umbilical vein endothelial cells. *Mol. Med. Rep.* **16**, 547–552 (2017).
8. Booij, J. C., Baas, D. C., Beisekeeva, J., Gorgels, T. G. M. F. & Bergen, A. A. B. The dynamic nature of Bruch's membrane. *Prog. Retin. Eye Res.* **29**, 1–18 (2010).
9. Curcio, C. A. & Johnson, M. Chapter 20 Structure, Function, and Pathology of Bruch's Membrane. in *Anatomy and Physiology* 465–481 (Elsevier Inc, 2013).
10. Aisenbrey, S. *et al.* Retinal pigment epithelial cells synthesize laminins, including laminin 5, and adhere to them through alpha3- and alpha6-containing integrins. *Invest. Ophthalmol. Vis. Sci.* **47**, 5537–5544 (2006).
11. Zarbin, M. A. Analysis of retinal pigment epithelium integrin expression and adhesion to aged submacular human Bruch's membrane. *Trans. Am. Ophthalmol. Soc.* **101**, 499–520 (2003).
12. Guillonneau, X. *et al.* In vitro changes in plasma membrane heparan sulfate proteoglycans and in perlecan expression participate in the regulation of fibroblast growth factor 2 mitogenic activity. *J. Cell. Physiol.* **166**, 170–187 (1996).
13. Kvansakul, M., Hopf, M., Ries, A., Timpl, R. & Hohenester, E. Structural basis for the high-affinity interaction of nidogen-1 with immunoglobulin-like domain 3 of perlecan. *EMBO J.* **20**, 5342–5346 (2001).
14. Rizzolo, L., Zhou, S. & Li, Z. The neural retina maintains integrins in the apical membrane of the RPE early in development. *Investig. Ophthalmol. Vis. Sci.* **35**, 2567–2576 (1994).
15. Fronk, A. H. & Vargis, E. Methods for culturing retinal pigment epithelial cells: a review of current protocols and future recommendations. *J. Tissue Eng.* **7**, 1–23 (2016).
16. Rowland, T. J. *et al.* Differentiation of human pluripotent stem cells to retinal pigmented epithelium in defined conditions using purified extracellular matrix proteins. *J. Tissue Eng. Regen. Med.* **7**, 642–653 (2013).
17. Rowland, T. J., Buchholz, D. E. & Clegg, D. O. Pluripotent human stem cells for the treatment of retinal disease. *J. Cell Physiol.* **227**, 457–466 (2012).
18. Subrizi, A. *et al.* Generation of hESC-derived retinal pigment epithelium on biopolymer coated polyimide membranes. *Biomaterials* **33**, 8047–8054 (2012).
19. Pennington, B. O., Clegg, D. O., Melkoumian, Z. K. & Hikita, S. T. Defined culture of human embryonic stem cells and xeno-free derivation of retinal pigmented epithelial cells on a novel, synthetic substrate. *Stem Cells Transl. Med.* **4**, 165–177 (2015).
20. Sorkio, A. *et al.* Structure and barrier properties of human embryonic stem cell-derived retinal pigment epithelial cells are affected by extracellular matrix protein coating. *Tissue Eng. Part A* **20**, 622–634 (2014).
21. Peng, S., Rao, V. S., Adelman, R. A. & Rizzolo, L. J. Claudin-19 and the barrier properties of the human retinal pigment epithelium. *Investig. Ophthalmol. Vis. Sci.* **52**, 1392–1403 (2011).
22. Rizzolo, L. J. Barrier properties of cultured retinal pigment epithelium. *Exp. Eye Res.* **126**, 16–26 (2014).
23. Benedicto, I. *et al.* Concerted regulation of retinal pigment epithelium basement membrane and barrier function by angiocrine factors. *Nat. Commun.* **8**, 15374 (2017).
24. Reichhart, N. & Strauß, O. Ion channels and transporters of the retinal pigment epithelium. *Exp. Eye Res.* **126**, 27–37 (2014).
25. Mitchell, C. H. & Reigada, D. Purinergic signalling in the subretinal space: a role in the communication between the retina and the RPE. *Purinergic Signal.* **4**, 101–107 (2008).
26. Peterson, W. M., Meggyesy, C., Yu, K. & Miller, S. S. Extracellular ATP activates calcium signaling, ion, and fluid transport in retinal pigment epithelium. *J. Neurosci.* **17**, 2324–2337 (1997).
27. Singh, R. *et al.* iPS cell modeling of best disease: insights into the pathophysiology of an inherited macular degeneration. *Hum. Mol. Genet.* **22**, 593–607 (2013).
28. Abu Khamidakh, A. E., dos Santos, F. C., Skottman, H., Juuti-Uusitalo, K. & Hyttinen, J. Semi-automatic method for Ca^{2+} imaging data analysis of maturing human embryonic stem cells-derived retinal pigment epithelium. *Ann. Biomed. Eng.* **44**, 3408–3420 (2016).
29. Sorvari, J., Viheriälä, T., Ilmarinen, T., Ihalainen, T. O. & Nymark, S. Analysis of ATP-induced Ca^{2+} responses at single cell level in retinal pigment epithelium monolayers. In *Advances in Experimental Medicine and Biology* Vol. 1185 (eds Bowes, R. C. *et al.*) 525–530 (Springer, Cham, 2019).
30. Korkka, I. *et al.* Functional voltage-gated calcium channels are present in human embryonic stem cell-derived retinal pigment epithelium. *Stem Cells Transl. Med.* **8**, 179–193 (2019).
31. Geiger, B., Spatz, J. P. & Bershadsky, A. D. Environmental sensing through focal adhesions. *Nat. Rev. Mol. Cell Biol.* **10**, 21–33 (2009).
32. Hongisto, H., Ilmarinen, T., Vattulainen, M., Mikhailova, A. & Skottman, H. Xeno- and feeder-free differentiation of human pluripotent stem cells to two distinct ocular epithelial cell types using simple modifications of one method. *Stem Cell Res. Ther.* **8**, 291 (2017).

33. Ho, M. S. P., Böse, K., Mokkapati, S., Nischt, R. & Smyth, N. Nidogens—extracellular matrix linker molecules. *Microsc. Res. Technol.* **71**, 387–395 (2008).
34. Petersen, O. H., Michalak, M. & Verkhratsky, A. Calcium signalling: past, present and future. *Cell Calcium* **38**, 161–169 (2005).
35. Strauß, O. Ca^{2+}-imaging techniques to analyze Ca^{2+} signaling in cells and to monitor neuronal activity in the retina. In *Retinal Degeneration* (eds Weber, B. & Langmann, T.) 297–308 (Humana Press, Totowa, NJ, 2012). https://doi.org/10.1007/978-1-62703-080-9_21.
36. Tovell, V. E. & Sanderson, J. Distinct P2Y receptor subtypes regulate calcium signaling in human retinal pigment epithelial cells. *Investig. Opthalmol. Vis. Sci.* **49**, 350 (2008).
37. Vitillo, L., Tovell, V. E. & Coffey, P. Treatment of age-related macular degeneration with pluripotent stem cell-derived retinal pigment epithelium. *Curr. Eye Res.* **45**, 361–371 (2020).
38. Brandl, C. *et al.* In-depth characterisation of Retinal Pigment Epithelium (RPE) cells derived from human induced pluripotent stem cells (hiPSC). *Neuromol. Med.* **16**, 551–564 (2014).
39. Reichman, S. *et al.* Generation of storable retinal organoids and retinal pigmented epithelium from adherent human iPS cells in xeno-free and feeder-free conditions. *Stem Cells* **35**, 1176–1188 (2017).
40. Li, Q.-Y. *et al.* Functional assessment of cryopreserved clinical grade hESC-RPE cells as a qualified cell source for stem cell therapy of retinal degenerative diseases. *Exp. Eye Res.* https://doi.org/10.1016/j.exer.2020.108305 (2020).
41. Gullapalli, V. K., Sugino, I. K. & Zarbin, M. A. Culture-induced increase in alpha integrin subunit expression in retinal pigment epithelium is important for improved resurfacing of aged human Bruch's membrane. *Exp. Eye Res.* **86**, 189–200 (2008).
42. Plaza Reyes, A. *et al.* Xeno-free and defined human embryonic stem cell-derived retinal pigment epithelial cells functionally integrate in a large-eyed preclinical model. *Stem Cell Rep.* **6**, 9–17 (2016).
43. Yurchenco, P. D. Basement membranes: cell scaffoldings and signaling platforms. *Cold Spring Harb. Perspect. Biol.* **3**, a004911 (2011).
44. Terranova, V. P., Rohrbach, D. H. & Martin, G. R. Role of laminin in the attachment of PAM 212 (epithelial) cells to basement membrane collagen. *Cell* **22**, 719–726 (1980).
45. Mahendra, C. K. *et al.* Detrimental effects of UVB on retinal pigment epithelial cells and its role in age-related macular degeneration. *Oxid. Med. Cell. Longev.* **2020**, 1–29 (2020).
46. Bennis, A. *et al.* Stem cell derived retinal pigment epithelium: the role of pigmentation as maturation marker and gene expression profile comparison with human endogenous retinal pigment epithelium. *Stem Cell Rev. Rep.* **13**, 659–669 (2017).
47. Rahner, C. *et al.* The apical and basal environments of the retinal pigment epithelium regulate the maturation of tight junctions during development. *J. Cell Sci.* **117**, 3307–3318 (2004).
48. Hazim, R. A. *et al.* Differentiation of RPE cells from integration-free iPS cells and their cell biological characterization. *Stem Cell Res. Ther.* **8**, 217 (2017).
49. Ishihara, J. *et al.* Laminin heparin-binding peptides bind to several growth factors and enhance diabetic wound healing. *Nat. Commun.* **9**, 2163 (2018).
50. Rizzolo, L. J., Peng, S., Luo, Y. & Xiao, W. Integration of tight junctions and claudins with the barrier functions of the retinal pigment epithelium. *Prog. Retin. Eye Res.* **30**, 296–323 (2011).
51. Tsukita, S., Tanaka, H. & Tamura, A. The Claudins: from tight junctions to biological systems. *Trends Biochem. Sci.* **44**, 141–152 (2019).
52. Zhang, H. *et al.* Comparison of two rabbit models with deficiency of corneal epithelium and limbal stem cells established by different methods. *Tissue Eng. Part C Methods* **23**, 710–717 (2017).
53. Berridge, M. J., Lipp, P. & Bootman, M. D. The versatility and universality of calcium signalling. *Nat. Rev. Mol. Cell Biol.* **1**, 11–21 (2000).
54. Skottman, H. Derivation and characterization of three new human embryonic stem cell lines in Finland. *Vitr. Cell. Dev. Biol. - Anim.* **46**, 206–209 (2010).
55. Hongisto, H. *et al.* Comparative proteomic analysis of human embryonic stem cell-derived and primary human retinal pigment epithelium. *Sci. Rep.* **7**, 1–12 (2017).
56. Vaajasaari, H. *et al.* Toward the defined and xeno-free differentiation of functional human pluripotent stem cell-derived retinal pigment epithelial cells. *Mol. Vis.* **17**, 558–575 (2011).
57. Schlie, S., Gruene, M., Dittmar, H. & Chichkov, B. N. Dynamics of cell attachment: adhesion time and force. *Tissue Eng. Part C Methods* **18**, 688–696 (2012).
58. Sorkio, A. E. *et al.* Biomimetic collagen I and IV double layer Langmuir-Schaefer films as microenvironment for human pluripotent stem cell derived retinal pigment epithelial cells. *Biomaterials* **51**, 257–269 (2015).
59. Schindelin, J. *et al.* Fiji: an open-source platform for biological-image analysis. *Nat. Methods* **9**, 676–682 (2012).
60. Schneider, C. A., Rasband, W. S. & Eliceiri, K. W. NIH Image to ImageJ: 25 years of image analysis. *Nat. Methods* **9**, 671–675 (2012).

Acknowledgements

The authors thank biomedical laboratory technicians Outi Melin, Hanna Pekkanen, and Emma Vikstedt for their technical assistance and contributions to cell culture. The authors acknowledge the Biocenter Finland and Tampere Imaging Facility for their services. This study was supported by the Academy of Finland grant numbers 287287, 304909, 308315, 319257, 323508), the Instrumentarium Science Foundation (170050, 180038), the Finnish Cultural Foundation (00171144, 00181174) and the Emil Aaltonen Foundation.

Author contributions

Study concept and design was mainly done by TI, SN, and HS. Experimental design and execution were performed by TV, AM, PG, and TI. Data analysis and interpretation were done by TV, JS, TOI, AM, PG, SN, and TI. Ca^{2+} imaging analysis tools were developed by JS. SS-W and BC provided expertise and resources on cell attachment studies. Manuscript writing was mainly performed by TV, SN and TI with contributions from all authors. All authors read, revised, and approved the final manuscript.

Competing interests

The authors declare no competing interests.

Additional information

Supplementary Information The online version contains supplementary material available at https://doi.org/10.1038/s41598-020-79638-8.

Correspondence and requests for materials should be addressed to T.I.

PUBLICATION II

Cell maturation influences the ability of hESC-RPE to tolerate cellular stress

Viheriälä T, Hongisto H, Sorvari J, Skottman H*, Nymark S*, Ilmarinen T

Stem Cell Research & Therapy (2022), 13:30
https://doi.org/10.1186/s13287-022-02712-7

Stem Cell Research & Therapy

RESEARCH Open Access

Cell maturation influences the ability of hESC-RPE to tolerate cellular stress

Taina Viheriälä[1], Heidi Hongisto[1,2], Juhana Sorvari[1], Heli Skottman[1†], Soile Nymark[1†] and Tanja Ilmarinen[1,3*]

Abstract

Background: Transplantation of human pluripotent stem cell-derived retinal pigment epithelium (RPE) is an urgently needed treatment for the cure of degenerative diseases of the retina. The transplanted cells must tolerate cellular stress caused by various sources such as retinal inflammation and regain their functions rapidly after the transplantation. We have previously shown the maturation level of the cultured human embryonic stem cell-derived RPE (hESC-RPE) cells to influence for example their calcium (Ca^{2+}) signaling properties. Yet, no comparison of the ability of hESC-RPE at different maturity levels to tolerate cellular stress has been reported.

Methods: Here, we analyzed the ability of the hESC-RPE populations with early (3 weeks) and late (12 weeks) maturation status to tolerate cellular stress caused by chemical cell stressors protease inhibitor (MG132) or hydrogen peroxide (H_2O_2). After the treatments, the functionality of the RPE cells was studied by transepithelial resistance, immunostainings of key RPE proteins, phagocytosis, mitochondrial membrane potential, Ca^{2+} signaling, and cytokine secretion.

Results: The hESC-RPE population with late maturation status consistently showed improved tolerance to cellular stress in comparison to the population with early maturity. After the treatments, the early maturation status of hESC-RPE monolayer showed impaired barrier properties. The hESC-RPE with early maturity status also exhibited reduced phagocytic and Ca^{2+} signaling properties, especially after MG132 treatment.

Conclusions: Our results suggest that due to better tolerance to cellular stress, the late maturation status of hESC-RPE population is superior compared to monolayers with early maturation status in the transplantation therapy settings.

Keywords: Human pluripotent stem cells, Retinal pigment epithelial cells, Oxidative stress, Cell therapy

Background

Retinal pigment epithelium (RPE) is a tight polarized monolayer of cells located under retinal photoreceptors at the back of the eye. RPE has many roles that altogether ensure proper visual function. The adjacent neural retina is exposed to highly oxidative environment, and due to this, one key function of RPE is to protect both itself and the retina against photo-oxidation [1, 2]. Exposure to chronic oxidative stress in the retina can lead to malfunction or death of RPE cells and retinal neurons and eventually contribute to the development of severe retinal degenerative diseases such as age-related macular degeneration (AMD) [3]. Unfortunately, current therapies mainly slow down the progression of the disease. Human pluripotent stem cell-based RPE (hPSC-RPE) transplantation is a promising approach for the treatment with safety and feasibility already under clinical investigation using either hPSC-RPE cell suspension or an intact cell sheet [4–8]. The hPSC-RPE used for cell therapy must endure high level of cellular stress caused by long time

*Correspondence: tanja.ilmarinen@tuni.fi
†Heli Skottman and Soile Nymark have contributed equally to this work
[3] BioMediTech, Faculty of Medicine and Life Sciences, Tampere University, Arvo Ylpön katu 34, 33520 Tampere, Finland
Full list of author information is available at the end of the article

periods in cell culture, cryopreservation for cell banking, potential live-cell shipment to clinical centers, and finally transplantation-related stress including immunosuppressive drugs, inflammation, and oxidative stress in the diseased eye. Human PSC-RPE cells cultured in vitro require time to mature and to gain functions characteristic to RPE, including upregulation of genes related to antioxidant functions as the culture ages [2, 9]. Previously, the developmental stage of non-polarized cadaveric adult human RPE stem cells has been shown to affect transplantation efficacy when suspension transplantation was used, with intermediate differentiation times (4 weeks) producing the most consistent vision rescue in a rat model [10]. Polarized human embryonic stem cell (hESC)-derived RPE cells cultured for 4 weeks, on the other hand, have been shown to decrease their sensitivity to oxidative stress compared to non-polarized cells, suggesting potential advantages of sheet transplantation over the suspension approach [11]. The reported culture times for hESC-RPE sheet transplantation in clinical trials vary between 3 and 20 weeks [6]. Yet, despite potentially highly impacting therapy efficacy, the development of tolerance to cellular stress during further in vitro maturation of hESC-RPE has not been examined. Although early polarized RPE cultures may be more plastic to environmental changes than cells cultured for longer time periods, they could also be functionally more immature and not possess intact signaling pathways for critical cellular functions. Among essential RPE functions are its barrier properties that ensure the proper movement of components between the blood supply and retina [12]. With phagocytosis, RPE disposes photoreceptor outer segments (POS) that photoreceptors renew daily [13]. In addition to barrier properties and phagocytosis, intact Ca^{2+} signaling is a critical indicator of proper RPE functionality. Ca^{2+} acts as a second messenger in RPE taking part in many processes all the way from cell differentiation to cell maturation [14, 15]. Importantly, Ca^{2+} signaling is linked to purinergic signaling in RPE: extracellular adenosine triphosphate (ATP) induces elevations in intracellular Ca^{2+} concentration regulating the chemical composition and the amount of water in the subretinal space and ensuring proper communication between RPE and the retina [16, 17]. We have previously shown that culture time of hESC-RPE improves the intercellular homogeneity of Ca^{2+} response properties in cell population [12]. In the current study, we evaluated the impact of culture time on the ability of the hESC-RPE to endure treatments with chemical stressors.

The present work demonstrates how maturation level of the cultured hESC-RPE cells affects their ability to tolerate cellular stress. Under normal circumstances, one of the functions of RPE cells is to demolish the accumulation of ROS. Addition of H_2O_2 increases the concentration of ROS mimicking the oxidative stress environment in the cells. ROS cause oxidative damage to cellular components such as proteins which need to be removed by proteasomes. Addition of MG132 prevents the normal behavior of proteasomes leading to the accumulation of toxic protein waste. Therefore, acute oxidative stress was induced with H_2O_2, and as oxidative stress is also known to inactivate the proteasome in RPE [18], normal function of proteases was prevented with a protease inhibitor MG132, mimicking the effects of chronic ROS exposure. These chemical stressors were used separately. The emphasis was placed on using physiologically relevant functional assays including phagocytosis and calcium imaging to assess the properties of intact RPE monolayers maturated on porous carrier substrate for 3 or 12 weeks. Time points were chosen to represent early and late maturation status based on our previous experience and earlier study following the development of barrier function of in vitro cultured hESC-RPE over time [12]. Our results indicate that the late maturity status of hESC-RPE cells can tolerate cellular stress more effectively than the population with early maturation status, with potential implications to hPSC-RPE cell therapy.

Methods

Cell culture, differentiation, and treatments of hESC-RPE

Human ESC Regea08/017 (46, XX) cell line was derived, characterized, differentiated with spontaneous differentiation protocol, and cultured as previously described [19]. The cells were cultured in xeno-free (XF) conditions throughout the differentiation of hESC to RPE and the further maturation of differentiated RPE cells. XF medium, which contains KnockOut™ Dulbecco's modified Eagle's medium (KO-DMEM, Gibco, Thermo Fisher Scientific) supplemented with 15% xeno-free KnockOut™ serum replacement (Gibco, Thermo Fisher Scientific), 2 mM GlutaMAX™ (Gibco, Thermo Fisher Scientific), 0.1 mM 2-mercaptoethanol (Gibco, Thermo Fisher Scientific), 1% MEM non-essential amino acids (Gibco, Thermo Fisher Scientific), and 50 U/ml penicillin–streptomycin (Gibco, Thermo Fisher Scientific), were changed three times a week. Cells were cultured in 37 °C with 5% CO_2.

For maturation, the hESC-RPE cells were thawed and seeded with a density of 2.5×10^5 cells/cm^2 on a porous polyethylene terephthalate (PET) hanging cell culture inserts (0.3 cm^2, pore size 1.0 um, Millipore or Sarstedt) or with a density of 2.1×10^5 cells/cm^2 on a 48 well plate, depending on the experiment. The surfaces were coated with a combination of Collagen IV (10ug/cm^2, Sigma Aldrich) and laminin 521 (1.8 ug/cm^2, Biolamina) in phosphate saline buffer (PBS, Gibco) containing Ca^{2+}

and Mg^{2+}. Cells were cultured for 3 or 12 weeks. Before each experiment, the cells were exposed to 1 μm MG132 (Calbiochem) protease inhibitor or 600 μm H_2O_2 solution (Sigma Aldrich) diluted in medium for 24 h. Control cells obtained fresh medium without the chemical stressors.

Mitochondrial Membrane Potential

For mitochondrial membrane potential measurements, a TMRE-Mitochondrial Membrane Potential Assay Kit (abcam, ab113852) was used according to manufacturer's instruction. Briefly, hESC-RPE cells were thawed on a 48 well plate and cultured for 3 and 12 weeks, respectively. 600 nM tetramethylrhodamine ethyl ester (TMRE) solution diluted in culture media was used, and 20 μM carbonyl cyanide 4-(trifluoromethoxy) phenylhydrazone (FCCP) served as a negative control compound. All steps were carried under light protection. Diluted TMRE was added to the cells and incubated for 20 min at + 37 °C, and a microplate reader was used to detect the fluorescence from the TMRE. Excitation and emission wavelengths of 549/575 nm were used. Negative controls were measured for both treated and non-treated cells. Results from the microplate reader were given as intensity values and the values are presented as boxplots. Control values were set to 100% and values from the treated cells were compared to the control cells as relative change in the fluorescence intensity. Higher fluorescence intensity corresponds to a higher value of mitochondrial membrane potential. 13–16 replicate wells from 3 maturation experiments were measured at both time points.

Transepithelial electrical resistance

Barrier development of hESC-RPE was measured from RPE cells cultured on PET hanging inserts. Transepithelial electrical resistance (TER) was measured using Millicell electrical resistance volt-ohm meter (Merck Millipore). Before each measurement, the cells were equilibrated for 10 min at room temperature (RT). Each hESC-RPE monolayer was measured twice, and the average TER values were calculated. PET insert without cells was used as a background and was subtracted from each TER value. Measurements were obtained at time points of 3 weeks and 12 weeks. In each insert, relative change was obtained by subtracting the value before the treatment from the value after the treatment and dividing this difference by the value before the treatment. Measurements were obtained from the control cells similarly and changes in these values were subtracted from the values of treated cells to obtain the final relative change caused by the treatments and compared to the controls. 6–14 replicate inserts from 2 to 3 maturation experiments were measured at both time points.

Immunofluorescence stainings

The hESC-RPE monolayers cultured on inserts were fixed for immunostainings at time points of 3 and 12 weeks. All steps were conducted at RT unless otherwise stated. The fixation was performed with 4% paraformaldehyde (Sigma Aldrich) in PBS for 15 min after which the cells were permeabilized with 0.1% Triton X-100 (Sigma Aldrich) in PBS for 15 min. This was followed by blocking with 3% bovine serum albumin (BSA, Sigma Aldrich) in PBS for 1 h. Primary antibodies for Zonula occludens (ZO-1, 1:200, 61-7300, Invitrogen), Na^+/K^+-ATPase (1:200, ab7671, Abcam), Connexin 43 (Cx43, 1:200, ab11370, Abcam), $P2Y_2$ (1:200, PA1-46150, Invitrogen) and claudin-19 (CL19, 1:200, MAB6970, R&D) were diluted in 3% BSA in PBS and incubated overnight at + 4 °C. The samples were washed several times with PBS followed by 1 h incubation with secondary antibodies donkey anti-mouse Alexa Fluor 488 (1:200, A21202, Life Technologies) and donkey anti-rabbit Alexa Fluor 568 (1:200, A10042, Life Technologies). F-actin was stained with Phalloidin (1:800, P1951, Sigma Aldrich). After incubation, the samples were washed with PBS and mounted with ProLong™ Gold Antifade Mountant with DAPI (Invitrogen, Thermo Fisher Scientific).

Z-stack images from the immunofluorescence-stained samples were captured with laser scanning confocal microscopes Zeiss LSM700, LSM780, or LSM800 with 63x/1.4 oil immersion objective. Images were converted to maximum intensity projections (MIP) with ImageJ [20, 21]. 2–5 replicate inserts from 2 to 3 biological replicates were immunostained and imaged at both time points.

Phagocytosis assay

POS fragments were isolated and purified from porcine eyes as described in [19]. The fragments were suspended in RPE medium containing 10% fetal bovine serum (FBS, Gibco). The POS-media were then added to the apical side of the cells cultured on inserts and incubated for 2 h at 37 °C with 5% CO_2. After this, the cells were washed with PBS, fixed, and immunostained as described above. POS particles were immunolabelled with primary antibody anti-opsin (1:1000, O4886, Sigma Aldrich) and actin filaments were stained with Phalloidin (1:800). 2–3 replicate inserts from 2–3 maturation experiments were used at both time points.

Z-stack images were acquired with laser scanning confocal microscope Zeiss LSM800 with 63x/1.4 oil immersion objective with interval of 100 nm. From each sample, five Z-stack images were captured from randomly selected areas. These images were resliced with ImageJ to 512 xz-slices which were converted to MIPs of 20 consecutive xz-slices, from which the internalized POS particles were then manually calculated. In addition,

the overall number of cells was calculated to obtain the average number of POS particles per cell.

Ca^{2+} imaging

For Ca^{2+} imaging, hESC-RPE cells were cultured on hanging inserts. Ca^{2+} imaging of the hESC-RPE monolayers was performed as previously described [12, 22] at time points of 3 weeks and 12 weeks. Briefly, the cells were loaded with Ca^{2+} sensitive dye fluo-4-acetoxymethyl ester (1 mM, fluo-4 AM; Molecular Probes, Thermo Fischer Scientific) for 45 min. Elliot buffer solution (pH 7.4, 330 mOsm) was used for washing the cells. During the imaging, the cells were perfused with Elliot alone or Elliot containing 100 µM ATP (Sigma Aldrich) with gravity-fed solution exchange system (AutoMate Scientific). All steps were performed at RT protected from light. Nikon Eclipse FN1 upright fluorescence microscope with a 25 × water immersion objective (NA = 1,10) was used for imaging. The cells were imaged for total of 10 min which included 2 min of baseline, 2 min of ATP stimulus, and 6 min of additional imaging. Data analysis wasconducted from three randomly selected regions of interest (ROIs). Each ROI was 200 × 200 pixels (104 × 140 µm) and from each ROI (approx. 200 cells/ROI) cells were outlined in ImageJ [20, 21]. The intensity data as a function of time was converted to a MATLAB (R2018b) form and analyzed using a script package as in [22]. Each cell was categorized in one of the two groups: cells that respond by Ca^{2+} elevation to the ATP stimulus and cells that do not respond to it. Responding cells were then further analyzed to determine the relative maximum amplitude of the Ca^{2+} response. 2–5 replicate inserts from 2 to 3 maturation experiments were measured at both time points. In each experiment day, both control inserts and inserts after the treatments were measured to overcome the possible effect of slight differences in the flow rate between experiment days visible in the data as a latency difference (see Fig. 5).

Cytokine array kit

Cells were cultured on hanging inserts, and at both time point, apical culture media were collected and frozen at − 80 °C. Secretion of multiple cytokines was measured from the collected media with Cytokine array kit (ARY005B, R&D Systems). 350 µl of media were used per sample and the assay was performed following manufacturer's protocol. Membranes were imaged with Bio-Rad X ChemiDoc XRS + with exposure time of 5–11 min (exposure time in which the control spots had reached maximal grey value were chosen). Intensities of the spots within each experiment were compared by using ImageJ and the results are presented as bar graphs. 2–4 replicate media samples from 2 biological experiments were measured at both time points. Only cytokines whose change compared to the control were congruent between 2 replicates were included.

Statistical analysis

All statistics were performed with Mann–Whitney *U* with GraphPad Prism (version 5.02) test to compare statistical significances. A p-value of < 0.05 was considered statistically significant.

Results

Mitochondria remained active after treatments with MG132 and H_2O_2

To assess functional consequences of the stressors rather than cell death, hESC-RPE cells cultured for 3 weeks (early maturation status, TER > 160 ohmcm^2) or 12 weeks (late maturation status, TER > 840 ohm cm^2) were treated with sublethal concentrations of MG132 or H_2O_2, as previously determined for mature hESC-RPE [23, 24]. Mitochondria are important organelles for the cell's normal behavior and highly susceptible to oxidative damage. It is known that mitochondrial membrane potential decreases in apoptosis [25]. To evaluate cell viability and to analyze the mitochondrial activity, mitochondrial membrane potentials were measured. TMRE accumulates to active mitochondria and can be visualized as increased fluorescence intensity. The measured intensities between the control and cells treated with MG132 or H_2O_2 differed significantly at both time points (MG132 at 3 weeks $p = 0.0186$ and 12 weeks $p < 0.0001$, H_2O_2 3 weeks $p = 0.0039$ and 12 weeks $p = 0.0210$). Cells after both treatments and at both time points revealed active mitochondria, on average with increased membrane potential compared to the control, indicating sublethal treatment range for both 3- and 12-week cultures (Fig. 1). Interestingly, there was larger variation in the values in the treated cells than in the control cells.

hESC-RPE with early maturation status is more susceptible to stress-induced changes in cellular barriers

The effects of MG132 and H_2O_2 on hESC-RPE's barrier properties were assessed by TER measurement and immunostainings with anti-ZO-1 and anti-CL19 antibodies. The stressed cells showed lower TER values compared to control cells at both time points (Fig. 2). However, the impact of the treatments on the tight junctions was larger with the cells of early maturation status. The MG132 treated cells had 45% ± 9 lower TER values than control cells ($p = 0.0001$) at the time point of 3 weeks. At 12 weeks the MG132 treated cells had only 22% ± 5 lower TER values than the control cells ($p = 0.0002$). Similarly, the treatment with H_2O_2 showed significantly lower TER values compared to the control

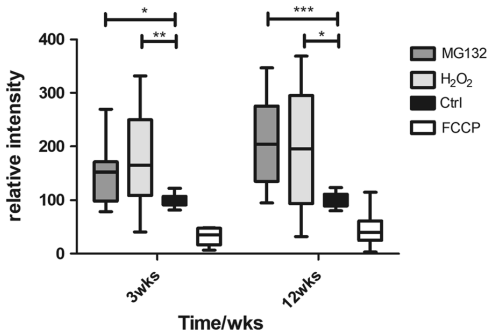

Fig. 1 Relative intensity of mitochondrial membrane potential values at time points of 3 weeks and 12 weeks. MG132 and H_2O_2 treated cells were compared to the control cells. FCCP represents a negative control compound. Mean of the control was set as 100%. Data represents means ± SD values from 13 to 16 replicates. *$p < 0.05$, **$p < 0.01$ and ***$p < 0.001$

cells at 3 weeks (22% ± 8 decrease, $p = 0.0056$) but at 12 weeks the decrease was not statistically significant (12% ± 14, $p = 0.0825$).

Of the tight junction proteins, ZO-1 is associated with the junctions from the early maturation process on, and its cellular localization was not affected by either of the treatments. Claudins, on the other hand, especially CL19 in RPE cells, are involved in the determination of the junctional properties, such as permeability and selectivity [26]. In early maturation status of hESC-RPE cells, CL19 is located on the apical surface whereas in polarized cells the localization is shifted to the tight junctions (as seen in control cells in Fig. 3). Consistent with the TER values, hESC-RPE cells treated with both MG132 and H_2O_2 showed a shift in the localization of CL19 from the junctions to the cytoplasm with the highest impact seen at 3 weeks.

Among interepithelial junctions are gap junctions that regulate cell–cell communication. Cx43 is a major gap junction protein expressed by RPE, and it has been reported that protection of RPE cells from oxidative stress-induced death is dependent on functional Cx43 channels [27]. In late maturation status, polarized RPE, Cx43 can be visualized as punctuate structures at the cell borders. MG132 treatment shifted the localization of Cx43 from the junctions to the cell membranes at 3 weeks, whereas at 12 weeks, the localization remained punctuate in junctions, yet, being not detectable in some cells. After the H_2O_2 treatment, the Cx43 localization was quite heterogenous, especially at the time point of 3 weeks. In some cells, Cx43 could not be detected indicating loss of expression, and in some cells the localization was shifted to apical membrane or the cytoplasm. At 12 weeks, Cx43 was accumulated in the apical surface.

In addition to the maintenance of transepithelial gradient, Na^+/K^+-ATPase has been shown to play a role in the function of tight junctions in mammalian cells, including RPE [28–30]. Similarly to native RPE, Na^+/K^+-ATPase is normally apically polarized in hESC-RPE.

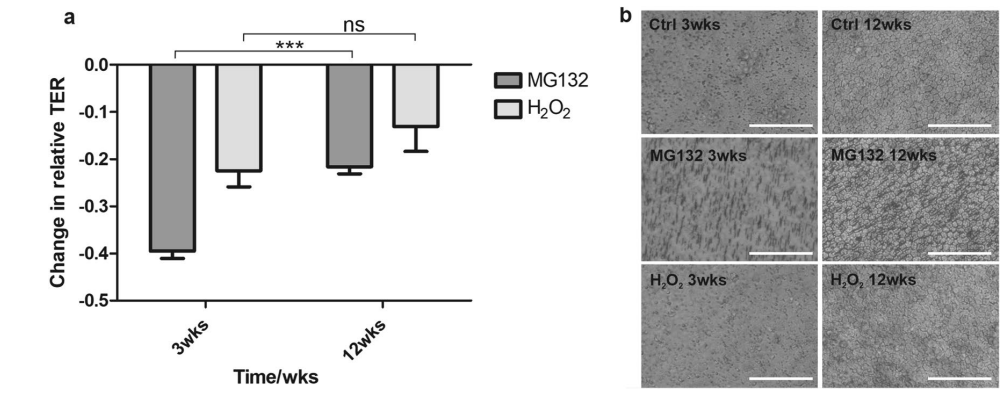

Fig. 2 **a** Relative change in TER values induced by the treatment with the stressors for early (3 weeks) and late (12 weeks) maturation status of hESC-RPE. Data shows the relative change in TER values before and after the treatments with MG132 and H_2O_2. Data represents means ± SD values from 6 to 14 replicates. Values that differ statistically are shown in the image with asterisks. **$p < 0.01$ and ***$p < 0.001$. **b** Phase contrast images of MG132 and H_2O_2 treatments and untreated hESC-RPE monolayers at time points of 3 weeks and 12 weeks. Images were taken from live cultures in inserts immediately after the treatments. At 3-weeks, the pores from the culture inserts are visible since the pigmentation of hESC-RPE cells is relatively low. At 12-weeks, hESC-RPE cells have gained pigmentation and therefore the pores are not visible. In addition, the cobblestone morphology of the hESC-RPE cells is clearer at 12-weeks compared to 3-weeks. Scale bar is 100 µm

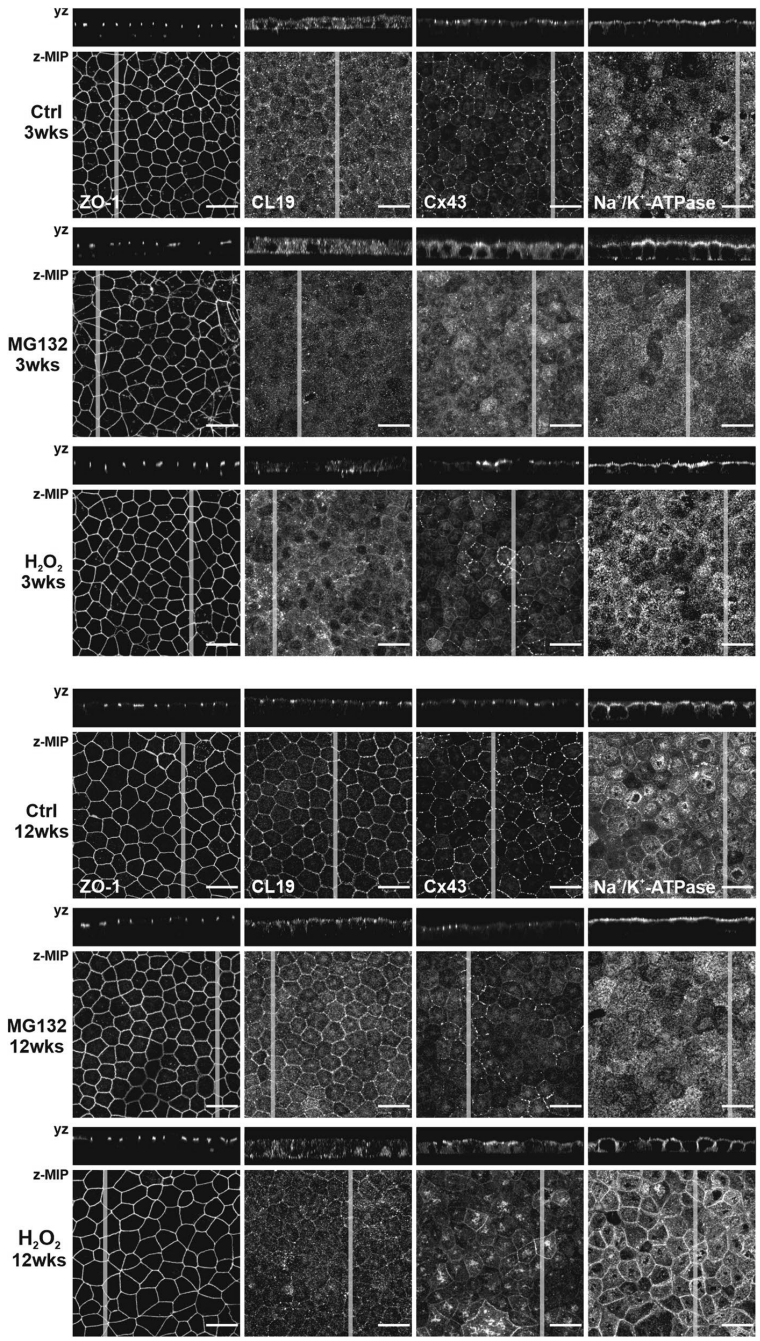

Fig. 3 Immunofluorescence images of localization of RPE proteins in control, MG132 and H_2O_2 treated hESC-RPE cells at time points of 3 weeks and 12 weeks. Each image consists of a laser scanning confocal microscopy *z*-maximum intensity projection (*z*-MIP) and *yz* cross-sections (MIP from 10 sections). Scale bar is 20 μm

Na^+/K^+-ATPase localization after MG132 treatment shifted more visibly to the apical membrane at both time points. Though, 3-week time point revealed also basolateral localization. H_2O_2 treatment did not have a major impact on the expression nor on the localization of Na^+/K^+-ATPase. Despite the changes in the TER, especially after MG132 treatment, and expression and localization of specific proteins, notable changes in the morphology and pigmentation were not observed (Fig. 2b). Morphological changes were further confirmed with confocal imaging (Fig. 3).

hESC-RPE with early maturation status are susceptible to MG132 but not H_2O_2-mediated reduction in phagocytosis activity

Previously, sublethal oxidative stress has been reported to reduce phagocytosis in an immortal RPE cell line ARPE19 [31]. Yet, the effect of oxidative stress to phagocytosis of hPSC-RPE cells is unknown. The susceptibility of hESC-RPE phagocytosis efficiency to cellular stress at different maturation stages was examined by exposing the cells to isolated porcine POS for 2 h immediately after 24-h MG132 or H_2O_2 treatments. The number of internalized POS particles identified by anti-opsin was counted from xz confocal images. Compared to control cells, only the MG132 treatment affected the POS intake efficiency and only in the 3-week cultured cells, indicative of a rather robust nature of the hESC-RPE phagocytic machinery, especially at the more advanced maturation stage (Fig. 4).

Ca^{2+} signaling was reduced especially in early maturation status after MG132 treatment

We and others have previously shown that examining Ca^{2+} signaling properties is a sensitive method for evaluating the quality and functionality of hPSC-RPE [12, 32]. In this study, Ca^{2+} signaling was analyzed by counting the number of cells responding to ATP stimulus by intracellular Ca^{2+} transients (Additional file 1: Fig.S1a and S1b) and calculating the relative amount of the responding cells (Fig. 5a). In addition, maximum response amplitudes as intensities relative to the baseline were analyzed. In control cells, ATP-induced Ca^{2+}-responses were extensively detected at both time points (3 weeks: 97% ± 3, 12 weeks: 98% ± 3), although a large variation in the maximum amplitudes was observed at the earlier time point (Fig. 5b) indicating heterogeneity of cells in the monolayer. At 12 weeks' time point, control cells were more homogenous regarding the maximum amplitudes (Fig. 5c). At 3 weeks, merely a few percent of cells treated with MG132 responded to the ATP stimulus by Ca^{2+} transients (3% ± 3) while at 12 weeks, this number was tenfold higher (31% ± 43). Cells treated with H_2O_2 showed overall more intracellular Ca^{2+}-activity compared to the MG132 treated cells: At 3 weeks, 43% ± 33 responded to the ATP stimulus and at 12 weeks, practically all cells (99% ± 0) responded to the ATP stimulus. Representative response curves from both time points are illustrated in Fig. 5d, e.

In addition to changes in the percentage of responding cells, the treatments induced changes in the response amplitude as well. At 3 weeks (Fig. 5b), both MG132 and H_2O_2 resulted in significantly lower maximum amplitudes compared to the control cells ($p < 0.0001$). At 12 weeks (Fig. 5c), MG132 treated cells remained in significantly lower levels in their Ca^{2+} response amplitudes compared to the control cells ($p < 0.0001$), but the cells treated with H_2O_2 showed no significant difference to the controls.

Addition of ATP to the apical side of RPE induces an intracellular Ca^{2+} transient primarily via apical $P2Y_2$ receptors [16]. In control cells, $P2Y_2$ was detected at the apical and lateral membrane at both timepoints (Fig. 5f). Interestingly, both treatments influenced the cellular localization of these receptors. At 3 weeks, the treatments shifted the localization of $P2Y_2$ away from the apical membrane towards the cytoplasm and the cell–cell junctions, especially with the MG132 treatment. At 12 weeks, the transition from the apical localization to the cytoplasmic was even further enhanced. In addition, the staining appeared homogenous around the monolayer in the control hESC-RPE, whereas the treated cells, especially with H_2O_2, showed heterogenous staining pattern containing cells in the monolayer with no $P2Y_2$ protein expression.

Cytokine expression during hESC-RPE maturation and stress induction

Paracrine signaling is an important way for the cells to communicate in different situations like inflammation. Especially in the cases where the ocular immune privilege has been disrupted either due to disease or surgical intervention, the expression of inflammatory cytokines or chemokines by the transplanted cells could increase the possibility of graft rejection. In our study, the untreated cells secreted a variety of different cytokines at both time points (Fig. 6a, b, Additional file 2: Fig. S2a and S2b, Additional file 3: Fig. S3a and S3b). Majority of the cytokines expressed at 3 weeks were downregulated at 12 weeks compared to the 3-week time point. Cell population with late maturation status revealed downregulated secretion of macrophage migration factor (MIF), plasminogen activator inhibitor-1 (Serpin E1/PAI-1) and monocyte chemoattractant protein-1 (CCL2/MCP-1) compared to cells with early maturation status. Stromal

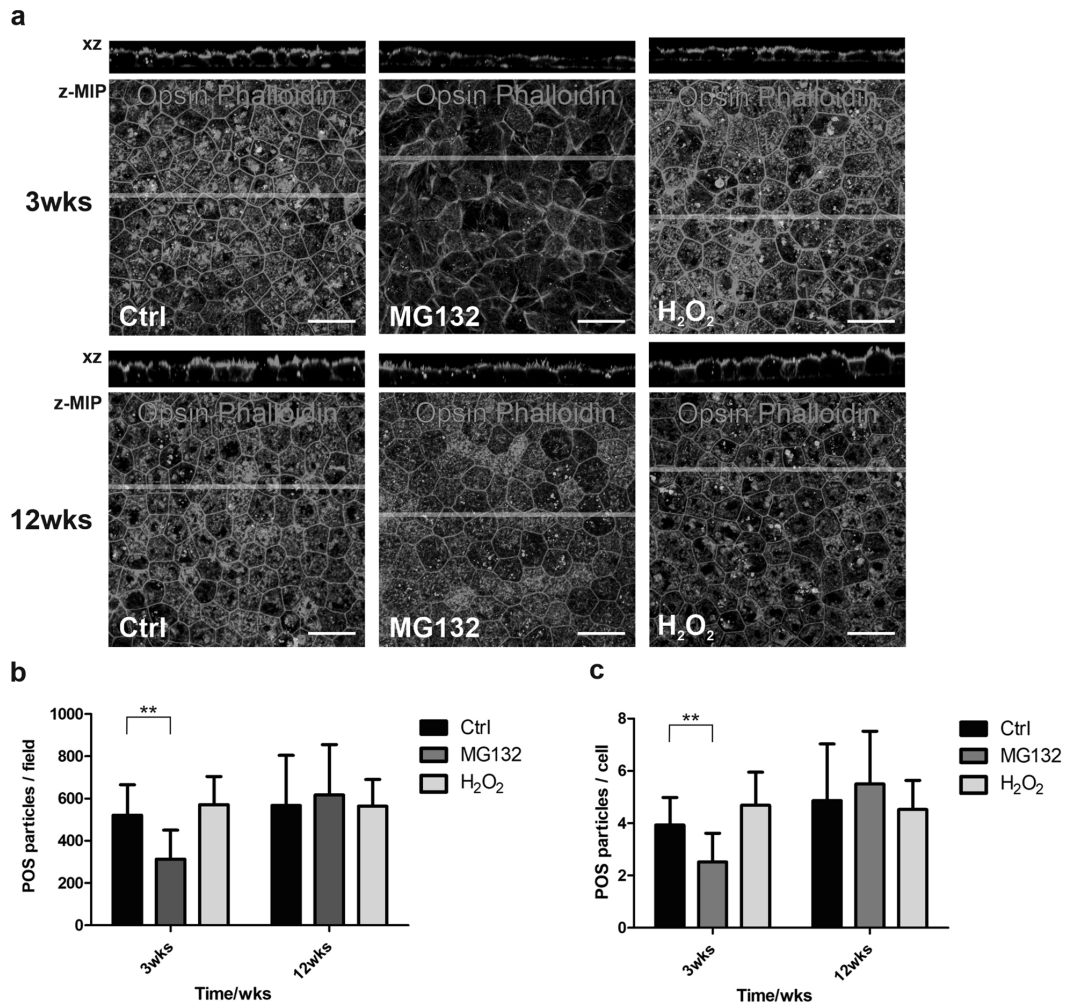

Fig. 4 Phagocytosis assay of hESC-RPE at time points of 3 weeks and 12 weeks. **a** Each image consists of a laser scanning confocal microscopy *z*-maximum intensity projection (*z*-MIP) and *xz* cross-sections (MIP from 20 sections) with POS particles (opsin staining) shown in green and F-actin (phalloidin staining) shown in red. Scale bar is 20 µm. POS particles inside the cells were calculated from xz cross-sections and are shown as **b** number of internalized POS particles per field (total field number 10–15 from 2 to 3 experiments) and **c** number of internalized POS particles per cell. Each field contains ca. 100 cells. Internalized POS particles were calculated as in [12]. Data represent means ± SD. $^{**}p < 0.01$

cell-derived factor 1 (CXCL12/SDF-1) was secreted only at the time point of 3 weeks. Intracellular adhesion molecule 1 (ICAM/CD54) was slightly upregulated at 12 weeks compared to the 3-week time point.

At the same time, the secretion levels of these cytokines were modestly altered after the treatment with MG132 or H_2O_2 (Fig. 6c–f, Additional file 2: Fig. S2c–f). Notably, expression of IL6 and IL8 were revealed only after the treatments. IL6 expression was observed repeatedly at the 12-week time point after H_2O_2 treatment (Fig. 6f, Additional file 2: Fig. S2f) and IL8 at the 3-week time point after MG132 treatment.

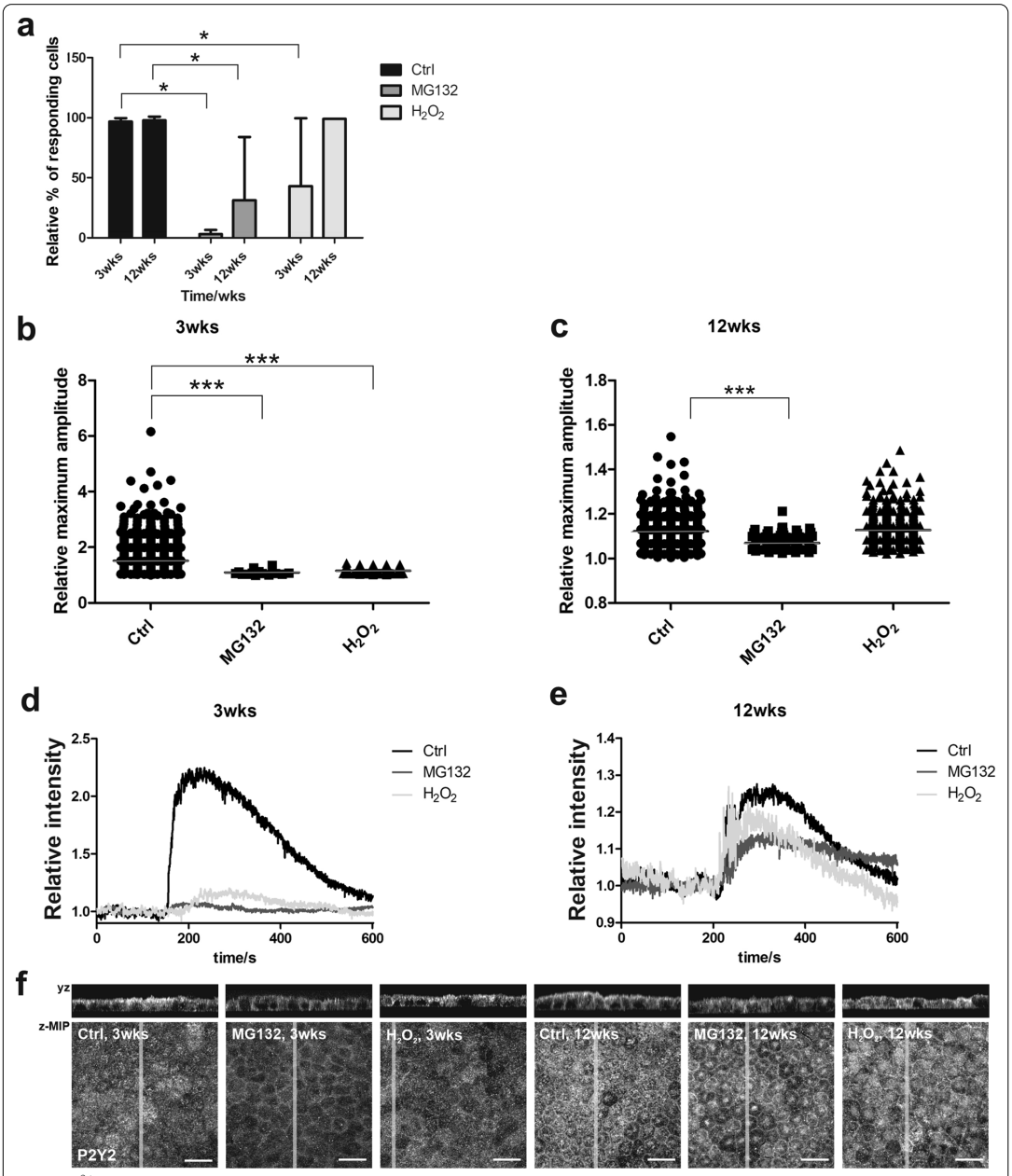

Fig. 5 Ca^{2+} signaling of control, MG132 and H_2O_2 treated hESC-RPE cells at time points of 3 and 12 weeks. Images represent **a** relative number of cells that respond to ATP stimulus at both timepoints, and relative maximum amplitudes at timepoints of **b** 3 weeks and **c** 12 weeks. Representative response curves at the timepoints of **d** 3 weeks and **e** 12 weeks. All results are conducted from 2 to 5 measurements. All data represents means ± SD. *$p < 0.05$ and ***$p < 0.001$. **f** Representative laser scanning confocal microscopy *z*-maximum intensity projections (*z*-MIP) and *yz* cross sections (MIP from 10 sections) of expression and localization of $P2Y_2$ receptor. Scale bar is 20 µm

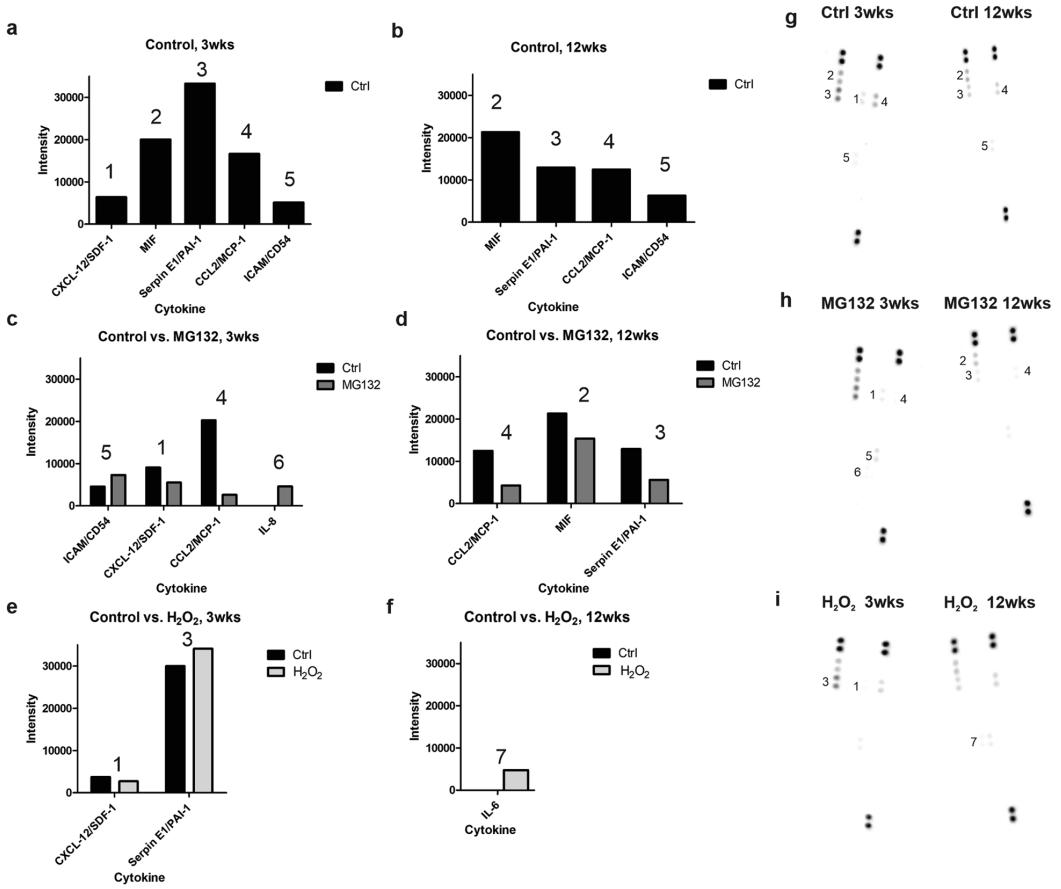

Fig. 6 Cytokine secretion of hESC-RPE cells. Intensity levels of secreted cytokines of control cells at **a** 3 weeks and **b** 12 weeks. Control values are values from membranes within each experiment ($n=2$ for 3 weeks and $n=1$ for 12 weeks). Intensity levels after MG132 treatment at **c** 3 weeks and **d** 12 weeks and after H_2O_2 treatment at **e** 3 weeks and **f** 12 weeks. **g**–**i** Cytokine array membranes illustrating spot intensities. Replicate experiment is shown in Additional file 2: Fig. S2

Discussion

Transplantation of RPE cells is a potential treatment strategy for retinal diseases such as AMD. The ability to differentiate RPE from hPSCs has offered a renewable cell source for therapeutical applications. For effective treatment, hPSC-RPE must exhibit the physiological characteristics of native human RPE. For therapeutic efficacy, it is important that the hPSC-RPE cells remain viable and are functional rapidly after transplantation in the challenging subretinal environment and in the presence of several additional stressors e.g. from the transplantation procedure itself and the environment of the diseased retina. Previously, hESC-RPE cell maturation level has been shown to affect their sensitivity to oxidative stress-induced cell death, however, the maturation status was evaluated only based on TER [11]. In addition, maturation level has been shown to affect transplant efficacy, but this has been evaluated only using the suspension transplantation approach [10]. In this study, most of the analyses were conducted with PET carriers which allow RPE maturation in monolayer format with physiologically relevant nutrient flow from the basolateral side and has also been used in transplantation setting [33]. We aimed to analyze the consequences of sublethal cellular stress induced by H_2O_2 and proteasome inhibitor MG132 to hESC-RPE with early versus late maturation status. Based

on our previous experience with hESC-RPE, expression and junctional localization of CL19 along with TER measurements are good indicators of functional maturation of the cells in culture, proper barrier function being a crucial property of RPE. Thus, in the current study, the maturation level was chosen mainly using these criteria and in accordance with our previous observations, junctional localization of CL19 was observed only after the 12-week culture time. Exposure to H_2O_2 is a widely used method to cause oxidative stress in cellular models and in RPE cells [34]. The ubiquitin-proteasome system on the other hand is responsible for degradation of damaged or redundant proteins which would otherwise accumulate as cellular debris and can be inactivated by oxidative stress [35].

Mitochondrial damage is adequate to initiate the degeneration of RPE leading to diseases such as AMD [36]. Mitochondria react rapidly and reversibly to many triggers from inside and outside the cell and have a key role for example in the activation of cell death [25]. Hence, we initiated this work by measuring the mitochondrial membrane potential after the treatment with MG132 or H_2O_2 to evaluate the fatality of the treatments, since mitochondrial membrane potential should decrease or cease in cell death [25]. Neither treatment showed signs of membrane potential decrease indicating that the treatments were not fatal to the cells. However, mitochondria protect themselves and other cellular components from oxygen damage [34] by activating defense mechanisms in response to cellular stressors. The subsequent increase in the need for energy could explain the increase in the mitochondrial membrane potential observed after the treatments. However, as cell populations are heterogenous in their responses, variation in the treated cells was large and included cells with remarkably lower membrane potentials compared to control.

RPE acts as a barrier between the choroid and subretinal space which is needed for proper neural homeostasis [37]. Tight junctional complexes between neighboring RPE cells ensure the proper functioning of this barrier. Tight junctions form in the apical periphery of contacting cells mediating the diffusion from the choroid to the subretinal space and vice versa. ZO1 and especially CL19 are responsible for the formation of the tight junction barrier in RPE and thereby take part in the modulation of transepithelial diffusion [38]. Disruption of this barrier enables an uncontrollable leakage of molecules and nutrients [37]. Transepithelial barrier can be measured with TER that we have previously shown to slowly increase during maturation as the tight junctions mature [12]. In addition, induction of oxidative stress has been shown to reduce TER which is usually a result of cell death [11, 24, 39]. In this study, as the TER reduced dramatically at 3 weeks after MG132 treatment, but the mitochondrial activity did not indicate cell death, tight junctions were analyzed in more detail. CL19 subcellular localization was altered at both time points with both chemical treatments, especially at 3 weeks after MG132 treatment. While CL19 localization was altered, the localization of ZO1 remained intact. Previously, Liu et al. [26] have demonstrated that CL19 knockdown has a similar effect with reduced TER and ZO1 remaining associated to apical junctional complex. Knockdown of CL19 has also been shown to affect phagocytosis [26], and similarly, in our study, the most pronounced reductions in CL19 junctional localization and in phagocytosis activity were correlated. Knockdown of CL19 reduced the rate of degradation but not binding or ingestion of POS in hiPSC-RPE [26]. However, in our study, the phagocytosis rate was analyzed after a short, 2-h incubation with POS, suggesting that the detected reduction in phagocytosis is more likely to reflect earlier events such as POS binding and/or internalization than degradation. Malfunctions in phagocytosis can lead to accumulation of POS particles and lipofuscin which together generate an enormous amount of reactive oxygen species (ROS) [26, 40]. One cause for the initiation of AMD is suggested to be the inability of RPE cells to demolish ROS [24]. Interestingly, in the study by Liu et al. [26], knockdown of CL19 activated AMPK, a protein kinase known to be activated by oxidative stress and linked to MER tyrosine kinase (MERTK) inactivation and inhibition of the internalization of POS in ARPE19 cells [41]. In the current study, phagocytosis was only reduced at 3-week time point and only with the MG132 treated cells. MG132 has been shown to activate AMPK in several cell types which were diminished by antioxidants [42], potentially suggesting a more developed antioxidant defense system in the more mature hESC-RPE at the 12-week time point.

In addition to tight and adherent junctions, cell–cell contacts in RPE consist of gap junctions. The gap junctions are formed by hemichannels, the basic components of which are connexins, Cx43 being the most widely expressed [27]. In the control hESC-RPE, Cx43 was localized in a similar manner on the apical and intercellular membrane than previously reported for mouse RPE and ARPE19 cells [43]. Cx43 has been suggested to have a protective role against oxidative stress, also in RPE cells where Cx43 knockdown increased the susceptibility of ARPE19 cells to oxidative stress-induced cell death [27, 44]. Oxidative stress was reported to alter the expression and subcellular localization of Cx43 in RPE by increasing its cytoplasmic aggregation, as was also seen in our study, especially in the cells with early maturation status followed by MG132 treatment and cells with late maturation status after H_2O_2 treatment. Connexins have a

half-life of only a few hours and depending on their stage of assembly, connexins can be degraded through different pathways [45]. In many cell types, treatment with proteasomal inhibitors leads to an increase in Cx43 immunoreactivity aggregates suggesting a role for proteasomes in the degradation of gap junctions. Gap junctions are also degraded via autophagy, an important homeostatic mechanism shown to be functional in hESC-RPE [23]. In many cell types, including RPE, proteasome inhibition seems to upregulate autophagy [46]. Although the maturation rate of the autophagic machinery in hESC-RPE during differentiation is not yet known, immature autophagy at the 3-week time point could at least partly explain the accumulation of Cx43 in the cells with early maturation status after MG132 treatment compared to the more mature hESC-RPE.

Na^+/K^+-ATPase maintains the transepithelial gradient [28]. In this study, the expression and apical localization of Na^+/K^+-ATPase were increased after the MG132 treatment. Proteins localized to plasma membranes are degraded via endocytosis but proteasomal inhibitors are known to inhibit endocytosis as well as degradation of proteins [47, 48]. The halftime of plasma membrane Na^+/K^+-ATPase in alveolar epithelium is 4 h [47]. Assuming that the regulation of Na^+/K^+-ATPase life cycle in RPE is similar, accumulation of Na^+/K^+-ATPase in the apical membrane within the timeframe of 24-h MG132 incubation can be perceived due to the malfunctions in endocytosis.

Purinergic signaling is important for the integrative functions of the retina and RPE. Intact ATP signaling can be considered as one key indicator of the hPSC-RPE authenticity, a prerequisite for the successful outcome of RPE transplantation therapy [32]. With our previously developed analysis tools for Ca^{2+} imaging [22], control cells demonstrated the ability to respond to the ATP stimulus already at the earlier time point. Further analysis revealed that the Ca^{2+} responses of the hESC-RPE with late maturation status cells were less exposed to the treatments compared to the population with early maturation status. The treatments affected the hESC-RPE cells so that the ability to respond was lost or the response was weaker compared to the control cells. We have previously shown that the higher maturation level increases the response amplitudes [12], although in this study, the maximum amplitudes were lower at 12 weeks compared to the cells with early maturation status. The comparison of the different maturation levels in Viheriälä et al. [12] was only 4 weeks, and in this study, the comparison is 9 weeks with completely different maturation levels. We also want to highlight that the increased pigmentation at 12 weeks can hinder the detection of the fluorescence signal, thus influencing the observed maximum amplitudes. In addition, the expression of the $P2Y_2$ receptor was increased during maturation suggesting that the low maximum amplitudes in control cells at 12 weeks were not due to compromised expression levels of the $P2Y_2$. However, the receptor was preserved better after the treatments at the 12 weeks, which could explain the better responses after the treatments at this time point. Differences in Ca^{2+} responses between MG132 and H_2O_2 treated cells could be, at least partly, explained by the $P2Y_2$ localization (Fig. 5f) which shifts from apical to more cytoplasmic, especially after the MG132 treatment at both time points.

RPE cells are known to be involved in immune responses and thereby secrete several immunomodulatory cytokines under normal conditions of the retina [49]. Their production is tightly regulated and can be modulated via various stimuli such as pathogens or other cytokines [50]. In addition, in some diseases like AMD, secretion of cytokines is dramatically upregulated [50]. RPE transplantation also has a risk of intraocular complications associated with inflammation and elevated levels of cytokines such as IFN-γ which is known to lead to upregulation of HLA-II expression in hPSC-RPE cells and immune reactions in HLA mismatched recipients [51–53]. Of the cytokines studied here, the untreated cells secreted CXCL-12/SDF-1, MIF, Serpin-1/PAI-1, CCL2/MCP-1, and ICAM/CD54, from which the CXCL-12/SDF-1 were secreted only at 3 weeks. In addition, IL6 and IL8 were secreted only after the treatments. Production of some of these cytokines by either primary or hPSC-RPE has been reported also previously by others [53, 54]. Being pro-inflammatory, these cytokines serve as important initiative signals for protective inflammation against pathogens. However, in the context of cell therapy, their secretion may increase the risk of graft rejection by e.g. chemoattraction of immune cells (CXCL12/SDF-1 [55], CCL2/MCP-1 [56], IL8 [56]) or influence angiogenesis (Serpin-1/PAI-1 [57], CCL2/MCP-1 [56]). The expression of CCL2/MCP-1 was downregulated after the MG132 treatment at both time points as has been shown previously for RPE by Liu et al. [58]. Secretion of MIF has been connected to proliferative vitreoretinopathy [39] and it has been shown to enhance migration and proliferation of RPE cells [59]. Interestingly, in two AMD patients treated with hESC-RPE, spreading of the pigmented area outward of the graft was noticed, potentially indicating migration of the hESC-RPE off the patch [6]. Of note, in our study, secretion of IL6, a mediator both in acute and chronic inflammatory responses, was expressed only after the treatment with H_2O_2 at both time points. In addition, IL8 was

expressed only after the MG132 treatment at 3-week time point. These findings are consistent with the earlier studies where have been shown the expression of IL6 and IL8 to be upregulated after the stimulation of H_2O_2 or MG132 [58, 60]. Despite the reported immunosuppressive properties of RPE cells, the production and induction of several proinflammatory molecules by hESC-RPE suggests that the use of immunosuppression in their transplantation is still essential [51].

RPE cells have robust defense mechanisms against oxidative stress, including pigmentation and efficient antioxidant and degradation systems [3], protecting e.g. tight junctions and therefore preventing the loss of critical RPE functions such as barrier integrity. The findings in the current study suggest that the development or maturation of these protective measures appears to correlate with the maturation of tight junctions and takes several weeks in hESC-RPE, rendering hESC-RPE with early maturation status vulnerable to even sublethal cell stress, potentially impairing critical RPE functions post-transplantation.

Conclusions

Based on the analyses conducted in this study, the hESC-RPE cells showed improved tolerance to cellular stress at the culture age of 12 weeks in comparison to 3 weeks. Toleration to cellular stress was studied with treatments of chemical stressors MG132 or H_2O_2. Treatments affected various hESC-RPE functional properties such as cellular barrier, rate of phagocytosis, Ca^{2+} signaling, and cytokine secretion. From these analyses, TER, phagocytosis, and Ca^{2+} signaling properties were reduced, and CL19 localization was shifted from apical to cytoplasmic at 3-week time point compared to 12 weeks, especially after MG132 treatment. Our results suggest the superiority of the more mature hESC-RPE population for successful cell therapy.

Abbreviations

RPE: Retinal pigment epithelium; hESC-RPE: Human embryonic stem cell-derived retinal pigment epithelium; Ca^{2+}: Calcium; H_2O_2: Hydrogen peroxide; AMD: Age-related macular degeneration; hPSC-RPE: Human pluripotent stem cell-derived retinal pigment epithelium; POS: Photoreceptor outer segment; ATP: Adenosine triphosphate; XF: Xeno-free; KO-DMEM: KnockOut™ Dulbecco's modified Eagle's medium; PET: Polyethylene terephthalate; TMRE: Tetramethylrhodamine ethyl ester; FCCP: Carbonyl cyanide 4-(trifluoromethoxy) phenylhydrazone; TER: Transepithelial electrical resistance; RT: Room temperature; PFA: Paraformaldehyde; PBS: Phosphate saline buffer; BSA: Bovine serum albumin; ZO-1: Zonula Occludens; Cx43: Connexin43; CL19: Claudin-19; MIP: Maximum intensity projections; FBS: Fetal bovine serum; Fluo-4 AM: Fluo-4-acetoxymethyl ester; ROI: Region of interest; MIF: Microphage migration factor; CCL2/MCP-1: Monocyte chemoattractant protein-1; ICAM/CD54: Intracellular adhesion molecule 1; CXCL12/SDF-1: Stromal cell-derived factor 1; Serpin-1/PAI-1: Plasminogen activator inhibitor-1; IL8: Interleukin8; IL6: Interleukin6; ROS: Reactive oxygen species; MERTK: MER tyrosine kinase.

Supplementary Information

The online version contains supplementary material available at https://doi.org/10.1186/s13287-022-02712-7.

Additional file 1. Fig. S1: Ca^{2+} signaling of control, MG132 and H_2O_2 treated hESC-RPE cells at time points of 3 and 12 weeks. Number of responding and non-responding cells at timepoints of a) 3 weeks and b) 12 weeks. Both time points include 2–5 replicate measurements. Bar data represents means ± SD. *$p < 0.05$.

Additional file 2. Fig. S2: Replicate of cytokine secretion of hESC-RPE. Intensity levels of secreted cytokines of control cells at a) 3 weeks and b) 12 weeks. Control values are average values from membranes within each experiment ($n = 2$ for 3 weeks and $n = 2$ for 12 weeks). Intensity levels after MG132 treatment at c) 3 weeks and b) 12 weeks and after H_2O_2 treatment at e) 3 weeks and f) 12 weeks. g)–i) Cytokine array membranes illustrating spot intensities.

Additional file 3. Fig. S3: Control membranes illustrating spot intensities from cytokine secretion assays of hESC-RPE at a) 3-week and b) 12-week time points. Exposure time in which the control spots (asterisks) had reached maximal grey value were chosen for each membrane.

Acknowledgements

We thank Outi Melin and Hanna Pekkanen for the technical assistance and contribution to cell production and Tampere Imaging Facility for their facilities. Marika Oksanen is also thanked for the assistance.

Authors' contributions

T.V., S.N., and T.I. designed the experiments. T.V. and H.H. performed the experiments. T.V. analyzed the data with contribution of S.N. and T.I. Ca^{2+} imaging analysis tools were developed by J.S. Funding acquisition H.S. Supervision T.I., S.N., H.S. Manuscript writing was mainly performed by T.V., T.I., and S.N. with contribution from all authors. All authors read and approved the final manuscript.

Funding

This research was supported by the Academy of Finland (Hongisto/315085, Skottman/323508, Skottman/304909, Nymark/287287, Nymark/323507), Finnish Cultural Foundation (00171144, 00181174), the Instrumentarium Foundation (170050, 180038), the Eye and Tissue Bank Foundation.

Availability of data and materials

All data used in this study are included in this article and additional files.

Declarations

Ethics approval and consent to participate

Tampere University has National Supervisory Authority for Welfare and Health (Dnro 1426/32/300/05) approval to conduct research on human embryos. The institute has also supportive statements of the Ethical Committee of the Pirkanmaa Hospital District to derive, culture, and differentiate hESC lines (Skottman/R05116). No new cell lines were derived for this study.

Consent for publication

Not applicable.

Competing interests

The authors declare that they have no competing interests.

Author details

[1]BioMediTech, Faculty of Medicine and Health Technology, Tampere University, Tampere, Finland. [2]Department of Ophthalmology, Institute of Clinical Medicine, University of Eastern Finland, Kuopio, Finland. [3]BioMediTech, Faculty of Medicine and Life Sciences, Tampere University, Arvo Ylpön katu 34, 33520 Tampere, Finland.

Received: 28 September 2021 Accepted: 10 January 2022
Published online: 24 January 2022

References

1. He Y, Ge J, Burke JM, Myers RL, Dong ZZ, Tombran-Tink J. Mitochondria impairment correlates with increased sensitivity of aging RPE cells to oxidative stress. J Ocul Biol Dis Inform. 2010;3(3):92–108.
2. Lidgerwood GE, Senabouth A, Smith-Anttila CJA, Gnanasambandapillai V, Kaczorowski DC, Amann-Zalcenstein D, et al. Transcriptomic profiling of human pluripotent stem cell-derived retinal pigment epithelium over time. Genom Proteom Bioinform. 2020. https://doi.org/10.1016/j.gpb.2020.08.002.
3. Plafker SM, O'Mealey GB, Szweda LI. Mechanisms for countering oxidative stress and damage in retinal pigment epithelium. In: International review of cell and molecular biology, vol. 298; 2012. p. 135–77. https://doi.org/10.1016/B978-0-12-394309-5.00004-3.
4. Schwartz SD, Regillo CD, Lam BL, Eliott D, Rosenfeld PJ, Gregori NZ, et al. Human embryonic stem cell-derived retinal pigment epithelium in patients with age-related macular degeneration and Stargardt's macular dystrophy: follow-up of two open-label phase 1/2 studies. Lancet. 2015;385(9967):509–16. https://doi.org/10.1016/S0140-6736(14)61376-3.
5. Sugita S, Mandai M, Hirami Y, Takagi S, Maeda T, Fujihara M, et al. HLA-matched allogeneic iPS cells-derived RPE transplantation for macular degeneration. J Clin Med. 2020;9(7):2217.
6. Da Cruz L, Fynes K, Georgiadis O, Kerby J, Luo YH, Ahmado A, et al. Phase 1 clinical study of an embryonic stem cell-derived retinal pigment epithelium patch in age-related macular degeneration. Nat Biotechnol. 2018;36(4):328–37. https://doi.org/10.1038/nbt.4114.
7. Kashani AH, Lebkowski JS, Rahhal FM, Avery RL, Salehi-Had H, Dang W, et al. A bioengineered retinal pigment epithelial monolayer for advanced, dry age-related macular degeneration. Sci Transl Med. 2018;10(435):1–11.
8. Mandai M, Watanabe A, Kurimoto Y, Hirami Y, Morinaga C, Daimon T, et al. Autologous induced stem-cell-derived retinal cells for macular degeneration. N Engl J Med. 2017;376(11):1038–46.
9. Vaajasaari H, Ilmarinen T, Juuti-Uusitalo K, Rajala K, Onnela N, Narkilahti S, et al. Toward the defined and xeno-free differentiation of functional human pluripotent stem cell-derived retinal pigment epithelial cells. Mol Vis. 2011;17:575.
10. Davis RJ, Alam NM, Zhao C, Müller C, Saini JS, Blenkinsop TA, et al. The Developmental stage of adult human stem cell-derived retinal pigment epithelium cells influences transplant efficacy for vision rescue. Stem Cell Rep. 2017;9(1):42–9.
11. Hsiung J, Zhu D, Hinton DR. Polarized human embryonic stem cell-derived retinal pigment epithelial cell monolayers have higher resistance to oxidative stress-induced cell death than nonpolarized cultures. Stem Cells Transl Med. 2015;4(1):10–20.
12. Viheriälä T, Sorvari J, Ihalainen TO, Mörö A, Grönroos P, Schlie-Wolter S, et al. Culture surface protein coatings affect the barrier properties and calcium signalling of hESC-RPE. Sci Rep. 2021;11(1):1–14. https://doi.org/10.1038/s41598-020-79638-8.
13. Strauss O. The retinal pigment epithelium in visual function. Physiol Rev. 2005;85(3):845–81.
14. Tonelli FM, Santos AK, Gomes DA, da Silva SL, Gomes KN, Ladeira LO, et al. Stem cells and calcium signaling. Adv Exp Med Biol. 2012;740:891–916.
15. Abu Khamidakh AE, dos Santos FC, Skottman H, Juuti-Uusitalo K, Hyttinen J. Semi-automatic method for Ca2+ imaging data analysis of maturing human embryonic stem cells-derived retinal pigment epithelium. Ann Biomed Eng. 2016;44(11):3408–20.
16. Mitchell CH, Reigada D. Purinergic signalling in the subretinal space: a role in the communication between the retina and the RPE. Purinergic Signal. 2008;4(2):101–7.
17. Peterson WM, Meggyesy C, Yu K, Miller SS. Extracellular ATP activates calcium signaling, ion, and fluid transport in retinal pigment epithelium. J Neurosci. 1997;17(7):2324–37.
18. Fernandes AF, Zhou J, Zhang X, Bian Q, Sparrow J, Taylor A, et al. Oxidative inactivation of the proteasome in retinal pigment epithelial cells: a potential link between oxidative stress and up-regulation of interleukin-8. J Biol Chem. 2008;283(30):20745–53.
19. Hongisto H, Ilmarinen T, Vattulainen M, Mikhailova A, Skottman H. Xeno- and feeder-free differentiation of human pluripotent stem cells to two distinct ocular epithelial cell types using simple modifications of one method. Stem Cell Res Ther. 2017;8(1):1–15.
20. Schindelin J. Fiji: an open-source platform for biological-image analysis. Nat Methods. 2012;9:676–82.
21. Schneider CA, Rasband WS, Eliceiri KW. NIH image to ImageJ: 25 years of image analysis. Nat Methods. 2012;9:671–5.
22. Sorvari J, Viheriälä T, Ilmarinen T, Ihalainen TO, Nymark S. Analysis of ATP-induced Ca2+ responses at single cell level in retinal pigment epithelium monolayers. Retin Degener Dis. 2019;1185:525–30.
23. Juuti-Uusitalo K, Koskela A, Kivinen N, Viiri J, Hyttinen JMT, Reinisalo M, et al. Autophagy regulates proteasome inhibitor-induced pigmentation in human embryonic stem cell-derived retinal pigment epithelial cells. Int J Mol Sci. 2017;18(5):1–17.
24. Juuti-Uusitalo K, Nieminen M, Treumer F, Ampuja M, Kallioniemi A, Klettner A, et al. Effects of cytokine activation and oxidative stress on the function of the human embryonic stem cell-derived retinal pigment epithelial cells. Investig Ophthalmol Vis Sci. 2015;56(11):6265–74.
25. Wang C, Youle RJ. The role of mitochondria in apoptosis. Annu Rev Genet. 2019;43:95–118.
26. Liu F, Peng S, Adelman RA, Rizzolo LJ. Knockdown of claudin-19 in the retinal pigment epithelium is accompanied by slowed phagocytosis and increased expression of SQSTM1. Investig Ophthalmol Vis Sci. 2021;62(2):1–3.
27. Hutnik CML, Pocrnich CE, Liu H, Laird DW, Shao Q. The protective effect of functional connexin43 channels on a human epithelial cell line exposed to oxidative stress. Investig Ophthalmol Vis Sci. 2008;49(2):800–6.
28. Reichhart N, Strauß O. Ion channels of the retinal pigment epithelium. In: Retinal pigment epithelium in health and disease; 2020. p. 65–84. https://doi.org/10.1007/978-3-030-28384-1_4.
29. Hu YJ, Wang YD, Tan FQ, Yang WX. Regulation of paracellular permeability: factors and mechanisms. Mol Biol Rep. 2013;40(11):6123–42.
30. Rajasekaran SA, Hu J, Gopal J, Gallemore R, Ryazantsev S, Bok D, et al. Na, K-ATPase inhibition alters tight junction structure and permeability in human retinal pigment epithelial cells. Am J Physiol Cell Physiol. 2003;284(653–6):1497–507.
31. Olchawa MM, Pilat AK, Szewczyk GM, Sarna TJ. Inhibition of phagocytic activity of ARPE-19 cells by free radical mediated oxidative stress. Free Radic Res. 2016;50(8):887–97.
32. Miyagishima K, Wan Q, Corneo B, Sharma R, Lotfi M, Boles NC, et al. In pursuit of authenticity: induced pluripotent stem cell-derived retinal pigment epithelium for clinical applications. Stem Cells Transl Med. 2016;5:1–13.
33. Liu Z, Ilmarinen T, Tan GSW, Hongisto H, Wong EYM, Tsai ASH, et al. Submacular integration of hESC-RPE monolayer xenografts in a surgical non-human primate model. Stem Cell Res Ther. 2021;12:1–16.
34. Ransy C, Vaz C, Lombès A, Bouillaud F. Use of H2O2 to cause oxidative stress, the catalase issue. Int J Mol Sci. 2020;21(23):1–14.
35. Blasiak J, Pawlowska E, Szczepanska J, Kaarniranta K. Interplay between autophagy and the ubiquitin-proteasome system and its role in the pathogenesis of age-related macular degeneration. Int J Mol Sci. 2019;20(1):210. https://doi.org/10.3390/ijms20010210.
36. Brown EE, DeWeerd AJ, Ildefonso CJ, Lewin AS, Ash JD. Mitochondrial oxidative stress in the retinal pigment epithelium (RPE) led to metabolic dysfunction in both the RPE and retinal photoreceptors. Redox Biol. 2019;24(March): 101201. https://doi.org/10.1016/j.redox.2019.101201.
37. Naylor A, Hopkins A, Hudson N, Campbell M. Tight junctions of the outer blood retina barrier. Int J Mol Sci. 2020;21(1):211. https://doi.org/10.3390/ijms21010211.
38. Liu F, Xu T, Peng S, Adelman RA, Rizzolo LJ. Claudins regulate gene and protein expression of the retinal pigment epithelium independent of their association with tight junctions. Exp Eye Res. 2020;198(198): 108157. https://doi.org/10.1016/j.exer.2020.108157.
39. Ko JA, Sotani Y, Ibrahim DG, Kiuchi Y. Role of macrophage migration inhibitory factor (MIF) in the effects of oxidative stress on human retinal pigment epithelial cells. Cell Biochem Funct. 2017;35(7):426–32.
40. Boulton M, Rózanowska M, Rózanowski B, Wess T. The photoreactivity of ocular lipofuscin. Photochem Photobiol Sci. 2004;3(8):759–64.
41. Qin S. Blockade of MerTK activation by AMPK inhibits RPE cell phagocytosis. Retin Degener Dis. 2016;854:773–8.
42. Jiang S, Park DW, Gao Y, Ravi S, Darley-Usmar V, Abraham E, et al. Participation of proteasome-ubiquitin protein degradation in autophagy and the activation of AMP-activated protein kinase. Cell Signal. 2015;27(6):1186–97.
43. Akanuma S, Higashi H, Maruyama S, Murakami K, Tachikawa M, Kubo Y, et al. Expression and function of connexin 43 protein in mouse and

human retinal pigment epithelial cells as hemichannels and gap junction proteins. Exp Eye Res. 2017;2018(168):128–37. https://doi.org/10.1016/j.exer.2018.01.016.
44. Giardina SF, Mikami M, Goubaeva F, Yang J. Connexin 43 confers resistance to hydrogen peroxide-mediated apoptosis. Biochem Biophys Res Commun. 2007;362(3):747–52.
45. Falk MM, Kells RM, Berthoud VM. Degradation of connexins and gap junctions. FEBS Lett. 2014;588(8):1221–9.
46. Zhan J, He J, Zhou Y, Wu M, Liu Y, Shang F, et al. Crosstalk between the autophagy-lysosome pathway and the ubiquitin-proteasome pathway in retinal pigment epithelial cells. Curr Mol Med. 2016;16(5):487–95.
47. Lecuona E, Sun H, Vohwinkel C, Ciechanover A, Sznajder JI. Ubiquitination participates in the lysosomal degradation of Na, K-ATPase in steady-state conditions. Am J Respir Cell Mol Biol. 2009;41(6):671–9.
48. Dada LA, Welch LC, Zhou G, Ben-Saadon R, Ciechanover A, Sznajder JI. Phosphorylation and ubiquitination are necessary for Na, K-ATPase endocytosis during hypoxia. Cell Signal. 2007;19(9):1893–8.
49. Holtkamp GM, Kijlstra A, Peek R, De Vos AF. Retinal pigment epithelium-immune system interactions: cytokine production and cytokine-induced changes. Prog Retin Eye Res. 2001;20(1):29–48.
50. Shi G, Maminishkis A, Banzon T, Jalickee S, Li R, Hammer J, et al. Control of chemokine gradients by the retinal pigment epithelium. Investig Ophthalmol Vis Sci. 2008;49(10):4620–30.
51. Idelson M, Alper R, Obolensky A, Yachimovich-cohen N, Rachmilewitz J, Ejzenberg A, et al. Immunological properties of human embryonic stem cell-derived retinal pigment epithelial cells. Stem Cell Rep. 2018;11(3):681–95. https://doi.org/10.1016/j.stemcr.2018.07.009.
52. Ilmarinen T, Thieltges F, Hongisto H, Juuti-uusitalo K, Koistinen A, Kaarniranta K, et al. Survival and functionality of xeno-free human embryonic stem cell-derived retinal pigment epithelial cells on polyester substrate after transplantation in rabbits. Acta Ophthalmol. 2019;97:688–99.
53. Sugita S, Mandai M, Kamao H, Takahashi M. Immunological aspects of RPE cell transplantation. Prog Retin Eye Res. 2021;84(January):100950. https://doi.org/10.1016/j.preteyeres.2021.100950.
54. Sugita S, Kamao H, Iwasaki Y, Okamoto S, Hashiguchi T, Iseki K, et al. Inhibition of T-cell activation by retinal pigment epithelial cells derived from induced pluripotent stem cells. Immunol Microbiol. 2015;56:1051–62.
55. Chan C, Shen D, Hackett JJ, Buggage RR, Tuaillon N. Expression of chemokine receptors, BLC and SDF-1, in the eyes of patients with primary intraocular lymphoma. Ophthalmology. 2003;110(02):421–6.
56. Detrick B, Hooks JJ. The RPE cell and the immune system. In: Retinal pigment epithelium in health and disease; 2020. https://doi.org/10.1007/978-3-030-28384-1_6.
57. Noe S, Frankenne F, Bajou K, Gerard R, Carmeliet P, Defresne MP. Influence of plasminogen activator inhibitor type 1 on choroidal neovascularization. FASEB J. 2001;15(6):1021–7.
58. Liu Z, Qin T, Zhou J, Taylor A, Sparrow JR, Shang F. Impairment of the ubiquitin-proteasome pathway in rpe alters the expression of inflammation related genes. Adv Exp Med Biol. 2014;801:237–50. https://doi.org/10.1007/978-3-319-17121-0.
59. Nishihira J. Macrophage migration inhibitory factor (MIF): its essential role in the immune system and cell growth. J Interferon Cytokine Res. 2000;20(9):751–62.
60. Wu WC, Hu DN, Gao HX, Chen M, Wang D, Rosen R, et al. Subtoxic levels hydrogen peroxide-induced production of interleukin-6 by retinal pigment epithelial cells. Mol Vis. 2010;16(April):1864–73.

Publisher's Note

PUBLICATION III

Functional voltage-gated calcium channels are present in human embryonic stem cell-derived retinal pigment epithelium

Korkka I, Viheriälä T, Juuti-Uusitalo K, Uusitalo-Järvinen H, Skottman H, Hyttinen J, Nymark S

Stem Cells Translational Medicine (2019), 8:179-193
https://doi.org/10.1002/sctm.18-0026

STEM CELLS TRANSLATIONAL MEDICINE®

TISSUE ENGINEERING AND REGENERATIVE MEDICINE

Functional Voltage-Gated Calcium Channels Are Present in Human Embryonic Stem Cell-Derived Retinal Pigment Epithelium

IINA KORKKA,[a] TAINA VIHERIÄLÄ,[a,b] KATI JUUTI-USITALO,[b] HANNELE UUSITALO-JÄRVINEN,[c,d] HELI SKOTTMAN,[b] JARI HYTTINEN,[a] SOILE NYMARK[a]

[a]Faculty of Biomedical Sciences and Engineering, BioMediTech, Tampere University of Technology, Tampere, Finland; [b]Faculty of Medicine and Life Sciences, BioMediTech, University of Tampere, Tampere, Finland; [c]Eye Centre, Tampere University Hospital, Tampere, Finland; [d]Faculty of Medicine and Life Sciences, Department of Ophthalmology, University of Tampere, Tampere, Finland

Correspondence: Soile Nymark, Ph.D., Arvo Ylpön katu 34, 33520 Tampere, Finland. Telephone: 358 40 849 0009; e-mail: soile.nymark@tut.fi

Received February 5, 2018; accepted for publication September 7, 2018; first published November 4, 2018.

http://dx.doi.org/10.1002/sctm.18-0026

Key Words. Retinal pigment epithelium • Voltage-gated Ca^{2+} channels • Stem cells • Patch-clamp • Vascular endothelial growth factor • Phagocytosis

ABSTRACT

Retinal pigment epithelium (RPE) performs important functions for the maintenance of photoreceptors and vision. Malfunctions within the RPE are implicated in several retinal diseases for which transplantations of stem cell-derived RPE are promising treatment options. Their success, however, is largely dependent on the functionality of the transplanted cells. This requires correct cellular physiology, which is highly influenced by the various ion channels of RPE, including voltage-gated Ca^{2+} (Ca_V) channels. This study investigated the localization and functionality of Ca_V channels in human embryonic stem cell (hESC)-derived RPE. Whole-cell patch-clamp recordings from these cells revealed slowly inactivating L-type currents comparable to freshly isolated mouse RPE. Some hESC-RPE cells also carried fast transient T-type resembling currents. These findings were confirmed by immunostainings from both hESC- and mouse RPE that showed the presence of the L-type Ca^{2+} channels $Ca_V1.2$ and $Ca_V1.3$ as well as the T-type Ca^{2+} channels $Ca_V3.1$ and $Ca_V3.2$. The localization of the major subtype, $Ca_V1.3$, changed during hESC-RPE maturation co-localizing with pericentrin to the base of the primary cilium before reaching more homogeneous membrane localization comparable to mouse RPE. Based on functional assessment, the L-type Ca^{2+} channels participated in the regulation of vascular endothelial growth factor secretion as well as in the phagocytosis of photoreceptor outer segments in hESC-RPE. Overall, this study demonstrates that a functional machinery of voltage-gated Ca^{2+} channels is present in mature hESC-RPE, which is promising for the success of transplantation therapies. STEM CELLS TRANSLATIONAL MEDICINE *2019;8:179–193*

SIGNIFICANCE STATEMENT

Human stem cells provide a promising cell source for the replacement of diseased retinal pigment epithelium (RPE) in the eye, and several clinical trials with cell transplantations are ongoing. The success of these therapies is largely dependent on the correct functionality of the transplanted cells. Still, cellular ion channels, vital for the proper RPE physiology, are inadequately characterized in stem cell-derived RPE. The results of this study demonstrate the presence and functionality of voltage-gated Ca^{2+} channels in mature human embryonic stem cell-derived RPE similar to native RPE, and provide insight into their physiological relevance. This work is a significant contribution toward a more detailed functionality confirmation of stem cell-derived RPE.

INTRODUCTION

Retinal pigment epithelium (RPE) is a monolayer of polarized cells located in the back of the eye between the photoreceptors and the choroid, and forms a part of the blood-retinal-barrier [1]. As a barrier, RPE regulates the transport of nutrients and ions between the bloodstream and the subretinal space. In addition, RPE performs essential functions for vision such as phagocytosis, secretion, visual cycle, and light absorption (reviewed in [2]). RPE also plays a critical role in the pathogenesis of several degenerative eye diseases such as age-related macular degeneration (AMD) [3] that is the leading cause of vision loss and blindness among the elderly worldwide [4]. Stem cells provide potential for the development of transplantation therapies producing a limitless source of RPE cells for the treatment of AMD and other RPE-originated retinal dystrophies [5]. Remarkably, such therapies are already being subjected to clinical trials for AMD and Stargardt's macular dystrophy [6–21]

as well as to several preclinical trials [5, 22–28]. Stem cell-derived RPE has been demonstrated to resemble native tissue in many respects: it has been shown to have a proteome closely similar to the native counterpart [29], phagocytose photoreceptor outer segment (POS) fragments [27, 28, 30–32], secrete vascular endothelial growth factor (VEGF) [32–34], and participate in the functional visual cycle [35, 36]. However, much is still not understood about the genetic characteristics of stem cell-derived RPE [37] or its behavior after transplantation [38]. Furthermore, there is only limited information about the functionality of ion channels [33] and Ca^{2+} signaling [31, 39, 40] in stem cell-derived RPE. In particular, studies about the voltage-gated Ca^{2+} (Ca_V) channels in these cells are lacking.

The correct operation of Ca_V channels is required in order for the stem cell-derived RPE to perform its critical functions in therapeutic use, since many of the important RPE functions are related to changes in intracellular Ca^{2+} concentration [2]. L-type Ca^{2+} channels have been identified in cultured and native RPE [41–55], where they participate in the transport of ions and water [42] as well as the regulation of POS phagocytosis [41], VEGF secretion [43], and RPE differentiation [2]. On the other hand, the malfunctioning of L-type Ca^{2+} channels in RPE has been linked to the pathogenesis of certain degenerative eye diseases [45, 56]. Of the L-type Ca^{2+} channels, RPE has been shown to express the subtypes $Ca_V1.1$–1.3 [46] with several studies suggesting that subtype $Ca_V1.3$ is the primary contributor to RPE physiology [41, 43, 46, 50–55]. Of the T-type Ca^{2+} channels, RPE has been reported to express the subtypes $Ca_V3.1$ and $Ca_V3.3$, and it has been speculated that these channels participate in the regulation of VEGF secretion [46]. To date, α subtypes of the third subfamily $Ca_V2.x$ have not been detected in RPE [46]. It is, however, unclear whether this impressive machinery of Ca^{2+} channels is present in stem cell-derived RPE, and raises a question about the resemblance of human embryonic stem cell (hESC)-derived RPE to native RPE.

To address this issue, we investigated the functionality and localization profile of Ca_V channels in hESC-RPE. Here, we present our patch-clamp recordings that reveal slowly inactivating L-type currents in hESC-RPE that are similar to native RPE. In some hESC-RPE cells, fast transient currents that resemble T-type currents were also recorded. When compared with mouse tissue, there were similarities, as well as certain differences, in the localization of Ca_V channels in hESC-RPE. With regard to physiology, we show that L-type Ca^{2+} channels participate in POS phagocytosis and the regulation of VEGF secretion in hESC-RPE. Overall, our results suggest that a functional machinery of voltage-gated Ca^{2+} channels is present in hESC-RPE, and thus strengthen the potential of stem cell-derived RPE in transplantation therapies.

Materials and Methods

Culture of hESC-RPE

In this study, we used the previously derived hESC lines Regea08/023, Regea08/017, and Regea11/013 [57]. The undifferentiated hESCs were maintained, cultured, and spontaneously differentiated as described before [58]. After approximately 72–124 days of differentiation in the suspension culture, the pigmented areas of the floating aggregates were manually separated. The pigmented cell clusters were dissociated with TrypLE Select (Invitrogen, UK) and seeded onto Collagen IV (5 μg/cm^2, Sigma-Aldrich, St. Louis, MO) coated 24-well cell culture plates (Corning CellBIND; Corning, Inc., Corning, NY) with a density of 5.5×10^5 cells/cm^2. The cells were cultured for approximately 22–73 days, and cells from several independent differentiation batches were used for the study.

The cells were passaged with a density of 2.5×10^5 cells/cm^2 onto polyethylene terephthalate coated hanging culture inserts (pore size 1 μm, Merck Millipore) treated with Collagen IV (10 μg/cm^2, Sigma-Aldrich) or with Collagen IV and laminin (1.8 μg/cm^2, LN521, Biolamina, Sweden). The cultures became confluent in 5 days on inserts, after which they were further cultured until mature monolayers were obtained (days post-confluence presented in each figure legend). For single cell patch-clamp experiments, the cells were detached from the inserts with TrypLE Select and let to adhere on cover slips treated with poly-L-lysine (Sigma-Aldrich).

Isolation of Mouse RPE

We used C57BL/6 mice at the age of 8–12 weeks where the development and maturation of RPE had been completed [59]. The mice were euthanized by CO_2 inhalation and cervical dislocation. The eyes were then enucleated and bisected along the equator. The eyecups were sectioned in Ames' solution (Sigma-Aldrich) with 10 mM HEPES and pH adjusted to 7.4, and the retina was gently removed leaving the RPE firmly attached to the eyecup. To isolate the RPE cells for patch-clamp recordings, the eyecup was incubated at 37°C in 5% CO_2 either in TrypLE Select for 15 minutes or in a solution containing (in mM) 135 TeaCl, 5 KCl, 10 HEPES, 3 EDTA-KOH, 10 glucose, and 25 U/ml activated papain (Sigma-Aldrich) for 30 minutes. After this, the eyecups were washed in the HEPES buffered Ames' solution supplemented with 1% bovine serum albumin (BSA; Sigma-Aldrich). The RPE was collected by gentle trituration, stored at 37°C in 5% CO_2 in the RPE culture medium and measured within 6 hours.

Ethical Issues

Approval for research with human embryos was given by the National Authority for Medicolegal Affairs, Finland (Dnro 1426/32/300/05). A supportive statement was received from the Local Ethics Committee of the Pirkanmaa Hospital District, Finland to derive and expand hESC lines from surplus embryos, and to use these cell lines for research purposes (R05116). No new cell lines were derived in this study. The procedures carried out with C57BL/6 mice were in accordance with the ARVO Statement for the Use of Animals in Ophthalmic and Vision Research and the Finnish Animal Welfare Act 1986.

Patch-Clamp Recordings

Patch-clamp recordings were performed at room temperature (RT) on single hESC-RPE and mouse RPE cells. Ionic currents were recorded using the standard patch-clamp technique in whole-cell configuration. To minimize potassium currents, patch pipettes (resistance 4–8 MΩ) were filled with a cesium based internal solution containing (in mM) 83 $CsCH_3SO_3$, 25 CsCl, 5.5 EGTA, 0.5 $CaCl_2$, 4 ATP-Mg, 0.1 GTP-Na, 10 HEPES, and 5 NaCl; pH was adjusted to ~7.2 with CsOH and osmolarity was adjusted to ~290 mOsm with sucrose. The internal solution contained 2 mM lidocaine *N*-ethyl chloride (Sigma-Aldrich) to exclude the possibility of the measured fast transient currents being carried

by sodium [60]. The tissue was perfused with a control external solution containing (in mM): 120 NaCl, 5 TeaCl, 1.1 $CaCl_2$, 1.2 $MgCl_2$, 10 HEPES, 5 glucose, and 10 $BaCl_2$. pH was adjusted to 7.4 with NaOH and the osmolarity was set to ~305 mOsm with sucrose. In some experiments, the $BaCl_2$ concentration was decreased to 1 mM, and this was compensated by increasing the NaCl concentration to 130 mM. In the experiments that used Ca^{2+} channel modulators, the control bath solution contained L-type Ca^{2+} channel activator 10 μM (-)BayK8644 (Sigma-Aldrich) or L-type Ca^{2+} channel inhibitor 10 μM nifedipine (Sigma-Aldrich). The recordings were made in voltage-clamp mode using the Axopatch200B patch-clamp amplifier connected to an acquisition computer via AD/DA Digidata1440 (Molecular Devices, CA). Potentials were corrected for a 10 mV liquid junction potential during data analysis. Access resistance was <25 MΩ and membrane resistance was >300 MΩ. The membrane capacitance was 33 ± 5 pF (mean ± SEM, n = 9) for hESC-RPE cells and 23 ± 3 pF (mean ± SEM, n = 3) for mouse RPE cells. The depletion of the currents in hESC-RPE cells in whole-cell configuration was −11 ± 3% during 19 ± 5 minutes (mean ± SEM, n = 3) measured using a 50 ms voltage step from −100 to 10 mV. The measurements lasted for a shorter time than that of depletion. Current–voltage (IV)-curves were obtained from the peak value of the current at given voltages. Conductance (G) was calculated as $G = I/(V–V_R)$, where V_R is the reversal potential.

Indirect Immunofluorescence Staining

For immunofluorescence staining, hESC-RPE monolayers and mouse RPE eyecups were fixed for 15 minutes with 4% paraformaldehyde. The hESC-RPE monolayers and mouse RPE eyecup whole mount preparations were permeabilized by 15 minutes incubation in 0.1% Triton X-100 (Sigma-Aldrich) at RT. This was followed by incubation with 3% BSA in phosphate-buffered saline (PBS) (Sigma-Aldrich) at RT for 1 hour. Primary antibodies for $Ca_V1.1$, $Ca_V1.2$, $Ca_V1.3$, $Ca_V3.1$, $Ca_V3.2$, $Ca_V3.3$ (1:100; Alomone Labs, Jerusalem, Israel), cellular retinaldehyde-binding protein (CRALBP; 1:500; Abcam, UK), zonula occludens (ZO-1; 1:50; Life Technologies), claudin-3 (1:80; Thermo Fisher Scientific), ezrin (1:100; Abcam, UK), acetylated α-tubulin (1:1,000; Sigma-Aldrich), and pericentrin (PCNT; 1:200; Abcam, UK) were diluted in 3% BSA-PBS and incubated for 1 hour at RT. The samples were then washed four times with PBS, followed by 1 hour incubation at RT with the secondary antibodies donkey anti-rabbit or anti-mouse Alexa Fluor 488 and donkey anti-rabbit or anti-mouse Alexa Fluor 568 (1:200; Life Technologies) as well as goat anti-rabbit or anti-mouse Alexa Fluor 488 and goat anti-mouse Alexa Fluor 568 (1:200; Thermo Fisher Scientific) diluted in 3% BSA-PBS. Phalloidin was visualized using Phalloidin-Atto 633 (1:100; Sigma-Aldrich), an Alexa Fluor 568 conjugate (1:400; Sigma-Aldrich) or an Alexa Fluor 647 conjugate (1:50; Life Technologies). The washes with PBS were repeated and the nuclei were stained with the 4′,6-diamidino-2-phenylidole included in the mounting medium (Life Technologies).

For paraffin embedded vertical sections, the hESC-RPE monolayers and mouse eyecups with retina attached were infused in paraffin blocks and cut into 7 μm vertical sections with a Leica SM2000 R or Leica SM2010 R sliding microtome (Leica Biosystems). The sections were then attached on glass coverslides by 1 hour incubation at 60°C. The samples were deparaffinized and hydrolyzed using xylene and ethanol series. Antigen retrieval was carried out by microwaving the samples in 10 mM sodium citrate in 0.05% Tween20 (Sigma Aldrich). The samples were blocked using 10% donkey serum and 5% BSA in tris-buffered saline (TBS) for 1 hour at 37°C. After this, they were washed twice in 0.02% Tween20-TBS. The Ca_V primary antibodies listed above, as well as Na^+/K^+-ATPase (1:200; Abcam) and Bestrophin-1 (1:500; Lagen laboratories) were diluted in 1% BSA-TBS and incubated overnight at 4°C. The samples were then washed twice with 0.02% Tween20-TBS. The secondary antibodies introduced above were diluted with 1% BSA-TBS and incubated for 1 hour at RT, followed by two washes and mounting as described above.

Confocal Microscopy and Image Processing

Confocal microscopy was performed with a Zeiss LSM780 or LSM700 laser scanning confocal microscope (LSCM) on an inverted Zeiss Cell Observer microscope (Zeiss, Jena, Germany) and Plan-Apochromat ×63/1.4 oil immersion objective. Voxel size was set to $x = y$ = 66 nm and z = 100–200 nm and image size to 512 × 512 or 1,024 × 1,024 pixels. Reflection imaging was conducted by collecting light from the 488 nm laser line by using 20/80 dichroic beam splitter and 480–492 nm emission window at the photomultiplier tube detector. The images were saved in czi-format and processed with ImageJ [61], adjusting only brightness and contrast, and panels were assembled using Adobe Photoshop CS6 (Adobe Systems, San Jose).

Pulse-Chase Phagocytosis Assay

Mature hESC-RPE monolayers on culture inserts were pre-incubated for 24 hours at 37°C in the control medium or in the presence of the L-type Ca_V modulators 10 μM (-)BayK8644, or 10 μM nifedipine, or T-type Ca_V inhibitor 5 μM ML218 (Sigma-Aldrich). For phagocytosis assay, POS fragments were isolated and purified from fresh porcine eyes obtained from a local slaughterhouse as described before [58, 62]. The POS particles were suspended to 10% fetal bovine serum (FBS) containing medium in control or in one of the drug containing conditions. In the pulse stage, equal amounts of POS containing media were added on the apical sides of the hESC-RPE inserts and incubated for 30 minutes at 37°C. For the chase stage, the media were changed back to 10% FBS medium with or without the drugs, and the hESC-RPE inserts were further incubated for 2 hours at 37°C. After this, the samples were fixed and stained as described above using the primary antibodies opsin (1:200; Sigma Aldrich) and ZO-1. The samples were imaged using the Zeiss LSM780 LSCM as described above but by imaging large random fields. The number of bound and internalized POS particles that were larger than 1 μm in diameter, were counted from maximum intensity projection images after performing Gaussian blur using ImageJ. The assay was performed with three inserts in each condition and data from 5 to 6 images from each of the three inserts was pooled together resulting in n = 15–16.

Enzyme-Linked Immunosorbent Assay for VEGF Secretion

Secretion of VEGF by mature hESC-RPE was assessed with a commercially available human VEGF Quantikine enzyme-linked immunosorbent assay (ELISA) kit (R&D Systems, MN) according to the manufacturer's instructions. Briefly, the polarized VEGF secretion in control conditions was studied by collecting medium samples separately from the apical and basolateral sides of the

insert after 24 hours incubation with three replicates. To test the effect of Ca_V channel modulators on VEGF secretion, we measured the total VEGF concentration secreted through both apical and basolateral cell membranes. The inserts were incubated 24 hours in different pharmacological conditions: in 1% FBS medium in control conditions, or in this medium together with 10 μM (-)BayK8644, 10 μM nifedipine or 5 μM ML218 with eight to nine replicates. The VEGF concentration from the collected medium samples was normalized to the number of cells based on cell counting under the Zeiss LSM780 LSCM using ×20 or ×63 objective.

Statistical Analysis

The data is stated as mean ± SEM (n, p), where n refers to the number of samples used to generate the data set and p refers to statistical significance. The data was tested for normality using the Shapiro–Wilk normality test. Some of the data sets did not meet the normality criteria. Thus, a pair-wise comparison of the test conditions to control condition was conducted using non-parametric Mann-Whitney U test to confirm the possible statistical significance between the experimental conditions.

Results

Currents Through Voltage-Gated Ca^{2+} Channels in hESC-RPE

In control conditions with 10 mM extracellular Ba^{2+}, whole-cell voltage clamp recordings revealed voltage-gated currents in single hESC-RPE cells (Fig. 1A) dissociated from a mature RPE monolayer (Fig. 1B). In response to a 50 ms voltage pulse from −80 to 60 mV in 10 mV steps, nine cells showed slowly or non-inactivating currents (Fig. 1C). Based on the normalized and averaged IV-curve (n = 9), the current activated at low potentials reaching maximum at 10 mV (Fig. 1D). The normalized and averaged GV-curve showed half maximum conductance at −7 ± 3 mV (n = 9) (Fig. 1E). Typical to L-type Ca^{2+} channels [47, 48], diminishing the Ba^{2+} content from 10 to 1 mM decreased the maximum current density from 2.4 ± 0.5 $pA{\cdot}pF^{-1}$ (n = 9) to 1.3 ± 0.3 $pA{\cdot}pF^{-1}$ (n = 7) (Fig. 1F). In addition, three cells showed fast transient currents (Fig. 1G) with inactivation time constant 6 ± 1 ms (n = 3). The current pattern indicated that hESC-RPE is likely to express both slowly inactivating L-type currents and fast inactivating T-type resembling currents. However, a detailed characterization of the fast inactivating currents was not possible as will be discussed later.

The Effects of L-Type Ca^{2+} Channel Activator and Inhibitor

The effects of (-)BayK8644 and nifedipine, well-characterized activator and inhibitor of the L-type Ca^{2+} channels, were tested for the slowly inactivating currents. These currents were increased by 10 μM (-)BayK8644 (Fig. 2A, 2C) and decreased by 10 μM nifedipine (Fig. 2B, 2D). Comparison with the control current at maximum amplitude revealed that the slowly inactivating current increased after (-)BayK8644 application by 80 ± 9% (n = 3, p < .05) (Fig. 2E) and decreased after nifedipine application by 56 ± 5% (n = 4, p < .05) (Fig. 2F). Both effects were statistically significant. These recordings confirm that the slowly inactivating currents were carried by the L-type Ca^{2+} channels.

Localization of Voltage-Gated Ca^{2+} Channels in hESC-RPE

To evaluate the localization of the Ca_V channels detected in the patch-clamp measurements in hESC-RPE, we performed antibody labeling against the L-type Ca^{2+} channels $Ca_V1.1$-$Ca_V1.3$ and the T-type Ca^{2+} channels $Ca_V3.1$-$Ca_V3.3$, together with markers for actin cytoskeleton, RPE maturity, and polarization. The hESC-RPE showed a typical expression of CRALBP (Fig. 3A) and Na^+/K^+-ATPase (Fig. 3F) on the apical side of the monolayer, as well as Bestrophin-1 primarily on the basolateral side (Fig. 3F). Zonula occludens (ZO-1) (Fig. 3B) and claudin-3 (Fig. 3C) co-localized on the cell–cell junctions with the circumferential bands of actin (phalloidin), characteristic to mature RPE [63]. This data, together with the TER value of over 200 Ω cm^2, strong pigmentation and cobblestone morphology (see Fig. 1B), indicate the maturity and polarization of our hESC-RPE.

The most prominent staining in hESC-RPE monolayers was detected for the subtypes $Ca_V1.3$ and $Ca_V3.1$, both localizing strongly at the apical membrane (Fig. 3D, 3E). Staining of these subtypes together with RPE microvilli marker ezrin revealed the localization of $Ca_V1.3$ right below the microvilli (Supporting Information Fig. S1A) and $Ca_V3.1$ at the microvilli (Supporting Information Fig. S1B). Since pigmentation hinders the visualization of the basolateral side (see yz confocal sections in Fig. 3), we performed immunostainings on paraffin embedded vertical sections of the hESC-RPE. This confirmed the apical localization of the subtypes $Ca_V1.3$ (Fig. 3H) and $Ca_V3.1$ (Fig. 3I) and revealed a pronounced basolateral localization of $Ca_V1.3$ (Fig. 3H). Furthermore, in hESC-RPE, we observed basolateral localization of $Ca_V1.2$ (Fig. 3G), and basolateral and junctional localization of $Ca_V3.2$ (Fig. 3J). The $Ca_V1.1$ and $Ca_V3.3$ subtypes were not detected (data not shown).

Voltage-Gated Ca^{2+} Channels in Mouse RPE

To compare the currents through voltage-gated Ca^{2+} channels in hESC-RPE with native tissue, patch-clamp recordings were performed from the cells of freshly isolated mouse RPE (Fig. 4). An investigation of currents in whole-cell configuration as a response to series of depolarizing voltage steps from −80 to +60 mV revealed slowly inactivating currents in the recordings (Fig. 4A). The currents activated at low potentials reaching the maximum at 20 mV in the normalized and averaged IV-curve (n = 4) (Fig. 4B). The half maximum conductance was reached at −6 ± 3 mV (n = 4) based on the normalized and averaged GV-curve (Fig. 4C). The maximum current density of the slowly inactivating current was 2.3 ± 0.6 $pA{\cdot}pF^{-1}$ (n = 4). Thus, the current characteristics of the voltage-gated Ca^{2+} channels in mouse RPE were comparable to those we identified in hESC-RPE.

Antibody labeling, similar to hESC-RPE, was performed on mouse RPE-eyecup whole mount preparations (Fig. 4D, 4E, Supporting Information Fig. S1C, S1D) and vertical sections of paraffin embedded eyecups (Fig. 4F–4I). The channel localization in mouse RPE followed similar characteristics as in hESC-RPE with the exception that the apically localized $Ca_V3.1$ was also detected at the basolateral side in mouse RPE (Fig. 4H). Furthermore, it is worth pointing out, that the uniform apical staining profile of $Ca_V1.3$ observed in hESC-RPE (Fig. 3D, 3H, Supporting Information Fig. S1A) was especially strongly detected in mouse RPE (Fig. 4D, 4G, Supporting Information Fig. S1C).

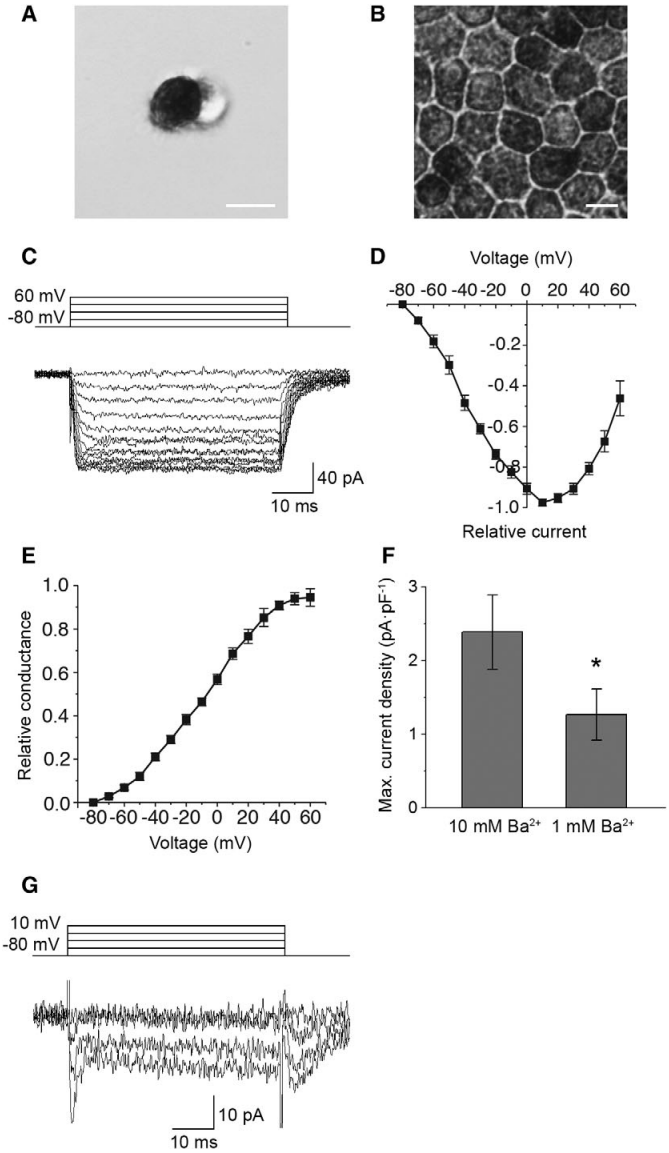

Figure 1. Voltage-gated currents in hESC-RPE. Examples of bright-field microscopy images of **(A)** a single hESC-RPE cell showing pigmented apical and non-pigmented basal sides and **(B)** a mature hESC-RPE monolayer with representative RPE morphology, scale bars 10 μm. Whole-cell voltage clamp recordings were carried out from single hESC-RPE cells. **(C):** A typical example of the slowly inactivating current elicited by 50 ms voltage steps from −80 to +60 mV in 10 mV increments. Normalized and averaged **(D)** IV-curve and **(E)** GV-curve of the slowly inactivating current (mean ± SEM, n = 9, cell lines 08/017 and 08/023, days post-confluence 73–128). **(F):** Averaged maximum current densities (obtained at 10 mV) of the slowly inactivating current in 10 mM Ba^{2+} (n = 9) and in 1 mM Ba^{2+} (n = 7, cell lines 08/017 and 08/023, days post-confluence 109–127). The difference in the current densities was statistically significant. **(G):** A typical example of the fast inactivating current elicited by 50 ms voltage steps from −80 to +10 mV in 10 mV increments (cell line 08/023, days post-confluence 109). *Statistically significant difference with $p < .05$.

VEGF Secretion in hESC-RPE

In hESC-RPE, characteristic to RPE physiology, VEGF secretion was polarized. Consistent with this, we found that the amount of VEGF secreted after a 24 hour incubation in control conditions was 588 ± 37 pg/10^5 cells to the apical side and 1,290 ± 38 pg/10^5 cells to the basolateral side (n = 3). Since the L-type Ca^{2+} channels have been reported to play an important role in VEGF secretion [43], we investigated the effect of their

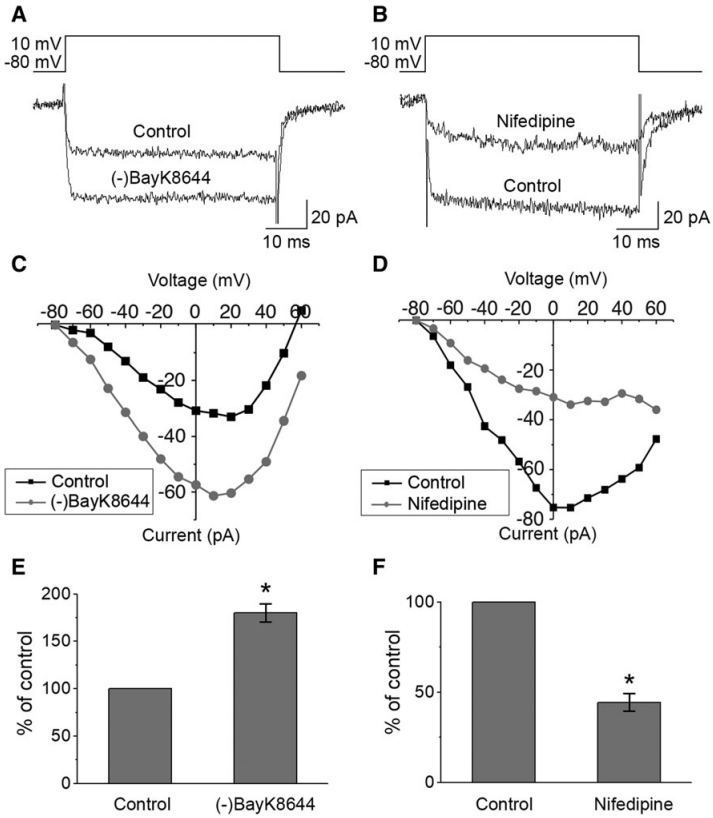

Figure 2. Responses of the currents to Ca^{2+} channel modulators. Whole-cell measurements of currents as responses to voltage pulses from −80 to +60 mV in 10 mV increments for 50 ms duration were performed before and after the application of the specific drugs. Examples of the effects of **(A)** L-type Ca^{2+} channel activator 10 μM (-)BayK8644 and **(B)** L-type Ca^{2+} channel inhibitor 10 μM nifedipine on Ba^{2+} currents in hESC-RPE and **(C, D)** the corresponding IV-curves, respectively. Changes in maximum current amplitudes presented as percentages from control conditions (mean ± SEM) show that both **(E)** activation with (-)BayK8644 (n = 3, cell line 08/017, days post-confluence 73–74) and **(F)** inhibition with nifedipine (n = 4, cell line 08/017, days post-confluence 73–99) resulted in statistically significant changes in the recorded currents. *Statistically significant difference with $p < .05$.

pharmacological modulation on the total amount of secreted VEGF in hESC-RPE. We followed the apical and basal secretion concurrently (Fig. 5) thus addressing the role of both apically and basally localized Ca^{2+} channels in the overall secretion. In control conditions, the total VEGF concentration in the medium after the 24 hour incubation was 1,950 ± 70 pg/10^5 cells (n = 9). Manipulation of the L-type Ca^{2+} channel activity directly affected the VEGF secretion as the activator (-) BayK8644 increased the secretion by 24 ± 9% (n = 9, $p < .05$) and the inhibitor nifedipine decreased the secretion by 19 ± 9% (n = 8, $p < .05$). Both effects were statistically significant. However, inhibition of the T-type channels by ML218 had little effect on the VEGF secretion (8 ± 14% increase, n = 8, $p > .05$).

Voltage-Gated Ca^{2+} Channels Regulate POS Phagocytosis in hESC-RPE

Previous studies indicate that L-type Ca^{2+} channels participate in the regulation of phagocytosis in RPE [41, 64]. Thus, we investigated the role of Ca_V channels in POS phagocytosis in hESC-RPE by pharmacologically modulating these channels during our phagocytosis assay. These experiments and subsequent labeling with opsin and ZO-1 showed a reduction in the total number of bound and internalized POS particles in the presence of either L-type channel activator or inhibitor, but an increase in the particle number in the presence of T-type channel inhibitor (Fig. 6). More specifically, the median value of POS particles in a randomly taken confocal image field decreased from the control conditions (n = 16, Fig. 6A, 6E) by 30% when the L-type channels were activated by (-)BayK8644 (n = 16, $p < .001$, Fig. 6B, 6E). A higher decrease of 62% occurred when the L-type Ca^{2+} channels were inhibited by nifedipine (n = 15, $p < .001$, Fig. 6C, 6E). Interestingly, we found that T-type Ca^{2+} channel inhibitor ML218 (Fig. 6D, 6E) increased the number of POS particles by 32% (n = 16, $p < .05$). All the effects were statistically significant.

Localization of $Ca_V1.3$ During hESC-RPE Maturation

It is well established that protein expression and localization change during RPE maturation [65]. We addressed this considering

the localization of the primary Ca_V channel subtype, $Ca_V1.3$, during hESC-RPE maturation. We immunolabeled $Ca_V1.3$ together with pericentrin (PCNT), a protein localized in the centrosomes at the base of the primary cilia, that have been recently shown to be important for RPE maturation [66, 67]. Figure 7 shows how the localization of these proteins changed remarkably during maturation. Fusiform hESC-RPE cells on the first day post-confluence (Supporting Information Fig. S2A) expressed $Ca_V1.3$ throughout the cell (Fig. 7A), and PCNT appeared as distinct puncta on the apical side. After 6 days post-confluence, the cells gained more epithelioid morphology (Supporting Information Fig. S2B) and $Ca_V1.3$ started to localize also to the apical and basal RPE cell membranes with brighter puncta forming on the apical side (Fig. 7B). Interestingly, these puncta showed co-localization with PCNT. The hESC-RPE cells obtained cobblestone morphology around 31 days post-confluence (Supporting Information Fig. S2C), and from this time point onwards, $Ca_V1.3$ was present more

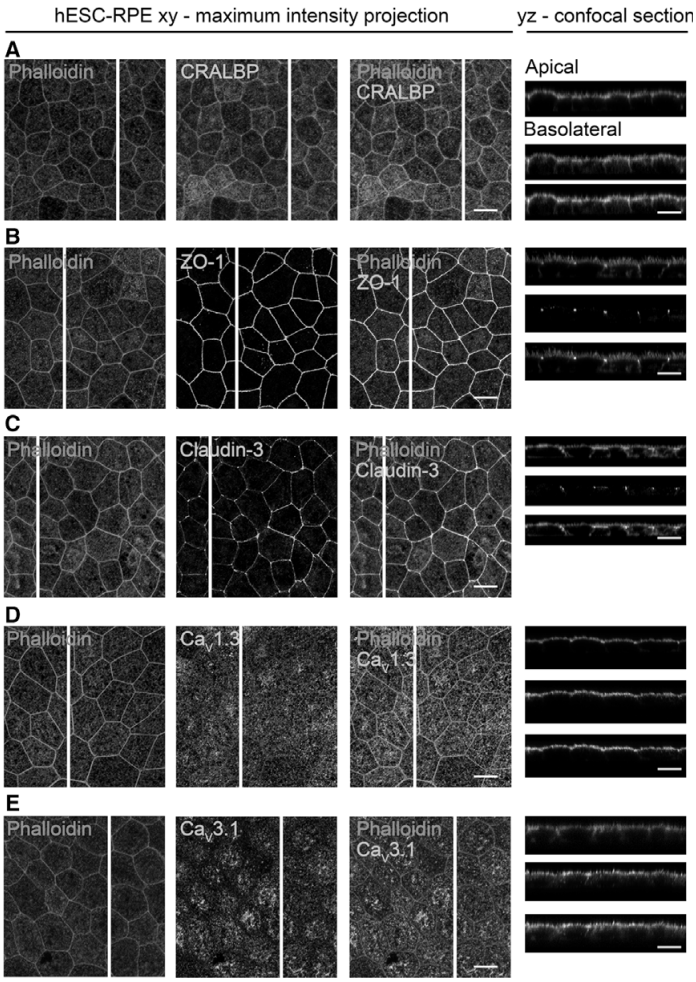

Figure 3. Localization of Ca_V channels in hESC-RPE. Immunostainings of RPE monolayers with xy-maximum intensity projections and yz-confocal sections (apical side upwards, localization of the section highlighted with a white bar). Actin cytoskeleton (phalloidin, red) labeled together with **(A)** RPE marker CRALBP (green, cell line 08/017, days post-confluence 91), **(B)** tight junction markers ZO-1, (green, cell line 08/017, days post-confluence 74) and **(C)** claudin-3 (green, cell line 08/017, days post-confluence 91), **(D)** L-type Ca^{2+} channel $Ca_V1.3$ (green, cell line 08/017, days post-confluence 109), and **(E)** T-type Ca^{2+} channel $Ca_V3.1$ (green, cell line 08/023, days post-confluence 66). Immunostainings of paraffin embedded hESC-RPE vertical sections with xy-maximum intensity projections (apical side upwards). **(F):** Cell polarization markers Na^+/K^+-ATPase (red) and Bestrophin-1 (green, cell line 08/023, days post-confluence 91). Cell nuclei (DAPI, blue) together with L-type Ca^{2+} channels **(G)** $Ca_V1.2$ (green, cell line 08/017, days post-confluence 84) and **(H)** $Ca_V1.3$ (green, cell line 08/023, days post-confluence 91), and T-type Ca^{2+} channels **(I)** $Ca_V3.1$ (green, cell line 08/017, days post-confluence 84) and **(J)** $Ca_V3.2$ (green, cell line 08/017, days post-confluence 84). Scale bars 10 μm. Abbreviations: Ca_V, voltage-gated Ca^{2+} channel; CRALBP, cellular retinaldehyde-binding protein; ZO-1, Zonula occludens; DAPI, 4′,6-diamidino-2-phenylidole; hESC, human embryonic stem cell; RPE, retinal pigment epithelium.

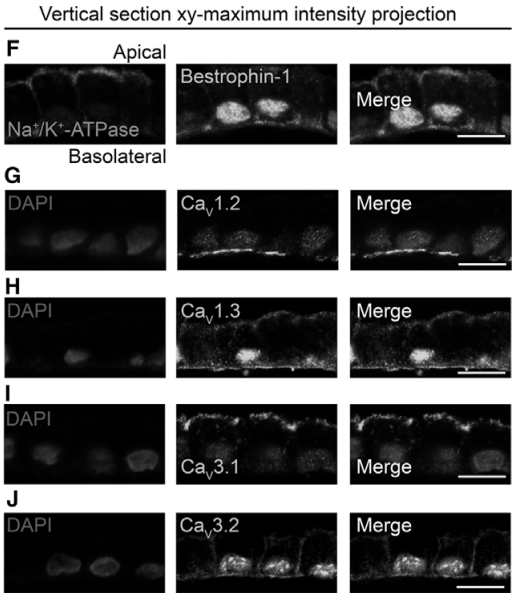

Figure 3. (Continued)

strongly on the apical and basolateral cell membranes (Fig. 7C). The apical side puncta were pronounced and appeared as one distinct cluster per cell co-localizing strongly with PCNT (Fig. 7C). Immunolabeling $Ca_V1.3$ with acetylated α-tubulin (Fig. 7E) showed the localization of $Ca_V1.3$ near the base of the primary cilia. With increasing maturation, the apical staining of $Ca_V1.3$ became more prominent and more homogeneous, while basolateral staining started to be difficult to detect due to increased pigmentation. At 84 days post-confluence (Fig. 7D), fairly uniform apical localization of $Ca_V1.3$ was present in hESC-RPE, although the puncta, co-localizing with PCNT, could still be distinguished. At this time point, PCNT localized near the apical centers of the cobblestone hESC-RPE cells (Fig. 7D, Supporting Information Fig. S2D), characteristic to mature RPE [67]. This data suggest that with increasing maturation, hESC-RPE started to gain the homogeneous apical localization of $Ca_V1.3$ detected in mouse RPE (Fig. 4D).

Discussion

Stem cell-derived RPE provides great potential for novel cell transplantation therapies and research has already proceeded to clinical trials [6–21]. Essential for the success of these therapies, stem cell-derived RPE has been shown to perform several key RPE functions [27–36]. However, the functionality of the ion channels and specifically the voltage-gated Ca^{2+} channels in these cells remain poorly known, even though many of the critical RPE functions are related to Ca^{2+} activity. This raises the question whether the stem cell-derived RPE destined for clinical purposes sufficiently resembles its native counterpart, and can thus replace the functions of lost cells. The present study addressed this issue by investigating the Ca_V channels in hESC-RPE. Using patch-clamp recordings and immunostainings, we showed the presence of functional L-type Ca^{2+} channels in hESC-RPE that are comparable to native mouse RPE.

In our study, two current types were detected, the slowly inactivating current and the fast inactivating current. We confirmed that the main current type, the slowly inactivating current, results from the activity of L-type Ca^{2+} channels since the current responses and IV-curves in this study resembled the previous recordings of L-type currents from various types of native RPE [43, 46–48]. Moreover, the sensitivity of the current to the L-type Ca^{2+} channel activator (-)BayK8644 [45–50, 53] and the inhibitor nifedipine [43, 44, 47, 48, 51] further indicated the presence of L-type currents in our measurements. The recorded current is likely to be carried primarily through $Ca_V1.3$ channels. This conclusion is based on the voltage-dependent activation of the currents at rather negative potentials [68], shape of the IV-curve characteristic to the $Ca_V1.3$ subtype [43, 46, 55], and slow inactivation of the current. It is still likely that $Ca_V1.2$ channels contribute to the recorded current as well, since our immunostainings confirmed the presence of both of the L-type Ca^{2+} channels, $Ca_V1.2$ and $Ca_V1.3$, in hESC-RPE. To date, $Ca_V1.3$ subtype has been reported to only localize basolaterally in murine [54] and porcine [55] RPE. Our data showed that both hESC- and mouse RPE express the $Ca_V1.3$ subtype also on the apical cell membrane, in addition to the basolateral membrane.

It is worth noting that patch-clamp recordings from primary RPE cultures show differences in L-type current characteristics when compared with our recordings from hESC-RPE [43, 45, 49, 50, 53], especially regarding the more negative activation threshold and the weaker slope of activation present in our study. The reason for this remains to be investigated, but it may be related to differences in phosphorylation, splicing variants, or the composition of the accessory subunits [69, 70]. Yet, the contribution of other Ca^{2+} conducting channels on the currents recorded in this study for hESC-RPE and native mouse RPE cannot be excluded. Several Ca^{2+}-conducting channels, such as store-operated Orai channels [71] and transient receptor potential (TRP) channels [41, 72–74], have important roles in the physiology of RPE. Relevant for this study, TRP channels are involved in the phagocytosis [41] and VEGF secretion [73]. In addition to these other Ca^{2+}-conductivities, the effect of cell dissociation to patch-clamp recordings needs to be taken into account. Cell–cell junctions break down in cell dissociation causing epithelial cells to lose their polarity, which compromises their normal ability to express and recycle proteins. This has a strong influence on the endocytotic processes that are important for the internalization of ion channels, regulating their numbers in the cell membrane [75]. Therefore, after cell dissociation, ion channels can be re-distributed to the intracellular compartments and those currents will thus be absent from the patch-clamp recordings.

In addition to L-type currents, our patch-clamp recordings revealed the presence of fast transient currents in hESC-RPE. The kinetics of these currents were comparable to those previously reported for the T-type Ca^{2+} channels in cultured human RPE [46], although faster than typically reported for other cell types (reviewed in [76]). Similar to the findings of the previous study [46], the fast transient currents were almost exclusively recorded in combination with the slowly inactivating current, which hindered their further analysis. In addition, TTX-sensitive currents can also contribute to the fast transient conductance

[60, 77] and make this current component extremely difficult to investigate. In immunostainings, we observed $Ca_V3.1$ and $Ca_V3.2$ in both hESC- and mouse RPE. $Ca_V3.1$ was localized apically at the microvilli in the both studied RPE cell types, while it was found also at the basolateral cell membrane in mouse RPE.

VEGF has a role in angiogenesis and vascular permeability, and therefore anti-VEGF agents are commonly used in the treatment of AMD [78]. In healthy RPE, VEGF secretion occurs in a polarized manner with significantly more pronounced secretion from the basal side [79, 80], as we showed here for hESC-RPE. This secretion is regulated by several factors including hyperosmolarity [81], hyperthermia [82], oxidative stress [83], and heat-sensitive TRPV channels [73]. Particularly relevant for this study, modulating the L-type Ca^{2+} channel activity has been shown to directly correlate with the VEGF secretion level [43]. Our ELISA results indicated similar behavior as the activator (-)BayK8644 increased the VEGF secretion and the inhibitor nifedipine decreased the VEGF secretion. This demonstrates that the L-type Ca^{2+} channels participate in the regulation of VEGF secretion in hESC-RPE. However, it is worth

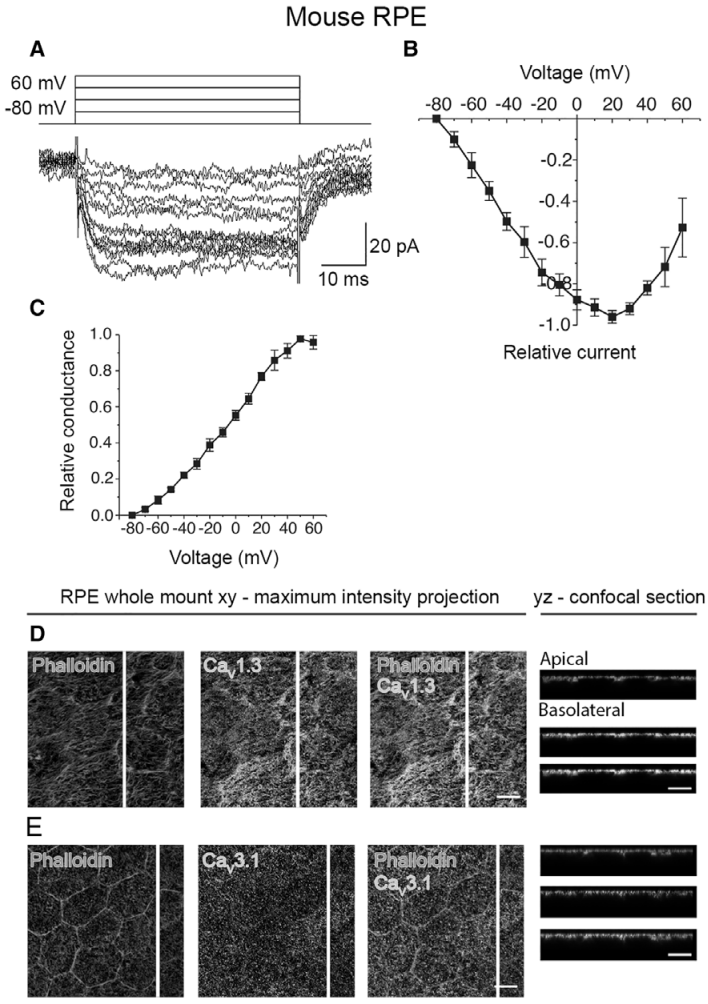

Figure 4. Ca_V channels in mouse RPE. **(A):** An example of the slowly inactivating L-type current measured in whole-cell configuration and elicited by 50 ms voltage steps from −80 to +60 mV in 10 mV increments. **(B):** Normalized and averaged IV-curve of the L-type current (mean ± SEM, n = 4). **(C):** Normalized and averaged GV-curve of the L-type current (mean ± SEM, n = 4). Localization of the Ca_V channels assessed by immunostainings of mouse RPE-eyecup whole mount preparations. Confocal images show the xy-maximum intensity projections and yz-confocal sections of the samples (apical side upwards, localization of the section highlighted with a white bar). Actin cytoskeleton (phalloidin, red) together with **(D)** L-type Ca^{2+} channel $Ca_V1.3$ (green), and **(E)** T-type Ca^{2+} channel $Ca_V3.1$ (green). Immunostainings of paraffin embedded vertical sections of mouse eyecups shown as xy-maximum intensity projections (apical side upwards). BF images together with L-type Ca^{2+} channels **(F)** $Ca_V1.2$ (green) and **(G)** $Ca_V1.3$ (green), and T-type Ca^{2+} channels **(H)** $Ca_V3.1$ (green) and **(I)** $Ca_V3.2$ (green). Scale bars 10 µm. Abbreviations: Ca_V, voltage-gated Ca^{2+} channel; BF, bright-field; RPE, retinal pigment epithelium.

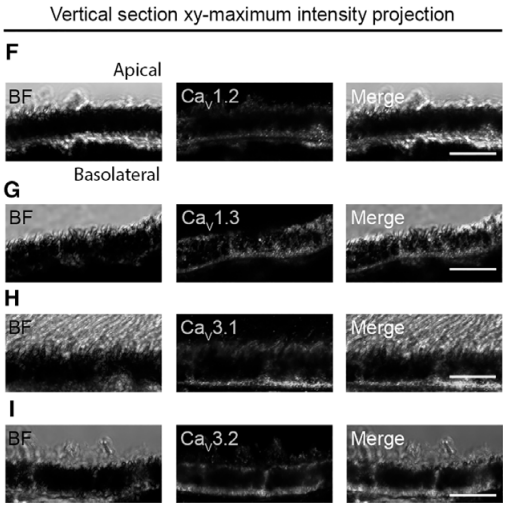

Figure 4. (Continued)

noting that the cell culture insert membrane with randomly spaced 1 μm holes may hinder both the diffusion of the drug to the basolateral cell membrane and the secretion of VEGF to the medium. Since the VEGF secretion is more pronounced in the basolateral side of the RPE, the structural constraints from the insert may lower the effect of pharmacological Ca^{2+} channel modulation on VEGF secretion.

Photoreceptor renewal is a critical task for RPE to maintain vision [2], and insufficient phagocytosis often leads to retinal diseases [84, 85]. Several ion channels, including the L-type Ca^{2+} channels, are known to have regulatory roles in phagocytosis in RPE [41, 64]. We found that in hESC-RPE, in line with the previous studies [64], inhibition of the L-type Ca^{2+} channels by nifedipine decreased the phagocytosis remarkably. On the other hand, activation of these channels by (-)BayK8644 also decreased the number of phagocytosed POS particles, although to a lesser extent. Interestingly, it was reported that in primary porcine RPE, the activation of L-type Ca^{2+} channels had no effect on phagocytosis, and this was suggested to be a consequence of the regulatory effect of bestrophin-1 setting a limit to L-type Ca^{2+} channel activity [41]. When comparing these results to our data, we want to point out that we used a pulse-chase POS phagocytosis assay, while Müller et al. [41] used an assay with continuous POS supply to the RPE cells that may lead to distinct outcomes. Moreover, it is possible that bestrophin-1 expression levels are much lower in hESC-RPE compared to primary porcine RPE [41] thus diminishing the regulatory effect of bestrophin-1 on L-type Ca^{2+} channels in our cells. Besides, the influence of Ca^{2+} in phagocytosis can also be inhibitory: increase in intracellular Ca^{2+} and subsequent activation of protein kinase C has been shown to reduce POS ingestion [86]. These observations indicate that the role for the L-type Ca^{2+} channels in the regulation of POS phagocytosis is a complex process (see also [41, 64]) and may include negative feedback mechanisms, especially after prolonged channel activation. Furthermore, it is known that these channels participate in the regulation of phagocytosis in concert with other ion channels including Ca^{2+}-dependent K^+ channels, bestrophin-1, TRPV [41], and most likely also the T-type Ca^{2+} channels. Our observation about the increased number of bound or ingested POS particles following T-type Ca^{2+} channel inhibition is similar to the effect of bestrophin-1 inhibition [41]. Analogous to bestrophin-1 [87], T-type Ca^{2+} channels are indicated to interact with the β subunits of the L-type Ca^{2+} channels [88]. This implies a possible role for the T-type channels to inhibit L-type channels through their interaction with β subunits. Taken together, these data demonstrate a need for further studies in elucidating the concerted functioning of Ca^{2+} conducting channels in the regulation of phagocytosis.

Regardless of the close resemblance between stem cell-derived and native RPE demonstrated for their proteome [29], capability of phagocytosis [27, 28, 30–32], VEGF secretion [32–34], and visual cycle [35, 36], many important differences have also been reported. These include a lower efficiency in the phagocytosis of POSs [89] as well as differences in growth factor secretion [90] and expression of adhesion junction and membrane transport genes [37]. We used mouse RPE as the native counterpart for hESC-RPE in our studies due to unavailability of live human RPE tissue. Previous work on gene and protein expression profiles of human and mouse RPE show high similarity regarding general biological functions, canonical pathways, and molecular networks [91, 92]. However, there are important species-specific differences between human and mouse RPE. These include immune regulation genes and genes related to the development of AMD and Usher syndrome [92] as well as the well-known anatomical differences such as the absence of macula in the mouse and differences in rod and cone types and distributions.

We studied the functionality of Ca_V channels in mature hESC-RPE where the localization of the primary Ca_V channel subtype, $Ca_V1.3$, started to resemble native RPE. During maturation, we observed significant changes in $Ca_V1.3$ localization in hESC-RPE implying that ion channels can be highly sensitive to the level of tissue maturity. This has been previously suggested at least for Bestrophin-1 in RPE [32, 93]. We

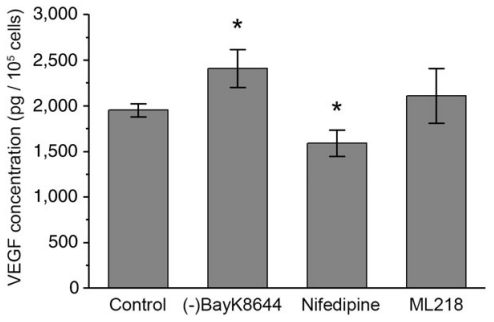

Figure 5. VEGF secretion from hESC-RPE. Total concentrations of VEGF secreted by the hESC-RPE after 24-hour incubation in control medium alone (n = 9) as well as in control medium with L-type Ca^{2+} channel activator 10 μM (-)BayK8644 (n = 9), L-type Ca^{2+} channel inhibitor 10 μM nifedipine (n = 8), or T-type channel inhibitor 5 μM ML218 (n = 8) (mean ± SEM, cell lines 08/023 and 11/013, days post-confluence 66–147). *Statistically significant difference with $p < .05$. Abbreviation: VEGF, vascular endothelial growth factor.

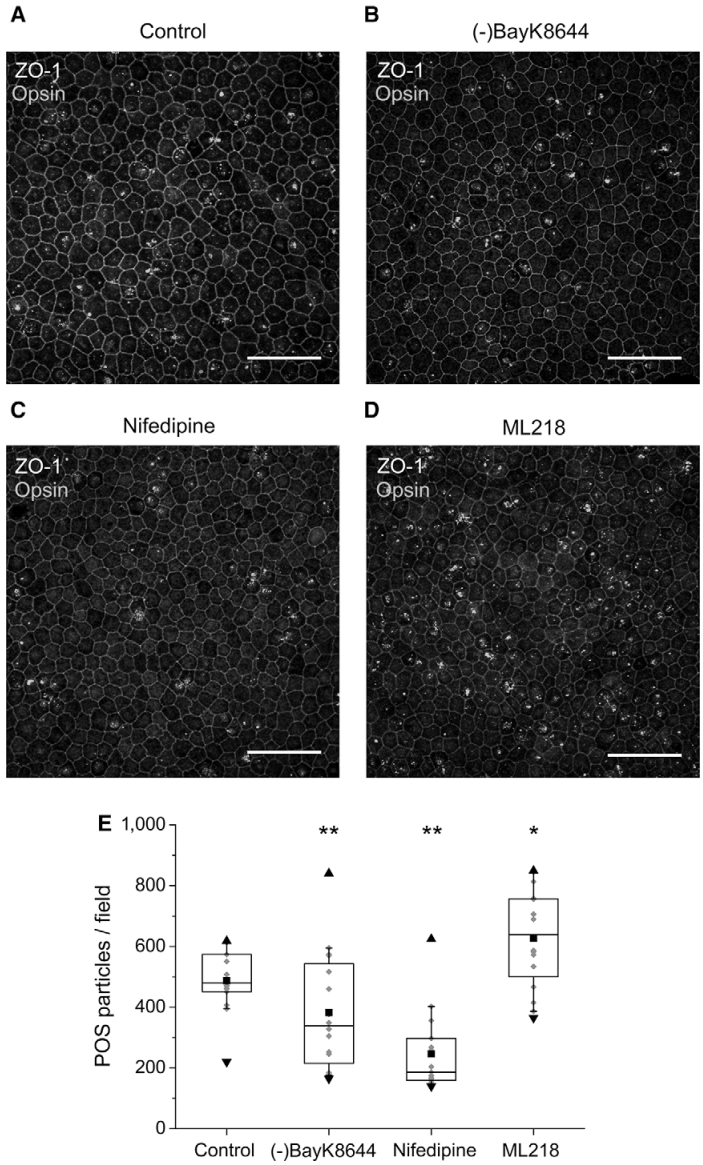

Figure 6. The effect of Ca_V channel modulators on POS phagocytosis in hESC-RPE. Mature hESC-RPE monolayers were incubated with purified porcine POSs in the pulse-chase phagocytosis assay. Xy-maximun intensity projections of the confocal images show both bound and internalized POS particles that were stained with opsin (green) together with the tight junction protein ZO-1 (gray) in **(A)** control conditions, and in the presence of Ca_V channel modulators **(B)** (-)BayK8644, **(C)** nifedipine, or **(D)** ML218. Scale bars 50 μm. **(E):** Quantification of POS particles in control conditions yielded the median value of 485 POS particles/field (n = 16). When modulating the Ca_V channels pharmacologically, the value changed in the presence of (-)BayK8644 to 339 POS particles/field (n = 15), nifedipine to 186 POS particles/field (n = 15), and ML218 to 639 POS particles/field (n = 16). The box limits 25%–75% of the gray data points; the whiskers include 10%–90% of the data; the center line shows the median value; the black square describes the mean; the black triangles present the minimum and the maximum values. Cell line 11/013, days post-confluence 147. Statistically significant differences with $*p < .05$ or $**p < .001$. Abbreviations: POS, photoreceptor outer segment; ZO-1, Zonula occludens.

showed that in mature hESC-RPE, $Ca_V1.3$ localized quite homogeneously on the apical and basolateral cell membranes. Intriguingly, in maturing hESC-RPE, $Ca_V1.3$ appeared as distinct foci that co-localized with PCNT to the base of the primary cilia. A similar punctuated appearance has been previously shown for TRP channel TRPM3 in human fetal RPE [94]. PCNT is

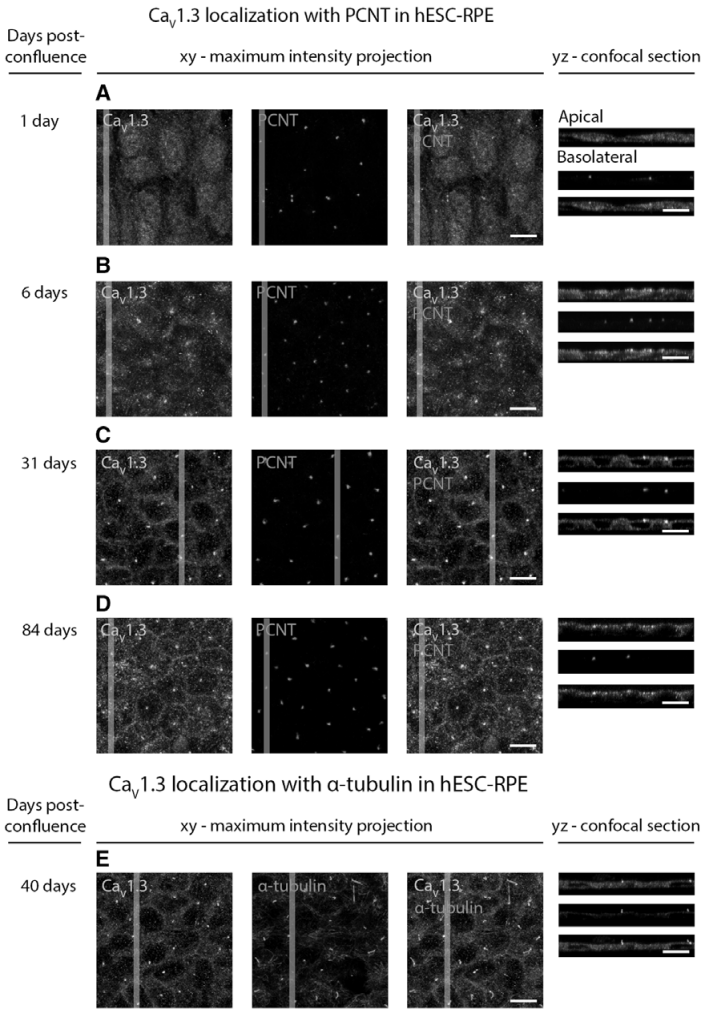

Figure 7. Localization of $Ca_V1.3$ during hESC-RPE maturation. Immunolabeling of $Ca_V1.3$ (green) together with centrosome protein PCNT (red) from post-confluence day 1 to post-confluence day 84 at four time points: **(A)** day 1, **(B)** day 6, **(C)** day 31, and **(D)** day 84 (cell line 08/017). **(E):** Labeling acetylated α-tubulin (red) together with $Ca_V1.3$ (green) shows the localization of $Ca_V1.3$ at the base of the primary cilia during maturation (cell line 08/017, days post-confluence 40). The confocal images are shown as xy-maximum intensity projections and yz-confocal sections (apical side upwards, localization of the section highlighted with a white bar). Scale bars 10 μm. Abbreviations: Ca_V, voltage-gated Ca^{2+} channel; hESC, human embryonic stem cell; RPE, retinal pigment epithelium; PCNT, pericentrin.

critical for the cilia formation, and relevant for our observations, PCNT is suggested to recruit protein complexes involved in cilia assembly and calcium signaling to the base of the primary cilia [66]. On the other hand, primary cilia has been shown to regulate L-type Ca^{2+} channel expression in mouse renal epithelial cells [95]. This occurs through Wnt signaling [95], and interestingly, recent work shows the importance of the regulation of Wnt signaling not only for RPE development [96] but also for RPE maturation [67]. Based on our data and taking into account these observations in the literature, it is possible, that $Ca_V1.3$ participates in ciliogenesis during RPE maturation or that its expression is coupled to the functioning of primary cilia in RPE maturation. This would not be surprising since primary cilia are important Ca^{2+} signaling organelles [97] with the expression of several different types of Ca^{2+} channels [98].

CONCLUSION

In this article, we demonstrate the presence of a functional machinery of voltage-gated Ca^{2+} channels in hESC-RPE, with L-type Ca^{2+} channel characteristics highly resembling the native RPE. We show a regulatory role for L-type Ca^{2+} channels in VEGF secretion and phagocytosis important for the

hESC-RPE functionality. We also provide novel information regarding the apical localization of $Ca_V1.3$ in RPE as well as its co-localization near the base of the primary cilia during hESC-RPE maturation. Our study represents an initial but significant progress toward a better understanding of Ca_V channels in stem cell-derived RPE, however, further studies are needed to elucidate the specific roles for T-type Ca^{2+} channels in RPE physiology. Overall, the results of the study are promising for the success of stem cell-based RPE transplantation therapies, but highlight the need for sufficient RPE maturation as a prerequisite for its fully functional Ca^{2+} machinery.

Acknowledgments

We thank Viivi Jokinen, Julia Johansson, Elina Hurskainen, Outi Heikkilä, Marja-Leena Koskinen, Outi Melin, Hanna Pekkanen, Outi Paloheimo, and Teemu Ihalainen for their technical assistance. The support from Tampere Imaging Facility and Tampere Facility of Electrophysiological Measurements is also greatly appreciated. This study was financially supported by the Academy of Finland (grant numbers 260375, 287287, 294054, 252225, 218050, 272808, 137801, 304909), the Emil Aaltonen Foundation, the Finnish Cultural Foundation, the Instrumentarium Science Foundation, the TEKES Human Spare Part Project and the Doctoral Programme of the President of Tampere University of Technology.

Author Contributions

I.V.: conception and design, collection and assembly of data, data analysis and interpretation, manuscript writing, final approval of manuscript; T.V.: collection and assembly of data, data analysis and interpretation, provision of study material, manuscript writing, final approval of manuscript; K.J.-U.: conception and design, collection and/or assembly of data, manuscript writing, final approval of manuscript; H.U.-J.: provision of study material, final approval of manuscript; H.S.: provision of study material, manuscript writing, final approval of manuscript; J.H.: financial support, manuscript writing, final approval of manuscript; S.N.: conception and design, financial support, collection and/or assembly of data, data analysis and interpretation, manuscript writing, final approval of manuscript.

Disclosure of Potential Conflicts of Interest

The authors indicated no potential conflicts of interest.

References

1 Strauss O. The retinal pigment epithelium in visual function. Physiol Rev 2005;85: 845-881.

2 Wimmers S, Karl MO, Strauss O. Ion channels in the RPE. Prog Retin Eye Res 2007; 26:263-301.

3 Ferrington DA, Sinha D, Kaarniranta K. Defects in retinal pigment epithelial cell proteolysis and the pathology associated with age-related macular degeneration. Prog Retin Eye Res 2016;51:69-89.

4 Wong WL, Su X, Li X et al. Global prevalence of age-related macular degeneration and disease burden projection for 2020 and 2040: A systematic review and meta-analysis. Lancet Glob Health 2014;2:e106-e116.

5 Riera M, Fontrodona L, Albert S et al. Comparative study of human embryonic stem cells (hESC) and human induced pluripotent stem cells (hiPSC) as a treatment for retinal dystrophies. Mol Ther Methods Clin Dev 2016;3:1-12.

6 Schwartz SD, Regillo CD, Lam BL et al. Human embryonic stem cell-derived retinal pigment epithelium in patients with age-related macular degeneration and Stargardt's macular dystrophy: Follow-up of two open-label phase 1/2 studies. Lancet 2015; 385:509-516.

7 Song WK, Park K, Kim H et al. Treatment of macular degeneration using embryonic stem cell-derived retinal pigment epithelium: Preliminary results in Asian patients. Stem Cell Reports 2015;4:860-872.

8 Schwartz SD, Tan G, Hosseini H et al. Subretinal transplantation of embryonic stem cell–derived retinal pigment epithelium for the treatment of macular degeneration: An assessment at 4 years. Invest Ophthalmol Vis Sci 2016;57:ORSFc1-ORSFc9.

9 Mandai M, Watanabe A, Kurimoto Y et al. Autologous induced stem-cell–derived retinal cells for macular degeneration. N Engl J Med 2017;376:1038-1046.

10 Southwest Hospital, China. Clinical study of subretinal transplantation of human embryo stem cell derived retinal pigment epitheliums in treatment of macular degeneration diseases. Available at https://www.clinicaltrials.gov/ct2/show/NCT02749734. Accessed January 9, 2018.

11 Chinese Academy of Sciences. Subretinal transplantation of retinal pigment epitheliums in treatment of age-related macular degeneration diseases. Available at https://www.clinicaltrials.gov/ct2/show/NCT02755428. Accessed January 9, 2018.

12 Cell Cure Neurosciences Ltd. Safety and efficacy study of OpRegen for treatment of advanced dry-form age-related macular degeneration. Available at https://www.clinicaltrials.gov/ct2/show/NCT02286089. Accessed January 9, 2018.

13 Astellas Institute for Regenerative Medicine. Long term follow up of sub-retinal transplantation of hESC derived RPE cells in Stargardt macular dystrophy patients. Available at https://www.clinicaltrials.gov/ct2/show/NCT02445612. Accessed January 9, 2018.

14 Astellas Institute for Regenerative Medicine. Safety and tolerability of sub-retinal transplantation of hESC derived RPE (MA09-hRPE) cells in patients with advanced dry age related macular degeneration (Dry AMD). Available at https://www.clinicaltrials.gov/ct2/show/NCT01344993. Accessed January 9, 2018.

15 Astellas Institute for Regenerative Medicine. Sub-retinal transplantation of hESC derived RPE(MA09-hRPE)cells in patients with Stargardt's macular dystrophy. Available at https://www.clinicaltrials.gov/ct2/show/NCT01345006. Accessed January 9, 2018.

16 Astellas Institute for Regenerative Medicine. Long term follow up of sub-retinal transplantation of hESC derived RPE cells in patients with AMD. Available at https://www.clinicaltrials.gov/ct2/show/NCT02463344. Accessed January 9, 2018.

17 Pfizer. Retinal pigment epithelium safety study for patients in B4711001. Available at https://www.clinicaltrials.gov/ct2/show/NCT03102138. Accessed January 9, 2018.

18 Federal University of São Paulo. Stem cell therapy for outer retinal degenerations. Available at https://www.clinicaltrials.gov/ct2/show/NCT02903576. Accessed January 9, 2018.

19 Chinese Academy of Sciences. Treatment of dry age related macular degeneration disease with retinal pigment epithelium derived from human embryonic stem cells. Available at https://www.clinicaltrials.gov/ct2/show/NCT03046407. Accessed January 9, 2018.

20 Pfizer. A study of implantation of retinal pigment epithelium in subjects with acute wet age related macular degeneration. Available at https://www.clinicaltrials.gov/ct2/show/NCT01691261. Accessed January 9, 2018.

21 da Cruz L, Fynes K, Georgiadis O et al. Phase 1 clinical study of an embryonic stem cell–derived retinal pigment epithelium patch in age-related macular degeneration. Nat Biotechnol 2018;36:328-337.

22 Li Y, Tsai Y, Hsu C et al. Long-term safety and efficacy of human-induced pluripotent stem cell (iPS) grafts in a preclinical model of retinitis pigmentosa. Mol Med 2012;18:1312-1319.

23 Lu B, Malcuit C, Wang S et al. Long-term safety and function of RPE from human embryonic stem cells in preclinical models of macular degeneration. Stem Cells 2009;27: 2126-2135.

24 Kanemura H, Go MJ, Shikamura M et al. Tumorigenicity studies of induced pluripotent stem cell (iPSC)-derived retinal pigment epithelium (RPE) for the treatment of age-related macular degeneration. PLOS ONE 2014;9(1):e85336.

25 Koss MJ, Falabella P, Stefanini FR et al. Subretinal implantation of a monolayer of human embryonic stem cell-derived retinal pigment epithelium: A feasibility and safety study in Yucatan minipigs. Graefes Arch Clin Exp Ophthalmol 2016;254:1553-1565.

26 Galloway CA, Dalvi S, Hung SSC et al. Drusen in patient-derived hiPSC-RPE models of macular dystrophies. Proc Natl Acad Sci USA 2017;114:E8214-E8223.

27 Thomas BB, Zhu D, Zhang L et al. Survival and functionality of hESC-derived retinal pigment epithelium cells cultured as a monolayer on polymer substrates transplanted in RCS rats. Invest Ophthalmol Vis Sci 2016;57:2877-2887.

28 Carr A, Vugler AA, Hikita ST et al. Protective effects of human iPS-derived retinal pigment epithelium cell transplantation in the retinal dystrophic rat. PLOS ONE 2009;4(12):e8152.

29 Hongisto H, Jylhä A, Nättinen J et al. Comparative proteomic analysis of human embryonic stem cell-derived and primary human retinal pigment epithelium. Sci Rep 2017;7:6016.

30 Subrizi A, Hiidenmaa H, Ilmarinen T et al. Generation of hESC-derived retinal pigment epithelium on biopolymer coated polyimide membranes. Biomaterials 2012;33: 8047-8054.

31 Singh R, Shen W, Kuai D et al. iPS cell modeling of Best disease: Insights into the pathophysiology of an inherited macular degeneration. Hum Mol Genet 2013;22: 593-607.

32 Brandl C, Zimmermann SJ, Milenkovic VM et al. In-depth characterisation of retinal pigment epithelium (RPE) cells derived from human induced pluripotent stem cells (hiPSC). Neuromolecular Med 2014;16:551-564.

33 Kokkinaki M, Sahibzada N, Golestaneh N. Human iPS-derived retinal pigment epithelium (RPE) cells exhibit ion transport, membrane potential, polarized VEGF secretion and gene expression pattern similar to native RPE. Stem Cells 2011;29: 825-835.

34 Blenkinsop TA, Saini JS, Maminishkis A et al. Human adult retinal pigment epithelial stem cell–derived RPE monolayers exhibit key physiological characteristics of native tissue. Invest Ophthalmol Vis Sci 2015;56:7085-7099.

35 Maeda T, Lee MJ, Palczewska G et al. Retinal pigmented epithelial cells obtained from human induced pluripotent stem cells possess functional visual cycle enzymes in vitro and in vivo. J Biol Chem 2013;288:34484-34493.

36 Muñiz A, Greene WA, Plamper ML et al. Retinoid uptake, processing, and secretion in human iPS-RPE support the visual cycle. Invest Ophthalmol Vis Sci 2014;55: 198-209.

37 Peng S, Gan G, Qiu C et al. Engineering a blood-retinal barrier with human embryonic stem cell-derived retinal pigment epithelium: Transcriptome and functional analysis. Stem Cells Translational Medicine 2013;2:534-544.

38 Stanzel BV, Liu Z, Somboonthanakij S et al. Human RPE stem cells grown into polarized RPE monolayers on a polyester matrix are maintained after grafting into rabbit subretinal space. Stem Cell Reports 2014;2: 64-77.

39 Miyagishima KJ, Wan Q, Corneo B et al. In pursuit of authenticity: Induced pluripotent stem cell-derived retinal pigment epithelium for clinical applications. Stem Cells Translational Medicine 2016;5: 1562-1574.

40 Abu Khamidakh AE, Dos Santos FC, Skottman H et al. Semi-automatic method for Ca2+ imaging data analysis of maturing human embryonic stem cells-derived retinal pigment epithelium. Ann Biomed Eng 2016; 44:3408-3420.

41 Müller C, Más Gómez N, Ruth P et al. CaV1.3 L-type channels, maxiK Ca2 +-dependent K+ channels and bestrophin-1 regulate rhythmic photoreceptor outer segment phagocytosis by retinal pigment epithelial cells. Cell Signal 2014;26:968-978.

42 Wimmers S, Halsband C, Seyler S et al. Voltage-dependent Ca2+ channels, not ryanodine receptors, activate Ca2+-dependent BK potassium channels in human retinal pigment epithelial cells. Mol Vis 2008;14: 2340-2348.

43 Rosenthal R, Heimann H, Agostini H et al. Ca^{2+} channels in retinal pigment epithelial cells regulate vascular endothelial growth factor secretion rates in health and disease. Mol Vis 2007;13:443-456.

44 Rosenthal R, Malek G, Salomon N et al. The fibroblast growth factor receptors, FGFR-1 and FGFR-2, mediate two independent signalling pathways in human retinal pigment epithelial cells. Biochem Biophys Res Commun 2005;337:241-247.

45 Mergler S, Steinhausen K, Wiederholt M et al. Altered regulation of L-type channels by protein kinase C and protein tyrosine kinases as a pathophysiologic effect in retinal degeneration. FASEB J 1998; 12:1125-1134.

46 Wimmers S, Coeppicus L, Rosenthal R et al. Expression profile of voltage-dependent Ca2+ channel subunits in the human retinal pigment epithelium. Graefes Arch Clin Exp Ophthalmol 2008;246:685-692.

47 Ueda Y, Steinberg RH. Voltage-operated calcium channels in fresh and cultured rat retinal pigment epithelial cells. Invest Ophthalmol Vis Sci 1993;34: 3408-3418.

48 Ueda Y, Steinberg RH. Dihydropyridine-sensitive calcium currents in freshly isolated human and monkey retinal pigment epithelial cells. Invest Ophthalmol Vis Sci 1995;36:373-380.

49 Strauss O, Mergler S, Wiederholt M. Regulation of L-type calcium channels by protein tyrosine kinase and protein kinase C in cultured rat and human retinal pigment epithelial cells. FASEB J 1997;11:859-867.

50 Strauss O, Buss F, Rosenthal R et al. Activation of neuroendocrine L-type channels (α1D subunits) in retinal pigment epithelial cells and brain neurons by pp60c-src. Biochem Biophys Res Commun 2000;270:806-810.

51 Rosenthal R, Bakall B, Kinnick T et al. Expression of bestrophin-1, the product of the VMD2 gene, modulates voltage-dependent Ca2+ channels in retinal pigment epithelial cells. FASEB J 2006;20: 178-180.

52 Wollmann G, Lenzner S, Berger W et al. Voltage-dependent ion channels in the mouse RPE: Comparison with Norrie disease mice. Vision Res 2006;46:688-698.

53 Rosenthal R, Thieme H, Strauss O. Fibroblast growth factor receptor 2 (FGFR2) in brain neurons and retinal pigment epithelial cells act via stimulation of neuroendocrine L-type channels (Cav1.3). FASEB J 2001;15: 970-977.

54 Reichhart N, Markowski M, Ishiyama S et al. Rab27a GTPase modulates L-type Ca2+ channel function via interaction with the II–III linker of CaV1.3 subunit. Cell Signal 2015;27: 2231-2240.

55 Reichhart N, Milenkovic VM, Halsband C et al. Effect of bestrophin-1 on L-type Ca2+ channel activity depends on the Ca2+ channel beta-subunit. Exp Eye Res 2010;91:630-639.

56 Rohrer B, Kunchithapautham K, Genewsky A et al. Prolonged src kinase activation, a mechanism to turn transient, sublytic complement activation into a sustained pathological condition in retinal pigment epithelium cells. Adv Exp Med Biol 2014;801: 221-227.

57 Skottman H. Derivation and characterization of three new human embryonic stem cell lines in Finland. In Vitro Cell Dev Biol Anim 2010;46:206-209.

58 Vaajasaari H, Ilmarinen T, Juuti-Uusitalo K et al. Toward the defined and xeno-free differentiation of functional human pluripotent stem cell-derived retinal pigment epithelial cells. Mol Vis 2011;17: 558-575.

59 Bodenstein L, Sidman RL. Growth and development of the mouse retinal pigment epithelium: I. Cell and tissue morphometrics and topography of mitotic activity. Dev Biol 1987;121:192-204.

60 Johansson JK, Ihalainen TO, Skottman H et al. Fast voltage sensitivity in retinal pigment epithelium: Sodium channels and their novel role in phagocytosis. bioRxiv 2017;223719.

61 Schneider CA, Rasband WS, Eliceiri KW. NIH Image to ImageJ: 25 years of image analysis. Nat Methods 2012;9:671-675.

62 Mao Y, Finnemann SC. Analysis of photoreceptor outer segment phagocytosis by RPE cells in culture. Methods Mol Biol 2013; 935:285-295.

63 Luo Y, Zhuo Y, Fukuhara M et al. Effects of culture conditions on heterogeneity and the apical junctional complex of

the ARPE-19 cell line. Invest Ophthalmol Vis Sci 2006;47:3644-3655.

64 Karl MO, Kroeger W, Wimmers S et al. Endogenous Gas6 and Ca2+-channel activation modulate phagocytosis by retinal pigment epithelium. Cell Signal 2008;20: 1159-1168.

65 Burke JM. Epithelial phenotype and the RPE: Is the answer blowing in the Wnt? Prog Retin Eye Res 2008;27:579-595.

66 Jurczyk A, Gromley A, Redick S et al. Pericentrin forms a complex with intraflagellar transport proteins and polycystin-2 and is required for primary cilia assembly. J Cell Biol 2004;166:637-643.

67 May-Simera HL, Wan Q, Jha BS et al. Primary cilium-mediated retinal pigment epithelium maturation is disrupted in ciliopathy patient cells. Cell Rep 2018;22: 189-205.

68 Koschak A, Reimer D, Huber I et al. a1D (Cav1.3) subunits can form L-type Ca2+ channels activating at negative voltages. J Biol Chem 2001;276:22100-22106.

69 Singh A, Gebhart M, Fritsch R et al. Modulation of voltage- and Ca2 +-dependent gating of CaV1.3 L-type calcium channels by alternative splicing of a C-terminal regulatory domain. J Biol Chem 2008;283:20733-20744.

70 Striessnig J, Pinggera A, Kaur G et al. L-type Ca2+ channels in heart and brain. Wiley Interdiscip Rev Membr Transp Signal 2014;3:15-38.

71 Cordeiro S, Strauss O. Expression of Orai genes and ICRAC activation in the human retinal pigment epithelium. Graefes Arch Clin Exp Ophthalmol 2011;249:47-54.

72 Martínez-García MC, Martínez T, Pañeda C et al. Differential expression and localization of transient receptor potential vanilloid 1 in rabbit and human eyes. Histol Histopathol 2013;28:1507-1516.

73 Cordeiro S, Seyler S, Stindl J et al. Heat-sensitive TRPV channels in retinal pigment epithelial cells: Regulation of VEGF-A secretion. Invest Ophthalmol Vis Sci 2010;51: 6001-6008.

74 Wimmers S, Strauss O. Basal calcium entry in retinal pigment epithelial cells is mediated by TRPC channels. Invest Ophthalmol Vis Sci 2007;48:5767-5772.

75 Balse E, Steele DF, Abriel H et al. Dynamic of ion channel expression at the plasma membrane of cardiomyocytes. Physiol Rev 2012;92:1317-1358.

76 Perez-Reyes E. Molecular physiology of low-voltage-activated T-type calcium channels. Physiol Rev 2003;83:117-161.

77 Strauss O, Wienrich M. Ca2+−conductances in cultured rat retinal pigment epithelial cells. J Cell Physiol 1994;160:89-96.

78 Kovach JL, Schwartz SG, Flynn HW Jr et al. Anti-VEGF treatment strategies for wet AMD. J Ophthalmol 2012;2012:1-7.

79 Klettner A, Kaya L, Flach J et al. Basal and apical regulation of VEGF-A and placenta growth factor in the RPE/choroid and primary RPE. Mol Vis 2015;21:736-748.

80 Blaauwgeers HGT, Holtkamp GM, Rutten H et al. Polarized vascular endothelial growth factor secretion by human retinal pigment epithelium and localization of vascular endothelial growth factor receptors on the inner choriocapillaris: Evidence for a trophic paracrine relation. Am J Pathol 1999;155: 421-428.

81 Hollborn M, Vogler S, Reichenbach A et al. Regulation of the hyperosmotic induction of aquaporin 5 and VEGF in retinal pigment epithelial cells: Involvement of NFAT5. Mol Vis 2015;21:360-377.

82 Faby H, Hillenkamp J, Roider J et al. Hyperthermia-induced upregulation of vascular endothelial growth factor in retinal pigment epithelial cells is regulated by mitogen-activated protein kinases. Graefes Arch Clin Exp Ophthalmol 2014;252: 1737-1745.

83 Kannan R, Zhang N, Sreekumar PG et al. Stimulation of apical and basolateral vascular endothelial growth factor-A and vascular endothelial growth factor-C secretion by oxidative stress in polarized retinal pigment epithelial cells. Mol Vis 2006;12: 1649-1659.

84 Gal A, Li Y, Thompson DA et al. Mutations in MERTK, the human orthologue of the RCS rat retinal dystrophy gene, cause retinitis pigmentosa. Nat Genet 2000; 26:270-271.

85 Vollrath D, Yasumura D, Benchorin G et al. Tyro3 modulates mertk-associated retinal degeneration. PLoS Genet 2015;11: e1005723.

86 Hall MO, Abrams TA, Mittag TW. ROS ingestion by RPE cells is turned off by increased protein kinase C activity and by increased calcium. Exp Eye Res 1991;52: 591-598.

87 Milenkovic VM, Krejcova S, Reichhart N et al. Interaction of bestrophin-1 and Ca2+ channel β-subunits: Identification of new binding domains on the bestrophin-1 C-terminus. PLoS ONE 2011;6(4):e19364.

88 Szklarczyk D, Franceschini A, Wyder S et al. STRING v10: Protein-protein interaction networks, integrated over the tree of life. Nucleic Acids Res 2015;43:447-452.

89 Mazzoni F, Safa H, Finnemann SC. Understanding photoreceptor outer segment phagocytosis: Use and utility of RPE cells in culture. Exp Eye Res 2014;126:51-60.

90 Sugino IK, Sun Q, Wang J et al. Comparison of FRPE and human embryonic stem cell–derived RPE behavior on aged human Bruch's membrane. Invest Ophthalmol Vis Sci 2011;52:4979-4997.

91 Yang X, Chung JY, Rai U et al. Cadherins in the retinal pigment epithelium (RPE) revisited: P-cadherin is the highly dominant cadherin expressed in human and mouse RPE in vivo. PLoS ONE 2018;13(1):e0191279.

92 Bennis A, Gorgels TG, Ten Brink JB et al. Comparison of mouse and human retinal pigment epithelium gene expression profiles: Potential implications for age-related macular degeneration. PLoS ONE 2015;10(10):e0141597.

93 Bakall B, Marmorstein LY, Hoppe G et al. Expression and localization of bestrophin during normal mouse development. Invest Ophthalmol Vis Sci 2003;44:3622-3628.

94 Zhao PY, Gan G, Peng S et al. TRP channels localize to subdomains of the apical plasma membrane in human fetal retinal pigment epithelium. Invest Ophthalmol Vis Sci 2015;56:1916-1923.

95 Muntean BS, Jin X, Williams FE et al. Primary cilium regulates CaV1.2 expression through Wnt signaling. J Cell Physiol 2014;229:1926-1934.

96 Westenskow P, Piccolo S, Fuhrmann S. Beta-catenin controls differentiation of the retinal pigment epithelium in the mouse optic cup by regulating Mitf and Otx2 expression. Development 2009;136:2505-2510.

97 Delling M, DeCaen PG, Doerner JF et al. Primary cilia are specialized calcium signalling organelles. Nature 2013;504:311-314.

98 Pablo JL, DeCaen PG, Clapham DE. Progress in ciliary ion channel physiology. J Gen Physiol 2017;149:37-47.

See www.StemCellsTM.com for supporting information available online.